



Pilkington Library

Author/Filing Title HIRATA, M

Accession/Copy No. 040165831

Vol. No.	Class Mark
---------------	------------------

	LOAN COPY	
--	-----------	--

0401658317



BADMINTON PRESS
UNIT 11 BROOK ST
SYSTON
LEICESTER LE7 1GB
ENGLAND
TEL: 0116 260 2917
FAX: 0116 260 6620

A fractal Approach to Mixing-microstructure-property
Relationship for Rubber Compounds

by

Mamoru Hirata


A doctoral thesis submitted in partial fulfilment
of the requirements for the award of
the degree of
Doctor of Philosophy
of the
Loughborough University

December 1997

Supervisor : Philip K. Feakley, Ph.D, FPRI

Institute of Polymer Technology and
Materials Engineering

© by Mamoru Hirata, 1997

 Loughborough University	
Library	
Date	June 98
Class	
Acc No.	040165831

K0629583

ACKNOWLEDGMENTS

I sincerely wish to thank my supervisor, Dr. Philip K. Freakley for his helpful guidance, suggestions and encouragement throughout the research period.

I gratefully acknowledge the financial provided by Bridgestone Corporation.

I also wish to express particular thanks to :

- Dr. David Southwart, Dr. Jane Clarke and Barry Clarke for their invaluable suggestions
- Member of the technical staff at IPTME for their co-operation during the course of this study
- Study mates in RuPEC group

ABSTRACT

The research is concerned with exploration of the utility of fractal methods for characterising the mixing treatment applied to a rubber compound and also for characterising the microstructure developed during mixing (filler dispersion). Fractal analysis is also used for characterisation of the fracture surfaces generated during tensile testing of vulcanised samples. For these purposes, Maximum Entropy Method and Box Counting Method are developed and they are applied to analyse the mixing treatment and the filler dispersion, respectively. These methods are effectively used and it is found that fractal dimensions of mixer-power-traces and fracture surfaces of vulcanised rubber decrease with the evolution of mixing time while the fractal dimension of the state-of-mix (filler dispersion) also decreases.

The relationship of the fractal dimensions thus determined with conventional properties, such as viscosity, tensile strength and heat transfer coefficient are then explored. For example, a series of thermal measurements are carried out during vulcanisation process and the data are analysed for determining the heat transfer coefficient. Nuclear Magnetic Resonance is used to obtain the properties of bound rubber and a quantitative analysis is also carried out and possible mechanisms for the relationships between the parameters are discussed based on existing interpretations.

Finally, the utility of the fractal methods for establishing mixing-microstructure-property relationships is compared with more conventional and well established methods. For this purpose, the fractal dimension of the state-of-mix is compared to conventional methods such as the Payne Effect, electrical conductivity and carbon black dispersion (ASTM D2663 Method C). It is found that the characterisation by the fractal concept agrees with the conclusions from these conventional methods. In addition, it becomes possible to interpret the relationships between these conventional methods with the help of the fractal concept.

Contents

	<u>Page No.</u>
Acknowledgments	i
Abstract	ii
Contents	iii
Lits of figures	vii
List of tables	xii
List of symbols	xiii
 Chapter 1: Introduction and objectives	 1
1.1 Preamble	1
1.2 Rubber Technology	1
1.2.1 The materials and ingredients	2
1.2.2 Polymer processing	6
1.2.3 The properties of rubber compounds	7
1.3 Fractals	8
1.4 Present problems of rubber technology	8
1.5 Objective	13
References	15
 Chapter 2: Literature review	 17
2.1 Fractals	17
2.1.1 The fractal concept	17
2.1.2 Classification of shapes	17
2.1.3 Dimension	19
2.1.4 Fractals	24
2.1.5 How to measure a fractal dimension	30
2.2. Rubber technology	37
2.2.1 Preamble	37
2.2.2 Raw materials	37
2.2.2.1 Scaling aspects of a polymer	37
2.2.2.2 Carbon black from fractal point of view	40

	<u>Page No.</u>
2.2.3 Rubber processing	42
2.2.3.1 Mixing	42
2.2.3.2 The state of mix of carbon black	51
2.2.3.3 Vulcanization	62
2.2.4 Ultimate properties of rubber vucanisate	70
2.2.4.1 Energy approach	70
2.2.4.2 Mechanism of carbon reinforcement	72
2.2.4.3 Medalia's interpretation of carbon reinforcement.	75
2.2.5 The meaning of Fractal Analysis and Fourier Transforms for Rubber Technology	77
2.2.6 Fractal applications	82
2.2.6.1 Polymer processing	82
2.2.6.2 Characterization of rubber properties	84
References	92
Chapter 3: Experimental work	98
3.1 Introduction	98
3.2 Material preparation	98
3.2.1 Materials and formulations	98
3.2.2 Mixing and operating conditions	98
3.2.3 Nomenclature of test samples	101
3.2.4 Fourier transform analysis of the mixer power chart	102
3.2.5 Measurement of electrical resistance of vulcanised compounds	103
3.2.6 Measurement of curing characteristics	105
3.2.7 Moulding	106
3.3 Measurements of rubber samples	106
3.3.1 Carbon black dispersion analysis	107
3.3.2 Measurements of fracture surface of tensile samples	108
3.3.3 Measurements of tensile strength	110
3.3.4 Measurements of viscoelastic and dynamic properties	110

	<u>Page No.</u>
3.3.5 Thermal properties	112
3.3.6 Bound rubber	113
References	115
Chapter 4: Results and Discussion	116
4.1 Introduction	116
4.2 General properties of tested samples	116
4.2.1 Tensile strength	117
4.2.2 Viscoelastic properties	118
4.2.2.1 Temperature dependence	118
4.2.2.2 The Payne effect	121
4.3 Fractal aspects of rubber properties	124
4.3.1 Fractal analysis of mixer power trace	124
4.3.2 Fractal analysis of the carbon black dispersion	132
4.3.3 Fracture surfaces of tensile strength samples	136
4.3.4 Relationships among Mixing, State of mix and fracture surface	141
4.3.4.1 Relationship between fractal dimensions of mixing and the state of mix	141
4.3.4.2 Relationship between the fractal dimension of the state of mix and fracture surfaces	146
4.3.4.3 Fractal application to vulcanized rubber properties	147
4.3.5 A new method to measure the state of mix	149
4.4 The influence of the state of mix on rubber properties	154
4.4.1 The influence of the state of mix on thermal properties ...	154
4.4.2 The relationship between bound rubber and the state of mix	158
References	161
Chapter 5: Conclusion and recommendations	162
5.1 Conclusions	162
5.1.1 Fractal application	162

	<u>Page No.</u>
5.1.2 A new method to evaluate the state of mix of filler dispersion	163
5.1.3 The influence of the state of mix on rubber properties	163
5.2 Recommendations	164
References	166
 Appendices :	
Appendix 1 : The definition of Peano curve	167
Appendix 2 : Fourier transform	171
Appendix 3 : Maximum entropy method	172
Appendix 4 : Analysis of random data	182
Appendix 5 : A random flight model as an example of random walk	185
Appendix 6 : Smith's fracture envelope	188
Appendix 7 : An analysis of flow in an internal mixer	192
Appendix 8 : ASTM D-2663, Method D	197
Appendix 9 : Experimental data	199
References	222

List of figures

	<u>Page No.</u>
Figure 1.1 Some typical monomers of elastomers and chemical structures	3
1.2 The temperature dependence of storage modulus of natural rubber	4
1.3 (a) An example of carbon black aggregate	5
1.3 (b) Categorization of carbon black based on its structures	5
1.4 A typical rubber fabrication factory and its processing equipment .	7
2.1 The first iterations of the Koch Curve	18
2.2 Approximation procedure replacing the original shape by triangle .	18
2.3 Two co-ordinate systems moving relative to each other with velocity V	19
2.4 Phase diagram for many particle systems	21
2.5 The Peano Curve. The fractal dimension of this curve is two	21
2.6 An example of a regular system with dimensions $d=1, 2$, and 3	22
2.7 Classification of fractal shape	25
2.8 The Sierpinski sponge. Its dimension is 2.7268	25
2.9 An example of random fractal. Its dimension is 1.11	26
2.10 A simple deterministic model of self affine fractal	28
2.11 An example of a random affine fractal	29
2.12 The method to determine the fractal dimension of a coast line by using circles	31
2.13 The method to determine the fractal dimension, the so called box counting method	31
2.14 A fractal model for the distribution of stars	33
2.15 The radii distribution of craters on the moon	35
2.16 Scaling concept of polymer chain. The chain consists of an imaginary sphere called a blob	38
2.17 Fractal dimension based on perimeter - area plot for 1000 N121 aggregates in the dry state	41
2.18 Correlation of the perimeter fractal with DBP absorption	41

	<u>Page No.</u>
2.19 A schematic drawing of rotors and mixing chamber	43
2.20 A typical mixer power trace of an internal mixer	44
2.21 A schematic model of an internal mixer	46
2.22 Schematic representation of an agglomerate. The cleavage occurs at the shaded plane	52
2.23 Onion model for carbon black incorporation into a polymer matrix	52
2.24 A model of dispersive mixing in an internal mixer	53
2.25 Dispersion analyser system for stylus roughness measurements	54
2.26 Stylus roughness traces and sample photographs	55
2.27 Carbon black agglomeration versus roughness factor from stylus measurement	56
2.28 Rheological properties of uncured compound with N220 in SBR1712 plotted against mixing time	60
2.29 Tensile strength of different elastomer compounds as a function of dispersion index	61
2.30 Typical cure curves at various temperatures	63
2.31 The structure of crosslinkings	63
2.32 Free radical mechanism as a model of vulcanisation	64
2.33 Thermal conductivity of carbon black loaded natural rubber	66
2.34 Temperature profile as a function of cure time and sample thickness	67
2.35 A trouser sample and measurement conditions	71
2.36 Crack growth versus tearing energy for NR(•) and SBR(×) gum vulcanisate	73
2.37 Four types of tear proposed by Medalia (schematic)	75
2.38 Electrical conductivity of SBR with 50 phr carbon black as a function of elongation	76
2.39 Rubber flow in an internal mixer	79
2.40 Relation between power spectrum density and frequency The circle and triangle correspond to rotor revolutions	83
2.41 Relation between fractal dimension and revolution ratio	83

	<u>Page No.</u>
2.42 Fractal area perimeter relationship for slit islands. Fractal dimension is 1.28	84
2.43 Cumulative spectrum for metal fracture surface	
Fractal dimension increment is 1.26	85
2.44 Impact energy versus fractal dimensional increment	86
2.45 Wear surface under the frictional force of 730 J m^{-2}	87
2.46 The effect of profilometer "radius" (disc diameter) on profilometer trace	88
2.47 Typical fractal plot profilometry data	88
2.48 Microscopic photograph of degraded SBR surface crazing	
200 hours ageing sample	90
2.49 A relationship between box size and the number of box that contains crazing images in it	90
2.50 Relation between the fractal dimension and ageing condition	91
3.1 Mixer power trace showing mixing process sequence	100
3.2 Power spectrum of a mixer power trace obtained by the Fourier transform	102
3.3 A simplified schematic of flow in the mixing chamber of an intermeshing rotor internal mixer	103
3.4 Schematic of the coaxial probe arrangement with air pressure mechanism	104
3.5 Details of the coaxial probe	104
3.6 A schematic cure curve. H is defined as the difference of maximum and minimum torque. $T_{0.9}$ is defined as the time to reach $0.9 \times H$ torque	106
3.7 Schematic explanation of experimental procedure for evaluating the state of mix of carbon black	107
3.8 Rodenstock RM 600 laser stylus	108
3.9 Temperature dependence of storage modulus. (AGL4)	111
3.10 The schematic explanation about the heat transfer measurements ...	112
3.11 An example of FID of LDPE sample	114

4.1 A normalised graph of tensile strength at break, where total internal mixer rotor revolutions is a product of rotor speed and mixing time	117
4.2 Temperature dependence of viscoelastic property of a NR (AGO5) sample	119
4.3 The influence of the state of mix on viscoelasticity. Badly mixed sample (AGL3) has a small E' than the better mixed compound (AGL5)	120
4.4 A result of the Payne Effect (SBR (AGL, M, N) sample)	121
4.5 A normalised graph of the Payne effect (NR(AGO, P, Q) samples) .	121
4.6 Determination of fractal dimension. From the slope of this graph, the fractal dimension is calculated	124
4.7 The relationship between mixing time and fractal dimensions of the mixer power chart (SBR sample)	126
4.8 Normalised relationship between mixing time and fractal dimensions. The absicca is a product of rotor speed and mixing time (SBR)	127
4.9 Mixer power trace of SBR compound. (a) 90 second Mixing (b) 420 second Mixing	128
4.10 Lines with a various fractal dimensions. D=1.0, 1.25, 1.5, 2.0 from the top to bottom	129
4.11 The relationship between mixing time and fractal dimensions (NR samples)	130
4.12 Comparison of power traces of SBR and NR compounds	131
4.13 An example of the box counting method to determine the state of mix of carbon black. (AGL)	132
4.14 A relationship between fractal dimension of carbon dispersion and mixing time (SBR samples)	133
4.15 A time dependence of the fractal dimension of the state of mix (SBR and NR have different formulations)	135
4.16 A contour profile of a fracture surface	136

	<u>Page No.</u>
4.17 A power spectrum of a fracture surface. The slope of the graph is used to calculate the fractal dimension. (AGL1)	137
4.18 A normalised fractal dimension of the fracture surface	138
4.19 A relationship between tensile strength and the fracture surface fractal dimension of SBR samples. Correlation coefficient is -0.675 ..	139
4.20 A relationship between tensile strength and the fractal dimension of NR samples. Correlation coefficient is -0.407	140
4.21 (a) The relationship between mixing and the state of mix (SBR compounds). Abscissa and ordinate are fractal dimensions of mixing and the state of mix respectively	141
4.22 (b) The relationship between mixing and the state of mix (NR compounds). Abscissa and ordinate are fractal dimensions of a mixing and the state of mix respectively	142
4.23 Electrical resistance versus fractal dimensions of the state of mix ..	143
4.24 A relationship between the Payne Effect and fractal dimensions of the state of mix. (top) SBR compound, correlation coefficient is 0.683 : (bottom) NR compound, correlation coefficient is 0.607 ..	145
4.25 Fractal application for the evaluation of the state of mix and the fracture surfaces. Abscissa and ordinate are fractal dimension of the state of mix and fracture surfaces, respectively	146
4.26 Tensile strength versus fractal dimension of mixer power traces ..	147
4.27 A fracture surface of tensile strength tested sample	150
4.28 The true surface roughness after removing a least square fitting surface	150
4.29 A two dimensional power spectrum for the true roughness of fracture surface	151
4.30 The new method to represent the state of mix by using 2D Fourier transformation	153
4.31 A temperature increase during vulcanisation	154
4.32 Thermal diffusivity as a function of the state of mix	155

	<u>Page No.</u>
4.33 Log resistivity versus mixing time for low structure black loaded samples	157
4.34 The relationship between mixing time and relaxation time of bound rubber	158
4.35 The relationship between the amount of bound rubber and mixing time	159
4.36 deGennes' model gives an ideal model for bound rubber	160

List of tables

	<u>Page No.</u>
Table 1.1 An example of the recipe for a rubber compound	2
3.1 Experimental formulation for SBR compounds (ASTM D3186)	99
3.2 Experimental formulation for NR compounds (ASTM D3184)	99
3.3 Nomenclature of test samples	101
3.4 Measuring condition of curing behaviour	105
3.5 Moulding conditions	106
3.6 Measuring condition of viscoelastic properties	110
3.7 The dynamic properties of rubber sample (AGL4)	111
4.1 Some thermal properties of polymer and carbon black	155
4.2 The relationship between NMR data and mixing time	158

List of Schemes

	<u>Page No.</u>
Scheme 1.1 Classification of research activity of polymer processing	9
1.2 The flow chart of research project	13

List of symbols

α	:	thermal diffusivity
α	:	slope of a power chart
α_1	:	extension ratio
β	:	slope of an power spectrum
γ	:	velocity average shear rate
ε	:	side length of the box
Θ	:	reduced temperature
λ	:	scaling factor
η	:	reduced position
μ_c	:	viscosity of fluid in channel
μ_t	:	viscosity of fluid at tip
ν	:	Flory number
ρ	:	distribution function
ρ_c	:	heat capacity
σ	:	stress at extension ratio α_1
σ	:	standard divination
τ	:	thermal diffusivity
a	:	surface area of trouser test
A	:	material constant for wear
b	:	scale parameter
BE	:	blending efficiency
C	:	correlation function
C_i	:	value of measured property of "i"th batch
C_p	:	concentration of segments

d	:	dimension parameter for each system
d_f	:	fractal dimension
D	:	fractal dimension
D_c	:	diameter at shaft
D_c	:	fractal dimension based on self - similarity
D_p	:	perimeter fractal dimension
D_s	:	dimension of a shape
D_t	:	diameter at tip
DM	:	degree of mixing
e	:	tip width
e_i	:	unit vector
E	:	modulus
E'	:	storage modulus
E_T	:	tear energy
E_o	:	modulus of pure gum
f	:	shape coefficient of carbon black (width/length)
f	:	frequency
f	:	ratio of pressure to drag flow
F	:	a function
F	:	tear force
F_{ent}	:	entropy for an segment
F_{rep}	:	repulsive energy
g	:	tip clearance
G	:	geometry constant
G	:	power spectrum
h	:	channel clearance
h	:	sample thickness
H	:	plate separation
H	:	Hurt exponent
I_v	:	uniformity index
j	:	imaginary symbol
k	:	thermal conductivity

L	:	length of an object (see also r)
M	:	intensity of FID signal
M	:	mass of an object
n	:	material constant for wear
N	:	number of boxes used for a box counting method
N	:	rotor speed
N_p	:	segment number
P	:	power
P	:	probability function
ΔP	:	pressure drop across flight
q	:	heat flux
Q_1	:	drag flow in channel
Q_2	:	drag flow at flight tip
Q_3	:	pressure flow in channel
Q_4	:	pressure flow at tip
r	:	length (see also L)
R	:	auto-correlation function
R_p	:	size of polymer chain
s	:	length of rotor
s_b	:	variance
s_x	:	variance
S	:	intensity of a power chart
S	:	shift factor
S	:	surface area of an object
t	:	time
t_{2a}	:	relaxation time for component a
t_{2b}	:	relaxation time for component b
T	:	temperature
T_g	:	glass transition temperature
T_m	:	melting temperature
V	:	volume of an object
V_z	:	velocity profile

W	:	wear rate
ΔW	:	tearing work
x	:	position parameter for an absolute co-ordinate system
x'	:	position parameter for an observation co-ordinate system
X	:	unknown measure of an object
y	:	position parameter for an absolute co-ordinate system
y'	:	position parameter for an observation co-ordinate system
z	:	position parameter for an absolute co-ordinate system
z'	:	position parameter for an observation co-ordinate system
Z	:	displacement for a random walk
Z	:	The Payne effect

Chapter 1

Introduction and objectives

1.1 Preamble

Rubber technology provides an interesting field of study because of the large number of potential applications and range of new concepts. The study of rubber technology includes rheological characterisation of polymer flow, chemical reactions such as vulcanisation and bound rubber formation, the material science of ingredients and many engineering subjects, such as fracture mechanics and adhesion.

In addition, process - (material microstructure) - property relationships are important for a wide range of materials, including metals, ceramics and polymers. The main feature of polymer technology can be seen in the strong relationship between processing and rubber properties. Selection of an appropriate processing treatment can have a substantial effect on the efficiency of manufacturing and the performance of the material during manufacture and the quality of the final products. There is still substantial scope for improvements in microstructure - process - property relationships at present.

The aim of this thesis is to explore the application of fractal concepts to characterise materials, processes and properties and their inter-relationships. Thus, it is necessary to understand the individual topics which make up rubber technology; and their inter-relationships. A short introduction to rubber technology is presented for this purpose. It provides a broad platform and an explanation of some of the key concepts of rubber technology. The meaning of fractals and their relevance to the objectives of this research are also given. The state of the art of rubber technology is also reviewed from a semi-historical point of view to clearly define directions for research in the field of rubber technology. Detailed objectives of the work reported in this thesis are given in the final section.

1.2 Rubber technology

Rubber technology may be effectively classified into three categories for the purpose of this research thesis ;

1. The materials and ingredients of rubber compounds.
2. Polymer processing.
3. The properties of rubber compounds.

1.2.1 The materials and ingredients

Rubber compounds

After the discovery of the vulcanisation process by Goodyear¹⁾, it was widely realised that the properties of vulcanised rubber could be substantially improved by a range of additives. The following formulation / recipe of a rubber compound illustrates a typical range of ingredients used to make a rubber compound.

Table 1.1 An example of the recipe for a rubber compound.

Elastomer	100 phr (parts per hundred rubber by weight)
Carbon black	20 - 150
Oil & Plasticiser	0 - 120
Sulphur	1 - 5
Crosslink activation system	
Stearic acid	1
Zinc oxide	3
Accelerator	
TBBS	1.25
(TBBS = N-tert-butyl-2-benzothiazylsulphenamide)	

The amounts of these ingredients are determined by the requirements of the final products. For example, typical amounts of carbon black for a vibration control system, a pneumatic tyre and automobile sealing strips are 20, 40 and 100 phr, respectively. The following are summaries of these ingredients.

Polymer

Polymers are generally high-molecular-weight, long-chain molecules. These long-chain molecules consist of a few types of repeating unit called monomers. It is convenient to

categorise pure and compound polymers as plastics, elastomers and fibres based on glass transition temperature (T_g) and crystallite melting points (T_m). The definition of these categories are as follows ²⁾.

1. Elastomers are polymers with crosslinks, or intense entanglements, or microcrystalline regions, whose T_g is such that $T_g + 75^\circ\text{C} < T_{\text{room}}$.
2. Fibres are highly crystalline polymers that can be easily oriented with T_m such that $T_m > T_{\text{room}} + 150^\circ\text{C}$.
3. Plastics fall into two categories. The first is glassy polymers which are amorphous substances where the T_g is such that $T_g > T_{\text{room}} + 75^\circ\text{C}$. The second is semicrystalline polymers which are substances of 50 - 90 % crystallinity where the T_g is much below T_m and much above T_{room} .

Some typical repeating units are shown in Figure 1.1.

No.	Rubber	ASTM Symbol	Chemical structure
1.	Isoprene rubber	NR	$\text{-(CH}_2\text{-C(CH}_3\text{)=CH-CH}_2\text{)-}$
2.	Natural rubber	IR	$\text{-(CH}_2\text{-C(CH}_3\text{)=CH-CH}_2\text{)-}$
3.	Butadiene rubber	BR	$\text{-(CH}_2\text{-CH=CH-CH}_2\text{)-}$
4.	1,2-butadiene rubber	1,2-BR	$\text{-(CH}_2\text{-CH=CH-CH}_2\text{)-}$
5.	Styrene-butadiene rubber	SBR	$\text{-(CH}_2\text{-CH=CH-CH}_2\text{)-}$ $\text{-(CH}_2\text{-CH(C}_6\text{H}_5\text{)-)-}$
6.	Chloroprene rubber	CR	$\text{-(CH}_2\text{-C(Cl)=CH-CH}_2\text{)-}$
7.	Nitril rubber	NBR	$\text{-(CH}_2\text{-CH=CH-CH}_2\text{)-}$ $\text{-(CH}_2\text{-CH(CN)-)-}$
8.	Butyl rubber	IIR	$\text{-(CH}_2\text{-C(CH}_3\text{)=CH-CH}_2\text{)-}$ $\text{-(CH}_2\text{-C(CH}_3\text{)=CH-CH}_2\text{)-}$
9.	Ethylene-propylene rubber	BPM EPDM	$\text{-(CH}_2\text{-CH}_2\text{)-}$ $\text{-(CH}_2\text{-CH(CH}_3\text{)-)-}$ $\text{-(CH}_2\text{-CH}_2\text{)-}$ $\text{-(CH}_2\text{-CH(CH}_3\text{)-)-}$ $\text{-(CH}_2\text{-CH(C}_6\text{H}_5\text{)-)-}$
10.	Styrene-chlorosulphonate	CSM	$\text{-(CH}_2\text{-CH}_2\text{)-}$ $\text{-(CH}_2\text{-CH(SO}_2\text{Cl)-)-}$ $\text{-(CH}_2\text{-CH(C}_6\text{H}_5\text{)-)-}$
11.	Acryl rubber	ACM ANM	$\text{-(CH}_2\text{-CH(CO}_2\text{R)-)-}$ $\text{-(CH}_2\text{-CH(CN)-)-}$ $\text{-(CH}_2\text{-CH(CO}_2\text{R)-)-}$ $\text{-(CH}_2\text{-CH(CN)-)-}$

Figure 1.1 Some typical monomers of elastomers and chemical structures ¹¹⁾.

Figure 1.2 shows an example of the temperature dependence of storage modulus of natural rubber (Hevea). The main difference between plastics and elastomers lies in the fact that the T_g of plastics (thermoplastics and thermosets : the former melts and the latter hardens through chemical reactions by raising temperature) is above room temperature and the T_g of elastomer is less than room temperature. In the case of elastomers a plateau region (the region of $-40\text{ }^{\circ}\text{C}$ to $200\text{ }^{\circ}\text{C}$ in **Figure 1.2**) can be seen around room temperature.

Recent developments of polymer technology include the invention of stereoregular type polymers (highly controlled tacticity polymer) and the discovery of living-polymers. The stereoregular type polymers were developed with the Ziegler-Natta catalysis system ³⁾ to produce highly controlled tacticity polymers. Living polymerisation was developed by Szwarc ⁴⁾ and enabled polymer molecular weight to be controlled allowing the production of monodispersed polymers.

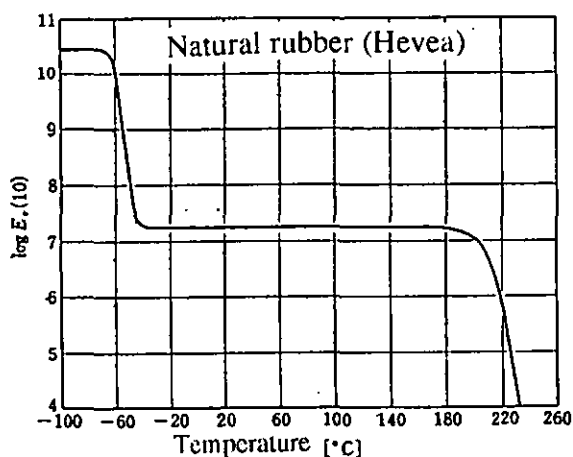


Figure 1.2 The temperature dependence of storage modulus of natural rubber ¹⁰⁾

The development of polymer technology enables polymers to be tailor made for specific purposes, thus improving the performance of commercial goods.

Particulate Filler

A particulate filler is used to obtain desired properties. A typical example is modulus and tensile strength which are difficult to control simply by polymer selections or use of other ingredients. There are two types of filler ; reinforcing and non-reinforcing. Typical reinforcing fillers are carbon black and silica. A typical non-reinforcing filler is calcium-carbonate for elastomers. One example of carbon black is shown in **Figure 1.3 (a)**. Two main material variables of carbon black are important for its effect on rubber properties. The first is its particle size and the other is the structure of carbon black agglomerates **Figure 1.3 (b)**. The particle size is normally characterised by its specific surface area (m^2/g) and the structure, which is a measure of aggregate geometry, specifically its ‘bulkiness’, is characterised by the amount of adsorbable DBP (dibutyl-phthalate). These characteristics are designed, mainly, depending on the purpose of final products.

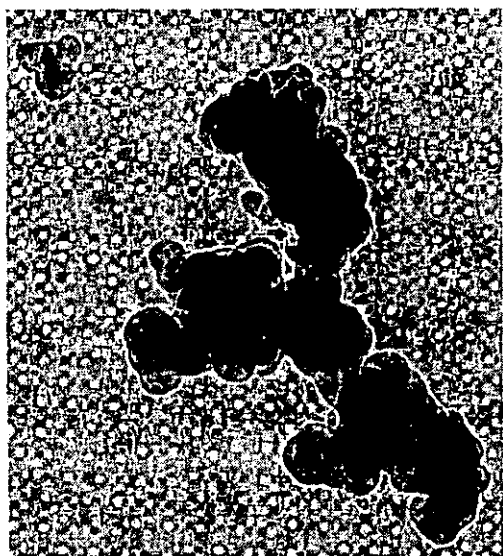


Figure 1.3 (a) An example of carbon black aggregate.⁶⁾

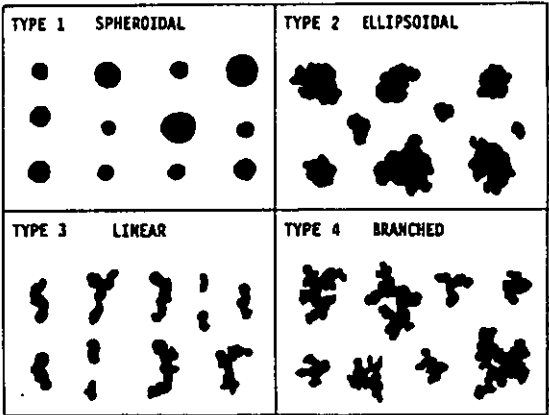


Figure 1.3 (b) Categorisation of carbon black based on its structures.³⁰⁾

Crosslinking system

Vulcanisation ingredients are one of the most basic additives in rubber compounds. The vulcanisation ingredients usually consist of two types of chemical agents. The first is chemicals which form crosslinks (sulphur or sulphur donor) and the other is chemicals which catalyse the vulcanisation process (accelerator and crosslink activation system).

The vulcanisation process was discovered by Goodyear ¹⁾ and accelerators were developed by Oenshlager ⁵⁾. Oenshlager also discovered that aniline greatly accelerated the rate of vulcanisation and that the combination of zinc oxide with organic accelerators improved the performance of products.

1.2.2 Polymer processing

Figure 1.4 shows a typical example of a rubber processing plant. The first stage is material preparation (left side in **Figure 1.4**) followed by a downstream shaping process (right side in **Figure 1.4**). Initially, matrix polymer and filler are mixed in an internal mixer and the mixed stock is combined with other ingredients on mills or in a screw extruder. These processes differ between factories. Sometimes only one stage mixing covers the rest of mixing process. The mixed rubber compound is introduced into an extruder or calender to form sub-components with the desired dimensions. These shaped materials are assembled at the next stage and finally brought to the vulcanisation process.

Rubber compounds are chemically active composites, so both the physical treatment and the heat history received during manufacture affect the material behaviour, placing specific requirements and boundary conditions on the selection and operation of the manufacturing process.

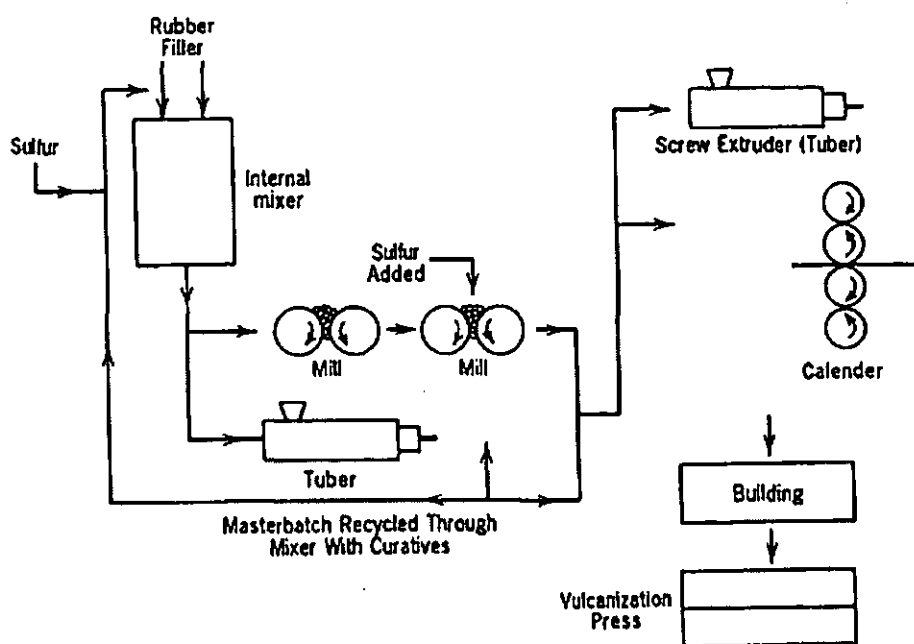


Figure 1.4 A typical rubber fabrication factory and its processing equipment ⁸⁾.

1.2.3 The properties of rubber compounds

The nature of research into rubber compounds is determined by the vulcanisation process. Pre-vulcanisation experiments and research can be conducted on the rheological behaviour of the material. Post-vulcanisation experiments and research can be conducted using methods ranging from simple tensile tests to evaluation of complex wear phenomena on the final products.

Rheological ⁶⁻¹¹⁾ study can be divided into two categories based on the amplitude which a material experiences under use. The first category involves small strains, typically within 10%. The study of the behaviour of vulcanised rubber mainly belongs to this category. This category has been extensively studied because it gives a consistent understanding of the relationship between the microstructure of polymers and their viscoelastic behaviour ^{9,10)}. A typical result is shown in **Figure 1.2**.

The second category treats material-behaviour under a large deformation. This field mainly consists of the formation of rheological or constitutive equations for unvulcanised

rubber compounds. It is mainly suited to the study of polymer flow during the processing stage. Two types of formulations are commonly used to analyse polymer flows. The first is based on a covariant derivation (Oldroyd derivation ¹²⁾) and the other is based on contravariant derivations (Jaumann derivation ⁷⁾). As Oldroyd ¹²⁾ pointed out, these formulations derive different results and experimental results suggest that the Oldroyd type formulation explains material behaviour better than the Jaumann type formulation. As yet this has not been properly evaluated.

1.3 Fractals

About twenty years ago, Mandelbrot ²⁸⁾ proposed the fractal concept ¹⁴⁾. It has been recognised that fractals can provide insights into a wide range of material phenomena. Metaphorically speaking, fractals can correspond to analytical mechanics in physics. Almost all of the topics which belong to mechanics, electromagnetism, quantum mechanics and field theory can be explained by using Hamiltonian or Lagrangian dynamics¹³⁾.

In the case of rubber technology, the application of fractals to the three main areas (raw materials-processing-vulcanised rubber properties) has already started. Unfortunately published literature is not available to illustrate the relationships between these areas. It is possible to explore the application of fractal concepts to rubber technology by reviewing these three areas from a fractal point of view. This research thesis provides an examination of the possibility of using fractal technology to provide a framework for the analysis of rubber processing and properties.

1.4 Present problems of rubber technology

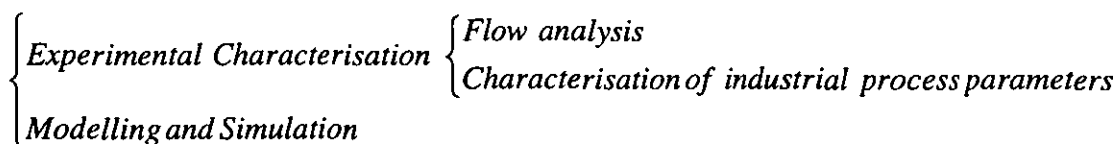
Rubber technology can be classified into three fields. As part of this definition both historical and contemporary issues are discussed to highlight and illustrate the context of this research thesis.

Materials and ingredients

Initial studies were completed by Staudinger ¹⁵⁾, Guth ¹⁶⁾ and Flory ¹⁷⁾. Staudinger established the concept that a polymer is made of high-weight molecules consisting of a few types of monomers (repeating units). After this was established, rubber elasticity attracted considerable research interest. The entropy concept of rubber elasticity was established by Guth and Flory. Recent research interest is mainly concerned with constitutive equations (rheology equations) because of the success of the tube-theory or the scaling concept by Doi, Edwards ¹⁸⁾ and deGennes ¹⁹⁾, respectively. The tube or scaling theory is closely related to fractal theory and their relationship is well established ²⁰⁾. The application of fractal technology has had considerable success in polymer physics in the form of the tube or scaling theory.

Polymer processing

Scheme 1.1 shows the classification of research activity in this field.



Scheme 1.1 Classification of research activity of polymer processing.

The initial characterisation of polymer processing, especially rubber processing, can be divided into two categories. The first is an experimental characterisation of rubber flow in an apparatus and the other is the simulation, or modelling, of this flow. Furthermore, the experimental characterisation is divided into two types of approach. One approach is the flow analysis of rubber compounds during mixing and the other approach is characterisation of industrial parameters such as a mixer power trace. An example of flow analysis is the flow visualisation techniques using a transparent polymer processing device initiated by Freakley ²¹⁾ and White ^{6,8)}. They found that there were five types of flow in an

internal mixer. These flows determine the efficiency of a mixing process and are dependent on both individual instrument design and operation conditions. This restriction prevents consistent interpretation of a mixing process by flow characterisation. The other approach is characterisation of the mixing process by using industrial parameters, such as mixer power, ram position and batch temperature. Unfortunately the interpretation of the mixing process is still qualitative, although these parameters are used to determine the terminal point of the mixing process. Quantitative interpretation of industrial parameters has not been carried out in relation to rubber flow in an internal mixer. The research to correlate polymer flow in an apparatus to industrial parameters may be developed by introducing a new parameter which relates to the flow characteristics of rubber compounds. Nishimoto²⁴⁾ initiated this type of research by quantitatively applying the fractal concept to the relationship between polymer flow in an internal mixer and a mixer-power trace.

The properties of rubber compounds

This category is a diverse field because of the requirements of the final products. It ranges from simple tensile properties to complicated phenomena like wear and adhesion. For example, abrasion is a complicated function of viscoelasticity, adsorption and tensile strength at break. It is very difficult to predict abrasion quantitatively and many experiments have to be done to predict it through empirical experiment. In spite of the recognition that it is necessary to consider many properties to understand one phenomenon, it appears, from experience, that tensile strength is the most important rubber property for industrial purposes. Two types of mechanisms have been proposed for the model of rubber fracture to explain the tensile strength at break. The first was the radical mechanism²⁵⁾ in which a radical produced by chain scission was transmitted chemically resulting in an instantaneous break-down at a fracture point. The other²⁶⁾ was the application of fracture mechanics developed for metallic materials. The radical mechanism was developed mainly by Bueche and the fracture mechanics was developed mainly by Thomas. These theories do not include the influence of reinforcing filler. Recently, Medalia²⁷⁾ summarised the existing research activities and proposed a “crack

deviation mechanism” for the action of reinforcing fillers. According to this theory, the fracture surface has to reflect the crack deviation caused by the reinforcing filler. Unfortunately published literature is not available to illustrate the fracture surfaces of elastomers to evaluate the validity of this mechanism.

Inter-relationships

The uniqueness of polymer technology lies in the fact that polymer processing and the properties of the final products are more closely related to each other than other materials. Thus an extensive consideration of the mechanism of processing and the behaviour of materials is required if accurately specified final products are to be obtained. To obtain this broad perspective, ranging from rubber processing to material science, it is necessary to “focus attention on underlying engineering and scientific principles, which are also the basics of the unifying elements to all processes” ²⁾. This research thesis is an examination of the possibility that fractal concepts could be used to characterise and unify polymer chemistry, rubber processing and the material sciences.

Four aspects from within the field of rubber technology were chosen to define the research with regard to the application of fractal technology to rubber processing and are as follows ;

1. Characterisation of polymer mixing.

This topic was directly developed from Nishimoto’s work ²⁴⁾. Mixing is very important and is the first step in rubber processing ; the quality of mixed rubber compound affects seriously the processability downstream. To characterise a mixing process, a mixer power trace is analysed by the fractal concept to provide a representative industrial parameter for mixing process.

2. Evaluation of the state-of-mix of carbon black in rubber compounds.

In the case of rubber compounds, the most important requirement at mixing stage is to achieve uniform the state of mix of carbon black, as the other ingredients of a compound can be distributed uniformly with a diffusion mechanism downstream. Although the

importance of the state of mix of carbon black has been recognised for a long time, research has not succeeded in explaining the complicated rubber properties with sufficient accuracy. Therefore, the characterisation of the state of mix was chosen to be the second topic for this research thesis. This topic can be regarded as an evolution of the work initiated by Freakley²⁹⁾.

3. An application of the relationship between the fractal concept and the rubber fracture mechanics.

The third topic is the characterisation of the fracture surface of a vulcanised rubber sample. It is necessary to evaluate the validity of Medalia's mechanism²⁷⁾ or to propose a potential experimental method. This topic is an attempt to characterise the fracture surface with the fractal concept.

4. The relationship between mixing, the state of mix and fracture mechanism.

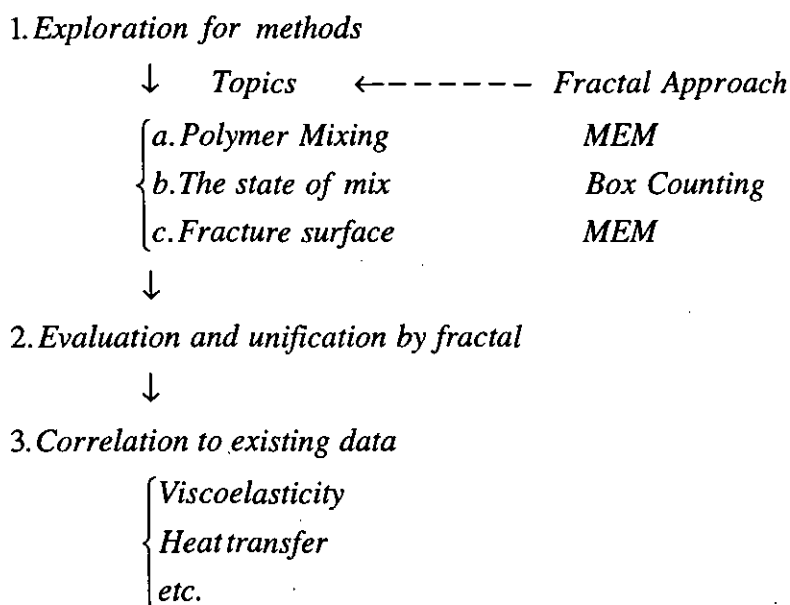
In addition to an examination of the applicability of the fractal concept to these three topics, it is also necessary to consider the relationship between operating conditions, the state of mix and the tensile strength at break. Fractals may provide an effective framework for dealing with this problem. In this thesis, the application of fractals to characterise the relationship between rubber mixing and the ultimate properties of the resulting compound is explored. Because of the lack of a consistent explanation for both unvulcanised and vulcanised properties, it is very difficult to obtain an optimum operation condition for rubber processing which satisfies many factors (processability, vulcanised properties and process cost). The application of fractals is expected to describe how these requirements can be optimised. Much research is currently being undertaken to characterise rubber properties from the fractal point of view. However, a systematic fractal application to rubber technology is not available at the moment. Such a systematic fractal application has the potential to connect existing research within a comprehensive theoretical framework.

1.5 Objectives

The first purpose of this thesis is to explore the utility of the fractal concept for the characterisation of ;

1. Rubber mixing
2. The state-of-mix of carbon black
3. Fracture surface
4. The inter-relationships of these properties

Scheme 1.2 shows the flow chart of the research in three stages ;



Scheme 1.2 The flow chart of research project.

The first step was an exploration of the tools and methods needed to analyse data.

The second step was an evaluation of the data by way of the fractal concept. The maximum entropy method (MEM) was used for the analysis of the mixer power-trace and of the fracture surface. A box counting method was used to evaluate the state of mix of carbon black in rubber compounds. With these analysis methods, the fractal dimension of a mixing (processing condition), the state of mix and fracture surface (vulcanised rubber

property) are characterised from the fractal point of view. Then, these three fractal dimensions are correlated and discussed in conjunction with tensile test data.

The third step was to explore the influence of the state of mix on the thermal properties and the state of bound rubber. A mechanism will be proposed to describe the influence of the state of mix on thermal properties.

References

- 1) C. Goodyear, U.S. Patent 3,633 (1844) ; "Gum Elastic", New Haven (1855)
- 2) Z. Tadmor, C.G. Gogos, "Principle of Polymer Processing", John-Wiley & Sons, (1979)
- 3) K. Ziegler, Angew. Chem., 76, 545 (1964)
- 4) M. Szwarc, J. Am. Chem. Soc., 78, 2656 (1956)
- 5) G. Oenschlager, Ind. Eng. Chem., 25, 232 (1933)
- 6) J. L. White, "Rubber Processing", Hanser (1977)
- 7) S. Middlemann, "Fundamentals of Polymer Processing", McGraw-Hill (1977)
- 8) J. L. White, "Principle of Polymer Engineering Rheology", Wiley Inter. Sci., (1990)
- 9) J. D. Ferry, "Viscoelastic Properties of Polymer", John Wiley & Sons., (1960)
- 10) A. V. Tobolsky, "Properties and Structure of Polymers", John Wiley & Sons., (1960)
- 11) Nihon Gomu Kyokai, "Gomu Gijyutu no Kiso", Gomu Kyokai (1983)
- 12) J. G. Oldroyd, Proc. Roy. Soc., A200, 523 (1950)
- 13) Y. Takahashi, "Kaiseki Rikigaku Nyumon", Kodan-sha (1977)
- 14) H. Takayasu, "Fractal Science", Asakura (1987)
- 15) H. Staudinger. "Die Hochmolekularen Organischen Verbindungen-Kaustushuk und Cellulose", Springer (Berlin, 1932)
- 16) H. Guth, H. Mark, Mh. Chem., 65,93 (1934)
- 17) P. J. Flory, "Principle of Polymer Chemistry", Cornell Univ. Press (1953)
- 18) M. Doi, S. F. Edwards, "The Theory of Polymer Dynamics", Clarendon (Oxford, 1986)
- 19) P. G. deGennes, "Scaling Concept in polymer", Cornell Univ. Press (1979)
- 20) D. Stauffer, "Introduction to Percolation Theory", Tayler & Francis (London, 1979)
- 21) P. K. Freakley, W. Idris, Rubb. Chem. Tech., 52,134 (1979)
- 22) K. Min, J. L. White, Rubb. Chem. Tech., 58,1024 (1985)
- 23) I. Mans-Zloczower, Z. Tadmor (ed.), "Mixing and Compounding of Polymer", Hanser (1995)
- 24) K. Nishimoto, N. Urabe, Nippon Gomu Kyokaishi, 65 (7), 82 (1992)

- 25) F. Bueche, "Physical Properties of Polymer", Interscience pub., (N.Y, 1962)
- 26) A. G. Thomas, J. Polym. Sci., 18,177 (1955)
- 27) A. I. Medalia, Rubb. Chem. Tech., 60,45 (1987)
- 28) B. B. Mandelbrot, "Fractals: Form, Chance and Dimension", Freeman, (San Francisco, 1977)
- 29) J. Clarke, P. K. Freakley, Plast. Rubb. and Comp. Process. and Appl., 24, 261 (1995)
- 30) C. R. Herd, G. C. McDonald, W. H. Hess, Rubb. Chem. Tech., 65, 107 (1992)

Chapter 2

Literature review

2.1 Fractals

2.1.1 The fractal concept

Fractal concepts ^{1 - 15)} are introduced here to ensure that the research thesis is self-contained and to demonstrate that it is possible to utilise fractals in the field of rubber technology.

2.1.2 Classification of shapes

It is possible to classify shapes into two categories. One is a shape which has a characteristic length and the other which does not have a characteristic length. In the case of a circle, a characteristic length is a radius and in the case of a house, it is the height or width of it. Any length can be chosen as long as it represents the typical length of the object. The feature of a shape which has a characteristic length is that the surface or the line which composes the shape is smooth. This means that the function of the surface or lines can be differentiated. Because of this character, many analytical methods are applicable to this class of shapes.

Other shapes do not have a characteristic length. Some examples of this class are the shapes of smoke, clouds, the surface of moon and the shape of a coast line. The surface of the moon is not smooth because of the craters on it. Some features can be seen in these categories. One is self-similarity and the other is self-affinity. These are systems that are invariant only under homogeneous or anisotropic magnification respectively.

For an example of self-similarity, let us take a famous curve called the Koch Curve. **Figure 2.1** and **Figure 2.2** show the curve and self-similarity is explained below.

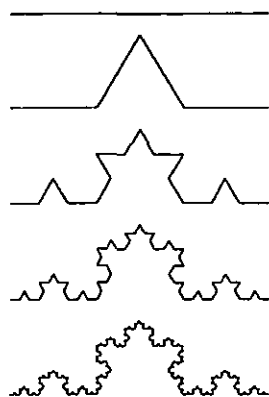


Figure 2.1 The first iterations of the Koch Curve.⁸⁾

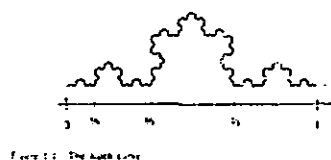


Figure 2.2 Approximation procedure replacing the original shape by triangle.⁸⁾

As a first approximation, the Koch Curve can be replaced by a triangle. This approximation is too rough to describe the shape of it so the same procedure is continued to approximate it by using triangles again. The rule for this approximation is that all the triangles should be similar. If this approximation is carried out infinitely, the Koch Curve is defined (**Appendix 1**). In this procedure, a triangle is replaced by smaller triangles which are similar to those in the previous steps. This characteristic, whereby the original shape can be approximated with a similar shape, is called “self-similarity”. Self similarity is applicable to both some mathematical shapes and also many natural shapes. The surface of the moon looks like the surface of an orange. The material fracture-surfaces under a microscope look like the surfaces of mountains. These observations come from the characteristic of self-similarity and they indicate that self-similarity is a common characteristic of the natural world.

Mandelbrot ¹⁾ investigated the characteristic of self-similarity and quantified it. Based on observations which were once discarded because of their complexity, he established a new branch of mathematics and called it “Fractals”.

2.1.3 Dimension

To identify a position on a line, one parameter (x) is necessary. In the case of a position on a plane surface, two parameters (x, y) are necessary. In the case of three dimensional space, it is necessary to use three parameters (x, y, z). As its natural extension, a surface or a solid body can be regarded as an ensemble of 2 or 3 parameters respectively.

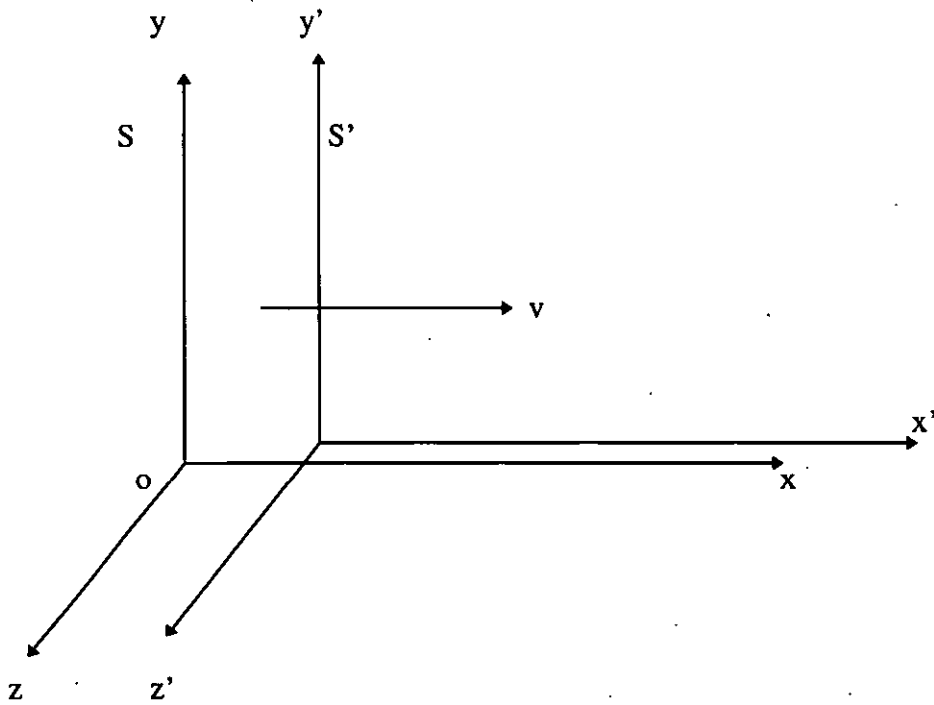


Figure 2.3 Two co-ordinate systems moving relative to each other with velocity V .

In classical physics, position parameters (x, y, z) and time (t) are considered independent. **Figure 2.3** shows an example of Newton's inertia theorem. In this case, a velocity (V) can be identified by two co-ordinate systems and its relationship can be given by the following equation.

$$x = x' - v t$$

$$y = y'$$

$$z = z'$$

$$t = t'$$

Equation 2.1

- x, y, z : Position parameter in an absolute co-ordinate system (S).
 x', y', z' : Position parameters in an observation co-ordinate system (S').
 t, t' : Time in an absolute and an observation co-ordinate system, respectively. (time is identical in both system in Figure 2.6)

For the same system, Einstein ¹⁶⁾ established the theory of “Special Relativity” which treats it as a four dimensional system. In his theory, three degrees of freedom are used to represent a position in space, and time is related to these positions as a fourth dimension. Einstein’s concept can be summarised as the Lorentz-transform for the same system.

$$x' = \frac{x - vt}{\sqrt{1 - (v/c)^2}}$$

$$y' = y$$

$$z' = z$$

$$t' = \frac{t - xv/c^2}{\sqrt{1 - (v/c)^2}}$$

Equation 2.2

The time becomes a dependent variable and is related to its position in an observation co-ordinate system.

In analytical physics ¹⁷⁾, a system comprising “m” particles is analysed as if it is a single particle. Figure 2.4 shows an example of such a system. One particle needs three position parameters and three velocities to define its physical condition. So, $(3+3) \times m = 6m$ parameters are necessary to characterise the behaviour of particles in the system. This space in which the co-ordinate system is located is known as “phase space”.

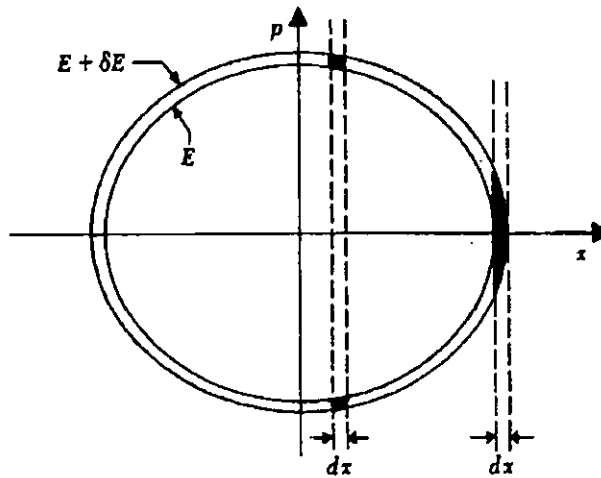


Figure 2.4 Phase diagram for many particle systems.²⁴⁾

There are some examples which do not follow this intuitive description. The Peano Curve is an example of this. **Figure 2.5** shows the Peano Curve on one surface although it is not necessary for it to exist on only one surface.

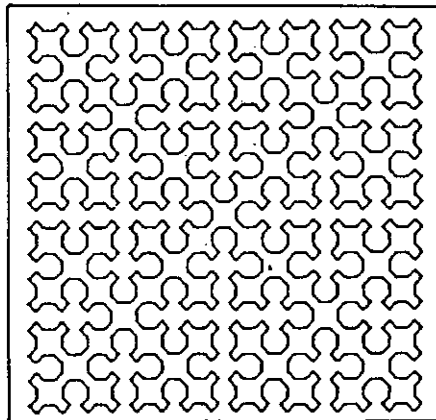


Figure 2.5 The Peano Curve. The fractal dimension of this curve is two.⁸⁾

It is possible to imagine a Peano Curve which spreads in three or more dimensions according to its definition (Appendix 1). In the two dimensional case (Figure 2.5), any position can be identified on a surface by using the Peano Curve (Appendix 1). Intuitively the Peano Curve in this case is a two-dimensional shape. However, the important characteristic of the Peano Curve lies in the fact that it needs only one parameter to identify a position on it. This fact conflicts with our own natural intuition. The conflict arises from the definition of “dimension” as being the degrees of freedom needed to unambiguously allocate a position in a co-ordinate system. It is important to consider the definition of dimension again to overcome this conflict. In the history of mathematics, this problem is known as the “1875-1922 Crisis”. Based on a topological concept, Menger¹⁸⁾ and Urysohn formulated the solution to this problem. It is possible to follow their results to reach the Fractal Dimension developed by Mandelbrot.

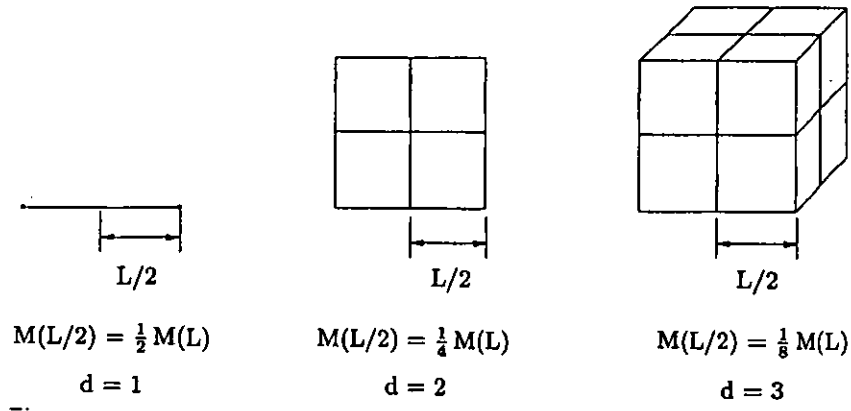


Figure 2.6 An example of a regular system with dimensions $d=1$, 2, and 3.¹³⁾

During the 1875 - 1922 Crisis, many types of definitions of dimensions were proposed. These new definitions of dimensions are theoretically important but to understand fractals, only a few new definitions are necessary. In this thesis, only two types of dimension which are based on self-similarity and self-affinity are used.

It is well known that in regular systems such as long wires, large thin plates, or large filled cubes, the dimension “d” characterises how the mass $M(L)$ changes with the linear size L for the system (**Figure 2.6**).

If a smaller part of the system of linear size bL ($b < 1$) is taken, then $M(bL)$ is decreased by a factor of b^d , i.e.,

$$M(bL) = b^d M(L) \quad \text{Equation 2.3}$$

The solution of the functional equation is simply $M(L) = AL^d$. Therefore, in the case of a line, the mass of the components of a line is one half if the line is divided into two equal pieces. (**Figure 2.6**) In the case of a plane, the mass of each segment becomes one fourth when a side is divided into equal lengths. In the case of a cube, the weight of segments becomes one eighth by the same procedure. These numbers “two, four, and eight” can be expressed as $(1/2)^1$, $(1/2)^2$, and $(1/2)^3$ respectively.

Thus the **Equation 2.3** becomes

$$M((1/2)L) = (1/2)^d M(L) \quad \text{Equation 2.4}$$

For each shape, “d” is

$$\begin{aligned} d = 1 & : \text{ for a line} \\ d = 2 & : \text{ for a plane} \\ d = 3 & : \text{ for a cube} \end{aligned}$$

There is no conflict between this dimension “d” and the traditional one. Furthermore, the characteristic of this definition is that it is not necessary for dimensions to be an integer. An alternative mathematical expression of this dimension, based on the number of segments, is given by taking logarithms of **Equation 2.3**.

$$Ds = \log b / \log a \quad \text{Equation 2.5}$$

Ds : Dimension of a shape
 a : Ratio between an original length and a changed one
 b : The number of segments

In the case of the Koch Curve, the similarity dimension (or what is called a Fractal dimension) is

$$Ds = \log 4 / \log 3 = 1.2618\ldots$$

Equation 2.6

This number seems very reasonable because the Koch Curve is more complicated than a simple line but it can not cover a plane like the Peano curve. The figure is not an integer but represents a reasonable result and can be regarded as a natural extension of conventional dimensions. It follows that the dimension of the Peano Curve is the same as a conventional one if this definition is applied to it. Thus the dimension of the Peano Curve in **Figure 2.5** is two. In the case of the Peano Curve in a space, its dimension becomes three.

2.1.4 Fractals

In the examples mentioned above, non-integer dimensions are encountered. The precise definition of a fractal by Mandelbrot is

“ A fractal will be defined as a set for which the Hausdroff-Besicovitch dimension strictly exceeds the topological dimension.” ¹⁾

It is not necessary to understand this mathematical expression perfectly. Based on this definition, two types of fractal sets have been identified. (**Figure 2.7**)

One is a self-affinity fractal and the other is a self-similarity fractal. They are defined as an invariant shape under isotropic or anisotropic magnifications respectively. These fractals are further divided into deterministic and random fractals. Deterministic or random fractals are defined by a repetition of a component shape. Furthermore, they consist of finitely ramified and infinitely ramified sets. A fractal is called “finitely ramified” if any bounded subset of the fractal can be isolated by cutting a finite number of bonds or sites. In the case

of the above example, the Koch and Peano Curves fall into the category of a self-similarity deterministic and finite-ramified group.

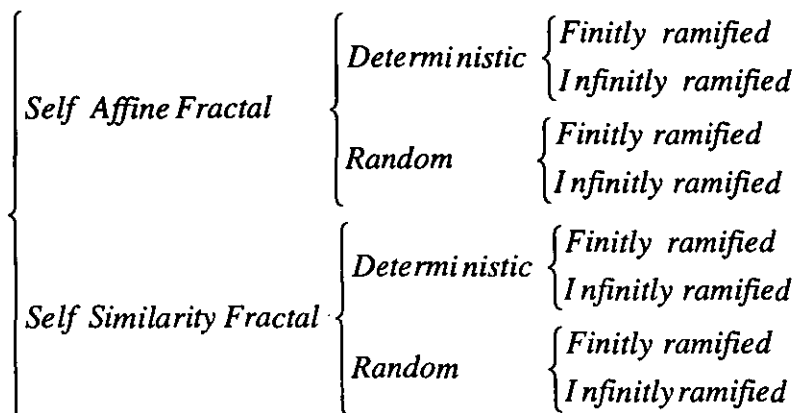


Figure 2.7 Classification of fractal shape.

The following are some examples of these categories which are relevant to this thesis.

The Sierpinski Sponge ¹⁹⁾

This example, the Sierpinski Sponge (**Figure 2.8**), belongs to the self-similarity and deterministic group.

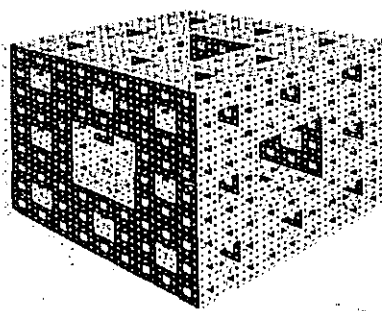


Figure 2.8 The Sierpinski sponge. Its dimension is 2.7268. ¹⁾

The Sierpinski Sponge is constructed by subdividing a cube into $3 \times 3 \times 3 = 27$ smaller cubes, and taking out the central small cube and its six nearest neighbour cubes. Each of the remaining 20 small cubes is processed in the same way and the whole procedure is iterated ad infinitum. After each iteration, the volume of the sponge is reduced by a factor of $20/27$, while the total surface area increases. At the limit of infinite iterations, the surface area is infinite, while the volume vanishes. Since $M((1/3)L) = (1/20)M(L)$, the fractal dimension is $d_f = \log 20 / \log 3 \approx 2.727$.

Random Sierpinski Sponge ²⁰⁾

For the contrast between a deterministic and a random fractal, another process based on the Sierpinski Sponge is given here. (Figure 2.9)

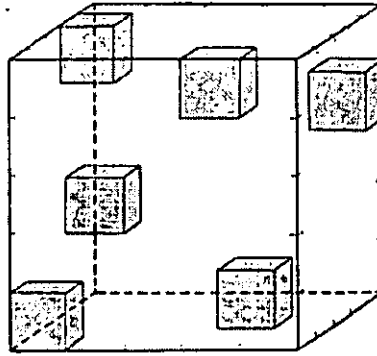


Figure 2.9 An example of random fractal. Its dimension is 1.11 . ^{1.8)}

In this example, the original cube is initially divided into $5 \times 5 \times 5 = 125$ segments. In this process, the mass of each segment is as follows :

$$M((1/5)L) = (1/5)^3 M(L)$$

Equation 2.7

thus, the cube's dimension will be three.

Next, six pieces are randomly selected and the others are removed. The fractal dimension of this set is then,

$$d_f = \log N / \log b = \log 6 / \log 5 = 1.11 \quad \text{Equation 2.8}$$

The important point in this example is its fractal dimension. In the case of deterministic fractals (deterministic Sierpinski Sponge), the dimension falls between two and three. This is a natural extension of our intuition because the Sierpinski Cube is neither a plane object nor a perfectly three dimensional one. In the case of a random Sierpinski Cube, the fractal dimension falls between one and two which appears to be counterintuitive. The ability of the fractal concept to provide insights into such counterintuitive results encourages the belief that the random Sierpinski Sponge may provide an effective model of carbon incorporation into a rubber matrix.

Self - affinity fractals

Self-affinity fractal systems are invariant only under anisotropic magnification. These shapes can be classified into two categories, regular and random fractals.

A simple model for a self - affinity, regular fractal is shown in **Figure 2.10**.

The structure is invariant under anisotropic magnification

$$\begin{aligned} x &\rightarrow 4x \\ y &\rightarrow 2y \end{aligned} \quad \text{Equation 2.9}$$

If a small piece is cut out of the original picture and the x axis is rescaled by a factor of 4 and the y axis by a factor of 2, exactly the original structure (anisotropy) can be obtained.

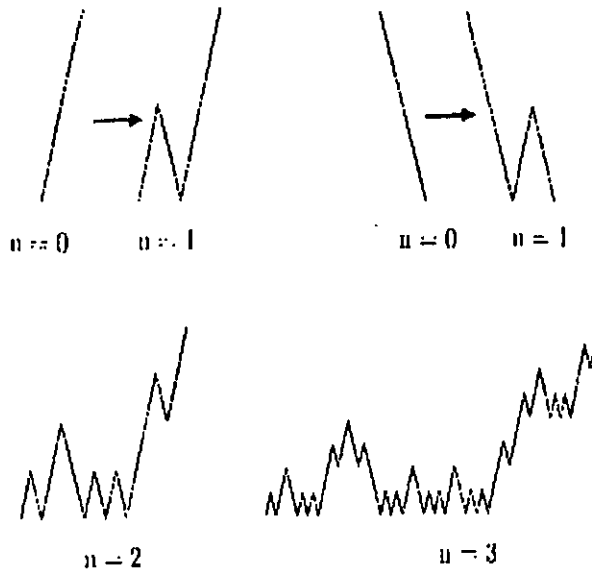


Figure 2.10 A simple deterministic model of self-affine fractal. ¹⁵⁾

In other words, if the form of the curve is described by the function $F(x)$, this function satisfies the equation

$$F(x) = 2F(x/2) = 4^{1/2} F(x/4) \quad \text{Equation 2.10}$$

In general, if a self-affine curve is scale invariant under the transformation,

$$\begin{aligned} x &\rightarrow ax \\ y &\rightarrow by \end{aligned} \quad \text{Equation 2.11}$$

the following relation is obtained.

$$F(bx) = aF(x) = b^H F(x) \quad \text{Equation 2.12}$$

Where the exponent

$$H = \log a / \log b$$

Equation 2.13

is called the Hurst Exponent. The solution of the functional equation is simply

$$F(x) = A x^H.$$

Equation 2.14

In the example in **Figure 2.10**, $H = 1/2$.

The next example, **Figure 2.11**, belongs to the random self-affine fractal type.

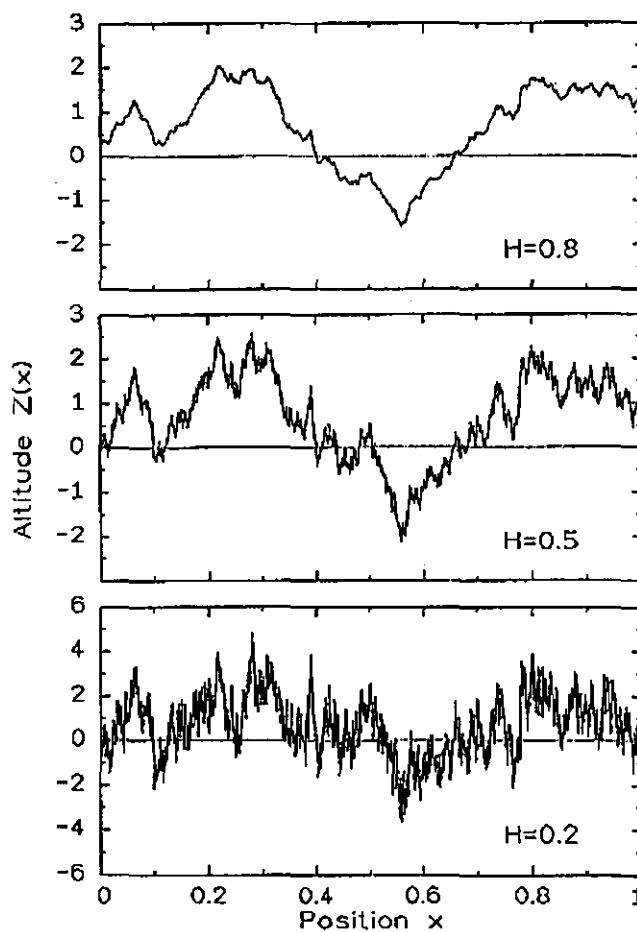


Figure 2.11 An example of a random affine fractal. ¹⁵⁾

This category is very important in the analysis of random walk (**Appendix 5**) and power-spectrum (**Appendix 4**).

Let us imagine a trace of random walk here (**Figure 2.11**). The abscissa is the time axis (t) and the ordinate is the displacement (Z).

$$Z(t) = \sum_{i=1}^t e_i$$

$$e_i = \pm 1$$

e : unit vector

Equation 2.15

Z(t) represents the distance of a random walk from a starting point. **Figure 2.11** presents some simulation results having a different Hurst Exponent. It is possible to consider these graphs of **Figure 2.11** as an example of time responses from some experimental instruments.

2.1.5 How to measure a fractal dimension

There are five ways to measure a fractal dimension. These are ;

- (1) Changing coarse graining level
- (2) Using the fractal measure relation
- (3) Using a correlation function
- (4) Using a distribution function
- (5) Using a power spectrum

Generally speaking, it has not yet been established that these five methods give the same dimension for the same shape. It is necessary to check each case independently. However many reported researches have given the same results and a conflict has not yet been found.

Changing coarse graining level

This method is carried out on approximate shapes which have a characteristic length (section 2.2.6). The most commonly used characteristic shapes are a circle or a box. **Figure 2.12** and **Figure 2.13** show the procedure to determine the fractal dimension by using these methods.

The first example starts from one end of the curve (**Figure 2.12**). Around this point, a circle with a certain radius is drawn. At the junction of the circle and the original line, another circle with the same radius is drawn. This procedure continues until the other end of the original line is reached. The relationship between the number and the radii of the circles is determined.

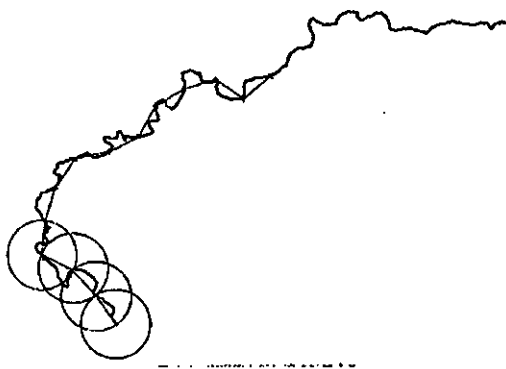


Figure 2.12 The method to determine the fractal dimension of a coast line by using circles. ⁸⁾

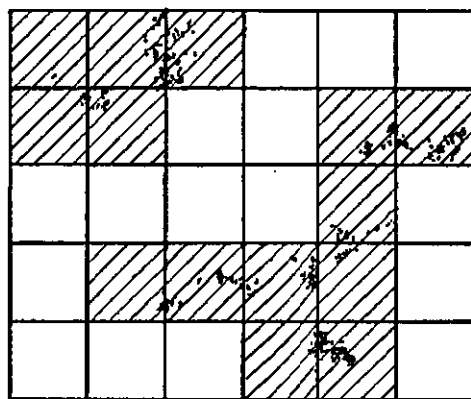


Figure 2.13 The method to determine the fractal dimension, the so called box counting method. ⁸⁾

Usually, the relationship between the number of segments and the dimension satisfies

$$N(r) \propto r^{-D}$$

Equation 2.16

Here, D stands for the dimension of the set (**Figure 2.15**).

As can be easily seen, in the case of a line, this relation should be

$$N(r) \propto 1/r = r^{-1} \quad \text{Equation 2.17}$$

It is possible to apply this procedure to the Koch Curve too. In this case, the relation follows

$$N(r) \propto r^{-\log_3 4} \quad \text{Equation 2.18}$$

(\log_3 is logarithm to base 3)

The second method divides the surface into small boxes which have a side length $1/r$ compared to the original one (**Figure 2.13**). It is necessary to count the number of boxes which contain the shape. The relationship between the number of boxes and the ratio r is given by

$$D_c = \lim_{\epsilon \rightarrow 0} \log N(\epsilon) / \log(1/\epsilon) \quad \text{Equation 2.19}$$

D_c : Fractal dimension based on self - similarity
 $N(\epsilon)$: A number of boxes which include the shape
 ϵ : Side length of the box

Using the fractal measure relation

Generally speaking, the quantities of length, area, volume and any unknown property have to satisfy the following relationship.

$$L \propto S^{1/2} \propto V^{1/3} \propto X^{1/D} \quad \text{Equation 2.20}$$

L, S, V, X : length, surface area, volume and unknown measure respectively.

Another example is given here to demonstrate how to measure the fractal dimension based on this method. (**Figure 2.14**)

Imagine a sphere around the weight centre of the field. The number of points $M(r)$ in the sphere is determined. If the weight points are uniformly distributed around the weight centre point, the amount of $M(r)$ will satisfy the following relation.

$$M(r) \propto r^3$$

Equation 2.21

As a natural extension of this process, if the unknown measure follows the relation of

$$M(r) \propto r^D$$

Equation 2.22

the dimension (D) can be regarded as a fractal dimension.

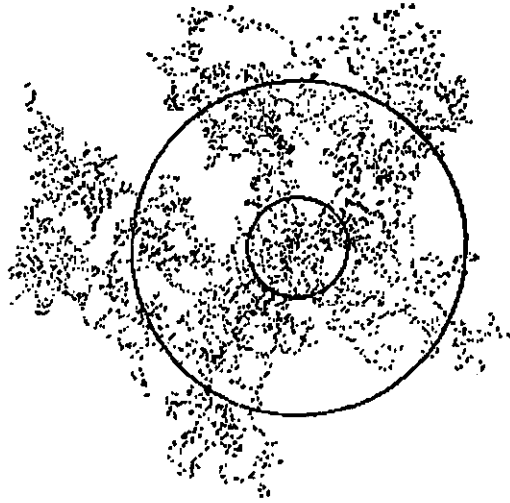


Figure 2.14 A fractal model for the distribution of stars. ⁸⁾

Using a correlation function

This method is closely related to the method mentioned above (**Appendix 4**). Because of the Wiener-Hinchin Relation (**Equation 2.31**), a correlation function or a power-spectrum can be discussed in the same way. There are some occasions in which it is easier to analyse the correlation function directly.

A distribution function $p(x)$ will be considered. The correlation function is defined as

$$C(r) = \langle p(x)p(x+r) \rangle$$

Equation 2.23

here the bracket stands for the mean value of a system.

If the distribution has fractal characteristics, the correlation function becomes

$$C(r) = r^{-\alpha} \quad \text{Equation 2.24}$$

and this power is related to the fractal dimension by the following relationship.

$$\alpha = d - D \quad \text{Equation 2.25}$$

where d : The dimension of space
 D : Fractal dimension

By plotting the independent variable against a measured correlation function a fractal dimension can be determined from experimental data.

Using a distribution function

The distribution of carbon agglomerates in a rubber compound is a typical example of the application of this method. It will be assumed that the representative size and its probability of number are r and $P(r)$ respectively (**Appendix 4**). If $F(r)$ stands for a probability density, the following relation is obtained between the probability and the probability density functions.

$$P(r) = \int_r^\infty F(x) dx \quad \text{Equation 2.26}$$

The fractal requires one condition for the function $P(r)$. In mathematics this condition is known as the “homogeneity relationship”. When the function $P(r)$ is homogeneous, it has to satisfy the following relationship.

$$P(r) \propto P(\lambda r) \quad \text{Equation 2.27}$$

λ : Scaling factor

The function does not change its formula under the variance change except for the inclusion of constants. It is known that only the power formula satisfies the requirement.

$$P(r) \propto r^{-D}$$

Equation 2.28

Many fractal examples are measured by using this method. The following is an example for the radii distribution of craters on the moon. (**Figure 2.15**)

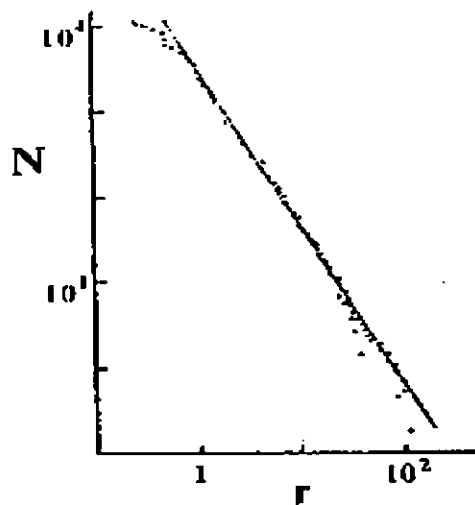


Figure 2.15 The radii distribution of craters on the moon.²²⁾

Using a power spectrum

Power-spectra are commonly used to characterise phenomena which change their results depending on time (**Appendix 2, 3, 4**). This method is very convenient because there are a variety of experimental evaluation methods. In the case of power-spectra, to change the coarse graining level means to change a cut-off frequency. It means that

$$S(f) \propto f^{-\beta}$$

Equation 2.29

and the relationship between a power β and a fractal dimension is given by

$$\beta = 5 - 2D$$

Equation 2.30

D : dimension of measured space

This fractal dimension does not conflict with the dimension from a correlation function in the above sub-section, because there is a relationship between a correlation function and a distribution power spectrum. It is called the Wiener-Hinchin Relationship.

$$G(\omega) = \int_{-\infty}^{\infty} R(\tau) \exp(-j\omega\tau) d\tau$$

Equation 2.31

$$R(\tau) = 1/2\pi \times \int_{-\infty}^{\infty} G(\omega) \exp(j\omega\tau) d\omega$$

G(ω)	: Power spectrum
R(τ)	: Auto-correlation function
j	: Imaginary symbol
ω	: Frequency
t	: Time

In this thesis, two types of method are employed. The first one is the coarse graining method mentioned in the earlier sub-section, and the other is a power-spectrum analysis introduced in this sub-section. The former is used for image analysis of the state of mix of carbon black and the latter is used for random data analysis. The choice of these methods depends on the characteristics of the experimental data and available instruments.

2.2 Rubber technology

2.2.1 Preamble

An effective explanation of rubber technology may be made by classifying it into three categories. The first category ^{25,29)} is the chemistry of the raw materials of the rubber compound, the second ³⁰⁻³²⁾ is polymer processing technology and the third ^{27-29,33-37)} is the material science of the vulcanized rubber properties. These interconnected fields each make a significant contribution to the understanding of every property of rubber. The aim of this thesis is to explore the possibility of applying the fractal concept as an integrated parameter between these fields for evaluating the total performance of a rubber compound.

The main aim of this chapter is to present a basic concept of rubber technology determined by these three fields. Some detailed theory is explained to propose a possible mechanism to correlate rubber properties with the fractal mechanism.

2.2.2 Raw materials

2.2.2.1 Scaling aspects of a Polymer

A polymer, especially an elastomer, is the matrix of rubber compounds. Polymers and related materials, such as plastics and thermosets are currently attracting very intensive research because of their widespread industrial use. Many new concepts, which have revealed the properties of such materials, have been applied to elastomers. The following example, the “scaling concept” ³⁶⁾, is a basic application of the fractal aspect of polymer properties.

The size of one polymer is discussed here. The “mean square length” is controlled mainly by two mechanisms. The first mechanism is the entropy effect which tends to contract the polymer chain to a small size. The polymer is best regarded as a chain of many small parts

called segments. These segments move very rapidly due to Brownian Motion. The total entropy of the system tends to be minimised because these segments are connected to each other through chemical bonds. The second mechanism is based on an exclusion effect. Because these segments have a finite size, they cannot occupy a certain point at the same time. These two mechanisms have a counter balancing effect and decide the size of the polymer in a certain condition.

The size of the polymer (R_p) naturally depends on its length which, in turn, is determined by the number of segments (N_p).

$$R_p \approx N_p^{\nu}$$

Equation 2.32

It is necessary to decide the power “ ν ” based on the mechanism mentioned above. This power “ ν ” is called the Flory Index.

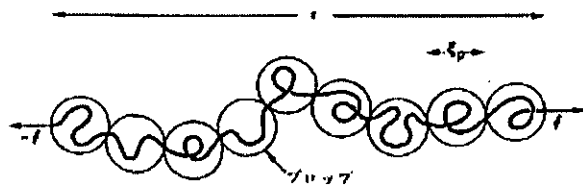


Figure 2.16 Scaling concept of polymer chain. The chain consists of an imaginary sphere called a blob. ³⁶⁾

Imagine that the N_p segments are restricted in an imaginary sphere (Figure 2.16) with a radius R_p . The concentration of segments in one blob (C_p) is given by

$$C_p \approx N_p / R_p^d$$

Equation 2.33

d: dimension of a space

Because of the exclusion effect, segments can't overlap each other. Such characteristics are measured by a repulsive force which is proportional to the concentration of the segments, per unit volume. This will be given by C_p^2 . Thus the total repulsive energy in the volume is given by

$$F_{rep} \approx R_p^d \times C_p^2 \approx N_p^2 / R_p^d \quad \text{Equation 2.34}$$

This is the total force which tends to expand the polymer chain. However an elongated long polymer chain has a big energy loss because of the entropy effect. Treating this effect using the random walk model (**Appendix 5**), the entropy effect is given by the term

$$F_{ent} \approx R_p^2 / N_p \quad \text{Equation 2.35}$$

Thus the total energy is the sum of both the entropic and exclusion effect.

$$F = F_{rep} + F_{ent} \quad \text{Equation 2.36}$$

If the segment number is fixed as N_p , the mean end-distance is the point where the free energy is minimum. By differentiating **equation 2.36**,

$$F \approx N_p^2 / R_p^d + R_p^2 / N_p \quad \text{Equation 2.37}$$

and after some calculation, the Flory Index is obtained.

$$v_F = 3 / (d + 2) \quad \text{Equation 2.38}$$

Equation 2.32 and **equation 2.38** tell us that the size of a polymer chain follows a power rule. Both the power rule and fractals are related concepts ³⁷⁾. Thus, it is possible to consider that the mechanism which decides the polymer size is a fractal phenomenon.

2.2.2.2 Carbon black from the fractal point of view

Morphological ³⁸⁻⁴¹⁾ characterisation of carbon black is an important aspect of the understanding of rubber reinforcement. In response to this considerable research to understand the essential parameters which control the properties of final products has been undertaken. However, satisfactory parameters have not yet been established because of the complexity of the problem.

The first attempt to quantify the character of carbon black was reported by Medalia and Heckman ⁴⁰⁾. In their research, they carried out image analysis of electron microscope photographs based on Euclidean Geometry. They were not able to correlate the colloidal characteristics of carbon with the physical properties of the rubber compound. To overcome this problem, Kayne ⁴²⁾ and Flock ⁴³⁾ applied Fractal Geometry to carbon black aggregate morphological characterisation, utilising the method of Richardson and Mandelbrot. Following on from their success and the development of the fractal concept, other fractal studies were carried out to obtain more precise parameters for carbon black. Gerspacher and O'Farrell ⁴⁴⁾ applied a new measuring method known as the perimeter-area relation (**section 2.1.5**) to evaluate the fractal dimension. Bournat, Oberlin ⁴⁵⁾, Ehrburgh, Dolle and Tence ⁴⁶⁾ used a mass-size method.

Another fractal approach has been carried out based on the importance of the carbon surface. Avnir and Farin ⁴⁷⁾ characterised the features of the carbon surface.

One example from such researches is shown here ⁴⁴⁾ (**Figure 2.17**).

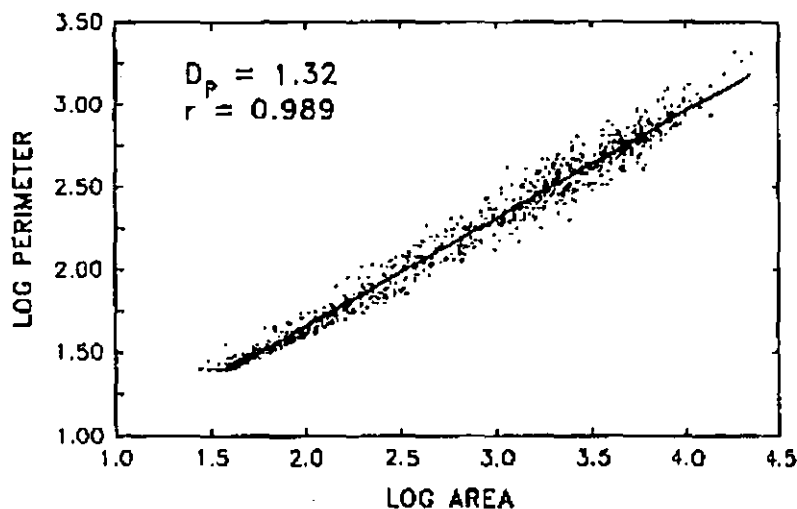


Figure 2.17 Fractal dimension based on perimeter - area plot for 1000 N121 aggregates in the dry state.⁴⁴⁾

This figure explains the relationship between surface area and perimeter. Based on this graph, the perimeter fractal dimension is decided from the slope of the regression line. The perimeter fractal is

$$D_p = 1.32$$

Equation 2.39

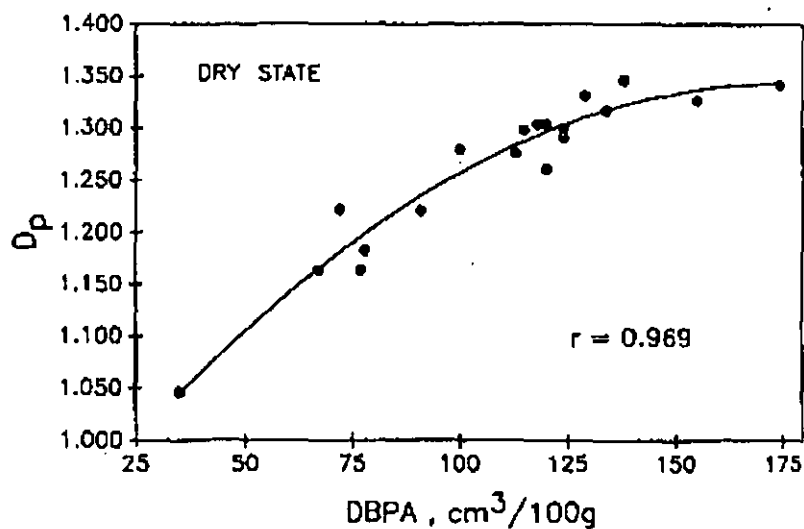


Figure 2.18 Correlation of the perimeter fractal with DBP absorption⁴⁴⁾

Figure 2.18 demonstrates the close relationship between the perimeter fractal dimension and the DBP (dibutyl phthalate) absorption value. The DBP value is defined as the amount absorbed per 100g carbon black. It is a measure of the complexity of the carbon black agglomerate. The important conclusion from this graph is that the fractal dimension does not conflict with existing data and that it is possible to correlate the fractal dimension to an existing parameter such as the DBP value.

It should be mentioned here that since the behaviour of the materials which make up the rubber compound is characterised by fractals, it is reasonable to suppose that the behaviour of the resulting compound itself will be similarly characterised.

2.2.3 Rubber processing

2.2.3.1 Mixing

The purpose of this chapter is to discuss the meaning of Fourier or fractal analysis, to relate existing research to this thesis. The rubber mixing process will be discussed from a mechanical point of view. For some mechanisms, there are models available to explain some aspects of the mixing process, so a mathematical model is described in a later section to clarify the mechanism of mixing. Following this, the state of mix of carbon black and its dispersive mechanism will be discussed. It is also important to know the mechanism of carbon black incorporation into a rubber matrix polymer because the evaluation of the state of mix of carbon black is directly connected to the mechanism of mixing. Finally, two aspects of the effect of the state of mix will be discussed. The first is the effect of the state of mix on heat transfer and the second is the relationship between bound rubber and the state of mix. In the case of heat transfer, it affects not only the physical properties of rubber but also the chemical properties through vulcanisation. A discussion of heat transfer and mechanism of bound rubber is thus required.

The mechanism of rubber mixing

Figure 2.19 shows the rotors and a chamber in an internal mixer. Rubber components are mixed in this region by the flow around the rotors. Five types of rubber flow are known⁴⁹⁻⁶⁷⁾. The first one is between a rotor tip and the chamber wall^{68,69)}; the second is a circulation in front of the rotor tip⁷⁰⁾ (Appendix 7); the third is a flow under a ram⁷¹⁾; the fourth one is a rubber exchange between the rotors⁶⁹⁾ and the fifth is a flow tangential to the rotors^{57,58)}.

Considering the flow pattern, there are two modes of flow which contribute to dispersive mixing. The first one is an elongational flow and the other is a shearing flow. The five types of flow in an internal mixer have various ratios of elongational to shear flow. For example, the flow just in front of the rotor tip is mainly dominated by elongational flows whilst the flow between rotor tip and chamber wall is mainly dominated by a shear flow. The details are dependent on machine design.

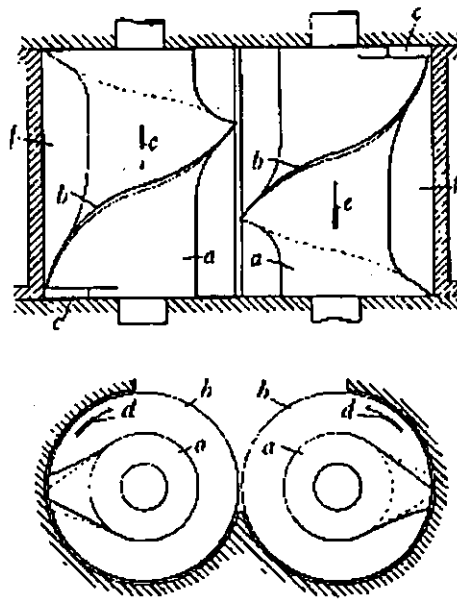


Figure 2.19 A schematic drawing of rotors and mixing chamber.⁴⁹⁾

Interpretation of the mixer power trace

Some information obtained from the study of an internal mixer may contribute to the understanding of the mechanism of rubber mixing. Typical information includes power traces, batch temperature, ram position and cooling water temperature. Among them, power traces are the most commonly used as a measure for quality control in industry. Here a basic interpretation of a power trace will be presented, (Figure 2.20), along with its mathematical treatment. Funt⁶⁹⁾ summarized existing research as follows ;

“The mechanism of rubber mixing in an internal mixer will be considered in a time sequence. Initially a mixture in the chamber consists of a rubber phase and a completely separate additive phase. As mixing proceeds, the additives are incorporated into the continuous rubber matrix as a dispersed phase. Solid particulate additives such as carbon black usually reinforce the rubber and raise the viscosity.

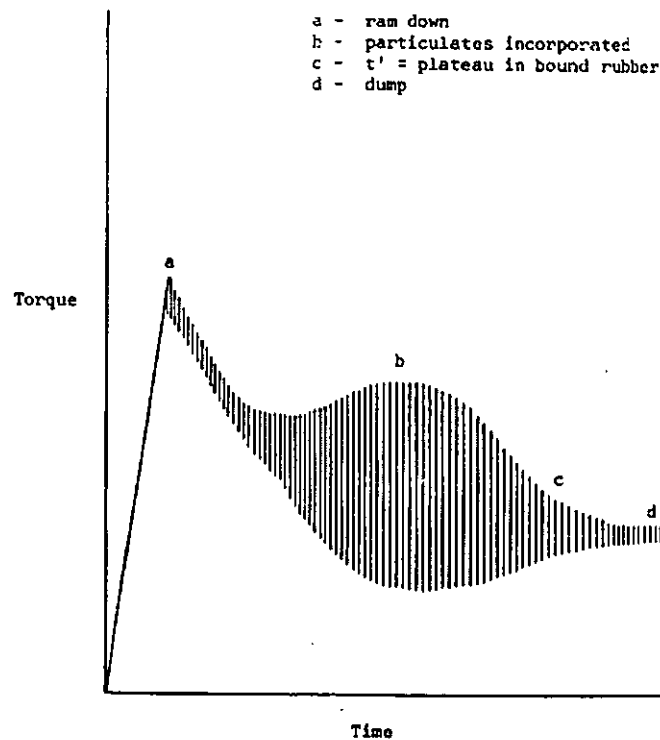


Figure 2.20 A typical mixer power trace of an internal mixer.⁶⁹⁾

This causes the torque to increase rapidly to a peak at time t_a as the particles form the dispersed phase. The continuing increase in temperature counteracts this effect and the torque decreases again until it reaches a steady state value which holds until the end of the mixing cycle at time t_d . The time t_b corresponds to the end stage of macroscopic carbon incorporation which is known as the “black incorporation time” (BIT). The mixing time t_c corresponds to the experimentally observed maximum in the die swell of extruded products which occurs when the bound rubber level reaches a plateau value and carbon dispersion has reached a steady state.”

The above explanation is a typical interpretation of a mixer power trace. There are, however, some problems with this interpretation. The first example is the dependence of a power trace on the composition of a rubber compound. Some NR rubber samples do not show black incorporation time (BIT) in the power trace. This means that the BIT and reinforcement do not correspond directly as Funt proposed. The next problem is the minimum line of the power trace. If only the viscosity change causes power to drop, the minimum line of the power trace should not increase after the BIT, so the power trace cannot be regarded as a function depending only on polymer viscosity. The fractal concept and the Fourier Transform can be used to explain such effects or extract more information from the power trace.

A mathematical treatment of a mixer power trace

In this thesis, the power trace is described by a fractal concept. It is therefore necessary to consider the relationship between the flow in an internal mixer and the power trace. The first analysis of an internal mixer was reported by Bolen and Colwell ⁷¹⁾ who used the simplified geometry shown in **Figure 2.21**.

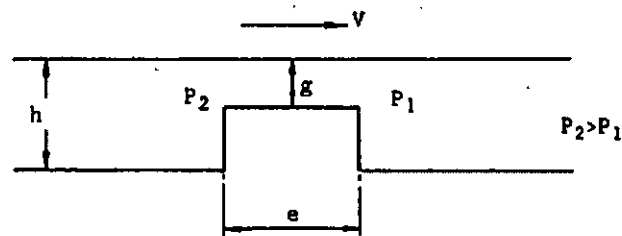
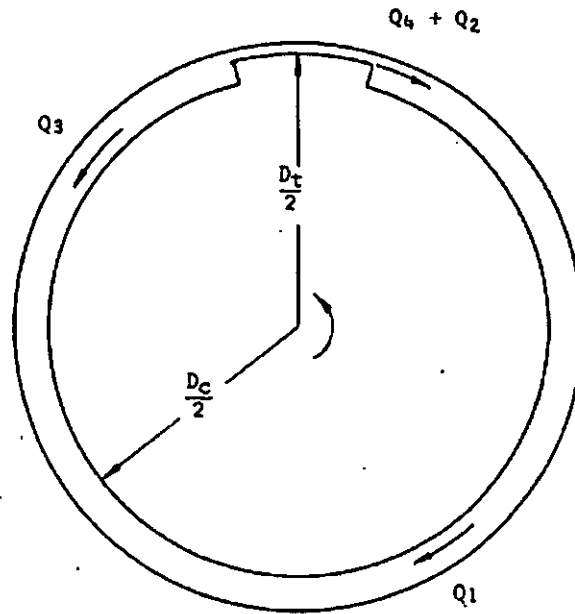


Figure 2.21 A schematic model of an internal mixer ⁷¹⁾

The following symbols are used ;

- Q_1 : drag flow in channel
- Q_2 : drag flow at flight tip
- Q_3 : pressure flow in channel
- Q_4 : pressure flow at tip
- g : tip clearance (constant)

h	: channel clearance
e	: tip width
s	: length of rotor
N	: rotor speed
D_c	: diameter at shaft
D_t	: diameter at tip
μ_c	: viscosity of fluid in channel
μ_t	: viscosity of fluid at tip
ΔP	: pressure drop across flight

The viscosity at the tip need not equal the viscosity in the channel if the viscosity is shear dependent, even for isothermal flow. The directions of the four flow components are shown in **Figure 2.21**. If it is assumed that the radius of the rotor is large compared to the parallel plates in a Cartesian n coordinate system, a constant viscosity solution for the drag flow components becomes :

$$\begin{aligned} Q_1 &= \pi D_c s h N / 2 \\ Q_2 &= \pi D_t s h N / 2 \end{aligned} \quad \text{Equation 2.40}$$

which is the total drag flow between parallel plates having a separation h (or g), and a relative velocity of

$$V = \pi n D \quad \text{Equation 2.41}$$

The pressure difference between the front and rear of the flight (ΔP) arises because of the difference in channel depth between the tip and the wall. The pressure flows for parallel plate geometry become

$$Q_3 = -\frac{sh^3\Delta P}{12\pi D_c\mu_c}$$

Equation 2.42

$$Q_4 = \frac{sg^3\Delta P}{12e\mu_t}$$

Since the mixer is a closed system, the flow past the tip must equal flow in the channel

$$Q_1 + Q_2 = Q_3 + Q_4$$

Equation 2.43

Substituting equation **Equation 2.40** into **Equation 2.43** and solving for the pressure drop yields

$$\Delta P = \frac{6\pi N(D_ch - D_tg)}{\left(\frac{h^3}{\pi D_c\mu_c} + \frac{g^3}{e\mu_t}\right)}$$

Equation 2.44

A velocity average shear rate ($\dot{\gamma}$) can be defined for both the tip and the channel

$$\dot{\gamma} = \frac{\int_0^h |u\gamma| dy}{\int_0^h |u| dy}$$

Equation 2.45

This is the same as a mass average shear rate. Let the ratio of pressure to drag flow be

$$f = Q_p/Q_d$$

$$f = Q_3/Q_1 \quad \text{for channel}$$

$$f = Q_4/Q_2 \quad \text{for tip}$$

Equation 2.46

Then the average shear rate, a function of f , is given by

$$\begin{aligned}\dot{\gamma} &= \frac{Q}{sx^2} \left[\frac{0.75\{(1+3f)^4 + 72f^2\}}{|1+3f|^3 + |1+9f|} \right] \quad \text{if } f < -1/3 \\ \dot{\gamma} &= \frac{Q}{sx^2} \left(\frac{2}{1+f} \right) \quad \text{if } -1/3 < f < 1/3 \\ \dot{\gamma} &= \frac{Q}{sx^2} \left[\frac{(1+3f)^4 + 144f^2 - (1+3f)^4}{72f^2(1+f)} \right] \quad \text{if } f > 1/3\end{aligned} \quad \text{Equation 2.47}$$

where $Q=Q_1$ and $x_2=h_2$ in the channel, $Q=Q_2$ and $x_2=g_2$ in the tip.

The velocity profile (V_z) for combined flow between parallel plates is given by

$$V_z = \frac{V}{H} y - \frac{y(H-y)}{2\mu} \frac{dp}{dz} \quad \text{Equation 2.48}$$

For plate separation H and relative velocity V , the shear rate may be calculated from

$$\dot{\gamma} = \frac{dv_z}{dy} = \frac{V}{H} - \frac{1}{2\mu} \frac{dP}{dz} (H - 2y) \quad \text{Equation 2.49}$$

The maximum shear stress will occur in the tip region where

$$\begin{aligned}H &= g \\ V &= \pi D_t N \\ \frac{dp}{dz} &= \frac{\Delta P}{e}\end{aligned} \quad \text{Equation 2.50}$$

The maximum shear rate and the maximum shear stress for a Newtonian fluid occur at $y=g$

$$\begin{aligned}
 \tau_{\max} &= \mu \gamma_{\max} \\
 &= \mu_t \left(\frac{V}{H} + \frac{H}{2\mu} \frac{dP}{dz} \right) \\
 &= \frac{\mu_t \pi D_t N}{g} \left\{ 1 + \frac{3 \left(\frac{D_c h}{D_t} - g \right)}{\frac{e h^3}{\pi g^2 D_c} + g} \right\}
 \end{aligned}
 \tag{Equation 2.51}$$

The torque on the rotor is given by

$$\begin{aligned}
 T &= \oint_{s_R} F dl \\
 &= \oint \tau A dl \\
 &= s \left[\tau_{t,y=0} \frac{e D_t}{z} + \tau_{y=0} (D_c - e) \frac{D_c}{z} \right]
 \end{aligned}
 \tag{Equation 2.52}$$

Substituting into **Equation 2.51** the appropriate values of V and H for the tip and for the channel and using a Newtonian fluid yields an expression for the torque T

$$T = \frac{\pi N \mu}{2} \left[1 + \frac{x}{a} \left(\frac{\pi x}{e} - \frac{1}{D_t} \right) - \frac{3\pi(x^2 a^2 - 1)}{1 + \frac{a^3 e}{x D_t}} \right]
 \tag{Equation 2.53}$$

$$\begin{aligned}
 \text{where} \quad a &= h/g \\
 x &= D_c/D_t
 \end{aligned}$$

and the shaft power required becomes

$$P = T N$$

Equation 2.54

Bolen-Colwell's Model tells us that power is a function of material property (μ), and other instrumental parameters (a , e , D_c , D_t , etc. in **Equation 2.53**). The model does not include real operating conditions. For example, the model does not include a starving or under-filled condition, the channels are considered to be fully filled with compound, it is a two dimensional model, so it does not include a flow tangential to the rotor and the viscosity is considered to be constant during operation. It is therefore necessary to include more factors in this model, as already indicated by the research into flow visualisation. Fractals and Fourier Transforms could be expected to combine such effects with this model.

2.2.3.2 The state of mix of carbon black

The following summarises and discusses the existing research which seeks to evaluate the state of mix of carbon black. It is obvious that the first step in the analysis of a mixing operation is to determine how good the mix actually is. It is therefore important to understand the existing procedures to detect the state of mix. Furthermore, the knowledge of the dispersion mechanism gives good information to improve the final product properties by achieving optimum conditions and also provides the ability to evaluate mixing data validity and its limitations.

Mechanism of carbon black dispersion in polymer matrix

Two mechanisms^{72, 73)} have been proposed for describing the dispersion of carbon black agglomerates. In the cleavage model, the traction forces on the surface of the agglomerate are below the critical value for fracture except near the particle equator where stresses are at a maximum. The agglomerate cleaves at this point into two almost equal parts. This

process is repeated on the subsequent fragments until the surface traction, which decreases as agglomerate size decreases, is no longer large enough to break agglomerates.

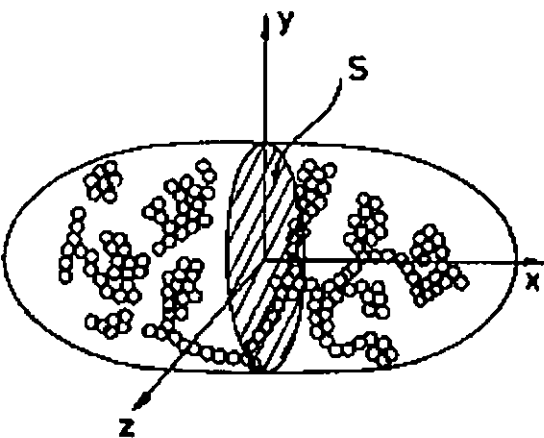


Figure 2.22 Schematic representation of an agglomerate. The cleavage occurs at the shaded plane.⁷²⁾

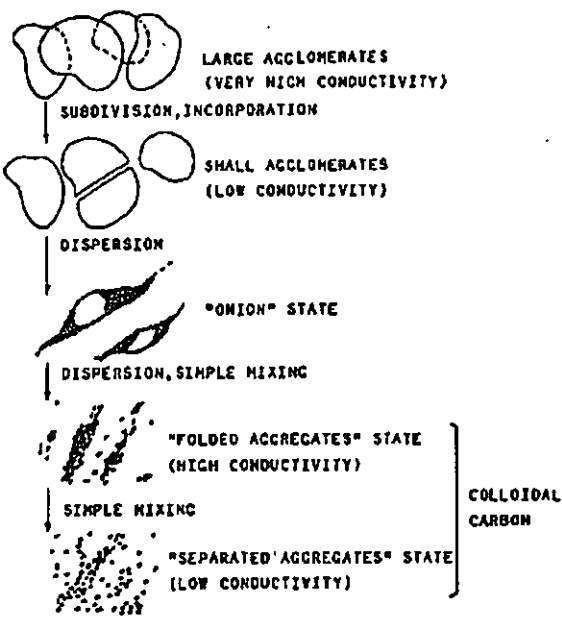


Figure 2.23 Onion model for carbon black incorporation into a polymer matrix.⁷³⁾

In the "onion peeling" model, the stresses generated at the agglomerate surface are large enough at any point on the surface to pull an aggregate or group of aggregates from the larger agglomerate. The aggregates which have been removed form a cloud around the initial agglomerate, partially shielding it from further size reduction. Agglomerate size reduction occurs as aggregates are swept from the cloud and fresh aggregates from the agglomerate replace them.

Both mechanisms are likely to occur in any mixing operation but the rate controlling mechanism will depend upon the carbon black type, pellet qualities, rubber properties and operating conditions such as temperature and rotor speed. In addition, a carbon black distribution is occurring at the same time by the flow in an internal mixer. Such flows are dependent on the mixing instrument.

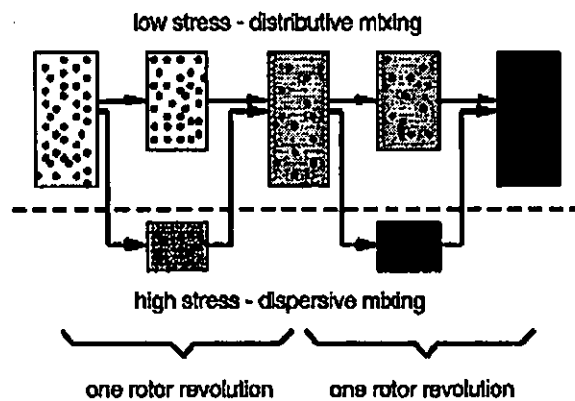


Figure 2.24 A model of dispersive mixing in an internal mixer. ⁷⁴⁾

Clarke and Freakley analysed dispersive mixing in an internal mixer ⁷⁴⁾. **Figure 2.24** shows their conclusions.

“In an internal mixer only a small part of the batch undergoes dispersive mixing at any one time and this portion is then distributively mixed into the bulk of the batch”

Existing methods for the evaluation of the state of mix

Many methods have been proposed for the evaluation of the state of mix. Eleven methods are mainly used for industrial and research purposes ⁷⁵⁾. These are

1. Optical microscopy ⁷⁶⁾
2. X-radiography ^{77, 78)}
3. Transmission electron microscopy ⁷⁹⁻⁸¹⁾
4. Scanning electron microscopy ⁸²⁾
5. Image analysis ⁸³⁾
6. Surface inspection ⁸⁴⁾
7. Stylus surface measurement ⁸⁵⁾
8. Optical scanning of surfaces ⁸⁶⁾
9. Optical extinction coefficient ⁸⁷⁾
10. Electrical conductivity ⁸⁸⁾
11. Pyrolysis gas chromatography ⁸⁹⁾

The details of these methods are provided by the references. Here, stylus surface measurements will be explained to show the kind of information such measurements can provide and because up-to-date stylus methods are used to characterise fracture surfaces in the experimental part of this thesis.

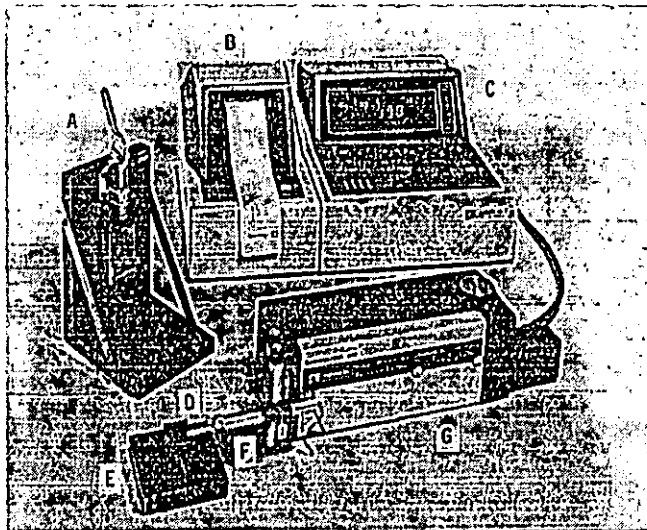


Figure 2.25 Dispersion analyser system for stylus roughness measurements ⁷⁵⁾

Stylus surface-roughness measurement is now a part of ASTM D2663 (Method C) for the analysis of dispersion of carbon black in rubber compounds. It is an indirect measure of dispersion because the stylus does not directly measure the pigment agglomerates. The apparatus is shown in Figure 2.25.

A test sample is prepared by a specimen cutter (A), and is put on the specimen holder (E, D). The Stylus probe (F) is operated by a drive unit (G) to traverse the sample surface at the speed of 0.25mm/s with 200 mg force. The results are recorded by a control unit (C) and are printed out (B). One example is shown in Figure 2.26.

The most pertinent measurements relative to dispersion are the total number of roughness [f] in peaks/cm, and the average peak height [h] measured in μm . The roughness factor is proportional to the total amount of filler agglomeration and is used to derive a dispersion index.

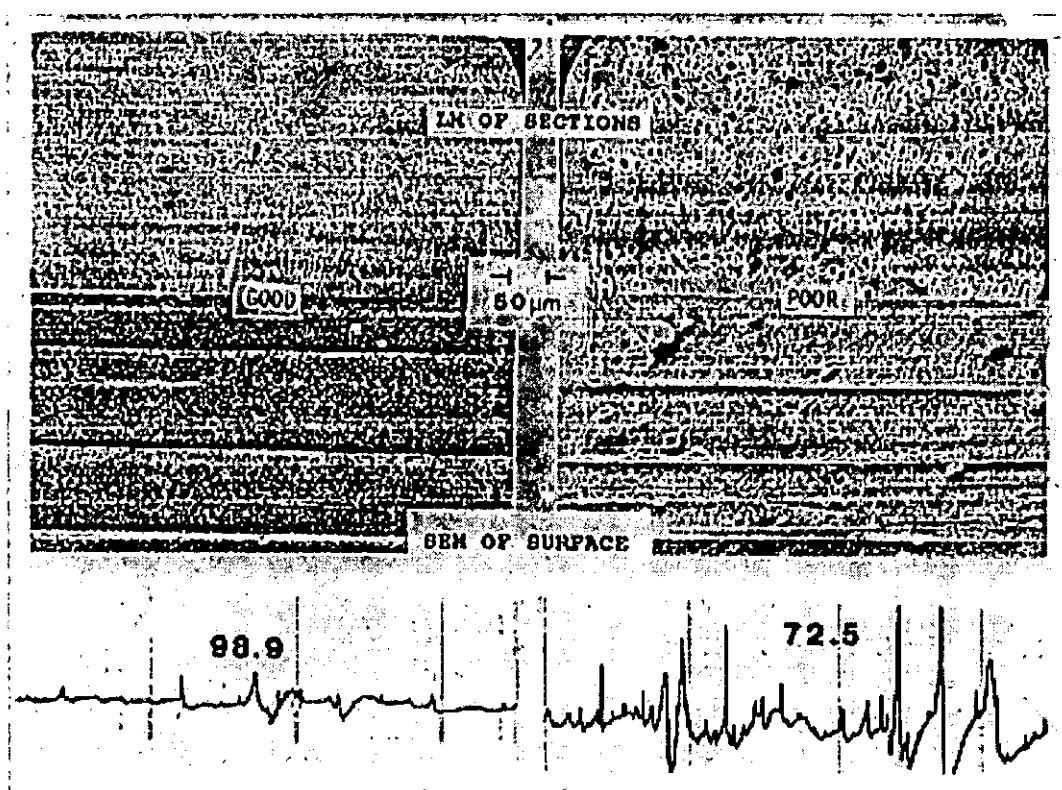


Figure 2.26 Stylus roughness traces and sample photographs.⁷⁵⁾

The results are usually calibrated against a more direct standard method such as ASTM D2663 method B. One example is shown in Figure 2.27.

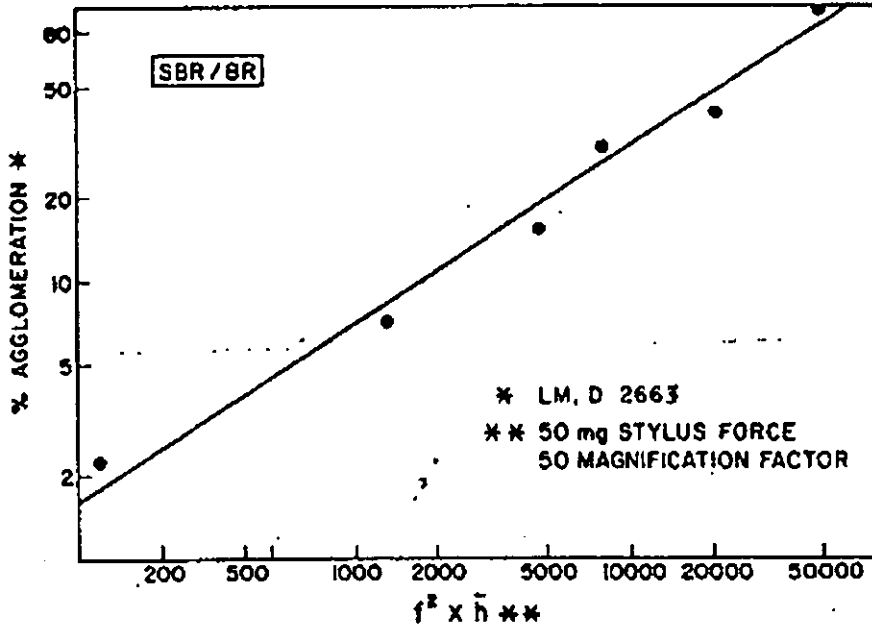


Figure 2.27 Carbon black agglomeration versus roughness factor from stylus measurement.⁷⁵⁾

Evaluation of the state of mix of carbon black

It is well known that the state of mix of rubber compound has a considerable influence on the properties of not only vulcanised rubber but also unvulcanised rubber. There are many reports which attempt to evaluate the state of mix. It is possible to classify this research into two categories depending on a scale of dispersion⁶⁹⁾. The first category examines macroscopic dispersion and the other examines microscopic dispersion. Corresponding to these categories, there are two types of method used to evaluate the state of mix. The first commonly used method is to count the visible carbon agglomerates per unit area using a microscope. The second commonly used method is to evaluate the electric resistance of the carbon black filled compound. These evaluations are related to some specific rubber

property and they are used to decide an effective time for the mixing of rubber compounds.

In the case of macroscopic dispersion, statistical methods have been used to evaluate the state of mix. Some of the earlier attempts to quantify the degree of mixing were made in the 1930's by Oyama ⁹⁰⁾. After attempts to rationalise empirical data on the kinetics of powder blending by qualitative statistical methods, the concept of the degree of mixing was put on a firm quantitative basis by Beaudry ⁹¹⁾.

Oyama measured the spatial variation of light absorption across the face of a cylinder containing clear and black particles. The maximum differences in absorption between any two locations at the beginning of the test and after various mixing times were measured. The degree of mixing (DM) was defined by

$$DM = 1 - \frac{\Delta i_{\max,t}}{\Delta i_{\max,0}}$$

Equation 2.55

Δi_{\max} : Maximum difference in light absorption

Beaudry was the first to use the quantitative results of the statistics of random sampling to describe blending. The variance among batches before (s_b^2) and after blending (s_x^2) were calculated.

$$s^2 = \frac{\sum C_i^2}{r} - \bar{C}^2$$

Equation 2.56

C_i : The value of measured property of "i" th batch

\bar{C} : Average value for all batches

the value of the variance for a theoretically perfectly random mixture (s_p^2) was calculated from the normal distribution having the same overall average composition. Then the limited blending ratio (γ) was calculated

$$\gamma = \frac{s_b^2}{s_p^2} \quad \text{Equation 2.57}$$

and the blending efficiency (BE) for any operation was also calculated

$$BE = \frac{\left(\frac{s_b^2}{s_x^2} \right)_{actual} - 1}{\gamma - 1} \times 100(\%) \quad \text{Equation 2.58}$$

This can be seen to be an extension of Oyama's Linear Function Principle where the statistical distribution of a measured property is used rather than the property itself. Many subsequent researches for the state of mix have been based on a combination of Oyama's and Beaudry's concepts. Lacy⁹²⁾ proposed a linear function of the variance

$$DM = \frac{s_0^2 - s^2}{s_0^2 - s_r^2}$$

$$s = [p(1-p)/n]^{1/2} \quad \text{Equation 2.59}$$

p : Average composition of n sample

$$s_0^2 = p(1-p)$$

$$s_r^2 = p(1-p)/n$$

Michael and Puzinowskas⁹³⁾ defined a uniformity index I_v

$$I_v = D_v / D_{v0}$$

$$D_v = \left[\sum_{i=1}^n (C_i - C_{av})^2 / n C_{av} \right]^{1/2} \quad \text{Equation 2.60}$$

$$D_{v0} = [(1 - C_{av}) / C_{av}]^{1/2}$$

The uniformity index varies from 1.0 for unmixed materials to 0 for a completely randomly mixed material.

Weidenbaum and Bonilla ⁹⁴⁾ used χ^2 as a measure of the state of mix. They suggested as the degree of mixing

$$DM = \sigma/s$$

Equation 2.61

where σ and s are the standard deviations of perfectly mixed material and the actual samples.

Smith ⁹⁵⁾ used a similar definition

$$DM = \sigma_0/s$$

Equation 2.62

$$\text{where } \sigma_0 = [p(1-p)]^{1/2}$$

Of the various definitions of the state of mix, either the variance of the measured property of the material or a linear function of the variance has proved to be the most useful in describing the efficiency of a mixing operation or the kinetics of mixing. Even though these proposals lead to some degree of success in the evaluation of the state of mix, they do not provide a clear relationship between the state of mix and rubber properties. Especially, these statistical approaches try to evaluate the state of mix by a mean value for the dispersion. The morphology of the state of mix is not explicitly incorporated in these researches. Fractal analysis of the state of mix is an attempt to include the effect of morphology.

Effect of the state of mix on rubber properties

In this section two aspects of the effect of the state of mix will be discussed. The first one deals with the rheological properties of unvulcanised rubber, the second with the tensile strength of single and blended polymer compounds.

The general effects of dispersion on rheological properties are illustrated by the work of Boonstra and Medalia⁹⁶⁾ (Figure 2.28).

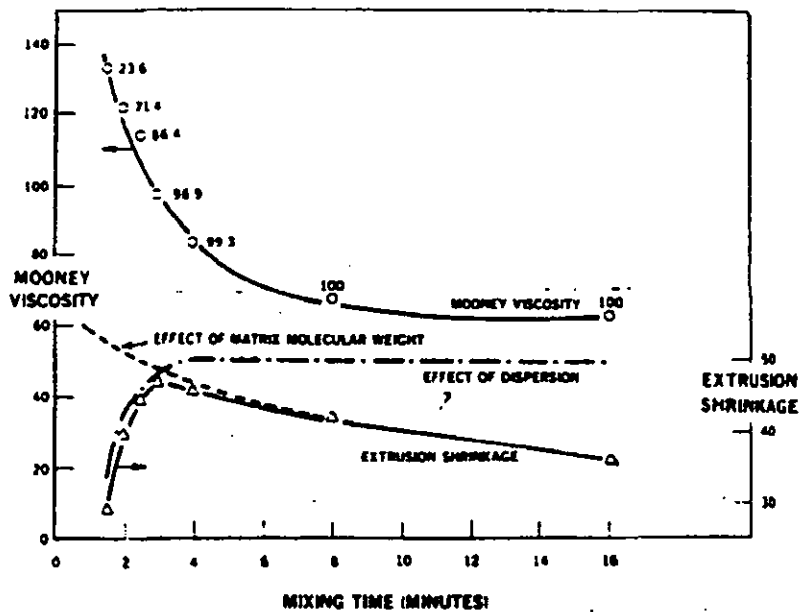


Figure 2.28 Rheological properties of uncured compound with N220 in SBR1712 plotted against mixing time.⁹⁶⁾

This shows a plot of mixing time versus Mooney Viscosity and extrusion shrinkage. The number beside each point on the Mooney Viscosity plot represents the % dispersion⁹⁷⁾ values using the Medalia Correction Factor⁹⁸⁾ for the amount of polymer occluded within the black agglomerates. Mooney Viscosity is lowest at the highest level of dispersion. High viscosity is attributed to the additional occlusion and partial immobilisation of polymer within the agglomerates at the lower dispersion levels⁹⁹⁾. The agglomerates affect

die swell in a similar manner. At the early stages of mixing, extrusion shrinkage is lowest and then increases up to the second power peak in the mixing circle. From that point on, extrusion shrinkage diminishes due to either polymer breakdown or selective adsorption of the high molecular weight polymer by the carbon black ^{100, 101}.

The second example is shown in Figure 2.29.

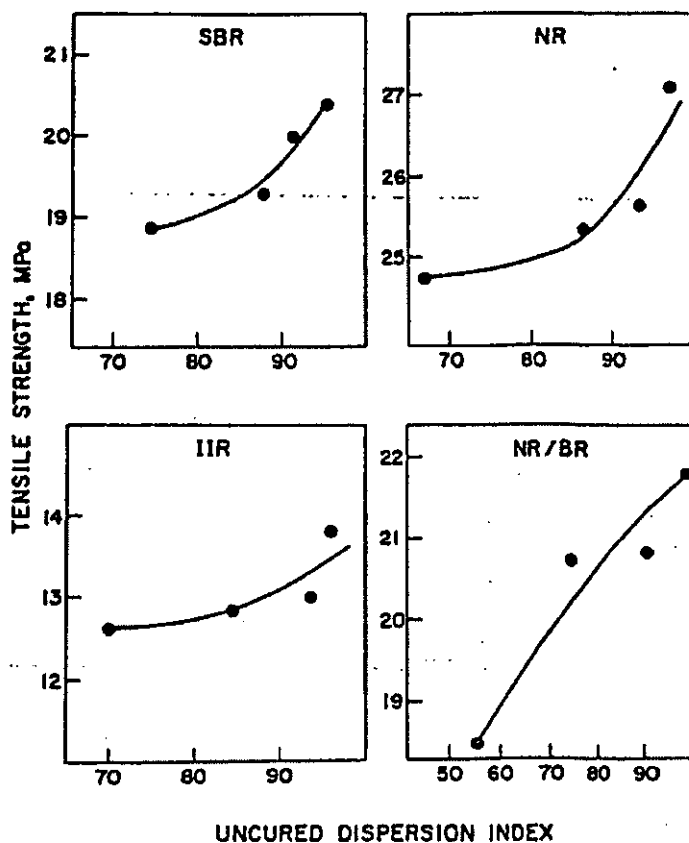


Figure 2.29 Tensile strength of different elastomer compounds as a function of dispersion index. ¹⁰²⁾

Generally speaking, filler agglomerates represent the most important aspect of dispersion in terms of failure properties such as tensile strength, elongation, fatigue life and abrasion resistance. **Figure 2.29** clearly shows that the tensile strength of SBR, NR, IIR are affected by carbon dispersion. In the case of the NR/BR blend, the distribution of carbon black within each polymer is another factor to be considered.

Figure 2.28 and **Figure 2.29** show that the dispersion index is important for both unvulcanised and vulcanised properties.

As will be discussed later, the location of carbon agglomerates (macroscopic morphology) in rubber compounds plays an important role in the fracture mechanism. The Medalia Correlation Factor includes a morphological effect for unvulcanised compounds. For example, it can be seen in the Guth-Gold-Einstein Equation that ;

$$E = E_0 (1 + 0.67fv + 1.62f^2v^2) \quad \text{Equation 2.63}$$

E, E₀ : modulus of a compound and gum respectively
v : volume ratio of carbon black
f : shape coefficient of carbon black (width/length)

The third term in the right hand side of **Equation 2.63** is a correction for the interaction between two particles and thus represents a simplified morphological effect.

In conclusion it can be said that the state of mix influences many properties of rubber compounds and should be considered when seeking to understand each property. One factor which causes the dispersion effect but has not been explicitly considered is the morphological state of the rubber compounds. The morphological effect should be taken into account to understand a phenomenon, as well as a statistical representation of carbon black the state of mix, such as that provided by ASTM D2663.

2.2.3.3 Vulcanisation

The state of mix exerts an influence on heat transfer which in turn exerts an influence on vulcanisation. Unfortunately no published literature regarding the effect of the state of mix on heat conduction was found, although some related literature was found. The basic mechanism of vulcanisation will be shown and the results used in the experimental work. This is followed by a discussion of the thermal properties and heat transfer, as the thermal properties of rubber compounds have a major effect on their overall performance. Finally, a basic treatment of heat transfer is given. These results will be utilised in the experimental work.

Vulcanisation process and mechanism

Vulcanisation ¹⁰³⁻¹⁰⁷⁾ is one of the most important processes of rubber technology.

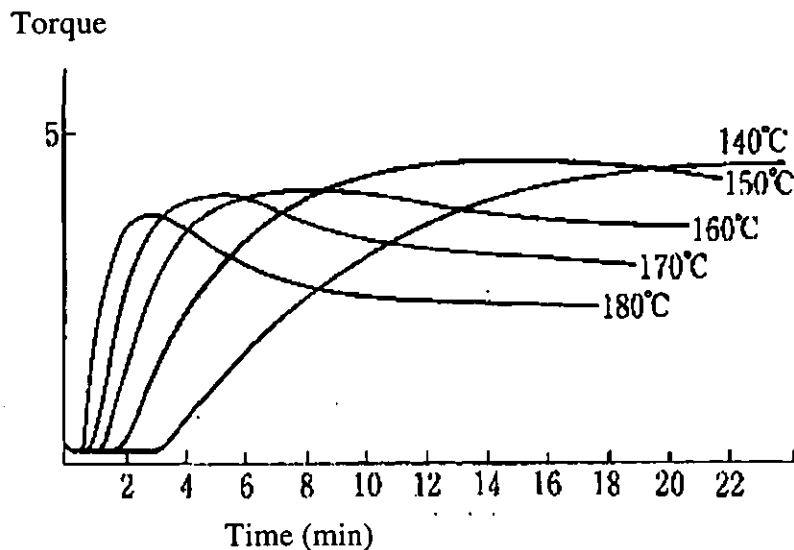


Figure 2.30 Typical cure curves at various temperatures. ¹⁰⁸⁾

Vulcanisation may be classified into two stages according to time sequence (Figure 2.30). The first stage ranges from the start of heating until the added sulphur makes a three dimensional polymer network. The second stage can be seen as a reversion in NR compounds. During the second stage, the sulphur which formed crosslink changes its character ¹¹⁰⁾ (Figure 2.31). The second stage ¹⁰⁸⁾ is one of the mechanisms of reversion in a cure curve, as well as chain scission of the matrix polymers.

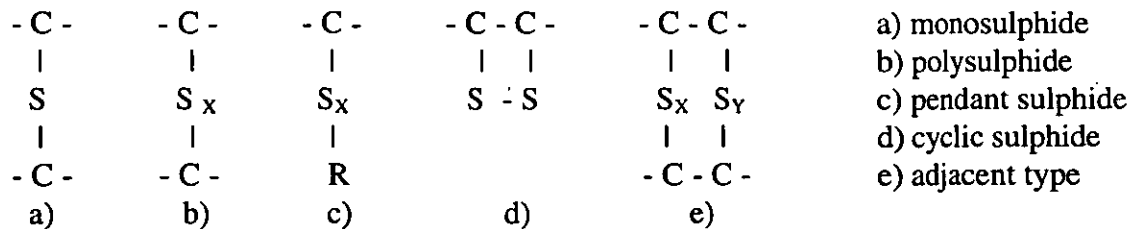


Figure 2.31 The structure of crosslinkings.

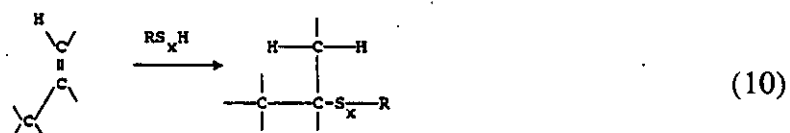
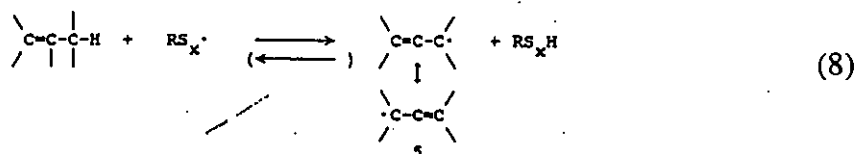
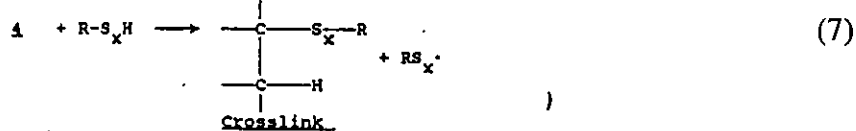
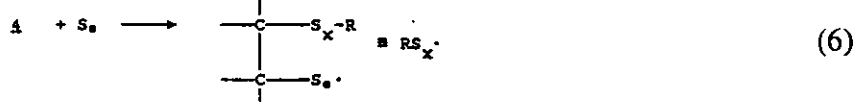
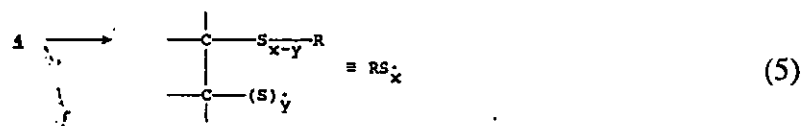
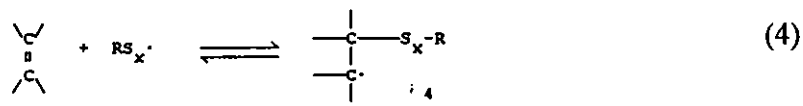
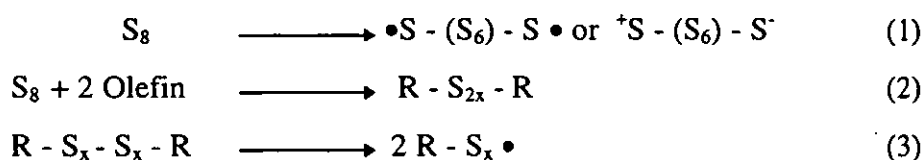


Figure 2.32 Free radical mechanism as a model of vulcanisation. ¹¹¹⁾

For the first stage of vulcanisation, three mechanisms are proposed. The first may be labelled as the free radical mechanism ^{111, 112)}. The second is an ionic mechanism ¹¹²⁾, and the third is a ligand-coupling mechanism ¹¹³⁾.

According to the postulated free radical mechanism, (Figure 2.32) the gradual formation of organic polysulphide molecules occurs in the initial stage of the reaction (2), perhaps via molecular assisted homolysis reactions. Polysulphide molecules would then serve as

the primary source of polysulphenyl radicals (3), which participate in a free radical chain reaction (4)-(9) and accelerate the reaction rate. According to Porter, the Arrhenius activation energy for the vulcanisation of rubbers by sulphur is 33 - 36 cal/mole.

Heat transfer

A polymer is a poor heat conductor. This property is used commercially for heat insulation purposes, but sometimes it can cause problems. For example, in the case of the pneumatic tyre, it may cause a tread separation or a burst due to a failure to dissipate hysteresis energy. It is very important to characterise the thermal character of rubber compounds. Thermal properties are, however, usually related to the vulcanisation process, where heat-transfer analysis is used to specify the conduction for a uniform cure and the necessary vulcanisate properties. It was found that the existing research mainly concentrated on operating methods to obtain a uniform temperature distribution or to predict a temperature distribution during vulcanisation, taking into account non-uniform, transient, temperature distribution as an operational parameter. Despite the importance of the vulcanisation process, research was not available concerning the thermal properties as a function of the state of mix.

Three types of research on the thermal properties of rubber compounds have been carried out. The first is the measurement of thermal properties ¹¹⁴⁾. It is difficult to simply define the heat capacity of carbon black because carbon black is shaped into small particles for handling purposes and a binder is used in the shaping process. During mixing, the binder is replaced by occluded or bound rubber. Furthermore, vulcanisation conditions depend on factors such as the process-line, operating conditions and economic restrictions. Such a complicated situation makes it difficult to precisely define properties and results in non-systematic measurements or, sometimes, a lack of data for desired conditions.

The second type of research is a numerical calculation ¹¹⁵⁾ of temperature distribution. In an industrial line, the shape of a mould may make a mathematical treatment very complicated. But recently developed numerical calculation methods and computers are solving this problem. The third type of research is a measurement of temperature during

vulcanisation and instrument development for experiments. The results from the measurements are compared to the calculated values based on the measured thermal properties. Typical examples from each field are shown below.

Hands and Horsfall ¹¹⁴⁾ carried out thermal measurement and proposed a power-series equation for calculating purposes. **Figure 2.33** shows one example of their results. It should be noticed that the thermal conductivity is dependent on temperature, decreasing in value by about 20 % from room temperature to a normal vulcanisation temperature. This change may result in a serious problem, especially in the case of thick products.

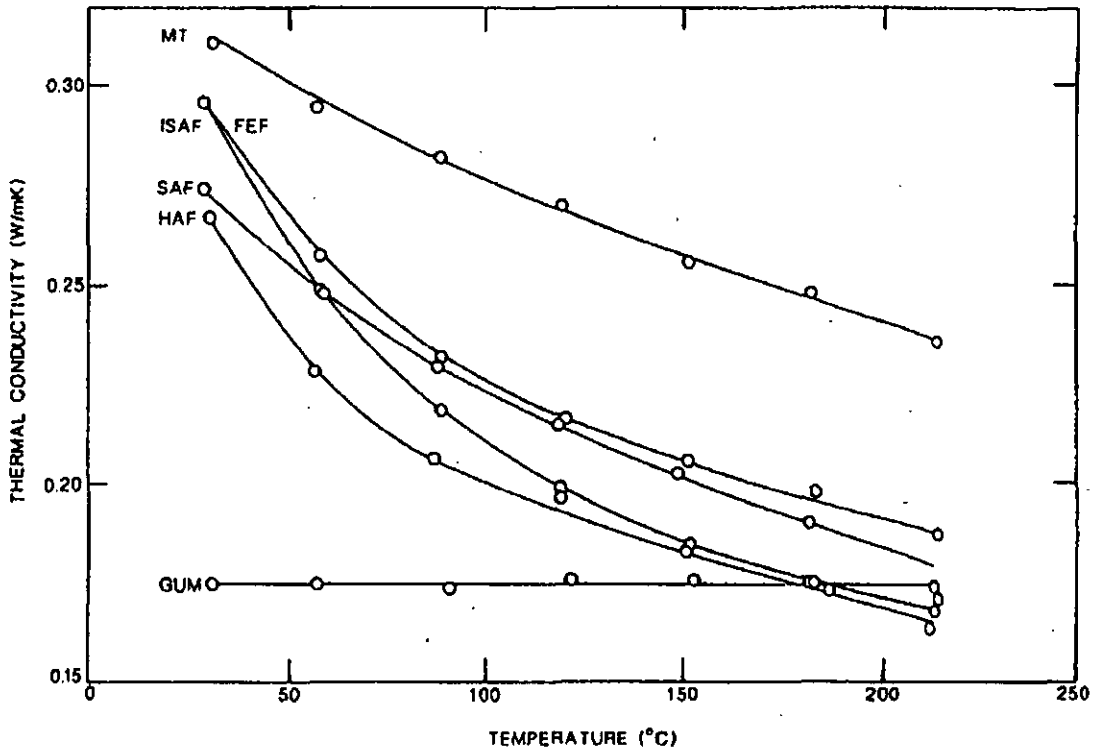


Figure 2.33 Thermal conductivity of carbon black loaded natural rubber. ¹¹⁴⁾

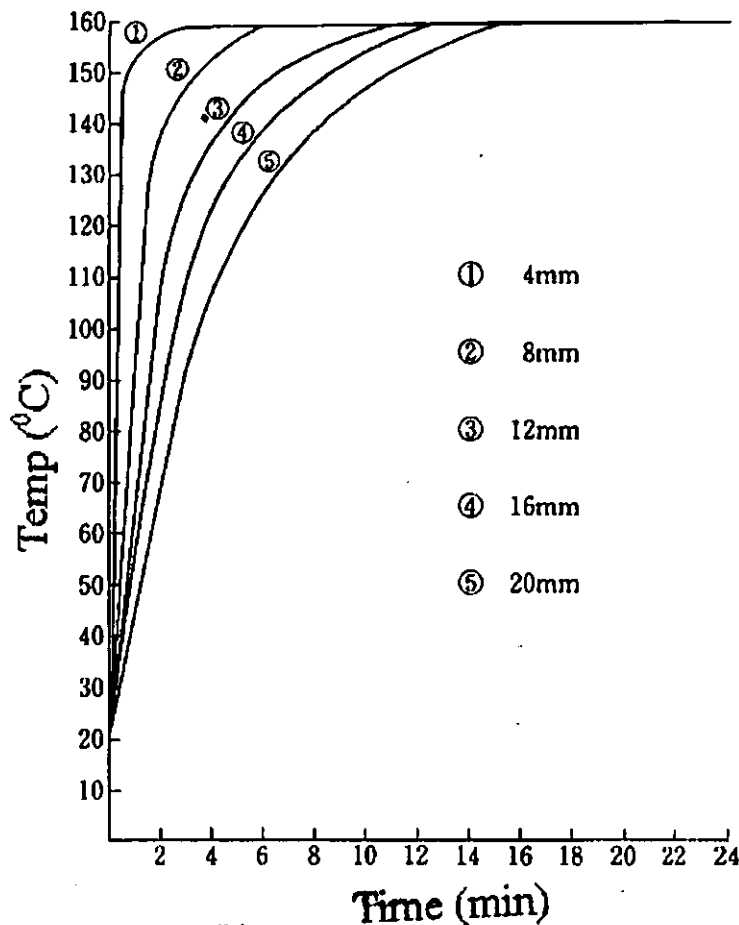


Figure 2.34 Temperature profile as a function of cure time and sample thickness. ¹⁰⁸⁾

Figure 2.34 shows one example of the temperature dependence of a thick sample. The experiments were carried out on a simple slab sample. The numbers in the graph show the thickness of the samples and the measurements were made at the centre of the samples. It takes 3 and 14 minutes for the samples of 4 and 20 mm thickness, respectively, to reach 150 °C from room temperature. It is well known that the rate of a chemical reaction strongly depends on temperature. As a rough measure, a 10 °C rise or fall results in a doubling or halving of the chemical reaction time. If the state of mix influences heat transfer then the state of mix must be considered to be an important factor for the vulcanisation process.

Mathematical model of heat transfer

A temperature difference between two points causes a heat transfer from the high temperature point to the low temperature point. Heat transfer is classified into three categories : conduction, convection, and radiation ¹¹⁶⁾. Heat conduction is a mechanism in which only heat energy is transferred by a medium. Convection is accompanied by mass transfer, an example of which is hot air blowing from a hair drier. In this case, hot air flow accompanies an air molecule transport. Radiation is defined as a heat transfer by means of electro-microwaves. A typical example is sunlight. Thermal energy is transferred as a light from the sun. Heat transfer by conduction is the most important factor in this thesis, so its treatment is given here.

Heat transfer is expressed by two equations.

$$q = -k \frac{\partial T}{\partial x}$$

$$\rho c \frac{\partial T}{\partial t} = k \frac{\partial^2 T}{\partial x^2}$$

Equation 2.64

q	:	heat flux (cal cm ⁻² sec ⁻¹)
T	:	temperature (K)
x	:	position parameter
k	:	thermal conductivity (cal cm ⁻¹ sec ⁻¹ K ⁻¹)
t	:	time (sec)
ρc	:	heat capacity (cal g ⁻¹)

The first equation is known as Fourier's Law of Heat Conduction, the second one is a second degree differentiation of Fourier's Law and it sometimes called the Diffusion Equation because of the similarity to the material diffusion equation. The second equation is usually used in the following form.

$$\frac{\partial T}{\partial t} = \alpha \frac{\partial^2 T}{\partial x^2}$$

Equation 2.65

α : thermal diffusivity (cm² sec⁻¹)

As an application of these methods, the heating of a finite slab is considered here ¹¹⁷⁾.

“A slab occupying the space between $y=\pm b$ is initially at temperature T_0 . At time $t=0$ the surfaces at $y = \pm b$ are suddenly raised to T_1 and maintained there. Calculate the temperature profile.”

This problem can be solved by using the following dimensionless quantities.

$$\begin{aligned}\Theta &= \frac{T_1 - T}{T_1 - T_0} \\ \eta &= \frac{y}{b} \\ \tau &= \frac{\alpha t}{b^2}\end{aligned}\quad \text{Equation 2.66}$$

Thus, the differential equations and boundary conditions are simply

$$\begin{aligned}\frac{\partial \Theta}{\partial \tau} &= \frac{\partial^2 \Theta}{\partial \eta^2} \\ I.C. \quad \text{at } \tau = 0, \quad \Theta &= 1 \\ B.C. \quad \text{at } \eta = \pm 1, \quad \Theta &= 0\end{aligned}\quad \text{Equation 2.67}$$

This equation can be solved by the method of separation of variables or Laplace Transformation. The solution is

$$\frac{T_1 - T}{T_1 - T_0} = 2 \sum_{n=0}^{\infty} \frac{(-1)^n}{(n + 1/2)\pi} \exp\left\{-(n + 1/2)^2 \frac{\pi^2 \alpha}{b^2} t\right\} \cos(n + 1/2) \frac{\pi y}{b}\quad \text{Equation 2.68}$$

When only the centre point is considered, the equation becomes,

$$\frac{T_1 - T}{T_1 - T_0} = 2 \sum_{n=0}^{\infty} \frac{(-1)^n}{(n + 1/2)\pi} \exp\left\{ -\left(n + 1/2\right)^2 \frac{\pi^2 \alpha}{b^2} t \right\} \quad \text{Equation 2.69}$$

When the terms higher than two in the series of the right term are ignored, the error is less than 5%. So, the final form becomes simply

$$\frac{T_1 - T}{T_1 - T_0} = \frac{4}{\pi} \exp\left(-\frac{\pi^2 \alpha}{4b^2} t \right) \quad \text{Equation 2.70}$$

Equation 2.70 is utilised in the experimental part of this thesis.

2.2.4 Ultimate properties of rubber vulcanisates

Among many rubber properties, tensile strength at break is the most important property for industrial purposes. In addition, this thesis will discuss the relationship between the fractal and the tensile strength at break as a representative vulcanised rubber property. It is therefore necessary to understand the fracture mechanics of rubber vulcanisates. In this section, current knowledge of the fracture mechanics will be discussed from the fractal standpoint.

2.2.4.1 Energy approach

Tensile strength at break can be discussed from the standpoint of energy balance. The energy approach originated from the discussion of tear, so, it is better to start from the energy approach to tearing.

Tearing is a complex ultimate property. A linear relationship cannot be assumed between stress and strain at the tear edge because a tear edge is exposed to high strain. The stress distribution around the edge also changes dramatically. Furthermore, the dynamic responses of materials under high stress control the mechanism by which the tear edge extends.

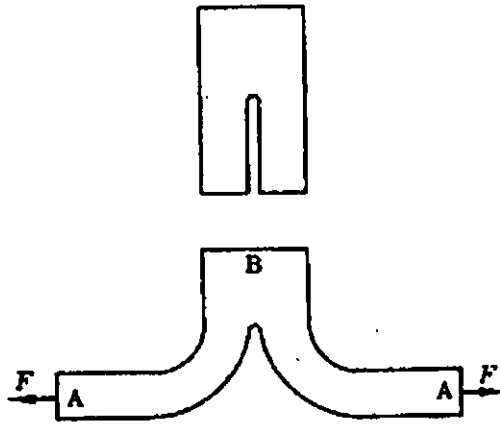


Figure 2.35 A trouser sample and measurement conditions. ¹¹⁹⁾

To avoid the analysis of such complicated situations, Thomas ^{118, 119)} treated the tear phenomena from the energy point of view. As shown in **Figure 2.35**, he used a trouser type sample as a model and considered only a steady tearing rate. In such a case, the distribution of the stress around the edge does not relate to the depth of the tear. Let F and ΔC be a force applied to a sample and a tear distance (at the point of A and B in **Figure 2.35**), respectively. The movement at the point A consists of two parts. The first part is the distance arising from the progress of the tear, and the second part is an elongation of the trouser sample under the force F . So, the total movement at A becomes $\alpha_1 \Delta C$. The energy of material elongation can be expressed as $\alpha_1 \Delta C$ (α_1 is an extension ratio). Therefore, the total energy which is necessary to tear a sample for a distance ΔC is

$$\Delta W = 2F\alpha_1 \Delta C \quad \text{Equation 2.71}$$

("2" arises from the fact that the sample has a two legs.)

It is necessary to decide the ratio between the energy which is used to tear a sample and the energy which is used to extend the sample. The energy (E) which is stored by the elongation at the legs can be written as

$$E = \int_{\alpha=1}^{\alpha_i} 2\sigma a(\Delta C) d\alpha \quad \text{Equation 2.72}$$

a : Surface area of trouser part
 σ : Stress at extension ratio α_i

As a first approximation, it is natural to regard this calculation as $(\alpha_i - 1)\Delta C$. If the legs of the sample are long enough so that α_i can be small and nearly “unity”, almost all the energy input to the sample will be used to increase the tear length. For a comparison between experimental data and equation 2.72, Thomas introduced tear energy E_T .

$$E_T = \Delta W / (h\Delta C) \quad \text{Equation 2.73}$$

h : sample thickness

By substituting equation 2.73 into equation 2.72, it becomes

$$E_T = 2F/h \quad \text{Equation 2.74}$$

Based on this equation, it becomes possible to obtain an intrinsic energy for tear by calculating it from experimental data. Equation 2.74 is the starting point of the following analysis.

2.2.4.2 Mechanisms of carbon black reinforcement

To understand the effect of carbon black on reinforcement, its effect on the various factors which influence the tearing energy must be examined, including threshold tearing energy, the energy dissipation mechanism and other factors ¹²⁰⁾. For example, its effect on modulus follows the well known relation ¹²¹⁾

$$E = E_0(1 + 0.67fv + 1.62f^2v^2) \quad \text{Equation 2.63}$$

The increase of the modulus results in an amplified stress and bigger energy dissipation during extension.

Threshold tearing energy

The concept of threshold energy of tearing has been demonstrated most convincingly in fatigue experiments (Figure 2.36). According to Thomas ^{2.99)}, the threshold energy is considered as the energy which must be put into an elastically effective network chain, mostly as distortion of chemical bonds, in order to raise the energy content of one of these bonds to its dissociation energy.

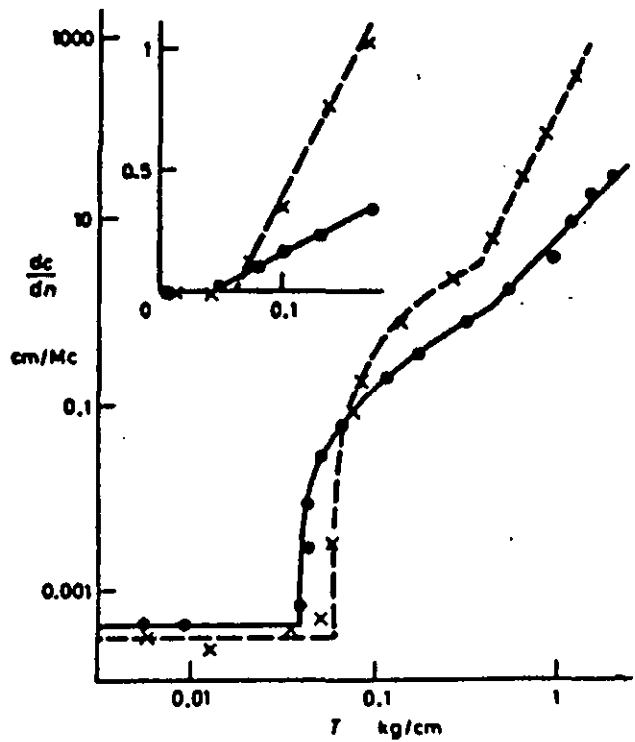


Figure 2.36 Crack growth versus tearing energy for NR(•) and SBR(×) gum vulcanisate. ¹²³⁾

The influence of carbon black on the threshold energy is discussed by Bhowmick, Gent and Pulford ¹²⁴⁾. In their experiment, it was found that the effect of a reinforcing carbon

black and a non-reinforcing carbon black on T_0 gave almost the same effect. Their result suggested that the influence of carbon black on T_0 was not a significant fact of carbon black reinforcement.

Energy dissipation mechanism

It is generally believed that dissipation of energy is essential for reinforcement. The research of energy dissipation can be classified into two categories. The first is a dynamic approach and the other a static approach. Medalia¹²⁰⁾ called them “viscous strengthening” and “high strain hysteresis”, respectively.

Viscous strengthening

Around a tear tip, the polymer suffers a large strain just before breaking down. The strain causes an energy dissipation and the tearing energy can be regarded as the necessary energy to cause the scission of the polymer chain plus the energy dissipated during stretching. The latter arises from molecular friction during stretching and is described by the WLF relationship. Both gum and carbon black filled compounds follow the WLF relationship (**Appendix 6**). There is no intrinsic difference between gum and carbon black filled compounds. Thus, the viscous strengthening cannot be regarded as a significant factor in carbon black reinforcement.

High stress hysteresis

High stress hysteresis derives from the following mechanisms¹²⁵⁻¹³⁰⁾.

1. Rearrangement of the rubber network, i.e., dragging the crosslinks into new locations.
2. Rearrangement of carbon black aggregates
3. Break down of carbon black network
4. Slippage and rupture of polymer or polymer-filler bonds.

These mechanisms were reviewed by Dannenberg and Brennan¹³¹⁾ for various elastomers. Their results showed that the type of carbon black had little effect on the extent of hysteresis or stress softening. Thus, high stress hysteresis cannot be regarded as a significant factor in carbon black reinforcement.

2.2.4.3 Medalia's interpretation of carbon black reinforcement

Medalia¹²⁰⁾ proposed a mechanism of carbon black reinforcement which can be regarded as the most comprehensive model at the moment. His model is used here for the basic theory of fractal application.

Medalia proposed a tear deviation mechanism for the carbon black reinforcement. He discussed two types of tear deviation. The first was a macroscopic and the other was a microscopic tear deviation. Figure 2.37 shows the tearing behaviour of a trouser specimen torn in the normal manner.

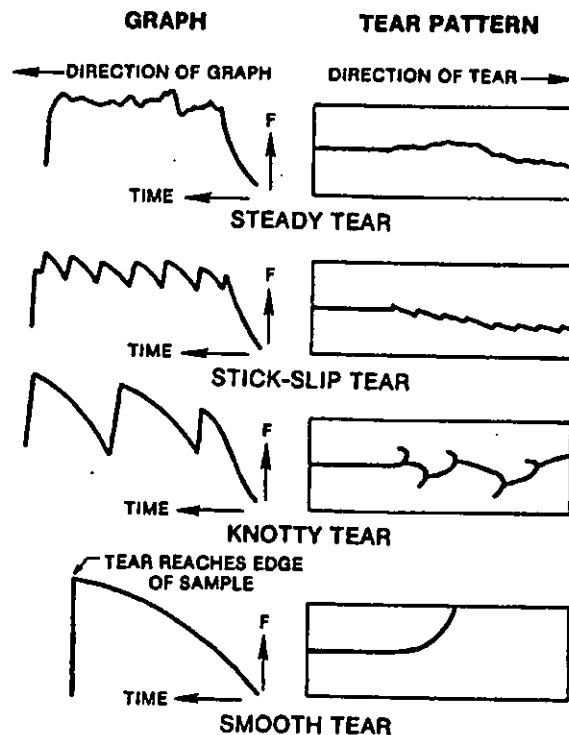


Figure 2.37 Four types of tear proposed by Medalia (schematic).¹³²⁾

Even in a steady state tear, there is generally some wandering which results in macroscopic surface roughness. Small deviations of the path produce stick-slip tears, and larger deviations result in knotty tears. In these models, when a tear deviates, the rate of tearing decreases and a stress builds up until a new tear is initiated. The force required to start tearing is proportional to the unstrained diameter of the tip of a tear, in accordance with **equation 2.71 - equation 2.74** derived by Thomas. For a knotty tear, where the curved knot is in effect the tip of the tear, large increases in force are required.

Medalia concluded that the addition of carbon black into rubber promoted tear deviation. The mechanism by which carbon black leads to tear deviation was presumed to be via the creation of barriers in the path of the tear. As evidence for his proposal, Medalia quoted some research results.

(a) The strongest evidence for formation of strands of aggregates comes from measurements of electrical conductivity¹³⁰⁾. The conductivity in the direction of stretching increases tremendously on stretching.

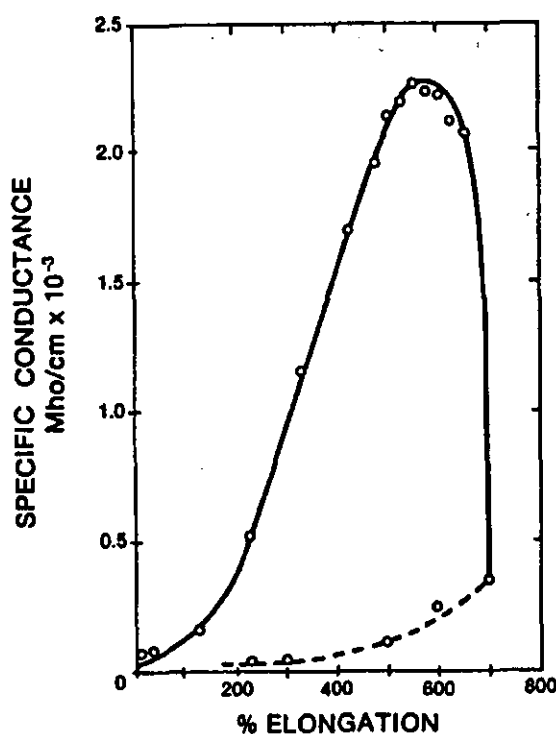


Figure 2.38 Electrical conductivity of SBR with 50 phr carbon black as a function of elongation.¹³⁰⁾

A 20 fold increase in longitudinal conductivity is shown in **Figure 2.38**, and earlier work by Voet ¹³³⁾, has shown an increase of up to 100 fold, with an anisotropy of up to 40. The decrease in conductivity at high elongation, in **Figure 2.38**, is due to the opening up of gaps here and there between the strands of aggregates. The gaps do not close readily on retraction, as shown by the dashed line of the figure.

(b) Direct evidence for tear deviation by clusters of carbon black comes from electron microscopy. Hess ⁷⁸⁾ has carried out extensive studies of the tearing of thin films of reinforced rubber in a transmission electron microscope and has noted that ;

“In all cases fairly large, highly wetted clusters of black tend to either halt the progress of the tear or divert its path. The presence of such clusters may be seen in electron micrographs of sections of filled rubber vulcanizates. On stretching, the aggregate within the clusters presumably reorient into strands.”

(c) Starcer et al ¹³⁰⁾ showed that their data for the statistics of rough tearing can be explained by the formation of anisotropic structures at the tip of the tear and that those structures are effective over a greater volume with black filled compounds than with gum vulcanizates.

2.2.5 The Meaning of Fractal Analysis and Fourier Transform for Rubber Technology

In this section, the significance of fractals for rubber technology will be discussed.

Polymer processing

If there is an available mathematical model for a mixing, it is possible to define the fractal dimension of a mixer power - trace mathematically. The definition of a fractal dimension is based on the Bolen-Colwell Model (section 2.2.3.1), but some important assumptions are pointed out later. The conclusion of the Bolen - Colwell Model is given by

$$T = \frac{\pi N \mu}{2} \left[1 + \frac{x}{a} \left(\frac{\pi x}{e} - \frac{1}{D_t} \right) - \frac{3\pi(x^2 a^2 - 1)}{1 + \frac{a^3 e}{x D_t}} \right] \quad \text{Equation 2.75}$$

where $a = h/g$
 $x = D_c/D_t$

To decide a fractal dimension, it is necessary to take a Fourier Transform of **Equation 2.75 (Appendix 2)**. To relate this equation to a mixer power trace, the viscosity (μ) of rubber must change during mixing. Hashizume proposed in his theory (**Appendix 7**) that another mechanism of polymer flow (④ in **Figure 2.39**) can be incorporated into the Bolen-Colwell Model. In addition, the Bolen-Colwell Model assumes a constant ratio of pressure flow to power flow at the rotor tip. This ratio, however, is a function of time due to the viscosity change through the state of mix of carbon black. For a simple treatment, **equation 2.75** can be separated into two terms. One is a time-dependent term and the other is a machine geometry constant.

$$T = \frac{\pi N \mu}{2} \left[1 + \frac{x}{a} \left(\frac{\pi x}{e} - \frac{1}{D_t} \right) - \frac{3\pi(x^2 a^2 - 1)}{1 + \frac{a^3 e}{x D_t}} \right]$$

$$= F(t) \times G \quad \text{Equation 2.76}$$

where $F(t)$: Time dependent term of torque
 G : Geometry constant

It is possible now to apply a Fourier Transform to **equation 2.76** to understand the meaning of fractal dimension from a mixer power trace (**Appendix 2**).

$$\int_0^\infty T(t) \exp(i\omega t) dt = G \int_0^\infty F(t) \exp(i\omega t) dt \quad \text{Equation 2.77}$$

The fractal dimension is derived from the slope of a power chart (α_f), and is given by differentiating equation 2.77 with by the frequency (ω).

$$\begin{aligned}\alpha_f &= \frac{d}{d\omega} \int_0^\infty NT(t) \exp(i\omega t) dt \\ &= NG \frac{d}{d\omega} \int_0^\infty F(t) G \exp(i\omega t) dt\end{aligned}\quad \text{Equation 2.78}$$

And the fractal dimension is decided by considering the space which an object occupies.

$$\alpha = d - D \quad \text{Equation 2.78}$$

Whatever the mathematical model, the fractal analysis in this thesis is based on the experimental data. It was considered to be more appropriate to consider the fractal analysis which gives the most macroscopic parameter and to modify the mathematical model by incorporating some discarded mechanisms. One of these, in the Bolen-Colwell Model, is the flow pattern within an internal mixer. It was shown that there are five types of flow in an internal mixer (section 2.2.3). Figure 2.39 shows one such flow.

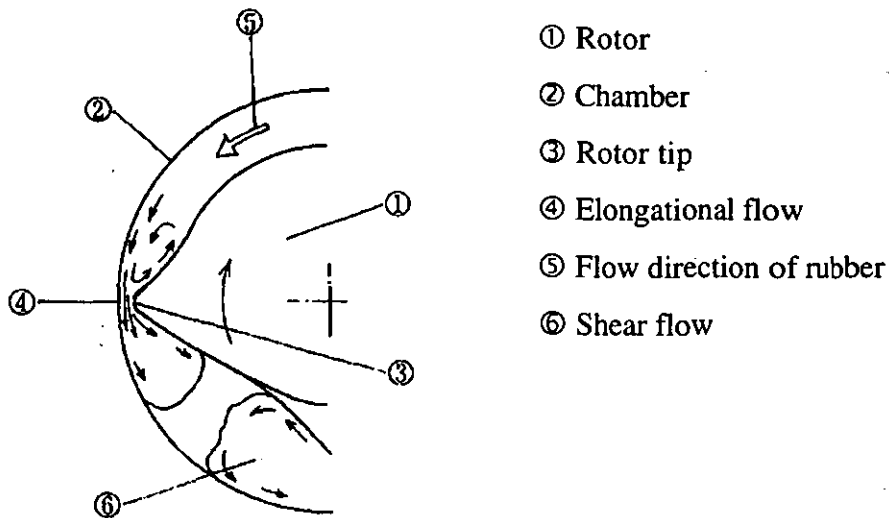


Figure 2.39 Rubber flow in an internal mixer. ¹⁰⁸⁾

The fractal is a macroscopic parameter for evaluating these flows by means of torque measurements during mixing. By combining fractal and other measurements like BIT, it is possible to obtain more information from a mixer power-trace. Furthermore, it becomes clear what the order of importance of such flows for a certain rubber compound or operating conditions are; and fractals may help us to make machines of desired efficiency. For example, the Fourier Transform gives us two types of clear peaks. According to Nishimoto (section 2.2.6.1), these peaks correspond to the rotation of rotors tips and wings. Nishimoto did not discuss the intensity of these peaks and their relation to the flows quantitatively but it is possible to assume that such peaks reflect the two main flows of polymer in an internal mixer. These are both the flow between rotor tip and a chamber wall (④), and the flow between rotors. By quantifying the intensities of such peaks and comparing them to mixing efficiency, it is possible to discuss the mechanism of flows in an internal mixer under a certain mixing condition or machine constants qualitatively. In addition, fractals give a total parameter for the mixing process and such quantified peak intensities give the significance of each flow. It is expected that the importance of the five flows in the mixing process can be elucidated by making a plot of the fractal dimension versus intensity.

Fractal for the state of mix

The significance of the fractal concept for the state of mix can be considered in two ways. First, as in other academic fields, it provides a new conceptual standpoint. Second, it may be used as a valuation of the morphology of the state of mix. The conceptual advantage arises from the ability of the fractal concept to link the measurements of polymer processing and vulcanised rubber properties. A single unified concept which can explain many aspects of rubber technology would be a considerable advantage. By using such a concept, the interrelationship of previously disparate information may yield significant insight into the mechanism of rubber technology. For example, the state of mix is evaluated by macroscopic, microscopic and indirect methods in section 3.2. These aspects are related to each other but research which treats the relationship between microscopic

dispersion and macroscopic is not available. In **Figure 2.20** and **Figure 2.28**, it is explained that carbon black agglomerates are incorporated into the polymer matrix before BIT. Microscopic dispersion continues after incorporation; however, it should be noticed that both phenomena are simultaneous and that incorporation and dispersion are affected by mixing conditions and formulations. BIT is a main industrial operating parameter, used to determine the end of the internal mixing process because there are milling stages downstream and microscopic dispersion is expected to proceed in such a process. Sometimes, however, the judgement by BIT presents a problem. Strongly occluded rubber prevents the carbon black from being dispersed more in downstream processes. To avoid such situations, it is necessary to consider the relation of the microdispersion and macrodispersion processes as they interact in a time sequence. Fractals are not affected by measurement magnification and can be expected to be one parameter which can connect these micro and macroscopic dispersions. Because fractals do not depend on scale, it is possible to apply fractal analysis to a desired scale by choosing suitable equipment. It is, therefore, possible to discuss micro and macro dispersion together by means of the fractal concept and it is expected that some new aspects of dispersion mechanisms will be revealed by the use of fractal measurements in this situation.

The second application of fractals is that they are expected to be a measure of morphology and characterise the size distribution function of the state of mix of carbon black by considering rubber properties. In **Figure 2.29**, the relationship between dispersion index and tensile strength is shown. It is known that there is a large scatter in the relationship between tensile strength and the dispersion index. One mechanism which contributes to such scattering is the morphology of the state of mix. Carbon agglomerates, which exist as a macroscopic chunk in a rubber compound, are a starting point for fracture. The position of carbon agglomerates in the rubber compound plays an important role because if a chunk of agglomerate is located in the centre of a sample, the fracture progress is absorbed by the surrounding rubber or carbon black network. If the agglomerate is located near the sample surface, the fracture results in catastrophic failure. Fractal analysis is expected to provide a method which can characterise such morphological effects.

Vulcanised rubber properties

The dual role of fractal analysis will be explained in this thesis. The first is to connect the processing conditions and vulcanised rubber properties. The second is a method of examining Medalia's interpretation of carbon black reinforcement. It is possible that further research will reveal the importance of fractals for rubber technology.

As already mentioned many times, only one scientific concept (fractal) connects the properties from polymer processing to vulcanised rubber properties. This means that the relationship between the mixing process and rubber properties becomes clearer than with existing methods.

The second purpose relates to the Medalia model of carbon reinforcement. As quoted above Medalia only proposed his interpretation based on existing results. It is necessary to discuss his proposal quantitatively and the fractal analysis presents one method to examine the validity of his proposal.

2.2.6 Fractal applications

2.2.6.1 Polymer processing

Nishimoto¹³⁴⁾ applied Fourier transforms to a mixer power trace. One example is shown in **Figure 2.40**. In **Figure 2.40**, there are two spectrum peaks (indicated by a circle and a triangle). By comparing the research of Toki^{54, 55)}, who analysed polymer flow in an internal mixer by using sensors, Nishimoto concluded that the peaks corresponded to the revolutions of rotor tips and wings. Nishimoto also applied fractal analysis to characterise the mixer power trace for NBR compounds. **Figure 2.41** shows the result. Nishimoto concluded that there is a maximum peak between 1.14 and 1.30 of the ratio of rotor revolution speed. However, Nishimoto did not discuss a theoretical relationship between the fractal dimension and mixing conditions.

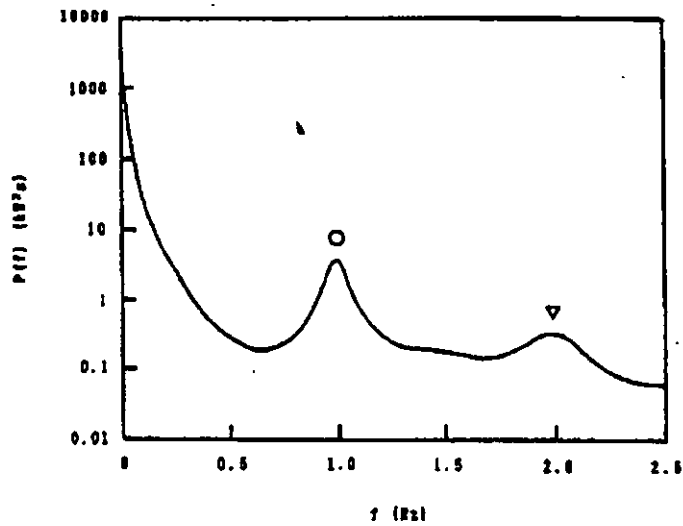


Figure 2.40 Relation between power spectrum density and frequency. The circle and triangle correspond to rotor revolutions.¹³⁴⁾

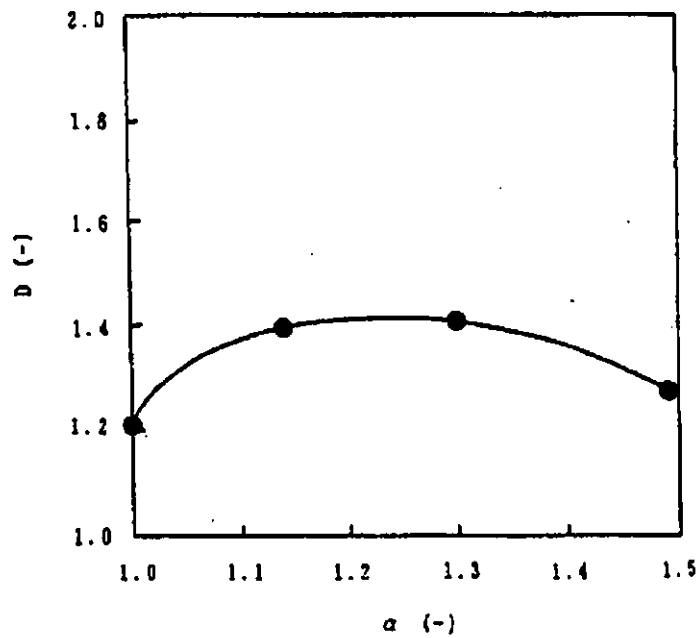


Figure 2.41 Relation between fractal dimension of mixing and revolution ratio.¹³⁴⁾

2.2.6.2 Characterisation of rubber properties

Fracture surface

Mandelbrot both developed and applied the fractal concept to characterise many natural phenomena. The following is one of his experiments to characterise a fracture mechanism.²³⁾

To characterise fracture surfaces, Mandelbrot applied two methods. The first was “fractal - area” perimeter relationship. In this method, a fractured steel specimen was plated with electroless nickel and mounted in an epoxy mount by vacuum impregnation in order to ensure edge retention. The specimen was then polished parallel to the plane of fracture. An “Island” of steel surrounded by nickel appeared which, on subsequent polishing, grew and merged. At each polishing step, the perimeter and area were measured and plotted on a double logarithmic scale graph (**Figure 2.42**). A fractal dimension of $D = 1.28$ was obtained by this method.

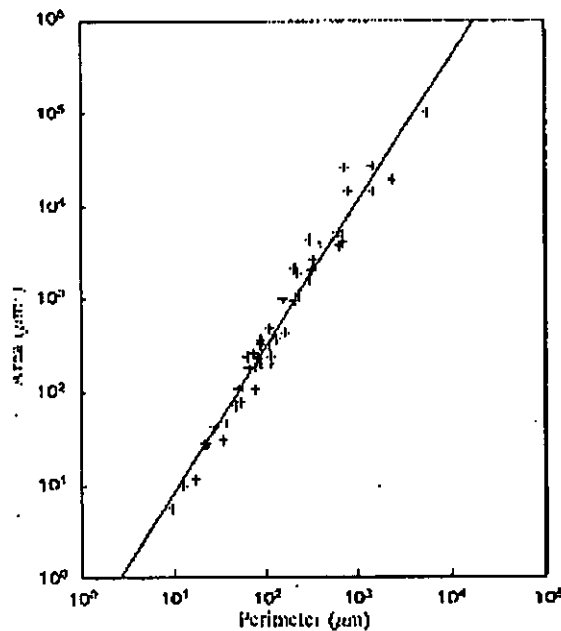


Figure 2.42 Fractal area perimeter relationship for slit islands. Fractal dimension is 1.28 .²³⁾

The second was a cumulative spectrum method. This method used fracture profile analysis based on Fourier Analysis (**Appendix 2**). Here, the plated and processed fracture was sectioned perpendicular to the fracture surface to expose it in profile. The profile's sample spectra exhibited wide oscillations. Some are statistical artefacts, but the others reflect fundamental lengths of the microstructure and their accompanying higher order harmonics. To average out some statistical fluctuations, five spectra were taken from serial sections, and integrated from high to low frequency (**Figure 2.43**). This method gave the fractal dimension as 1.26. The fractal dimensions from each method are identical within the range of statistical error.

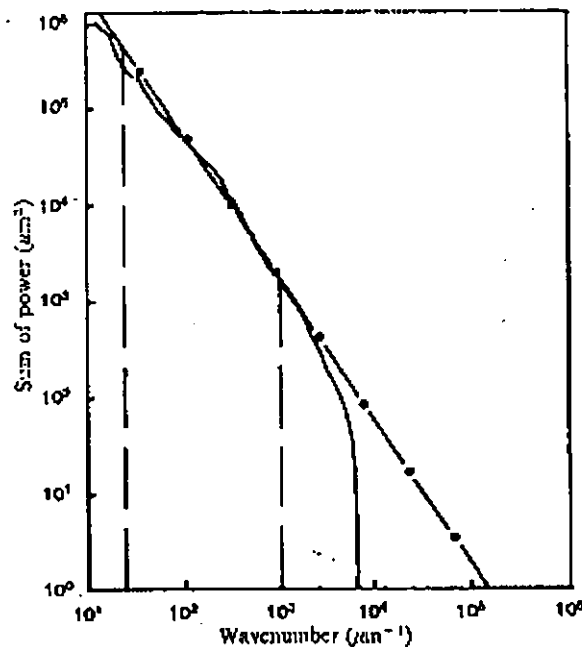


Figure 2.43 Cumulative spectrum for metal fracture surface. Fractal dimension increment is 1.26 .²³⁾

It is necessary to connect fractal results to existing data to reveal the fracture mechanism. The Charpy Impact Test was adopted for this purpose (**Figure 2.44**).

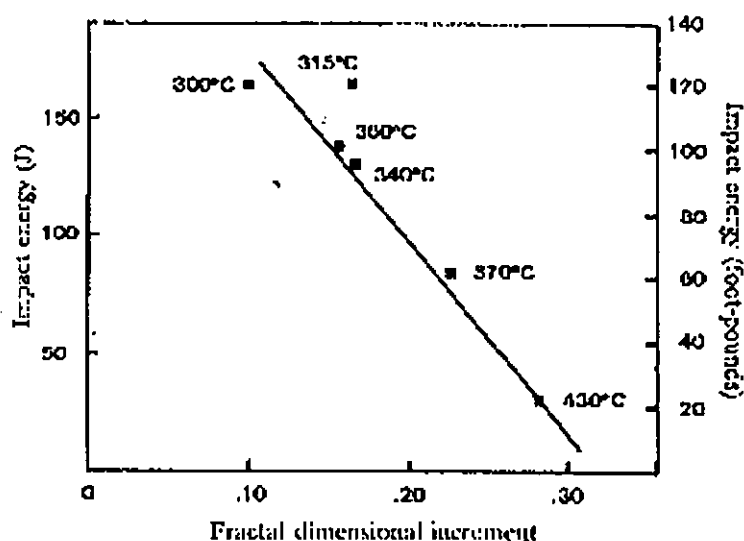


Figure 2.44 Impact energy versus fractal dimensional increment. ²³⁾

Based on this data, Mandelbrot suggested a possible explanation for the fracture mechanism. In his view, in a fracture that is transgranular (that is, runs through the grains) and involves a typical form of the notion of percolation ³⁷⁾, for example, during fracture of a ductile material, any voids forming around inclusions increase in size and coalesce into void sheets which ultimately form the fracture surface. If the growth of a void were independent of its neighbours or its position in the specimen, the percolation process would control the fracture mechanism. The relation of the percolation process and fractal geometry are already established ³⁷⁾, thus, it is quite possible for the fracture surface to show a fractal geometry. This indicates that it may be possible to observe fractal geometry on the fracture surface of rubber compounds.

Abrasion

Wear ¹³⁵⁾ is one of the most important factors involved in the application of rubber to industrial purposes. Shallamack ¹³⁶⁾ explored the abrasion formation mechanism; then Thomas ¹³⁷⁾ and Southern ¹³⁸⁾ developed a fatigue model based on fracture mechanics

concepts. More recently, Gent and Pulford ¹³⁹⁾ and Zang ¹⁴⁰⁾ have shown that wear involves tensile failure and chemical effects as well as fatigue.

Stupak and Donovan ¹³⁵⁾ applied fractal geometry to analyse abrasion patterns and correlate their feature to viscoelastic properties. Their results are quoted here because they provide an example of fractal application to rubber. Their method was very simple and it clearly shows how the fractal concept is easily applied to many fields.

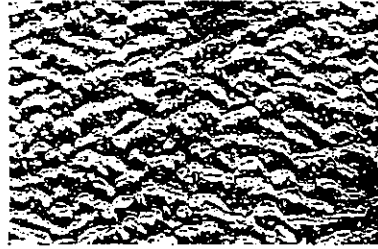


Figure 2.45 Wear surface under the frictional force of 730 J m^{-2} . ¹³⁵⁾

In their research, samples were prepared by a modified blade abrader. **Figure 2.45** shows one example of an abrasion pattern. The wear profiles were determined by using a profilometer. The profilometer traces were mounted on thick paper and the relief images were produced. These relief images were then used for perimeter determination where discs of various diameters were rolled along the relief profile. The discs had a hole in the centre which allows a pencil lead to record their path on the paper. Small discs conformed closely to the irregular outline, however large discs were unable to penetrate into many of the irregularities. The length of each path was measured with an architect's scale, and was normalised by dividing by the projected length of the original profilometer trace. (**Figure 2.46**)

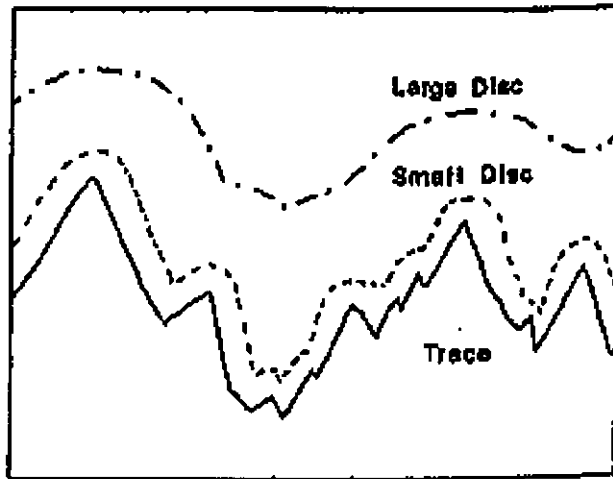


Figure 2.46 The effect of profilometer "radius" (disc diameter) on profilometer trace. ¹³⁵⁾

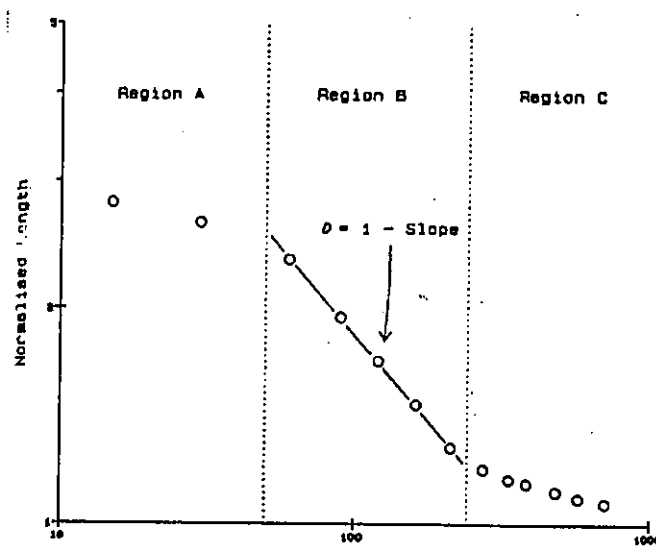


Figure 2.47 Typical fractal plot profilometry data. ¹³⁵⁾

It is clearly shown in **Figure 2.47** that the wear profile or abrasion pattern follows the fractal concept in some regions. Based on this fractal result, the wear condition and its

fractal dimension were considered and some relations between the fractal behaviour of wear mechanism and viscoelastic properties were suggested. Based on these results, a wear topography and fractal relation was proposed.

$$W = A(L \log S)^n \quad \text{Equation 2.80}$$

where W : Wear rate
 A , n : Material constants for wear
 S : Shift factor

Surface crazing morphology

Surface crazing plays an important role in the durability of manufactured rubber goods. It is, therefore, a problem which has attracted much research interest. Surface crazing can be classified into two categories ^{141, 142)}. The first is ozone crazing and the other one is light crazing. The main feature of ozone crazing is cracks which run normal to direction of stretching in a stretched sample exposed to an ozone atmosphere. The feature of light crazing is crazing in all directions by the catalytic effect of light on the sample surface. To characterise crazing, it is common to compare the crazing to a standard sample. For example, Newton ¹⁴³⁾ classified crazing into five categories by comparing it to photographs of standard samples. Edwards ¹⁴⁴⁾ adopted a similar, but more dynamic, evaluation system which also classified crazing into five categories.

The complexity arises from the fact that it is not straight forward to evaluate a craze pattern because of its non-Euclidean shape. Nishimoto ¹⁴⁵⁾ recently applied the fractal concept to evaluate the craze pattern and succeeded in characterising it.

In Nishimoto's experiment, SBR rubber samples are degraded by a weatherometer. One example of crazing is shown in **Figure 2.48**.

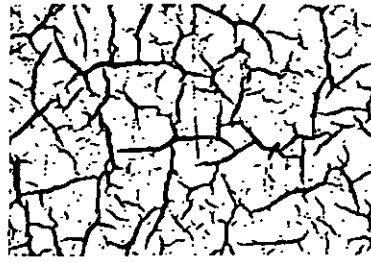


Figure 2.48 Microscopic photograph of degraded SBR surface crazing. 200 hours ageing sample.¹⁴⁵⁾

The crazing pattern on the samples is characterised by using the box counting method. **Figure 2.49** shows an example of such analysis.

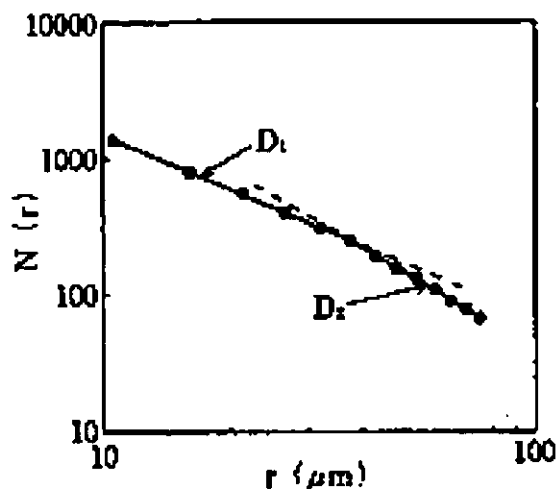


Figure 2.49 A relationship between box size and the number of box that contains crazing images in it.¹⁴⁵⁾

In this figure, the crazing pattern has two types of fractal dimension. According to Graf¹⁴⁶⁾, these two types of dimension, the smaller and the bigger one, correspond to the complexity of microscopic crazing structure and a structural pattern spanning the whole

sample. In their experiment, the small fractal dimension reflected the complexity of each crazing pattern itself and the bigger dimension reflects the total pattern of crazing.

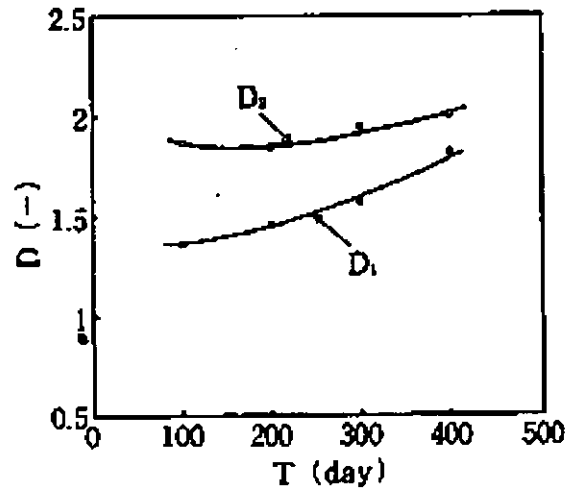


Figure 2.50 Relation between the fractal dimension and ageing condition. ¹⁴⁵⁾

To characterise these fractal dimensions, they compared the results according to ageing time. **Figure 2.50** shows a regular increase of fractal dimension according to ageing time. The result corresponds to the apparent fact that the crazing becomes bigger and more complex as the ageing period increases. Based on these results, Nishimoto proposed the use of fractal dimension as a measure for evaluating the crazing pattern but have not yet explained what kind of mechanism causes the crazing pattern to exhibit fractal geometry.

References

- 1) B. B. Mandelbrot. "Fractals: Form, Chance and Dimension", Freeman, (San Francisco 1977) : "The Fractal Geometry of Nature", Freeman, (San Francisco 1987)
- 2) H. Jones, in "Fractals and Chaos", ed. by T.Crilly, R.A.Earschaw, H.Jones (Springer, New York 1991)
- 3) H. O. Peigen, H. Juergens, D. Saupse, "Chaos and Fractals", Springer Verlag, (New York, 1992)
- 4) J. Freder, "Fractals", Plenum, (New York, 1988)
- 5) T. Vicsek, "Fractal Growth Phenomena", World Scientific, (Singapore, 1989)
- 6) D.Avnir (ed), "The Fractal Approach to Heterogeneous Chemistry", John Wily, (New York, 1992)
- 7) M.Barnsley, "Fractals Everywhere" (Academic Press, San Diego 1988)
- 8) H. Takayasu, "Fractal in Physical Sciences", Manchester University Press, (Manchester, 1990)
- 9) H. G. Schuster, "Deterministic Chaos - An introduction", Physik Verlag, (Weinheim, 1984)
- 10) H. O. Peitgen, P. H. Richer, "The Beauty of Fractals", Springer Verlag, (Heidelberg, 1986)
- 11) H. E. Stanley, N. Ostrowsky (eds), "Correlation and Connectivity : Geometric Aspects of Physics, Chemistry and Biology", Kluwer, (Dordrecht, 1990)
- 12) H. O. Peigen, H. Juergens, D. Saupse, "Chaos and Fractals", Springer Verlag, (New York, 1991)
- 13) A. Bunde, S. Havlin (eds), "Fractal and Disordered Systems", Springer Verlag, (Heidelberg, 1991)
- 14) J. F. Gouyet, "Physique et Structures Fractals", Masson, (Paris, 1992)
- 15) A. Bunde, S. Havlin (eds), "Fractals in Science", Springer Verlag, (Heidelberg 1994)
- 16) D. F. Lawden, "An Introduction to Tensor and Relativity", Methuen & Co. Ltd (London, 1962)
- 17) D.Ter.Haar, "Elements of Hamiltonian Mechanics", Pergamon Press (Oxford, 1971)

- 18) K. Menger, "What is dimension ?", Amer. Math. Month., 50, 2-7, (1943)
- 19) W. Sierpinski, "Sur une courbe dont tout point est un point de ramification.", Co,ptes Rendus (Paris, 1916)
- 20) K. Murayama, "Amorphous and Fractal" in Fractal Science, ed. H. Takayasu, Asakura shyoten (Tokyo, 1987)
- 21) C. K. Peng, S. Havlin, Phys. Rev. E, 47, 899 (1993)
- 22) H. Mizutani, "Science of Crater", Tokyo University Press (1980)
- 23) B. B. Mandelbrot, D. E. Passoja, A. J. Pully, Nature 308, 19, 721 (1984)
- 24) F. Reif, "Fundamentals of statistical and thermo physics", McGraw Hill (1965)
- 25) P. J. Flory, "Principle of Polymer Chemistry", Cornel Univ. Press, (1953)
- 26) M. Doi, S.F.Edwards, "The theory of Polymer Dynamics", Clarendon (Oxford, 1986)
- 27) M.Doi, "Introduction to Polymer Physics", Oxford Univ. Press (1995)
- 28) G. Krause, "Reinforcement of Elastomer", Wiley (Interscience), (New York, 1986)
- 29) J. B. Donnet, "Carbon black Physics, Chemistry and Elastomer reinforcement", Dekker, (New York, 1965)
- 30) P. K. Freakley, "Theory and practice of engineering with rubber", Applied Science (London, 1978)
- 31) J. L. White, "Principle of Polymer Engineering Rheology", Wiley (New York, 1990)
- 32) J. L. White, "Rubber Processing : Technology, Materials and Principles" Hanser/Garddner (New York, 1995)
- 33) J. D. Ferry, "Viscoelastic Properties of Polymers", John Wiley & Sons (New York 1960)
- 34) A. V. Tobolsky, "Properties and Structure of Polymers", John Wiley & Sons (New York, 1960)
- 35) F. Buecke, "Physical Properties of Polymers", John Wiley & Sons (New York, 1962)
- 36) P. G. deGennes, "Scaling concept in polymer", Cornell Univ.Press (1979)
- 37) D. Stauffer, "Introduction to Percolation Theory", Tayler & Francis (London, 1985)
- 38) G. Kraus, Fortschr. Hochololym.-Forsh., 8, 155 (1971)
- 39) W. H. Hess, L. Ban, G. C. McDonald, E. Urban., Rubb. Chem. Tech., 46, 204 (1971)
- 40) A. I. Medalia, F. A. Heckman., J. Colloid. Interface Sci., 36, 173 (1971)

- 41) W. H. Hess, L. Ban, G. C. McDonald, E. Urban., *Rubb. Chem. Tech.*, 46, 204 (1973)
- 42) B. H. Kayne, *Powder Tech.*, 21,1 (1978)
- 43) A. G.Flook, *Powder Tech.*, 21, 295 (1978)
- 44) M. Gerspacher, C. P. O'Farrell, *Elastomerics*, 123 (4), 25 (1991)
- 45) X. Bourrat, A. Oberlin, *Carbon* 26 (1), 100 (1988)
- 46) F. Ehrburger-Dolle, M. Tence, *Carbon* 28 (2), 448 (1990)
- 47) A. V. Avnir, D. Farin, *J. Chem. Phys.*, 79 (7), 3566 (1983)
- 48) C. R. Herd, G. C. McDonald, W. M. Hess, *Rubb. Chem. Tech.*, 65, 107 (1992)
- 49) W. Prager, J. K. Talbot (in E.C.Berhadtd ed) "Processing of Thermoplastic Materials", McGraw Hill (1953)
- 50) S. Shiga, M. Furuta, *Nippon Gomu Kyokaishi*, 55, 491 (1982)
- 51) S. D. Lee, J. L. White, N. Nakajima, R. Brozokowski, *Kautsch. Gummi Kunstst* 42, 992 (1989)
- 52) J. Kim, J. L. White, *Nihon Rheorogi Gakkaishi*, 17, 203 (1989)
- 53) J. Kim, J. L.White, W. Szydlowski, *Int. Polym. Process*, 4, 9 (1989)
- 54) S. Toki, M. Takeshita, Y. Morimoto, M. Okuyama., presented at a meeting of Rubber division ACS. Houston, Oct.25 (1983)
- 55) S. Toki, *Nippon Gomu Kyokaishi*, 62, 132 (1989)
- 56) P. K. Freakley, R. P. Patel., *Rubb. Chem. Tech.*, 58, 751 (1987)
- 57) L. Min, J. L. White, *Rubb. Chem.Tech.*, 58, 1024 (1985)
- 58) L. Min, J. L. White, *Rubb. Chem.Tech.*, 60, 361 (1983)
- 59) L. Min, *Int. Polym. Process*, 1, 179 (1987)
- 60) L. Min, *Adv. Polym. Tech.*, 7, 243 (1987)
- 61) N. Tokita, J. L. White, *J. Appl. Polym. Sci.*, 10, 1011 (1966)
- 62) J. L. White, N. Tokita, *J. Appl. Polym. Sci.*, 12, 1589 (1968)
- 63) A. Morikawa, J. L.White, K. Min, *Int. Polym. Process*, 4, 23 (1989)
- 64) A. Morikawa, J. L. White, K. Min, *Adv. Polym. Tech.*, 8, 383 (1989)
- 65) D. K. Setsua, J. K. White, *Kautshuk Gummi Kunstst*, 44, 542 (1991)
- 66) D. K.Setsua, J. K. White, *Polym. Eng. Sci.*, 31, 1742 (1992)
- 67) K. Kawasaki, K. Tagi, *Int. Polym. Process.*, 3, 173 (1990)

- 68) J. E. Point, US Patent (filed Jan. 21, 1914) 1,138,410 (1915)
- 69) J. M. Funt, "Mixing of rubber", RAPRA Publ., Shawbury, U.K., (1977)
- 70) S. Hashizume, Nihon Rheorogi Gakaishi, 15, 19 (1987)
- 71) W. R. Boden, R. E. Colwell, Soc. Plast. Eng. J., 14 (8), 24 (1958)
- 72) I. Manas-Zloczower, A. Nir, Z. Tadmor., Rubb. Chem. Tech. 55, 1250 (1982)
- 73) S. Shiga, M. Furuta., Rubb. Chem. Tech., 50, 292 (1977)
- 74) J. Clarke, P.K.Freakley, Plast. Rubb. and Comp. Process. and Appl., 24, 261 (1995)
- 75) W. M. Hess., Rubb. Chem. Tech., 64, 386 (1991)
- 76) ASTM D2663 (Method A)
- 77) W. M. Hess., Rubb. Chem. Tech., 35, 228 (1962)
- 78) W. M. Hess, F. P. Ford, Rubb. Chem. Tech., 36, 1175 (1963)
- 79) J. S. Trent, S. I. Scheinbein, P. R. Coucham, Macromolecules, 16, 589 (1983)
- 80) L. C. Sawyer, D. T. Grubb, "Polymer Microscopy", Chapman and Hall, (London, New York, 1982)
- 81) L. C. Ban, K. S. Campo, Rubb. Chem. Tech., 64, 126 (1991)
- 82) L. E. Porter, Rubber World, 189 (2), 35 (1983)
- 83) W. M. Hess, G. C. McDonald, E. Urban, Rubb. Chem. Tech., 46, 204 (1963)
- 84) B. Topcik, Rubber Age, 80, 105 (7), 25: 105 (8), 35 (1973)
- 85) ASTM D2663 (Method D)
- 86) P. C. Ebell, D. A. Hemsley., Rubb. Chem. Tech., 54, 698 (1981)
- 87) J. Jansen, G. Krause, Rubb. Chem. Tech., 53, 48 (1980)
- 88) A. I. Medalia, Rubb. Chem. Tech., 59, 432 (1986)
- 89) J. E. Callan, W. M. Hess, E. Scott, Rubb. Chem. Tech., 44, 814 (1971)
- 90) Y. Oyama, Sci. Papers Inst. Phys. Chem. Rev., (Tokyo), 37 (951), 17 (1940)
- 91) J. P. Beaudy, Chem. Eng., 55 (7), 112 (1948)
- 92) P. M. C.Lacy, J. Appl. Chem., 4,257 (1954)
- 93) A. S. Michael, U. Fuzinauskas, Chem. Eng. Prog., 50 (12), 604 (1954)
- 94) S. S. Weidenbaum, C. F. Bonilla, Chem. Eng. Prog., 51 (1), 273 (1955)
- 95) J. C. Smith, Ind. Eng. Chem., 47, 2240 (1955)
- 96) B. B. Boonstra, A. I. Medalia, Rubb. Chem. Tech., 36, 115 (1964)

- 97) C. H. Leigh - Dugmore, *Rubb. Chem. Tech.*, 29, 1303 (1956)
- 98) A. I. Medalia, *Rubb. Chem. Tech.*, 34, 1134 (1961)
- 99) I. Pliskin, *Rubb. Chem. Tech.*, 46, 1218 (1973)
- 100) L. L. Ban, W. M. Hess, L. A. Papazian, *Rubb. Chem. Tech.*, 47, 858 (1974)
- 101) G. R. Cotton, *Rubb. Chem. Tech.*, 48, 548 (1975)
- 102) W. H. Hess, V. E. Chirico, P. C. Vegvari, *Elastomer*, 112 (1), 24 (1980)
- 103) A. Y. Coran, *Rubb. Chem. Tech.*, 68, 351 (1995)
- 104) G. Bertrand, J. Olivie, *Prog. Rubb. Plast. Tech.*, 3 (2), 1 (1987)
- 105) P. Quirk, *Prog. Rubb. Plast. Tech.*, 4 (1), 31 (1988)
- 106) T. Kempermann, *Rubb. Chem. Tech.*, 61, 422 (1988)
- 107) M. A. Fath, *Rubber World*, 210 (1), 24 (1994)
- 108) Nihon Gomu Kyokai ed., "Gomu Gijyutu no kiso" The Soc. Rubb. Ind., (1988)
- 109) F. R. Eirich, "Science and Technology of rubber", Academic Press (London, 1978)
- 110) B. A. Pogadkin, *Rubb. Chem. Tech.* 29, 555 (1956)
- 111) R. Quirk, *Prog. Rubb. Plast. Tech.*, 4 (1), 31 (1988)
- 112) M. Porter, "Organic chemistry of sulphur", Plenum Press, (New York, 1988)
- 113) S. Osae, *Polym. Appl.*, 14, 117 (1993)
- 114) D. Hans, F. Hortall, *Rubb. Chem. Tech.*, 50, 253 (1977)
- 115) H. P. Schlenger, *Rubb. Chem. Tech.*, 56, 304 (1983)
- 116) M. Oezisik, Y. Bayazituglu, "Element of Heat Transfer", McGraw Hill (1988)
- 117) R. N. Bird, W. E. Stewart, E. N. Light, "Transport Phenomena", John Wiley & Sons (1960)
- 118) A. G. Thomas, *J. Polym. Sci.*, 18, 177 (1955)
- 119) A. G. Thomas, *J. Appl. Polym. Sci.*, 3, 168 (1960)
- 120) A. I. Medalia, *Rubb. Chem. Tech.*, 60, 45 (1987)
- 121) E. Guth, *J. Appl. Phys.*, 16, 20 (1945)
- 122) G. J. Lake, A. G. Thomas, *Kautsch. Gummi Kunstst.*, 20, 211 (1967)
- 123) G. J. Lake, A. G. Thomas, *Proc. Roy. Soc. London, Ser. A* 300, 108 (1967)
- 124) A. K. Bhomich, A. N. Gent, C. T. R. Pulford, *Rubb. Chem. Tech.*, 56, 226 (1983)
- 125) L. Muellins, *Trans. Inst. Rubb. Ind.*, 35, 213 (1963)

- 126) E. H. Andrew, A. J. Walsh. *J. Polym. Sci.*, 33, 39 (1958)
- 127) T. L. Smith, *J. Poly. Sci.*, 32, 99 (1958)
- 128) A. N. Gent, A. W. Henry, *Proc. Int. Rubb. Conf.*, 5th Brighton, England 193 (1967)
- 129) A. W. Henry, Ph.D thesis, The university of Akron Dept. Chem. (1961)
- 130) R. G. Starcer, E. D. von Meerwall, F. N. Kelly, *Rubb. Chem. Tech.*, 58, 913 (1985)
- 131) E. M. Dannenberg, J. J. Bronnan, *Rubb. Chem. Tech.*, 39, 597 (1966)
- 132) J. Glucklich, R. F. Landel., *J. Appl. Polym. Sci.*, 20, 121 (1976)
- 133) A. Voet, J. C. Morawski, *Rubb. Chem. Tech.*, 47, 765 (1974)
- 134) K. Nishimoto, N. Urabe, *Nippon Gomu Kyokaishi*, 65 (7), 82 (1992) : 65 (8),
51 (1992)
- 135) P. R. Stupak, J. A. Donovan, *J. Mater.Sci.*, 23, 2230 (1988)
- 136) A. Shallamack, *Rubb. Chem. Tech.*, 55, 209 (1968)
- 137) A. G. Thomas, *Rubb. Chem. Tech.*, 48, 902 (1974)
- 138) E. Southern, A. G. Thomas, *Rubb. Chem. Tech.*, 52, 1008 (1979)
- 139) A. N. Gent, C. T. Purford, *J. Appl. Polym. Sci.*, 28, 943 (1983)
- 140) S. W. Zang, *Rubb. Chem. Tech.*, 57, 755 (1984)
- 141) A. Kondo, *Gomu*, 15, 23 (1968)
- 142) M. Urabe, *Koubunshi*, 18, 174 (1969)
- 143) R. G. Newton, *Rubb. Chem. Tech.*, 18, 504 (1945)
- 144) D. C. Edwards, R. C. Klingender, *Rubber Age*, 96, 65 (1964)
- 145) K. Nishimoto, Y. Nagai, T. Akiyama, N. Mifune., *Nippon Gomu Kyokaishi*, 66 (8),
546 (1993)
- 146) J. G. Graf, *Powder Tecch.*, 67, 83 (1991)

Chapter 3

Experiments

3.1 Introduction

As mentioned in chapter 1, the purpose of this project is to apply the fractal concept to various rubber properties and to obtain a perspective of the relationship of rubber mixing processing to vulcanised properties. For this purpose, the following objectives were carried out.

- (a) The first experiment was to analyse the mixing mechanism. Many researchers have shown that power traces provide much useful data during mixing. Considering this situation, a power trace is analysed by applying Fourier transform.
- (b) The second experiment was to evaluate the state of mix and its influence on rubber properties. A macroscopic carbon black dispersion was evaluated by a box counting method.
- (c) The next experiment was to evaluate the behaviour of the vulcanisates. Tensile strength is the most commonly used property for this purpose and was selected here.
- (d) The relationship between the mixing, the state of mix, tensile strength and fracture surfaces were evaluated and analysed.

To analyse these experiments, fractal methods were applied to each experiment. These methods are not new research procedures, but some of them have not yet been applied to rubber technology.

3.2 Material preparation

3.2.1 Materials and Formulations

For comparison purposes, two formulations are adopted based on different matrix polymers by referring to the American Standard Test of Materials (**Table 3.1 and Table 3.2**). In the case of the SBR formulation, SBR1502 was used. The carbon black is N330 supplied by Cabot.

In the NR formulation, SMR 20 (Standard Malaysian Rubber) is used as the matrix polymer. The other ingredients are as used for the SBR formulation.

Table 3.1 Experimental formulation for SBR compounds (ASTM D3186)

No.	Ingredients	Amount (phr)	Supplier
1	Styrene butadiene Rubber	100	Goodyear
2	Carbon Black N330	40	Cabot
3	Zinc oxide	3	Schill Seilacher
4	Stearic Acid	1	Schill Seilacher
5	TBBS * ¹⁾	2	Schill Seilacher
6	Sulphur	2	Schill Seilacher

*1) N-Cyclohexyl-2-benzthiazyl sulphenamide

Table 3.2 Experimental formulation for NR compounds ASTM (D3184)

No.	Ingredients	Amount (phr)	Supplier
1	Natural Rubber	100	Malaysia
2	Carbon black N330	40	Cabot
3	Zinc Oxide	5	Schill Seilacher
4	Stearic Acid	1	Schill Seilacher
5	CBS * ²⁾	1	Schill Seilacher
6	Sulphur	2.5	Schill Seilacher

* 2) N-Tert-Butyl-2-Benzothiazole sulphenamide

3.2.2 Mixing and operating conditions

A Francis Shaw K1 Internal mixer (chamber volume 5.5 litres) was used for the mixing. The conditions were as follows.

Rotor speed was 30, 50, 70 rpm.

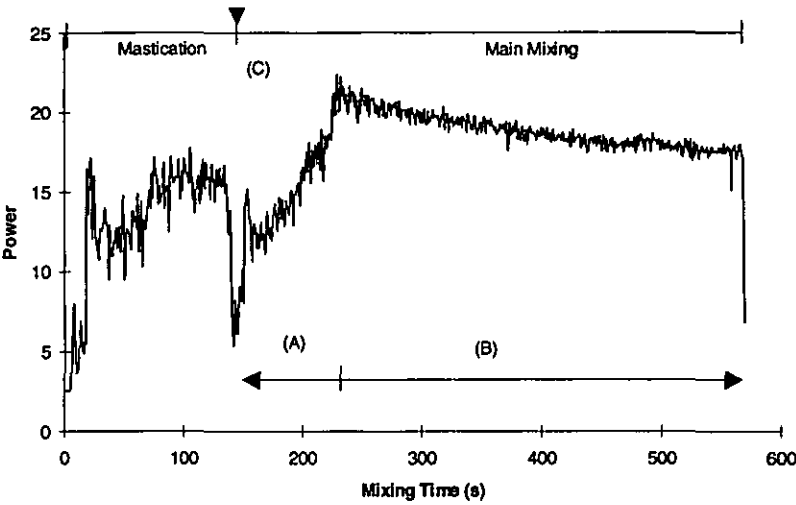
Fill factor was 0.5

Circulating cooling water temperature of rotor was 40°C

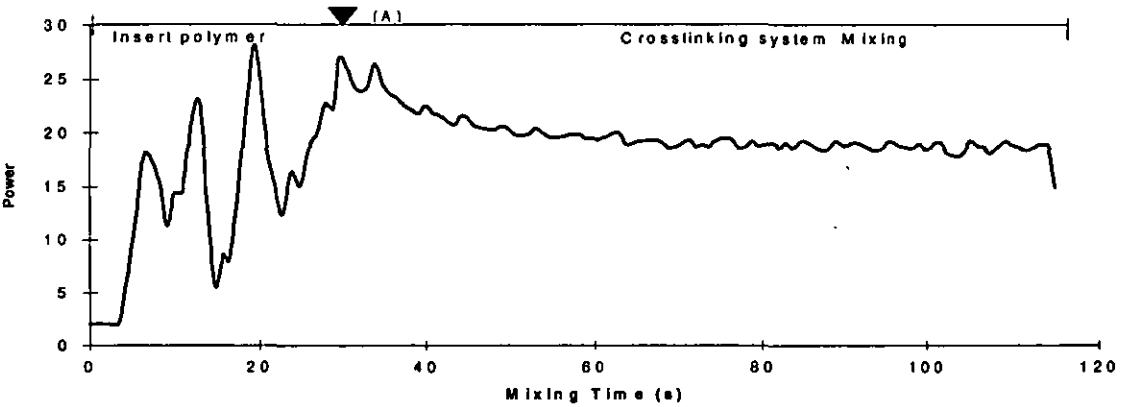
The mixing pattern was two stage mixing.

The main reason for using two stage mixing was to avoid scorch (premature cross linking) problems during mixing. To change the state of mix of carbon black, various mixing times after adding the carbon black into the polymer were adopted (90, 180, 300, 360, 420 seconds) for three rotor revolution speeds (30, 50, 70 rpm). The **Figure 3.1** shows the

mixing sequence schematically. At first (Figure 3.1 (a)), polymer was supplied into the internal mixer and masticated for two minutes. Then the carbon black was added and mixed for the selected time to obtain samples which had various states of mix. When a certain mixing time had passed, the rubber compounds were discharged from the mixer and passed once through the two roll mill to minimise any further mixing. These rubber compounds were left at room temperature for two hours to cool them down to room temperature.



(a) First stage mixing. (A), (B) and (C) in the graph stand for Incorporation, Dispersion and Carbon black addition, respectively.



(b) Second stage mixing. (A) in the graph stands for the addition of crosslinking system.

Figure 3.1 Mixer power trace showing mixing process sequence.

Then the mixed compounds were cut into strips for re-feeding into the mixer for the second mixing. At the beginning of the second stage (**Figure 3.1 (b)**), sulphur and accelerator were added and mixed for one and half minutes. After the second mixing stage, the mixed rubber compounds were passed once through the two roll mill.

3.2.3 Nomenclature of test samples

Table 3.3 shows the nomenclature of samples. The sample is classified into six categories based on both the formulation and the rotor revolution speed (**Table 3.3 (a)**). Furthermore, each category is classified into five series based on mixing time (**Table 3.3 (b)**). Therefore, tested samples are labelled by being based on both the formulation and the total rotor revolutions (the multiple of rotor speed and mixing time).

Table 3.3 Nomenclature of test samples.

(a) Sample name and its matrix polymer.

Sample name	Polymer	Rotor speed (rpm)
AGL	NR	30
AGM	NR	50
AGN	NR	70
AGO	SBR	30
AGP	SBR	50
AGQ	SBR	70

(b) Sample number and its mixing conditions.

Sample	Number	Rotor Speed (rpm)	Mixing Time (min)	Total revolution (cycles)
AGL	1	30	1.5	45
AGL	2	30	3.0	90
AGL	3	30	5.0	150
AGL	4	30	6.0	180
AGL	5	30	7.0	210

3.2.4 Fourier transform analysis of the mixer power chart

An example of a power chart, which was taken during mixing, is shown in **Figure 3.1**. The duration after adding carbon black and before dumping in the first stage (**Figure 3.1 (a)**) was used to characterise the mixing behaviour of the carbon black with the matrix polymer.

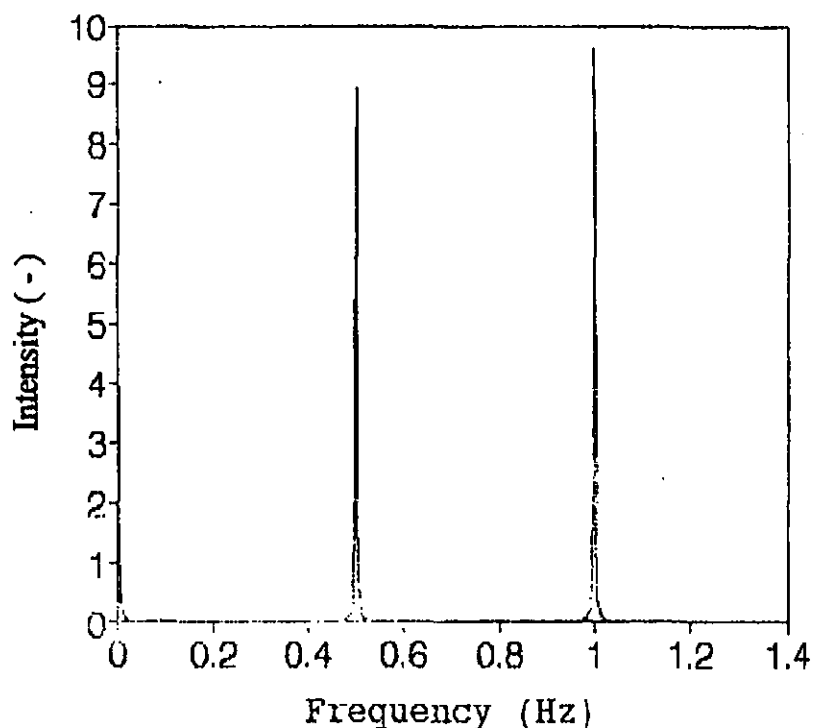


Figure 3.2 Power spectrum of a mixer power trace obtained by the Fourier transform (rotor speed is 30 Hz).

The Fourier Transform (FT: see **Appendix 2**) was applied to the power charts and the results were analysed by using fractal method. In this experiment, the Maximum Entropy Method (MEM, see **Appendix 3**) was used to obtain precise data. **Figure 3.2** shows the result of the Fourier transform analysis. There are two types of peak in the chart. One corresponds to the rotation of the tips on the rotor (**Figure 3.3**). The other peak (in the zero area) corresponds to the total shape of the power chart and this peak was used to obtain a fractal dimension to characterise the mixing behaviour.

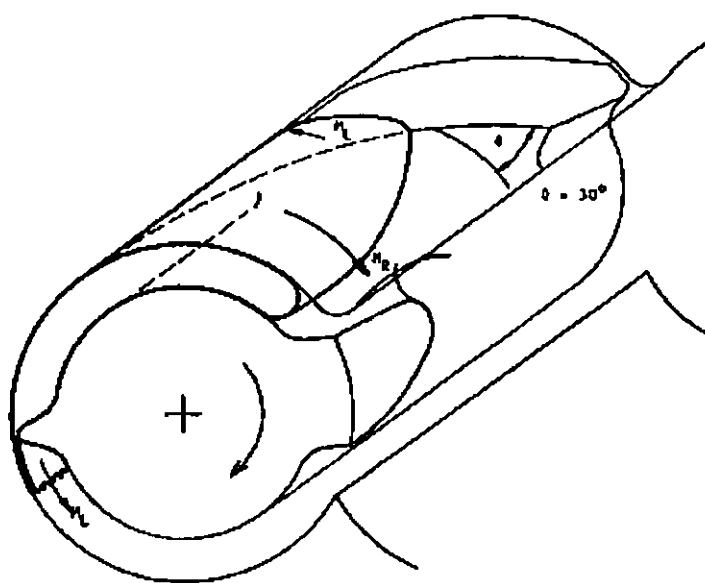


Figure 3.3 A simplified schematic of flow in the mixing chamber of an intermeshing rotor internal mixer. ¹⁾

3.2.5 Measurement of electrical resistance of unvulcanised compounds

Electrical resistance was measured to correlate the fractal method for evaluating the state of mix to existing data. This electrical resistance measurement is a widely accepted method for evaluating the state of mix of carbon black. The measurements were carried out by Bridgestone Corporation (Kodaira, Tokyo). The main ideas and construction of the apparatus are based on Boonstra's method. ²⁾

"Boonstra utilised a coaxial probe that was specifically designed for dispersion analysis of rubber compounds. **Figure 3.4** and **Figure 3.5** shows schematic details of the apparatus. The rubber sample is compressed within a stainless-steel cylinder using a piston. The wall of the cylinder forms the ground or negative electrode, and the positive electrode is a small metal rod down the centre of the tube, which is insulated from the cylinder by a PTFE disc. The depth of the ring-shaped cavity at the bottom, which houses the specimen, is 2.00 mm. The optimum air pressure for the piston (100 mm diameter) is 210 kPa.

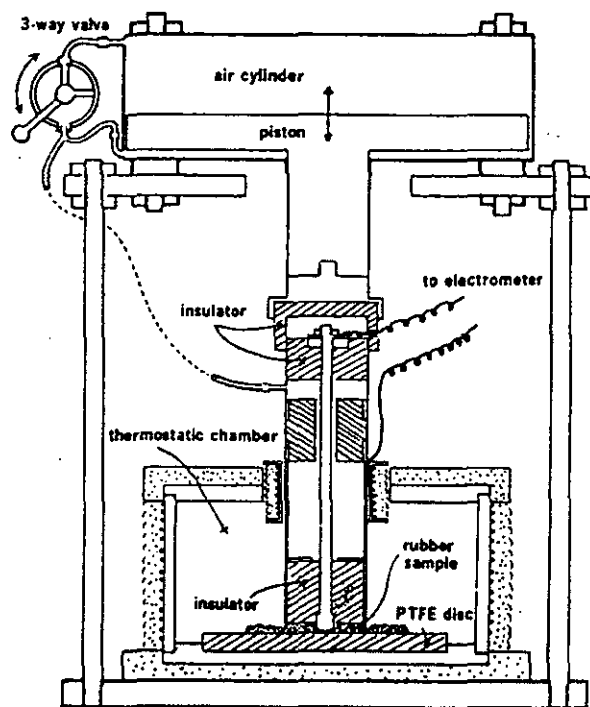


Figure 3.4 Schematic of the coaxial probe arrangement with air pressure mechanism ²⁾

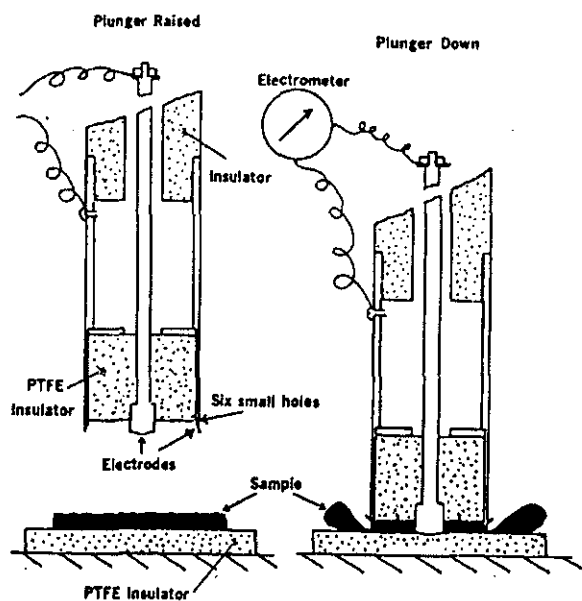


Figure 3.5 Details of the coaxial probe. ²⁾

Resistivity is measured at a time of 60 s after the piston reaches its lowest point (1 to 2 s) at a temperature of 60 °C. Resistivity decreases significantly in the direction of higher temperature. Therefore, the temperature of the test specimen is controlled quite closely (± 1 °C). ”³⁾

Rectangular samples of unvulcanised rubber (50 × 50 × 20 mm) were cut out from the mixed rubber compound by means of a knife or scissors. Before the electrical resistance measurements, the sample was placed in a heating oven at 60 °C for 30 minutes to ensure a temperature equilibrium in the bulk of the sample. During measurements, three readings were taken at 15, 30 and 60 seconds after starting the test to check the resistance decrease but only the value taken at 60 seconds was used in this experiment.

3.2.6 Measurement of curing characteristics

A Wallace Precision Cure Analyser (Wallace PCA) was used for measuring the curing behaviour of mixed rubber compound. The operating conditions are listed in **Table 3.4**.

Table 3.4 Measuring condition of curing behaviour

Parameter	Condition
Temperature (°C)	150
Pressure (kPa)	600
Frequency (Hz)	1.7
Strain (%)	0.14

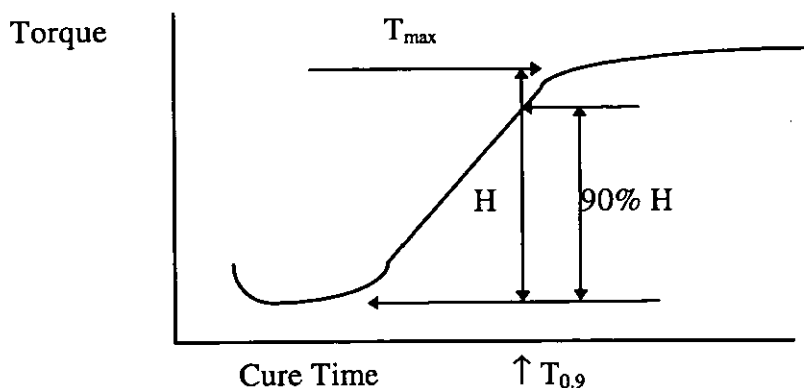


Figure 3.6 A schematic cure curve. H is defined as the difference of maximum and minimum torque. $T_{0.9}$ is defined as the time to reach $0.9 \times H$ torque.

By using this machine, the data about maximum (T_{max}) and minimum (T_{min}) torque, and curing time at $T_{0.9}$ (time to 90% of maximum crosslink density) can be obtained. $T_{0.9}$ data is used to determine the cure time for the following vulcanisation process. One schematic example is shown in **Figure 3.6**. $T_{0.9}$ is defined as a time to reach 90% torque of the difference between the maximum and minimum torque (H).

3.2.7 Moulding

Vulcanisation was carried out by using a hydraulic press. Slab sheets with 2 mm thickness were prepared for the experiments. **Table 3.5** shows the moulding conditions. The cure time depends on each sample. $T_{0.9}$ (90% cure time) cure was carried out based on the measurements of curing characterisation mentioned above.

Table 3.5 Moulding conditions

Parameter	Condition
Temperature ($^{\circ}\text{C}$)	150
Pressure (MPa)	9.8

3.3 Measurements on rubber samples

3.3.1 Carbon black dispersion analysis

The box counting method was used to measure the fractal dimension of carbon black dispersion. **Figure 3.7** shows the procedure.

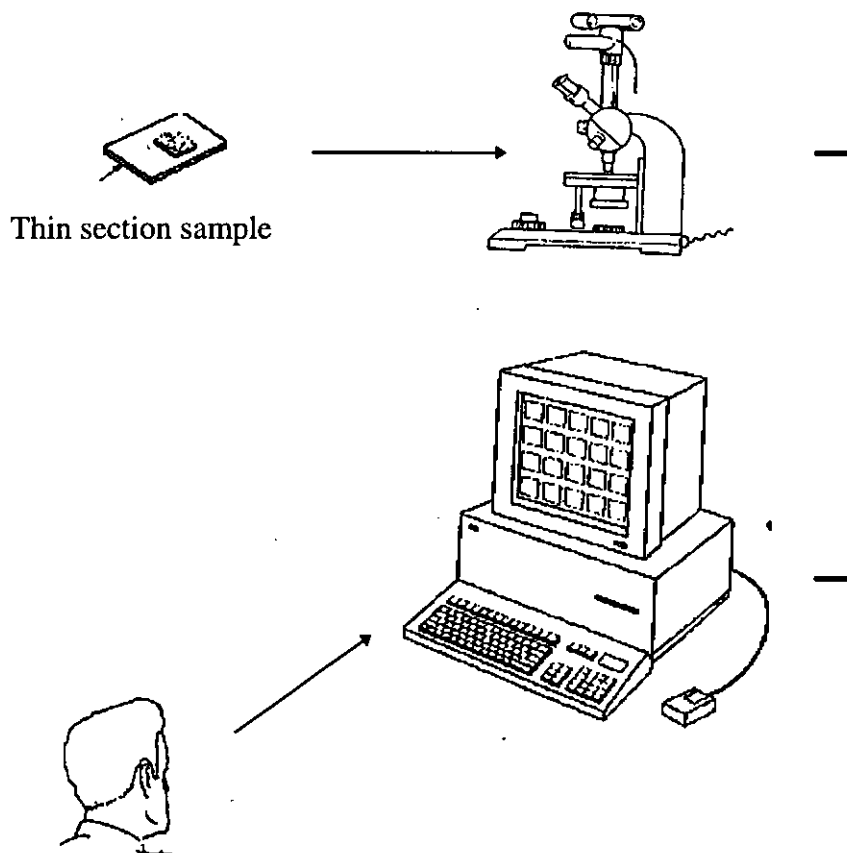


Figure 3.7 Schematic explanation of experimental procedure for evaluating the state of mix of carbon black.

By using a microtome, thin section samples from the vulcanised rubber sheet moulded for the tensile test were prepared³⁾ and they were put on to a slide glass. A light microscope and video system were then used to magnify the sample. Total magnification was 720. Four transparency sheets, which have different mesh sizes, were used to count the boxes (lattices on the transparency sheet). The box sizes on the transparency sheets were 1, 2, 3

and 4 cm. These transparency sheets were put on the CRT screen and the boxes which contained carbon black agglomerates were identified visually and subsequently counted by a software package named VIDS V (Sunptotics, UK).

3.3.2 Measurements of the fracture surface of tensile samples

Figure 3.8 shows a schematic procedure for measurements of the fracture surface.

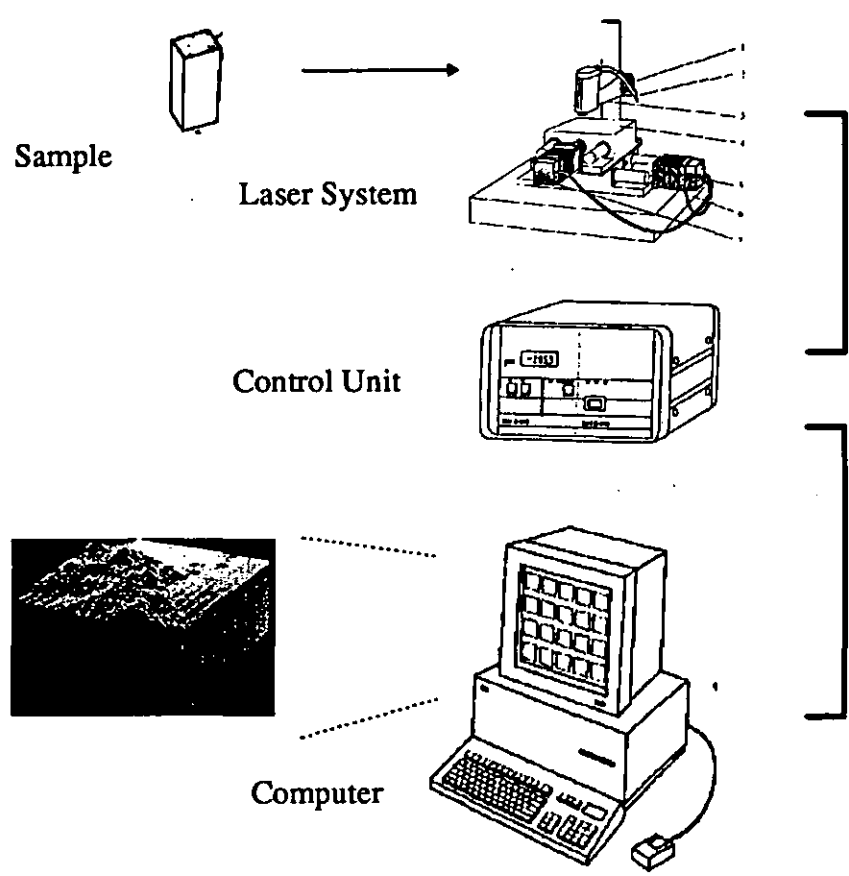


Figure 3.8 Rodenstock RM 600 laser stylus ⁴⁾

Fracture surfaces of tensile test samples were measured by the RM 600 Laser stylus, made by Rodenstock. This machine comprised two units, a laser system and a control unit. The control unit works as a digitiser for connecting the laser unit to a computer. The laser system consisted of two parts.

① The horizontal position control unit : A platform is shifted by two stepping motors, which enable controlled movements in the order of 0.01 mm. A rubber sample was fixed on this measuring platform. The control unit operated the motors and detected the horizontal positions.

② Roughness detection unit : A laser sensor detected the roughness on the sample surface with a resolution of $\pm 1\mu\text{m}$. Then, the computer displayed the measured roughness on a screen.

The computer was able to operate many mathematical treatments with the software package supplied by Rodenstock.

Two types of surface measurements were carried out.

(1) Two dimensional measurement

This method was used for both two dimensional Fourier analysis and roughness measurements with a new procedure proposed in this research thesis (section 4.3.5). These experiments were carried out by using the software package (mathematical package) to obtain a whole picture of the fracture surfaces ⁹⁾. During the experiments, 2.5×2.5 mm areas of sample surfaces were detected with the $10\mu\text{m}$ mesh. Sometimes a smaller area in the measured surface was used for the further experiments to avoid an apparent scratch on the sample surface. The software package corrected for any error due to the sample not lying flat on the platform. By this procedure, a true roughness could be detected which roughness was used for two dimensional Fourier analysis.

(2) One dimensional measurement

A line measurement was used for obtaining suitable data to detect the fractal dimensions of the fracture surface. For this purpose, a line detection of the surface roughness was carried out at intervals of $10\mu\text{m}$ on at least 10 positions to obtain a statistical mean value. Again, each line spectrum had a resolution power of $10\mu\text{m}$ order. These measured data were stored by a computer and used later for the fractal analysis by using the maximum entropy calculation program (refer to Appendix 3).

In both experiments, the fracture surfaces of tensile test specimens were measured. This enables us to correlate the fractal dimension to tensile strength and the state of mix.

3.3.3 Measurement of tensile strength

The vulcanised samples were cut into dumbbell shapes by using a standard die cutter according to BS 903 type 1. The stress strain tests of these samples were carried out with a Hounsfield 500L testing machine at room temperature. This machines detects the tensile strength and the elongation at break, and five moduli at any extension ratios.

3.3.4 Measurements of viscoelastic and dynamic properties

Rheolometer Solid IR (Toyo Seisakusyo, Japan) in the Bridgestone Corporation was used to measure these properties. The operating conditions were as follows.(Table 3.6)

Table 3.6 Measuring condition of viscoelastic properties.

Sample dimension (mm)	20 × 4 × 2
Rate of Temp. Increase (°C/min)	3
Temp. range (°C)	-70 to 70
Frequency (Hz)	50
Amplitude (%)	0.1(<0°C) or 1 (>0°C)

Two types of viscoelastic properties were measured. An example of the temperature and strain dependence of samples is shown in Figure 3.9 and Table 3.7 respectively.

(1) The temperature dependence of dynamic modulus. This measurement was carried out to check the general properties of rubber samples. The important point is the transient region from glassy state to rubber-like state. It is well established that the slope reflects the crosslink density including temporary entanglements and physical hindrance²⁾. Therefore, the slope reflects the state of mix of carbon black because the dispersed carbon black contributes to temporary or permanent crosslinks.¹⁰⁾

(2) The strain dependence (the Payne effect). This measurement was carried out to evaluate the state of mix, but it is rather difficult to compare the original data between samples because even if the difference among samples is merely the state of mix, it results in a difference of modulus through the crosslink density difference. One way to compensate for such differences and extract only the effect of the state of mix is to use

normalised data. In this case, according to Payne ⁶⁾, the strain dependence is defined as a ratio of the infinite modulus. (Equation 3.1)

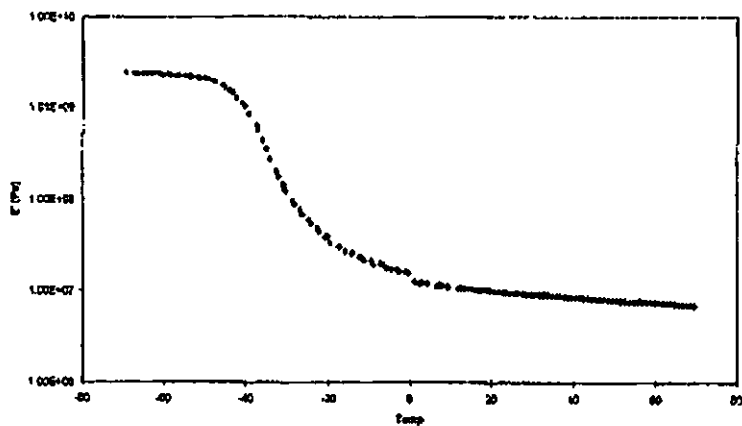


Figure 3.9 Temperature dependence of storage modulus. (AGL4)

Table 3.7 The dynamic properties of rubber samples. (AGL4)

Strain	E' (MPa)	E'' (MPa)	Tanδ
0.10	1.19×10 ⁷	1.34×10 ⁶	0.113
0.19	1.18×10 ⁷	1.49×10 ⁶	0.126
0.29	1.15×10 ⁷	1.60×10 ⁶	0.140
0.48	1.12×10 ⁷	1.73×10 ⁶	0.155
1.02	9.87×10 ⁶	1.72×10 ⁶	0.174
1.98	9.11×10 ⁶	1.66×10 ⁶	0.183
2.95	8.53×10 ⁶	1.52×10 ⁶	0.179
3.93	8.08×10 ⁶	1.40×10 ⁶	0.174

$$Z = 100 \times (E'_{\max} - E'_{\min}) / E'_{\min}$$

Equation 3.1

Z

: The Payne effect (%)

E'_{\max} , E'_{\min}

: Maximum and minimum modulus respectively

There is an alternative way to evaluate the same effect instead of using E'. For example, E'' or tanδ can be used instead of E'. But the above method is the simplest way to correlate the test data to the other existing data ⁷⁻⁹⁾.

3.3.5 Thermal properties

Figure 3.10 shows the procedure to measure the heat diffusivity. For the experiments, the AGL sample was used. A slab sheet was prepared by using the special mould (see the following explanation) at first .

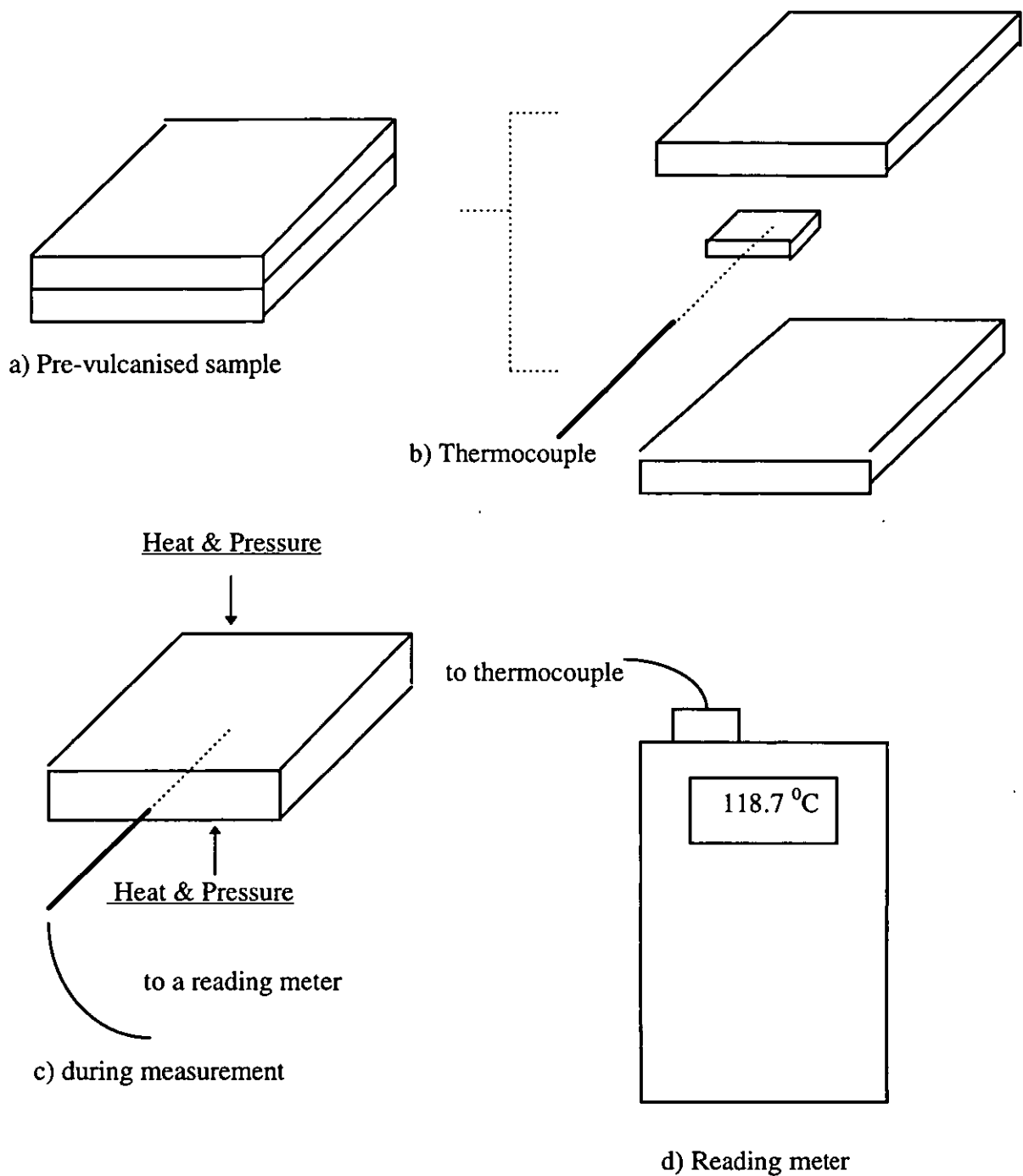


Figure 3.10 The schematic explanation about the heat transfer measurements.

The dimension of the mould is $12 \times 12 \times 1.5$ cm and it has a small hole to allow a thermocouple to be put into its centre. The slab sheet was cut into two pieces and an unvulcanised rubber sample was put in the centre of the slab. Then the ensemble ; which include the slab sheet, a measuring sample, the mould and thermocouple at the centre ; was put in the hydraulic press to carry out the temperature measurement. Vulcanisation temperature was set at 170°C and the pressure was 9.8 MPa. During the vulcanisation, the temperature of the rubber sample was measured using the thermocouple and a reading detector, over a period of 20 minutes. The mathematical model to analyse the data is given in section 2.2.3.

3.3.6 Bound rubber

Many researches ¹¹⁻¹³⁾ reveal that bound rubber has a large influence on vulcanised rubber properties. To correlate the mixing time to bound rubber, NMR (nuclear magnetic resonance) analysis was applied here. Concerning this experiment, Bridgestone Corporation supplied experimental facilities. The NMR machine was a PC90 produced by Bruker. Experimental temperature was 40°C . Solid echo pulse sequence ¹⁴⁻¹⁶⁾ having a 6 μs interval was used to obtain Free Induction Decay (FID) from NMR. A FID was recorded for one second and stored by a digitizer. A computer program was used to analyse the stored FID. Non linear least squares fitting was used to determine the components of the FID.

One example of the non linear least squares fitting is shown in Figure 3.11. The FID consists of the three types of responses shown below ;

$$M(t) = a \exp\left(-\frac{t}{t_{2a}}\right) + b \exp\left(-\frac{t}{t_{2a}}\right) + c \exp\left\{-\left(\frac{t}{t_{2b}}\right)^2\right\} \quad \text{Equation 3.1}$$

where M : Intensity of FID signal
 t : Time
 a,b,c : The ratio of compound components
 t_{2a}, t_{2b} : Relaxation time of each component

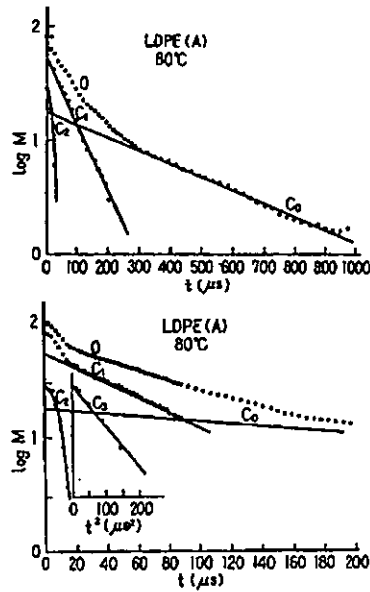


Figure 3.11 An example of FID of LDPE sample ¹⁶⁾

The first and second terms on the right hand side are Lorentz type decay and correspond to the slow relaxation movement of the compound component. The third term corresponds to Gaussian type decay and corresponds to the quick relaxation component. From a physical point of view, the former corresponds to the bulk rubber and crosslink segments and the latter corresponds to bound rubber around carbon black. In the case of rubber compounds, it is necessary to detect the FID for more than 30 seconds to decompose the first and second term in the **Equation 3.1**. In other words, it is impossible to decompose bulk rubber segments and crosslinks from the FID by recording it for only 1 second. Thus, the FID is decomposed into two components during this experiment.

References

- 1) P. K. Freakley, S. R. Patel, Polym. Eng. Sci., 27 (18), 1358 (1987)
- 2) A. I. Medalia, Rubb. Chem. Tech., 53, 48 (1980)
- 3) B. B. Boonstra, Rubb. Chem. Tech., 195, 50 (1977))
- 4) Rodnestock, "User manual RM600 Laser Stylus"
- 5) Rodenstock, "User manual of Laser Stylusl"
- 6) A. R. Payne, J. Appl. Polym. Sci., 7, 873 (1963)
- 7) G. Kraus, "Science and Technology of Rubber", Academic Press (New York, 1978)
- 8) K. A. Burgess, F. Lyon, W. S. Stoy, "Encyclopaedia of Polymer Science and Technology", Wiley Interscience (New York, 1965)
- 9) L. Mullins, Rubb. Chem. Tech., 42, 339 (1969)
- 10) G. Kraus, "Reinforcement of Elastomers", Wiley Inter science (New York, 1965)
- 11) D. Rivin, J. Aron, A. I. Medalia, Rubb. Chem. Tech., 41, 330 (1968)
- 12) W. F. Watson, Ind. Eng. Chem., 47, 1281 (1955)
- 13) J. B. Donnet, G. Heinrich, G. Riess, Rev. Gen. Cauotch. Plas., 38, 1803 (1961):
41, 519 (1964)
- 14) T. C. Farrar, E. D. Becker, "Pulse and Fourier Transform NMR", Academic Press (1971)
- 15) A. Abragam, "The Principle of Nuclear Magnetism", Oxford Univ. Press (1961)
- 16) K. Fujimoto, T. Nishi, Nihon Gomu Kyokaishi, 45 (7), 640 (1972)

Chapter 4

Results and Discussion

4.1 Introduction

In this chapter, the validity of fractal applications to rubber technology is discussed in the light of the experimental results. The topics and purposes ;

(1) General properties.

The purpose of this section is to check the validity of tested samples. Tensile strength and viscoelasticity were utilised.

(2) Fractal applications.

Fractal analysis is applied to rubber mixing, the state of mix, fracture surface and their relationships. These discussions explore the applicability of fractals to rubber properties.

(3) The influence of the state of mix on rubber properties.

The influence of carbon black dispersion on thermal properties and bound rubber, which have not been discussed with the relation of the state of mix quantitatively before, are discussed.

For simplicity, raw data is summarised in the Appendices, so only essential data is shown.

4.2 General properties of tested samples

A discussion of the general properties of samples tested has two purposes.

(1) To check the validity and reliability of the measurements of the tested samples.

The experimental results are discussed here and their value or trends in relationships to existing data and experience are considered.

(2) To introduce a normalising method due to Clarke and Freakley¹⁾.

Clarke and Freakley explored the importance of carbon black dispersion and suggested a normalising method for the evaluation of rubber properties as they are influenced by the state of mix. Their method is utilised in the following discussion to identify trends in the physical properties of rubber compounds.

4.2.1 Tensile strength

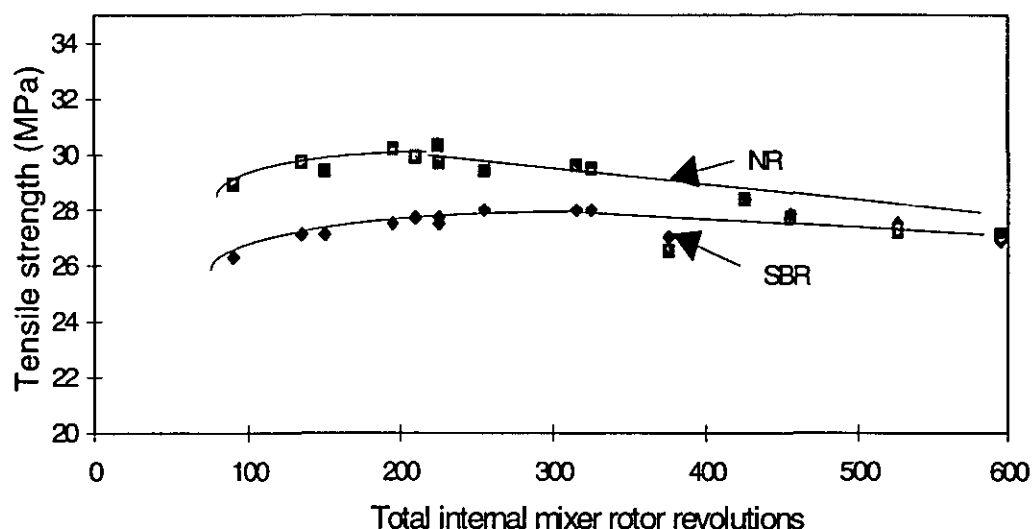


Figure 4.1 A normalised graph of tensile strength at break, where total internal mixer rotor revolutions is a product of rotor speed and mixing time.

(Ref. 3.3.3)

Figure 4.1 shows a normalised graph of the tensile strength of samples. Results for two types of compounds, NR and SBR, are reported in this thesis. It should be noted that the formulations of NR and SBR samples are different but the vulcanisation was regulated by adopting the best cure time in all compounds. The shapes of the curves in **Figure 4.1** are typical and are due mainly to two phenomena.

(1) The nature of the matrix polymer.

Generally speaking, the NR compound has a higher tensile strength than the SBR compound because of the elongational effect, such as crystallisation. This tendency becomes more apparent in high temperature environments. At higher temperatures, crystallisation is impossible but the elongational alignment of the polymer molecules remains more apparent in the NR compound than in the SBR compound.

(2) The dependence of tensile strength on mixing conditions.

In a short mixing time or where the total rotor- revolution number is low, the carbon black dispersion is not good. This results in a low tensile strength at break which is clearly demonstrated by **Figure 2.29** in section 2.2.3.2. As the state of mix is improved, the tensile strength improves and reaches a maximum value, after which it decreases due to the mastication effect becoming more dominant than the improvement of the state of mix. This phenomenon is more apparent with higher molecular weight compounds than those with lower molecular weight. **Figure 4.1** shows the phenomenon clearly. SBR is more resistant to mastication than NR and the NR compound has a higher molecular weight than the SBR sample. Therefore, the decay of tensile strength of the NR compounds beyond the maximum is more pronounced than for the SBR compound.

The experimental samples exhibited properties which were in broad agreement with those previously described in the literature ²⁾ which confirms the validity of the results from these experiments.

4.2.2 Viscoelastic properties

Viscoelastic properties are very useful to judge the quality of rubber samples for the following reasons.

- (1) A variety of properties can be derived from a single experiment.
- (2) The relationship between viscoelastic properties and molecular structure is well established ³⁾.

Thus viscoelastic properties are examined here to assess the behaviour of samples at different states of mix and to make comparison with existing data.

4.2.2.1 Temperature dependence

Figure 4.2 shows the temperature dependence of an NR sample. There are three distinct regions in the graph :

- (1) The first region, found at very low temperatures, is where the sample takes on a glassy state.
- (2) The second region, found at high temperatures, is where normal polymers exhibit a rubber-like state.

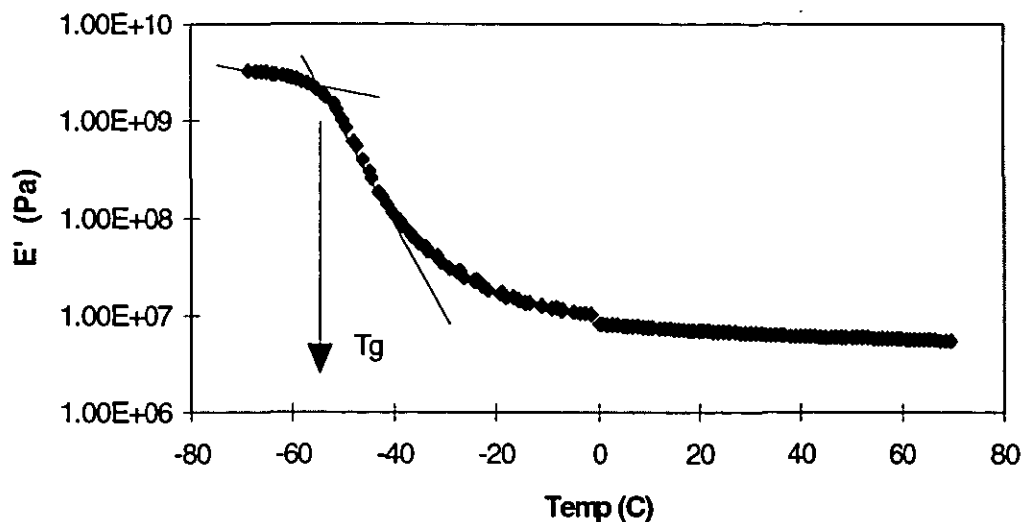


Figure 4.2 Temperature dependence of viscoelastic property of a NR (AGO5) sample. (Ref. 3.3.4)

(3) A third transition region is found between the two regions already described. This transition region reflects the state of mix of carbon black because its slope is a function of crosslinks and entanglement (here entanglement means temporary entanglement of polymer chains, phantom crosslinks and polymer segments physically trapped by carbon black). Changes of the state of mix affect the relaxation spectrum, resulting in a change of the slope in temperature dependence described by the Williams- Landel- Ferry equation (WLF) ³⁻⁶. Generally, a pure gum rubber has a steep slope and carbon black filled compounds have a shallow slope because of the increased range of the relaxation mechanism. The angle of a slope also depends on the state of mix. **Figure 4.3** shows such behaviour.

There are two important features in **Figure 4.2** ;

- ① A glass transition temperature.

It depends on molecular structure, weight and ingredients in the compounds, but is mainly controlled by molecular structure and it is a well defined characteristic of each compound. In the case of NR compounds, it is well known that the glass transition temperature is round about $-55\text{ }^{\circ}\text{C}$, with small variations ²⁻⁴⁾. As can be seen from **Figure 4.2**, the NR samples for this project take almost the same value as in reported data. The glass transition temperature (T_g) is defined as a transition point from glassy state to transient region ²⁻⁴⁾ and confirms the validity of the results reported here.

② A discontinuity at zero degrees (the Payne effect).

The discontinuity arises from the experimental conditions required to obtain a maximum response from the equipment. At this temperature, the strain was changed from 0.1 to 1.0 %. The theory of rubber elasticity ⁷⁾ shows the following relation (**Equation 4.1**). The modulus has to be constant according to **Equation 4.1** because there is no strain factor in the equation. The **Figure 4.3** did not agree with the **Equation 4.1**. The conflict is known as the Payne Effect. The tested sample shows a characteristic typical of existing data and again, confirms the validity of the results.

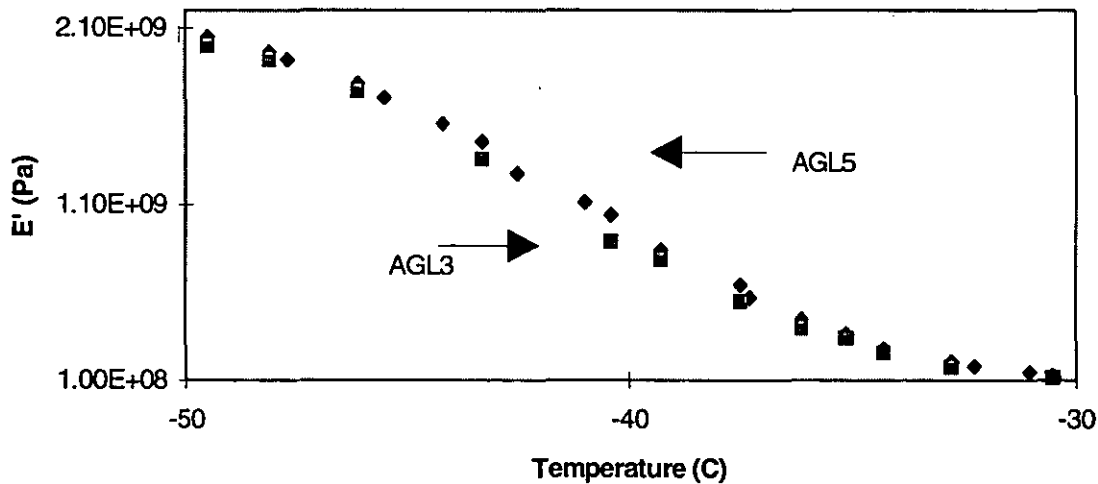


Figure 4.3 The influence of the state of mix on viscoelasticity. Badly mixed sample (AGL3) has a small E' than the better mixed compound (AGL5). (Ref. 3.3.4)

$$E = \nu RT(1 - 2 M_c / M_n)$$

here ν : Crosslink density (mol / cm^3)

R : Gas Constant ($8.317 \text{ J} / \text{mol deg}$)

T : Absolute Temperature

M_c : Mean Molecular Weight of Segments

M_n : Mean Molecular Weight of Matrix Polymer

Equation 4.1

4.2.2.2 The Payne Effect

The Payne Effect reflects the way in which the filler-network-structure change affects the various strain ratios.

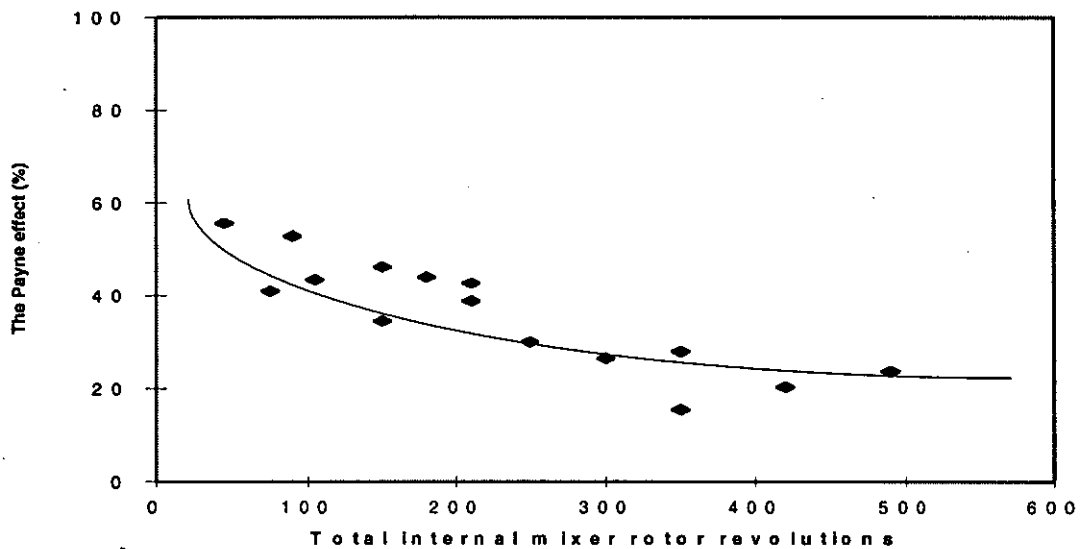


Figure 4.4 A result of the Payne Effect (SBR (AGL, M, N) sample). (The definition of the Payne Effect here is given in Equation 3.1)

Figure 4.4 shows results for the SBR samples. The relationship between the total rotor revolution number and the Payne Effect is obvious from the figure. This relationship arises for the following reasons :

“This behaviour is due to breakdown of the agglomerates formed as the primary product of the mixing. Immediately after, and even during (mixing), their formation (incorporated carbon) these concentrated agglomerates are subjected to high shear forces that tend to break down again into smaller and smaller unit the final dispersion is reached. This picture can be considered as representing the general process of mixing of particulate filler with a high-viscosity vehicle, although the effect will not be so evident with coarse fillers.” ²⁾

Figure 4.5 shows a normalised data of NR compounds plotted against the accumulated rotor revolution number. The mechanism and reasoning for the SBR samples are also applicable for this graph.

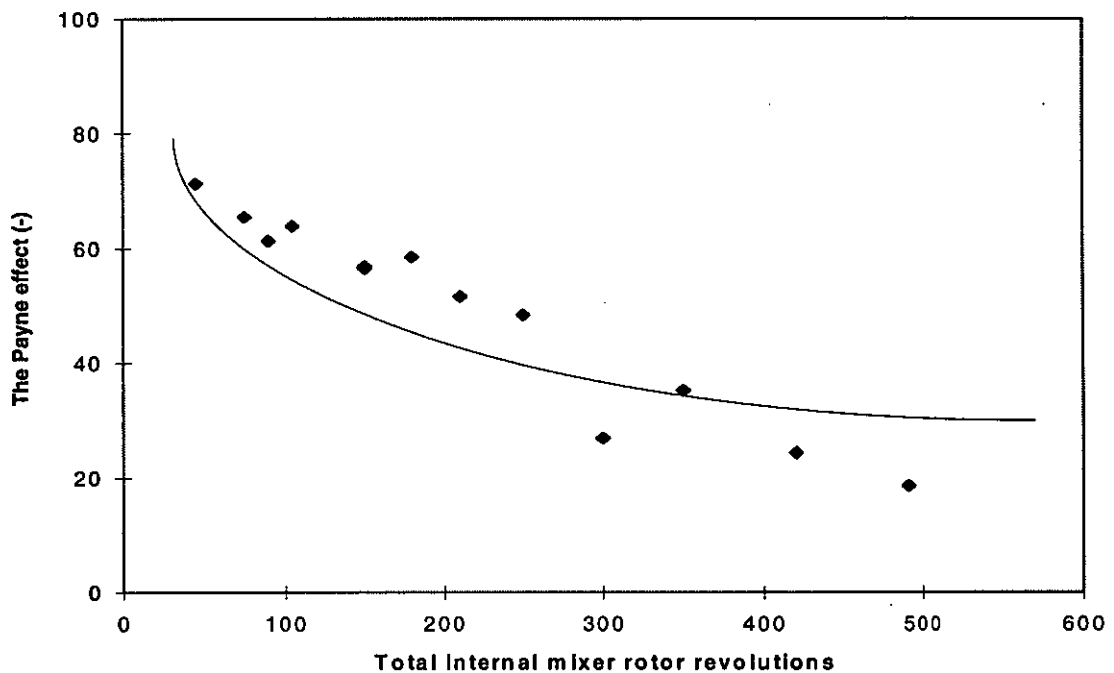


Figure 4.5 A normalised graph of the Payne effect (NR(AGO, P, Q) samples).

(Ref. 3.3.4)

By comparing Figure 4.4 to Figure 4.5, it can be seen that the Payne Effect of the SBR sample is smaller than for the NR sample. It corresponds to the shorter BIT (black incorporation time) and higher viscosity of NR compared with SBR. The shorter the BIT, the more time compounds have to develop the breakdown of the agglomerates because the shorter BIT means a longer carbon black dispersion process in a fixed mixing time. The higher the viscosity, the more extensively carbon black dispersion develops because the higher viscosity means bigger shear or elongational force during mixing. Thus the strain dependence becomes bigger when it is compared to similar mixing conditions. It could be reasonable to hypothesise that if the Payne Effect is compared at the same state of mix, its value has to be almost the same.

It can be concluded that the Payne Effect can be used as a measure of the state of mix because of the mechanism shown here. This data will be correlated to other measurements in later sections.

4.3 Fractal aspects of rubber properties

4.3.1 Fractal analysis of the mixer power trace

Three topics will be discussed in this section.

- (1) The validity of the fractal analysis, checked by comparing it to existing data.
- (2) The relationship between mixing time and fractal dimensions. Here, a normalising method is discussed for relating the mixing process to the fractal concept.
- (3) Comparison of the mixing behaviour of SBR and NR compounds.

The validity of fractal application to the analysis of a mixer power trace

A mixer power trace is one type of power spectrum. Therefore, the fractal method mentioned in section 2.1.5 is applicable to its analysis. The relationship between the power of a mixer power trace and frequency is given by **Equation 4.2**.

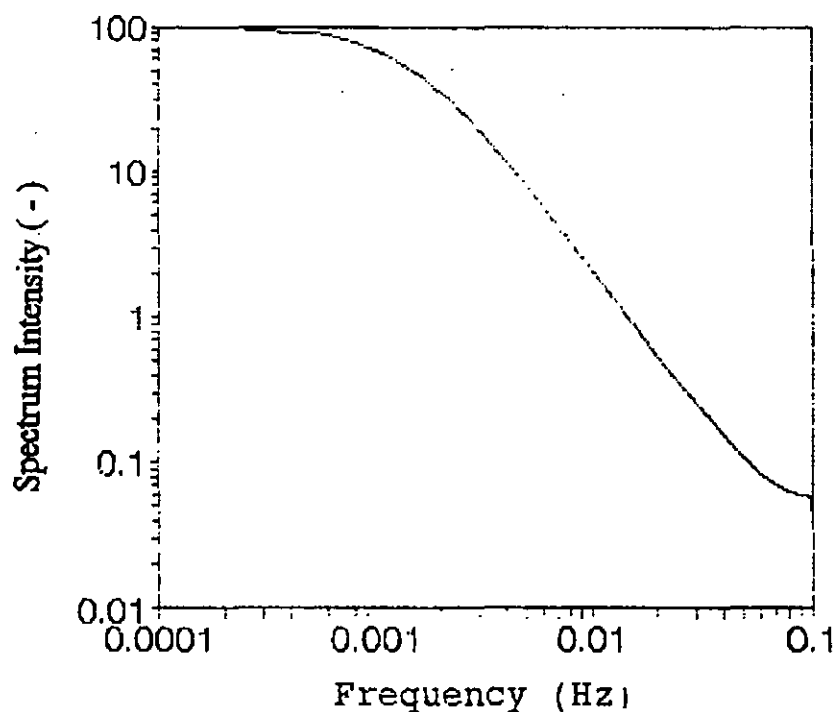


Figure 4.6 Determination of fractal dimension. From the slope of this graph, the fractal dimension is calculated. (Ref. 3.2.4)

$$S(f) \propto f^{-\beta}$$

$$D_f = 5 - 2\beta$$

Equation 4.2

- S : Intensity of power spectrum
- f : Frequency
- β : A power
- D_f : Fractal dimension

Figure 4.6 demonstrates one example of the log - log plot to decide the fractal dimension from the power trace of the mixing process. (**Figure 4.6** is a re-scaled graph of the zero region in **Figure 3.2**) From the slope of the figure, the power β is decided at first, then the fractal dimension is calculated from **equation 4.2**. In this case, the value is,

$$D_f = 1.58$$

Equation 4.3

Some literature is available to check the validity of the data. Nishimoto ⁸⁾ reported the fractal dimension as ranging from about 1.1 to 1.6. As shown in **section 2.2.3**, the flow pattern in a mixer is mainly dominated by a recirculation (one type of turbulence, see **Appendix 7**) in front of the rotor tip. Many reports have been published recently about the fractal character of turbulence. Lovejoy ⁹⁾ reported one such quantity. He analysed the fractal dimension of a cloud. (The shape of the cloud is a fractal because of the turbulence in the atmosphere.) His measurement gives a fractal dimension for the cloud as

$$D_f = 1.35$$

Equation 4.4

The figure is in broad agreement with the result obtained in this study. Unfortunately, a procedure to derive a fractal dimension from the basic equation (Navier - Stokes Equation) of hydrodynamics has not been carried out, so the data obtained here is justified only on the basis of existing data.

As a conclusion to this subsection, it can be said that the fractal analysis adopted here gives a reasonable value by comparison with existing data.

Exploration of the relationship between mixing and a fractal dimension

The fractal dimensions of mixer power traces are shown in **Figure 4.7** as a function of mixing time.

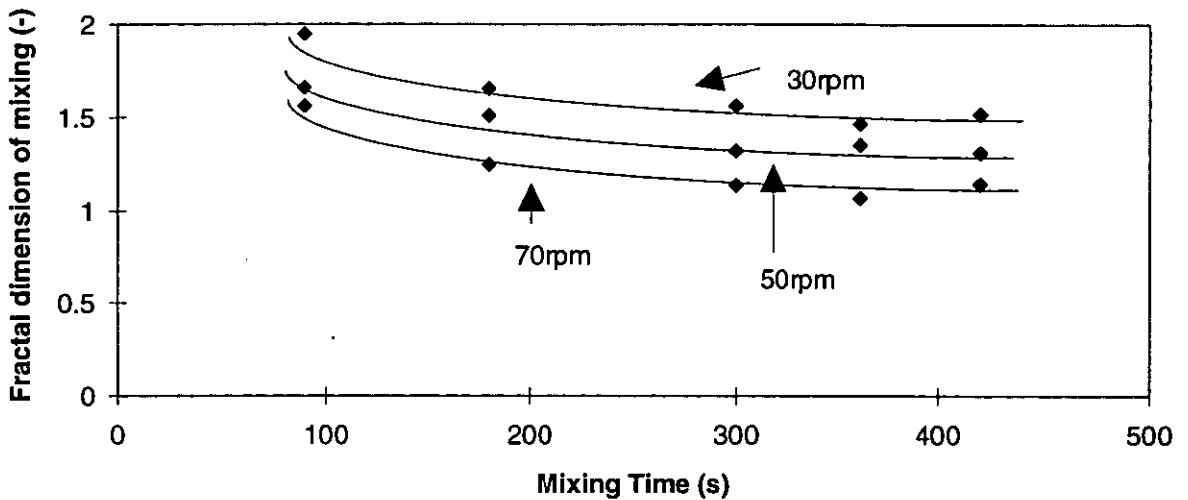


Figure 4.7 The relationship between mixing time and fractal dimensions of the power trace (SBR samples). (Ref. 3.2.4)

There are two features in the graph.

- (1) The relationship between mixing time and fractal dimension. The longer the mixing time, the smaller the fractal dimension.
- (2) The second point is that the greater the number of revolutions, the smaller the fractal dimension when compared at a certain mixing time.

These two features can be integrated by introducing a normalising method. Clarke and Freakley ¹⁾ proposed that the accumulated rotor revolution number mainly controls the state of mix in a certain condition. Their proposal is applied to the fractal analysis and is shown in **Figure 4.8**. In **Figure 4.8**, the abscissa is a multiplication of mixing time and a

rotor revolution speed. Thus, it stands for the total rotor revolution number during a mixing.

It is obvious from the graph that the fractal dimension of a mixing is characteristic of a mixing process and is related to the total rotor revolution number.

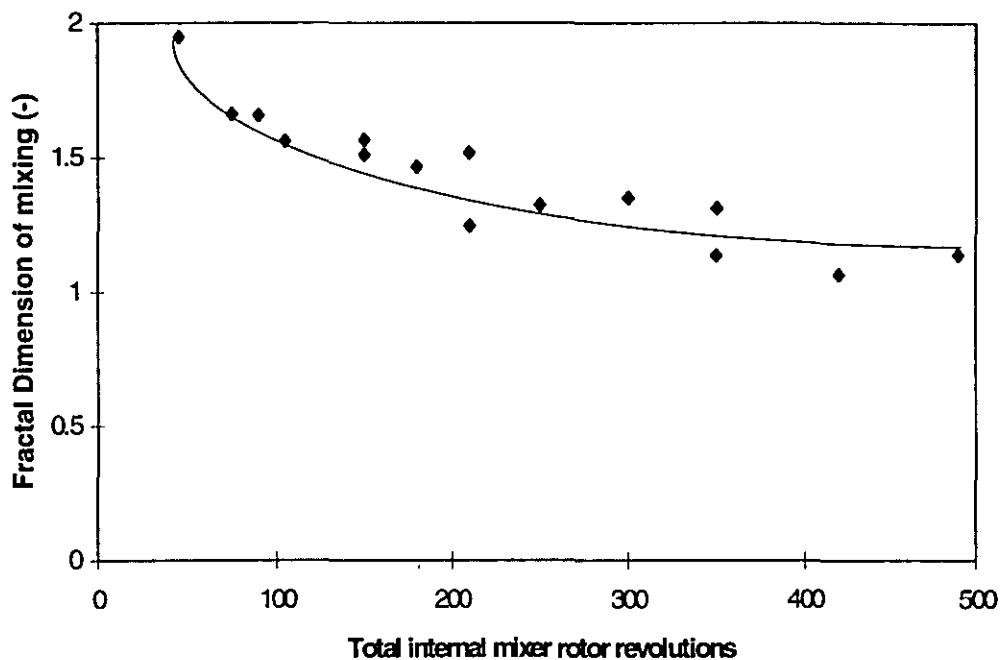
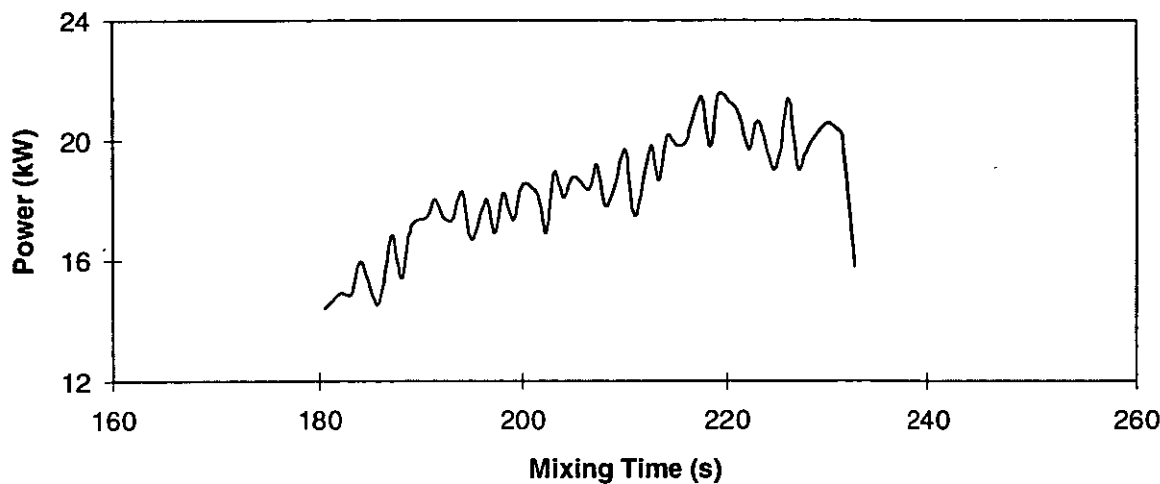


Figure 4.8 Normalised relationship between mixing time and fractal dimensions. The abscissa is a product of rotor speed and mixing time (SBR). (Ref. 3.2.4)

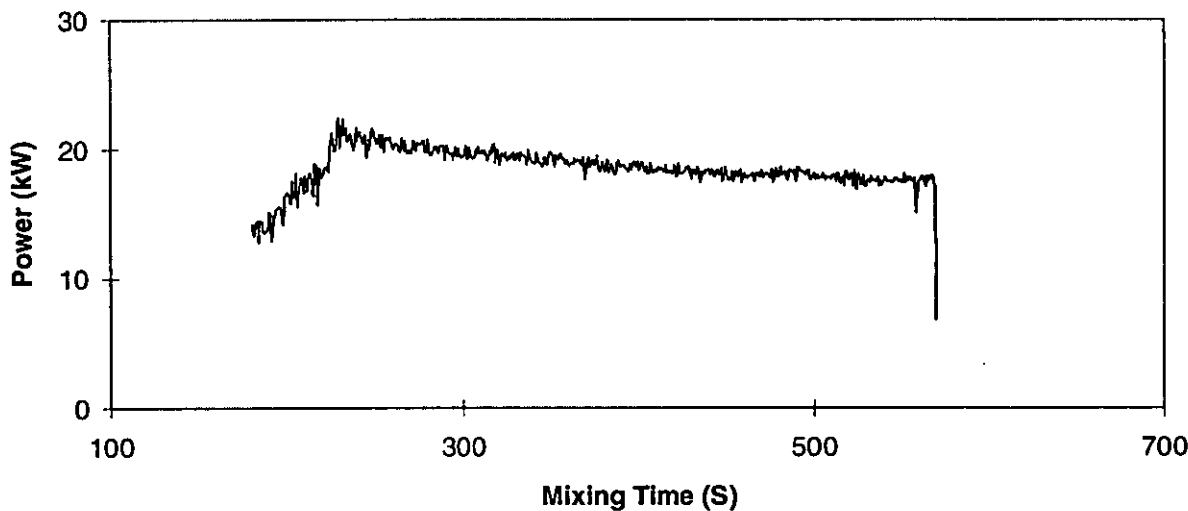
These two features arise from the fact that the fractal dimension reflects the total shape of a mixer power chart. The power chart with a big fractal dimension tends to cover a larger two dimensional surface with its trace while a power chart with a small fractal dimension tends to be a simple line.

This explanation is confirmed by checking the original power chart shown in **Figure 4.9**. In the following discussion ; (1) only mixing regions and (2) the ratio of fluctuation to mean value should be considered. (Therefore, the mastication stage (0 to 180 seconds) is not shown in **Figure 4.9**.)

In the case of graph (a) of **Figure 4.9**, the fluctuation of the power trace is more prominent than in graph (b) also the power trace tends to cover more of the whole plane than the corresponding long time mixing in graph (b). Therefore, the power trace of graph (a) is more complicated than graph (b) and results in a bigger fractal dimension.



(a) 90 second mixing after mastication (AGL1)



(b) 420 second mixing after mastication (AGL5)

Figure 4.9 Mixer power trace of SBR compound. (a) 90 second Mixing (b) 420 second Mixing. (Ref. 3.2.2)

This interpretation can be confirmed by carrying out the simulation of a power chart. Takayasu ¹⁰⁾ simulated a line having various fractal dimensions.

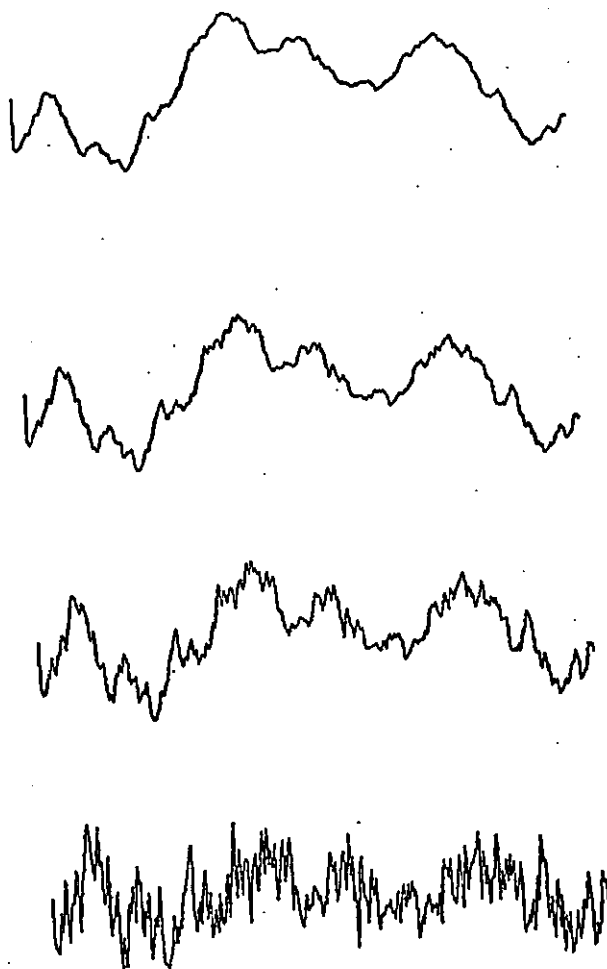


Figure 4.10 Lines with a various fractal dimensions. $D=1.0, 1.25, 1.5, 2.0$ from the top to bottom. ¹⁰⁾

As it can be seen from **Figure 4.10**, fractal dimension increases as a line becomes more complicated.

The comparison of mixing behaviour between SBR and NR samples

The normalised data of SBR and NR samples are shown as in **Figure 4.8** and **Figure 4.11**. The interpretation used for the SBR sample is also applicable to the NR compound. By comparing the normalised data of SBR and NR compounds, it is obvious that the NR

compound has a smaller decay of fractal dimension than the SBR. This phenomena arises from the slower carbon black incorporation of SBR compounds and a smaller fractal dimension of mixing at the end of a mixing process.

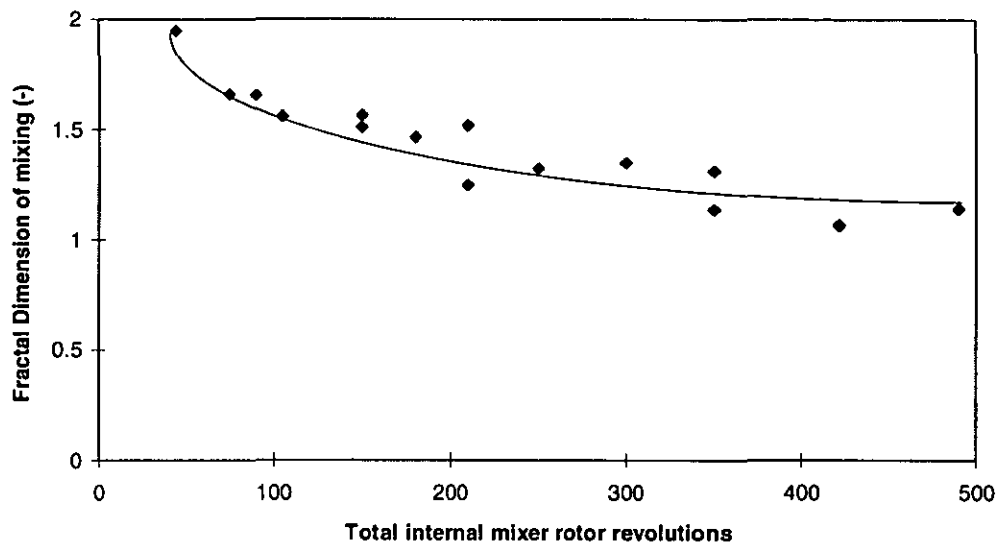


Figure 4.8 (Repeated) Normalised relationship between mixing time and fractal dimensions. The abscissa is a product of rotor speed and mixing time (SBR samples).

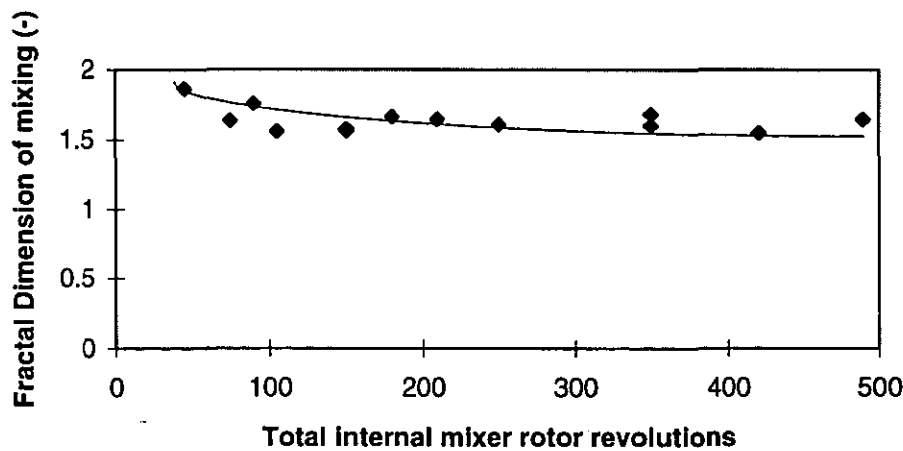
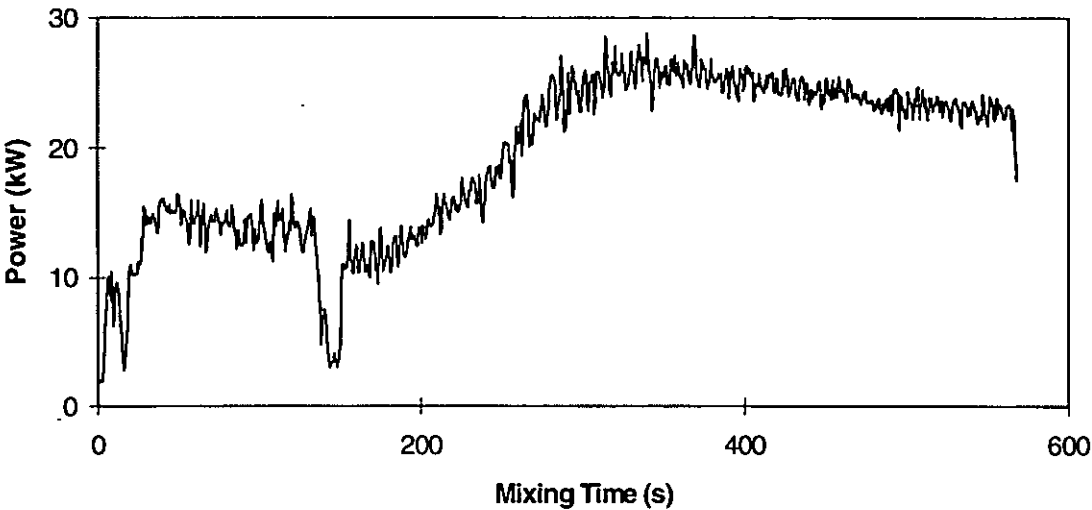
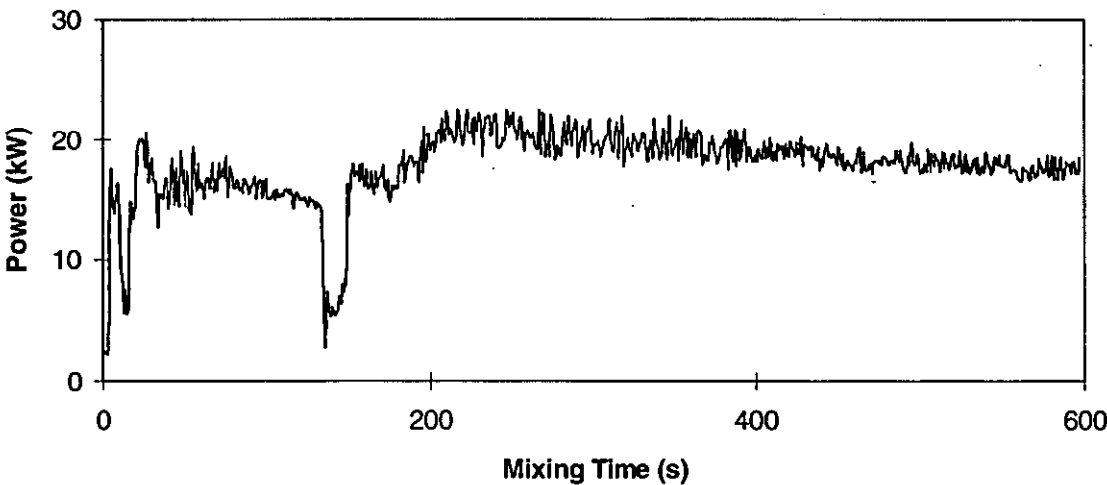


Figure 4.11 The relationship between mixing time and fractal dimensions (NR samples). (Ref. 3.2.4)

This can be confirmed from the original power chart (Figure 4.12).



(a) The power trace of SBR compound. (AGM5)



(b) The power trace of NR compound. (AGP5)

Figure 4.12 Comparison of power traces of SBR and NR compounds. (Ref. 3.2.2)

The steady state value of the fractal dimension of mixing is influenced by two factors. These are : (1) the fluctuation related to rotor revolutions and (2) the total tendency

arising from the physical property change during the mixing process. In the case of the SBR formulation (Figure 4.12 (a)), these two features are more prominent than for NR (Figure 4.12 (b)) compounds and result in the larger fractal dimension of SBR compounds at the steady state.

4.3.2 Fractal analysis of the carbon black dispersion

Despite considerable research, the relationship between carbon black and rubber properties has not yet been well established because of the difficulty in evaluating the state of mix by using a single measurement method. In this section, the fractal concept is applied to evaluate the state of mix. The following three topics are discussed.

- (1) The validity of fractal application to carbon black dispersion.
- (2) The relationship between fractal dimensions of carbon black dispersion and mixing.
- (3) The comparison of carbon black dispersion between the NR and the SBR samples.

The validity of fractal application to carbon black dispersion

A box counting method was used to decide the fractal characteristics of the state of mix (section 2.1.5). Then, a log - log plot was constructed. Figure 4.13 demonstrates the validity of the fractal concept as a means of evaluating the state of mix because the graph follows a power rule.

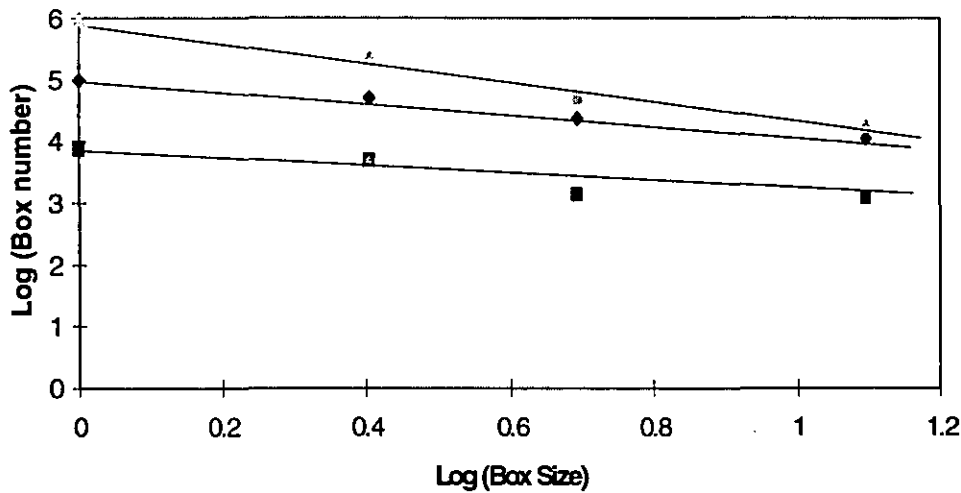


Figure 4.13 An example of the box counting method to determine the state of mix of carbon black (AGL). (Ref. 3.3.1)

In the **Figure 4.13**, some experimental scattering is detected. Two main factors contribute to this :

- (a) The lack of objectivity. The experiments were carried out visually, not by using a reliable computer software package. Visually, it is very difficult to judge consistently whether a box contains carbon black or not.
- (b) The box counting method. In this method, the box size (mesh size) had to be changed for the determination of fractal dimensions. The precision decreases as the box size increases. In the big box size region, the data points in **Figure 4.13** show the scattering caused by this factor. To overcome this, it is better to adopt a suitable range of microscope magnification, by considering the precision of experimental instruments.

The relationship between fractal dimension of carbon black dispersion and mixing

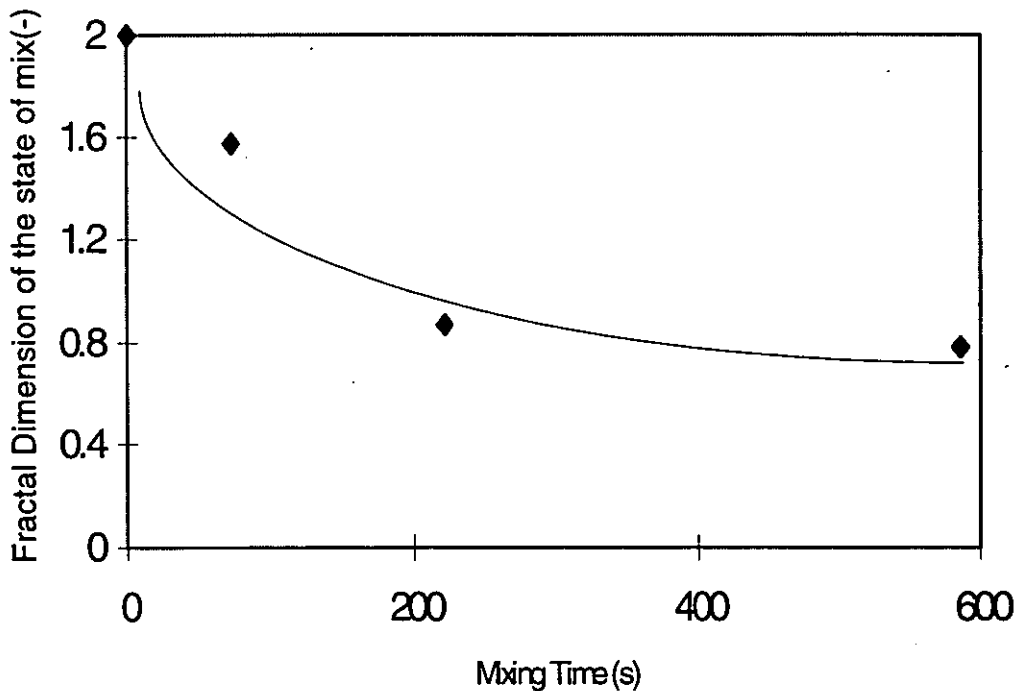


Figure 4.14 A relationship between fractal dimension of carbon black dispersion and mixing time (SBR samples).

Figure 4.14 shows the relationship between the fractal dimension of carbon black dispersion and mixing time. The fractal dimension of carbon black dispersion becomes smaller and approaches constant value as mixing evolves. These phenomena can be explained by the following mechanism.

Initially, added carbon black in a system simply covers the surface of the matrix polymer in an internal mixer. Then carbon black is incorporated into the polymer matrix. The incorporated carbon black reduces its size by both shear and elongational forces during mixing. Dispersed aggregate can not be seen by light microscopy. This means that the texture or complexity of the surface disappears as carbon black dispersion is improved. Therefore, the longer a mixing time, the smaller the fractal dimension of carbon black dispersion.

Three characteristic points in **Figure 4.14** have to be considered.

(1) The starting point of mixing

In **Figure 4.14**, the number “2” is a theoretical value because a surface completely covered by carbon black is a two-dimensional distribution. The extrapolation from the experimental data agrees with the theoretical value. This fact demonstrates the validity of fractal analysis used here.

(2) The middle point of mixing

As can be seen from **Figure 4.14**, the fractal dimension at 210 seconds approaches a steady value. It is reasonable to consider that this point could be regarded as the terminal point for industrial operations because there is no significant improvement of the state of mix.

(3) The end point of mixing

It is necessary to consider the meaning of a steady state fractal dimension, $d=0.78$. The figure is smaller than one and it means that the carbon black dispersion in the matrix is almost randomly distributed at this stage (see **section 2.1.4**). This conclusion is reasonable from our experience which tells us that well - mixed samples have a random carbon black dispersion.

The comparison of carbon black dispersion between NR and SBR compounds

Figure 4.15 shows the relationship between mixing time and the fractal dimensions of SBR and NR samples. The SBR and NR samples have different formulations, therefore it is not easy to compare the results between the SBR and NR formulation.

Two features have to be mentioned here :

(a) The first feature is the plateau value of the fractal dimension at long mixing times. The surface density of the detected agglomerates in the thin section sample mainly contribute to the difference in the fractal dimension between SBR and NR samples. It is known that NR compounds show a quicker black incorporation time than SBR. Thus, an NR compound reduces the number of carbon black agglomerates more extensively than does an SBR compound. This mechanism results in a smaller value of the fractal dimension of the NR compound.

(2) The second phenomenon is the rate of decay of the fractal dimension. The fractal dimension at zero mixing time could be two. If the value shown in Figure 4.15 is extrapolated to two, it is obvious that NR has a bigger rate of decay than the SBR system. Again, the mechanism mentioned above is applicable to the phenomenon.

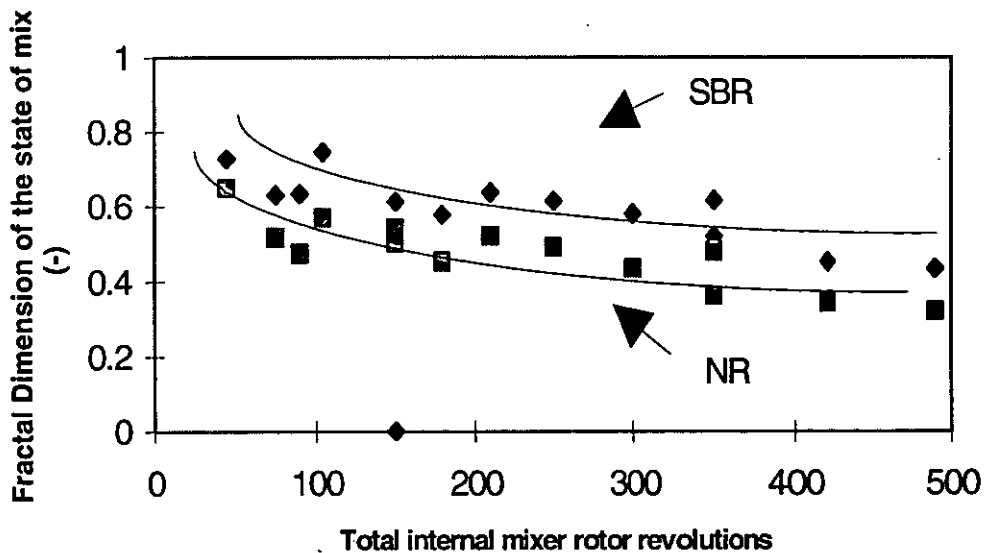


Figure 4.15 A time dependence of the fractal dimension of the state of mix. (SBR and NR have different formulations). (Ref. 3.3.1)

4.3.3 Fracture surfaces of tensile strength samples

In this section, the application of fractals to characterise a fracture surface will be discussed. This section consists of three subsections.

- (1) The validity of fractal application to fracture characterisation
- (2) The relationship between mixing and the fractal dimension of a fracture surface
- (3) The relationship between tensile strength and fractal dimension of a fracture surface

The validity of fractal application to fracture surface

To apply the fractal concept to the fracture surface of rubber samples, the contour profile was measured (section 3.3.2). Figure 4.16 shows one example of such an experiment.

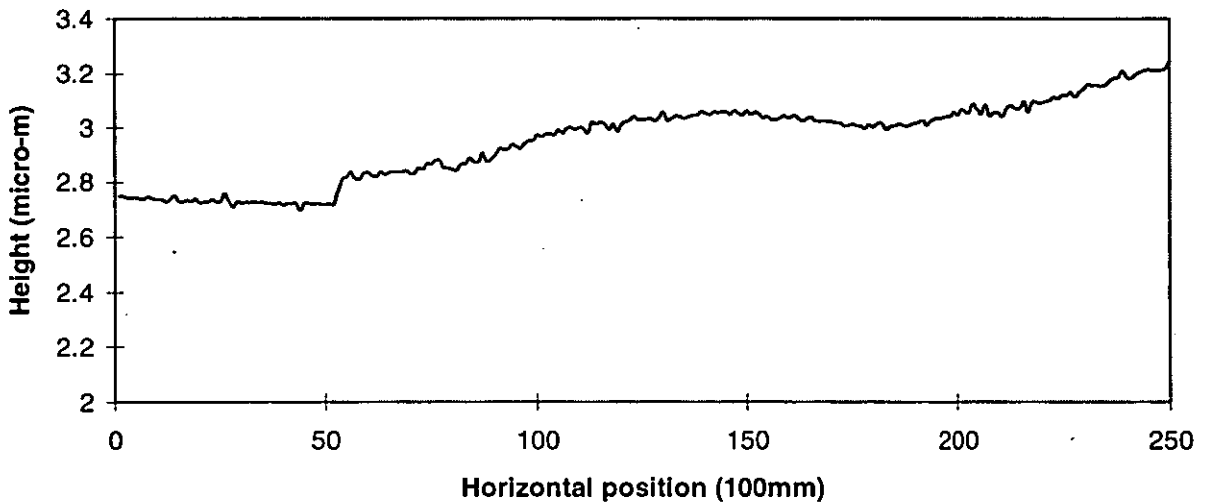


Figure 4.16 A contour profile of a fracture surface. (Ref.3.3.2)

To carry out a Fourier analysis, it is possible to apply the same type of software as was used for the analysis of the mixer power trace (**Appendix 3**). One calculation result is shown in **Figure 4.17**.

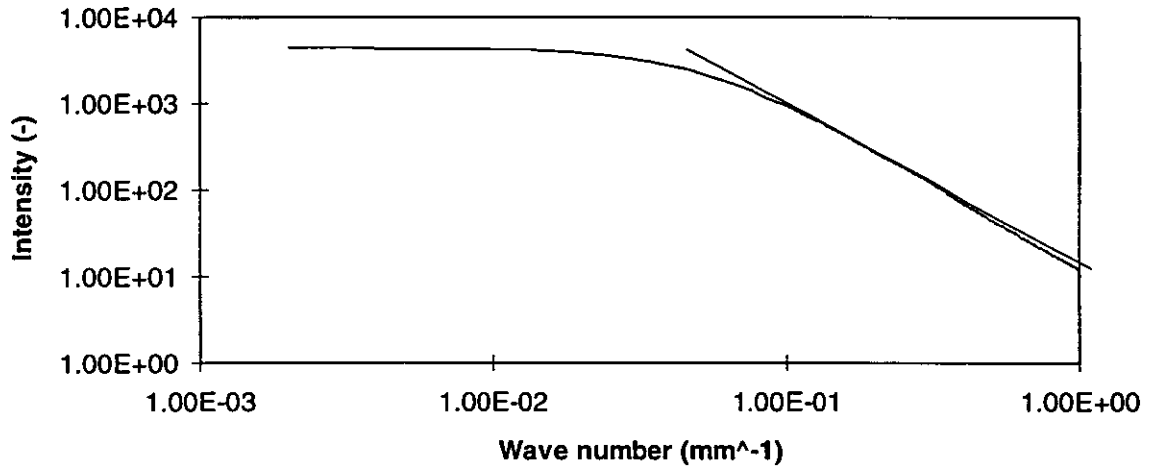


Figure 4.17 A power spectrum of a fracture surface. The slope of the graph is used to calculate the fractal dimension (AGL1).

Figure 4.17 shows clearly that a power rule is applicable to characterise a fracture surface. Therefore, it confirms the validity of the fractal application to the fracture surface analysis (see the regression line around the large wave number region).

The relationship between mixing and the fractal dimension of a fracture surface

In the case of a fracture surface, the relationship between a fractal dimension and a power is given by

$$\beta = 7 - 2D$$

Equation 4.5

β : A power from an experiment

D : A fractal dimension

The fractal dimensions of tested samples are listed in **Appendix 9**. As for the other analyses, normalised data are shown in **Figure 4.18**.

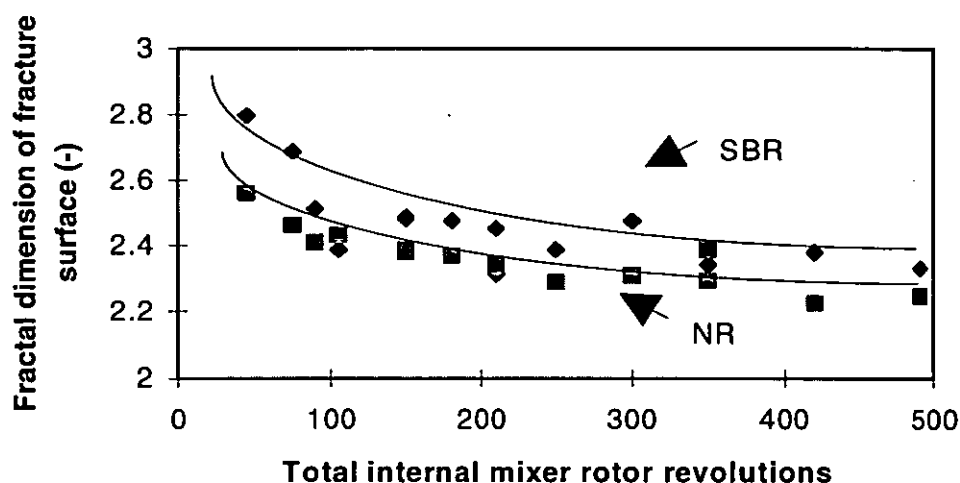


Figure 4.18 A normalised fractal dimension of the fracture surface (◆ SBR ■ NR). (Ref. 3.3.2)

For both SBR and NR samples, the fractal dimensions decrease as mixing proceeds. As mentioned before, the fractal dimension represents the characteristic of the whole of the measured surface. The smoother the fracture surface, the smaller the fractal dimension. It is easily observed that a badly mixed compound has a rough fracture surface, while a well mixed compound has a smooth fracture surface. **Figure 4.18** quantifies such observations based on the fractal concept.

In **Figure 4.18**, NR has a smaller fractal dimension than SBR. Such a difference may arise from the difference in the formulations or carbon black incorporation speed. Although the mechanisms which cause the differences were not the subject of this research thesis, it is possible to propose that residual carbon black agglomerates in the samples control the roughness of the fracture surface because they tend to be both an initiation point of a fracture process and a source of increased fracture energy due to stress intensification. As previously seen, NR compounds have a shorter carbon black incorporation time than SBR compounds. Therefore NR compounds experience a longer dispersion process than SBR compounds when they are compared at the same total rotor revolutions. Through this mechanism, the difference of carbon black incorporation time during mixing resulted in the

difference in fractal dimension of fracture surface of SBR and NR compounds in **Figure 4.18**.

The relationship between tensile strength and the fractal dimension of fracture surface

Figure 4.19 and **Figure 4.20** show the relationship between tensile strength and the fractal dimension of the fracture surface. In the case of NR compounds, tensile strength at break is very sensitive to the mastication effect. To reduce the effect, the data for periods longer than 300 cycles (see **Figure 4.1** in section 4.2.1) are not plotted in **Figure 4.20**.

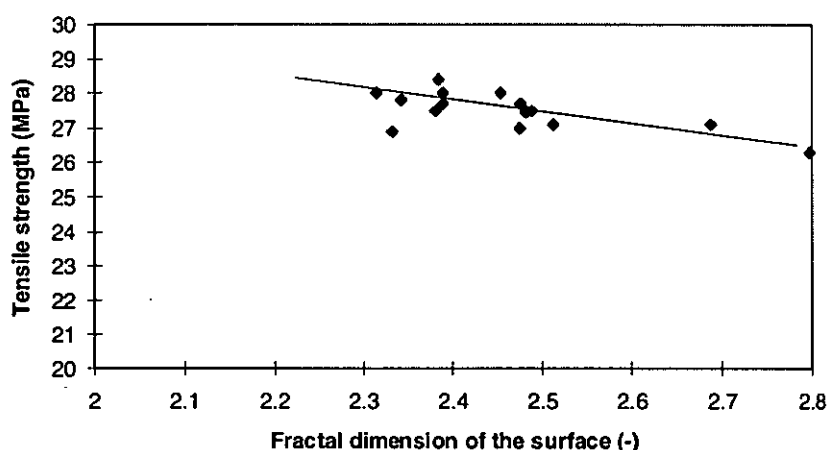


Figure 4.19 A relationship between tensile strength and the fracture surface fractal dimension of SBR samples. Correlation coefficient is -0.675. (Ref. 3.3.2)

There are two prominent characteristics :

(1) The relationship between fractal dimension of fracture surface and the tensile strength.

In both SBR and NR compounds, the tensile strength is proportional to the fractal dimension of the fracture surfaces. In this experiment, the difference was only mixing time in each series of SBR and NR compounds. Other factors which may contribute to tensile strength are not taken account of here. Therefore, the reason why a relatively straight

relationship between the fractal dimension of fracture surface and the tensile strength was obtained arises from the fact that the state of mix mainly controls the tensile strength in each compound. It can be concluded that a smaller fractal dimension means a bigger tensile strength because a smaller fractal dimension means that a compound is in a well - mixed state which results in a bigger tensile strength.

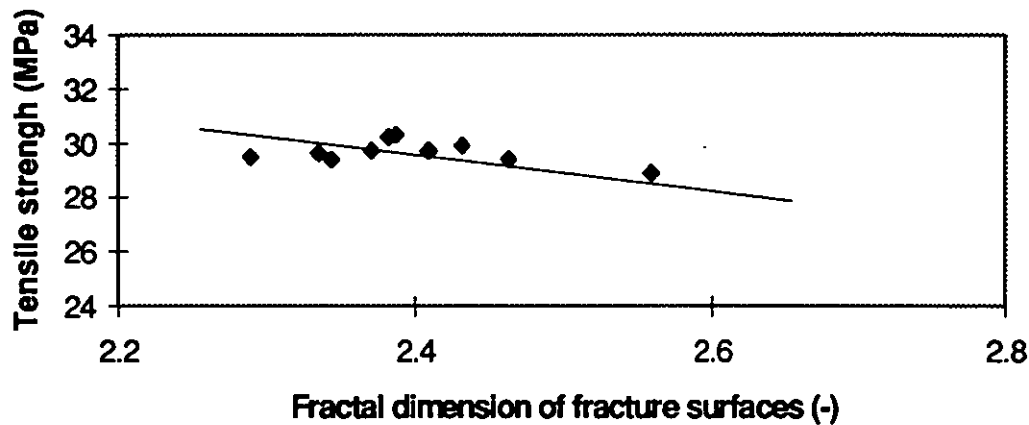


Figure 4.20 A relationship between tensile strength and the fractal dimension of NR samples. Correlation coefficient is -0.407. (Ref. 3.3.2)

(2) The scattering in the graphs.

There is some scattering in both graphs but the scattering is bigger in the NR samples than the SBR samples. The bigger scattering arises from the fact that the tensile strength is a function of many factors. For example, tensile strength is a function of molecular weight, the state of cure and the combination of ingredients. Especially, it is well known that NR has extra mechanisms which SBR does not have. An elongational crystallisation and a mastication during mixing are examples of such mechanisms. Although the mastication effect is minimised by choosing a shorter mixing time, its effect is still present. The more extensive the mastication, the smaller the tensile strength. The extra mechanisms such as mastication are not characterised by the fractal method and result in a bigger scatter in NR compounds than SBR compounds.

To conclude, it can be said that the fractal concept can be a basic aid for understanding the relationship between tensile strength and carbon black dispersion.

4.3.4 Relationships among mixing, state of mix and fracture surfaces

The relationships between mixing, state of mix and vulcanised properties will be discussed in this section. For convenience, these relationships are discussed separately.

4.3.4.1 Relationship between fractal dimensions of mixing and the state of mix

In this subsection, two topics will be discussed.

- (1) The relationship between mixing and carbon black dispersion from the fractal point of view.
- (2) The relationship between fractal and existing methods for evaluating carbon black dispersion.

The second topic is discussed from a microscopic and macroscopic point of view.

The relationship between mixing and carbon black dispersion

In **Figure 4.21** and **Figure 4.22**, a simple fractal relationship between the state of mix of carbon black and mixing conditions can be seen. (In the case of NR compounds, long - time mixing data (more than 250 cycles) is not plotted, to reduce the mastication effect.)

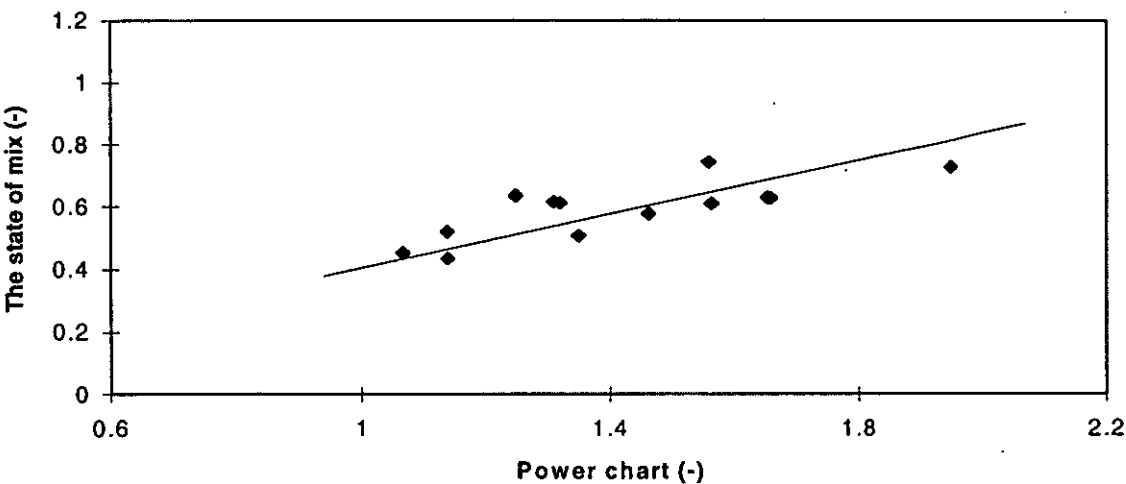


Figure 4.21 (a) The relationship between mixing and the state of mix (SBR compounds). Abscissa and ordinate are fractal dimensions of mixing and the state of mix respectively. (Ref. 3.2.4, 3.3.1)

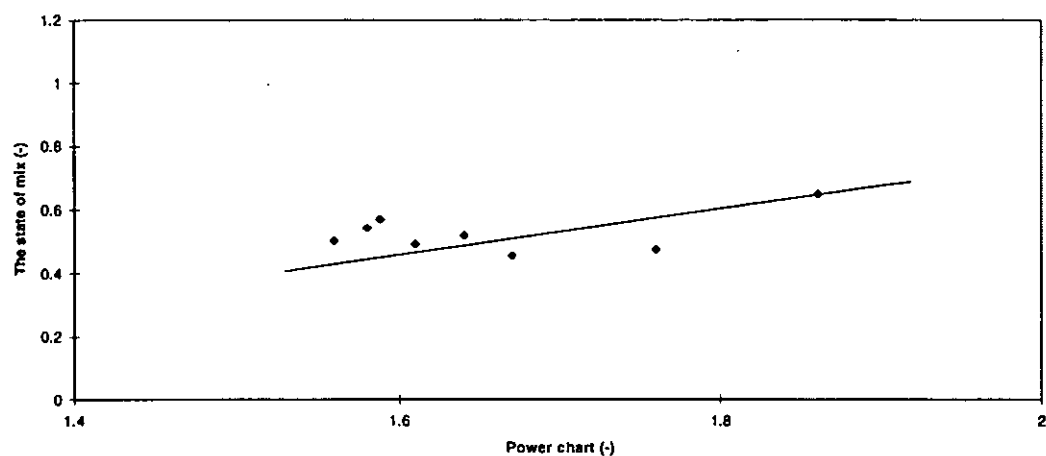


Figure 4.22 (b) The relationship between mixing and the state of mix (NR compounds). Abscissa and ordinate are fractal dimensions of a mixing and the state of mix respectively. (Ref. 3.2.4, 3.3.1)

From these figures, it is apparent that the SBR compound is better behaved than the NR compound because the NR compound shows a bigger scattering than the SBR compound.

Two factors contribute to the above fact :

(1) Experimental procedure: The data scattering arises from the fact that the fractal dimension of the carbon black dispersion is more reliable in the SBR compounds than the NR samples because measurements of the carbon black dispersion become increasingly difficult as carbon black is incorporated into the matrix polymer and NR has a quicker carbon black incorporation than SBR. Therefore the NR has a relatively bigger scattering than the SBR samples.

(2) Experimental range : This factor arises from the fact that the fractal dimension adopted here for evaluating the carbon black dispersion is one measure for macroscopic evaluations. There are two types of carbon black dispersion based on its scale. The first one is a macroscopic and the other is a microscopic dispersion. In this experiment, an optical microscope is used to carry out a box counting method. Therefore, the fractal dimension used here for evaluating the state of mix is mainly in the range of macroscopic evaluation. However the fractal dimension of a mixing process reflects both macro and

microscopic carbon black dispersion mechanisms, the validity of which can be seen by comparing the data shown in the following subsection.

The relationship between the fractal and existing methods for evaluating carbon black dispersion

Two other measurements were carried out to evaluate the state of mix.

(1) The first was the electrical resistance (section 3.2.5). This method reflected the dispersion at microscopic level more sensitively because the carbon black agglomerates result in a good electrical path.

(2) The other was the Payne Effect (section 3.3.4). This method reflected both macro and microscopic carbon black dispersion together because the modulus of a compound is controlled by both carbon black network (macroscopic dispersion) and bound rubber (microscopic dispersion).

A comparison of the fractal dimension of the state of mix to the electrical resistance and the Payne Effect allowed us to interpret the meaning of the fractal dimension of the state of mix.

(1) Electrical resistance and the fractal dimension of carbon black dispersion

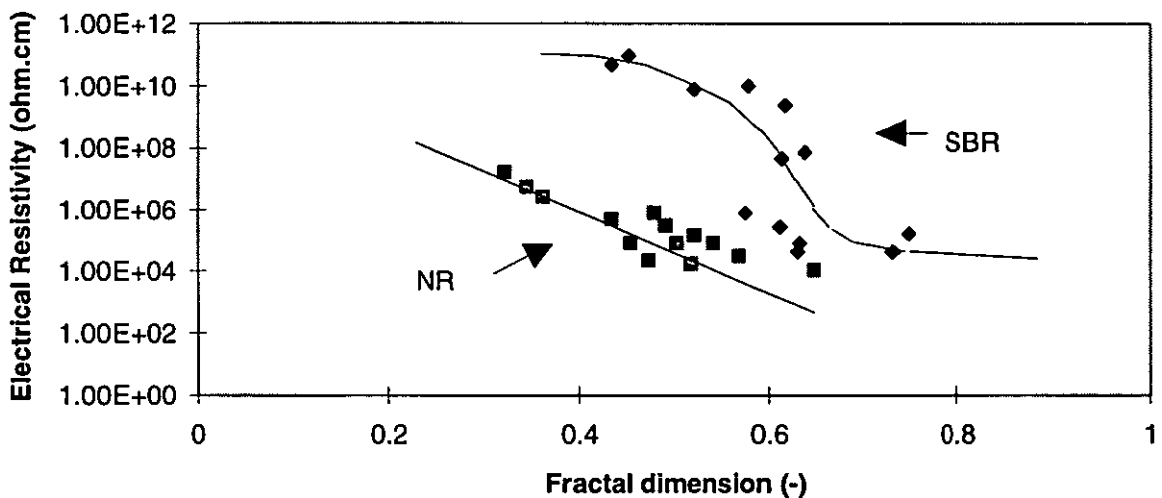


Figure 4.23 Electrical resistance versus fractal dimensions of the state of mix. (Ref. 3.2.5)

To consider the microscopic dispersion effect, the relationship between electrical resistance and the fractal dimension of carbon black dispersion is shown in **Figure 4.23**. As can be seen from the graph, the relationship is not simple in the SBR compounds. In addition, there is a threshold around 0.6 of the fractal dimension in the SBR compounds. This point can be regarded as the point where the macroscopic carbon black agglomerates disappeared. The point naturally depends on the rate of carbon black incorporation into the matrix polymer. In the case of NR compounds, the threshold can not be seen in **Figure 4.23** because the carbon black incorporation in an NR compound is quicker than in an SBR compound. Therefore, in this experimental range, it was impossible to check the threshold.

The difference of electrical resistance between SBR and NR compounds has also to be considered. In **Figure 4.23**, the electrical resistance of the NR compound is smaller than that of the SBR compounds, even in the case of well mixed samples. It is reported ¹¹⁾ that NR is more sensitive to the amount of carbon black than SBR, resulting in a smaller electrical resistance. Although this sensitivity can be regarded as a main factor of the difference, a mechanism was not suggested in the original paper.

(2) The Payne Effect

Figure 4.24 shows the Payne Effect as a typical example of viscoelastic behaviour. In both NR and SBR compounds, the relationship between the fractal dimension of the state of mix and the Payne Effect becomes more straightforward than in **Figure 4.23**. It means that the fractal dimension of the state of mix is more sensitive to the macroscopic dispersion than microscopic dispersion, as expected.

To conclude; the fractal concept for the state of mix is one method for correlating the mixing process to the carbon black dispersion. In the present work, the fractal method is more sensitive at a macroscopic level of carbon black dispersion and is therefore more useful as a measure of properties which are sensitive to macroscopic dispersion.

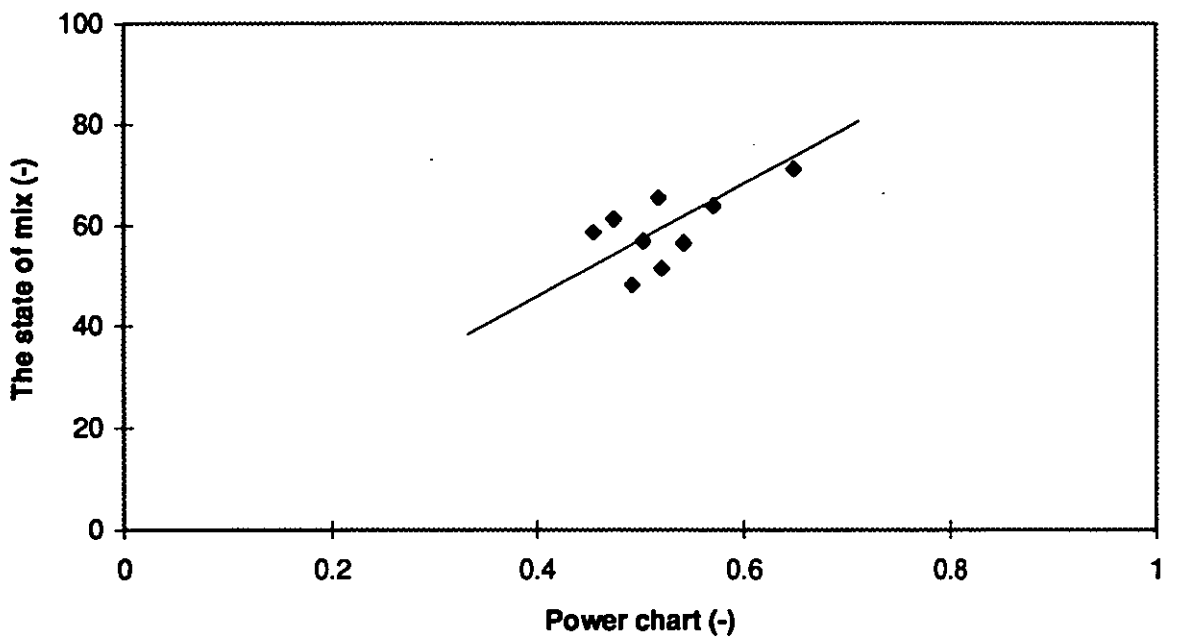
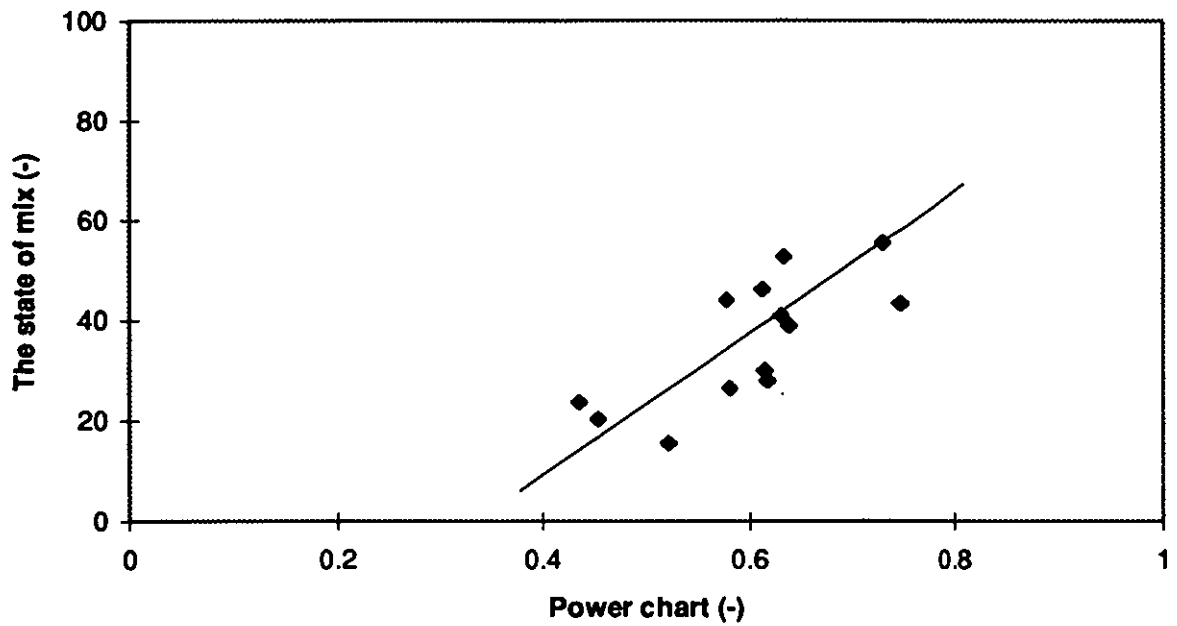


Figure 4.24 A relationship between the Payne Effect and fractal dimensions of the state of mix. (top) SBR compound, correlation coefficient is 0.683 : (bottom) NR compound, correlation coefficient is 0.607. (Ref. 3.3.4)

4.3.4.2 The relationship between fractal dimensions of the state of mix and fracture surfaces

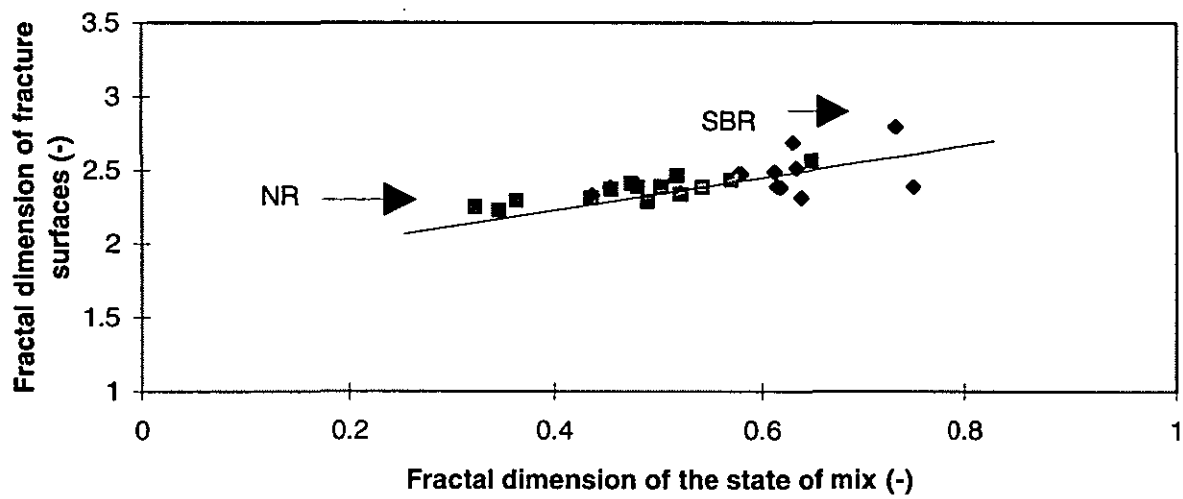


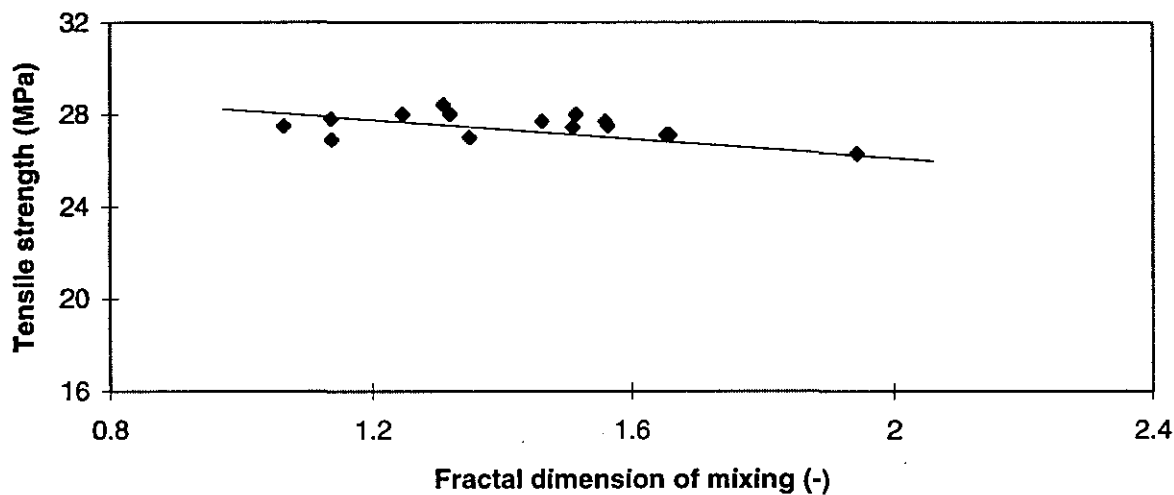
Figure 4.25 Fractal application for the evaluation of the state of mix and the fracture surfaces. Abscissa and ordinate are fractal dimension of the state of mix and fracture surfaces, respectively. (Ref. 3.2.4, 3.3.2)

Figure 4.25 shows a fractal relationship between the state of mix and the fracture surfaces using the fractal concept. It is clear from this graph that the fractal dimensions connect both properties quite well.

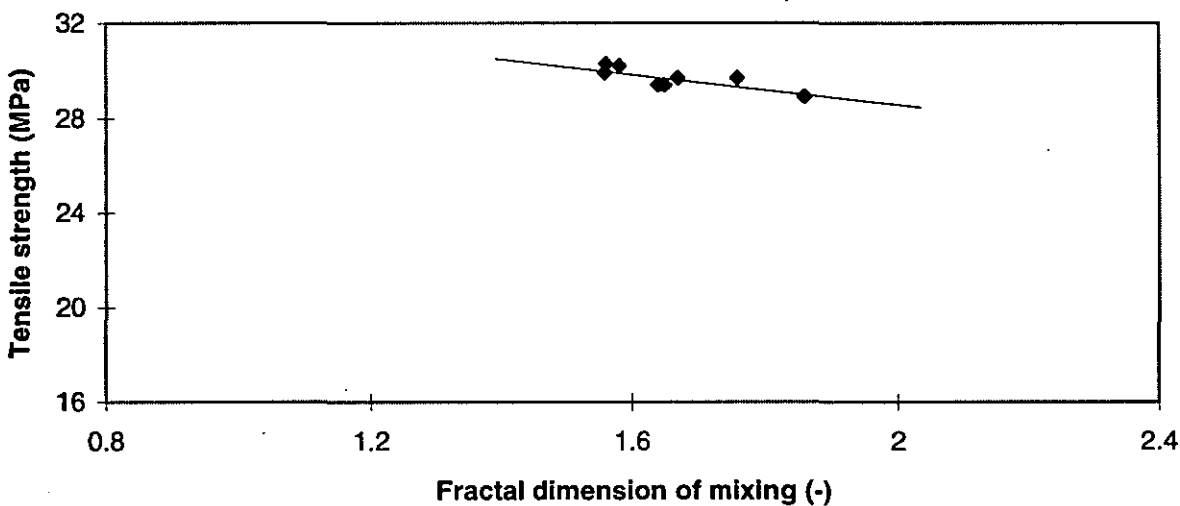
Although only one line is drawn in the graph, it should not be considered that the fractal dimension of fracture surfaces is only a function of the state of mix. An overlap of the plots found here in **Figure 4.25** for SBR and NR compounds is merely a coincidence. Each compound is expected to have its own intrinsic line.

4.3.4.3 Fractal application to vulcanised rubber properties

Figure 4.26 shows the relationship between fractal dimensions of the mixer power trace and the tensile strength at break. In the case of NR compounds, the data longer than 250 cycles in mixing is not plotted to avoid the large mastication effect.



(a) SBR compounds



(b) NR compounds

Figure 4.26 Tensile strength versus fractal dimension of mixer power traces. (Ref. 4.2.4)

It can be seen that the tensile strength of SBR and NR compounds have a linear relationship with the fractal dimension of mixing. The tensile strength at break is inevitably a function of molecular weight, ingredients, mixing conditions and cure conditions. In the experiment, the differences among samples in series of SBR and NR compounds are confined to mixing time and rotor revolution speed. Thus, it is reasonable to suggest that the state of mix of carbon black is the most important factor in this experiment.

The above reasoning can be confirmed by considering the difference of the relationship of tensile strength and fractal dimension of the fracture surface between the SBR and NR samples. There are two features in the difference :

① The scattering in the graph : There is an extra mechanism, such as elongational crystallisation, which controls the tensile strength in the NR compounds. This extra mechanism was not included in the fractal characterisation of mixing and resulted in the bigger scattering of tensile strength.

② The slope of the graph : The dependence of tensile strength on fractal dimension (the slope in the graph) is bigger in NR compounds than in SBR compounds. As being seen before, a NR compound has a bigger decay of the fractal dimension of mixing than the SBR compound. Therefore, the carbon black dispersion played a more important role in the NR compounds than in the SBR compounds and resulted in a larger dependence of tensile strength on the carbon black dispersion, as characterised by the fractal dimension.

To conclude : The fractal concept can be applied to the characterisation of mixing conditions, the state of mix and vulcanised rubber properties. Furthermore, it has a role in correlating their interrelationship within a single concept.

4.3.5 A new method to measure the state of mix

The purpose of this section was to propose a new method of measuring the state of mix. This proposal was derived from an improvement in experimental equipment.

Two topics are discussed : The merit of the new procedure and the interpretation of the new method.

The merit of the new procedure

The equipment, Rodenstock RM600, can be regarded as an up-to-date equivalent of the ASTM D2663 technique. The instrument and its software packages reduce some experimental difficulties of the ASTM D2663 method dramatically.

(1) It presented few practical difficulties.

Using ASTM D2663 (Method C, **Figure 2.25** and **Figure 2.26**), two types of information were obtained. These were f (total amount of roughness in peaks/cm) and h (the average peak height in μm). Because of the characteristics of the data, it was necessary to treat them statistically. The new method reduces the repetition of the experimental procedures to obtain the statistical data by applying a two dimensional Fourier Transformation.

(2) The data reliability was expected to be better than ASTM D2663.

The value (f) represented two dimensional surface information only with one dimensional observation (a line scanning) in ASTM D2663. In the new method, the total amount of surface roughness was represented by a wavenumber arising from a two dimensional Fourier Transformation resulting in a more reliable treatment of surface roughness.

With value (h), it was difficult to remove the slope of the surface which required careful adjustment of the experimental conditions. In the new method, averaging the surface slope could be removed by applying a filter function (a least-square fitting surface). The importance of the filter function lies in the fact that a somewhat complicated surface shape can be applied to remove the error arising from the experimental procedure.

Interpretation of the new method

Result from the new method is shown in **Figure 4.27** and **Figure 4.28**.

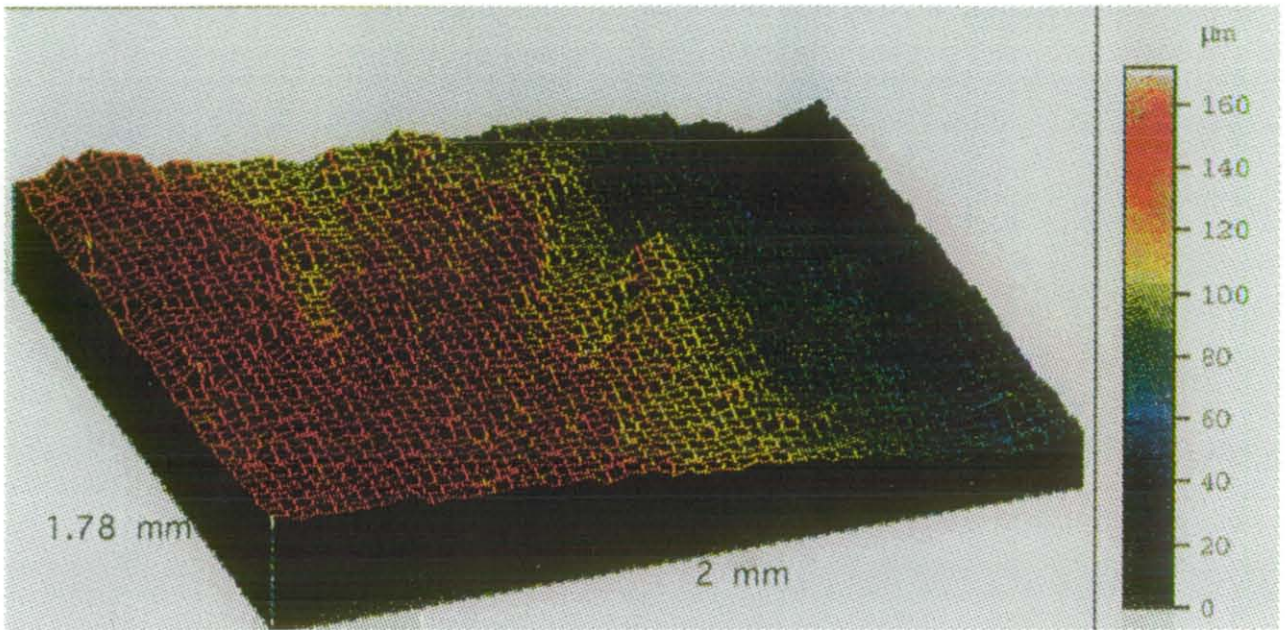


Figure 4.27 A fracture surface of tensile strength tested sample (a screening sample).

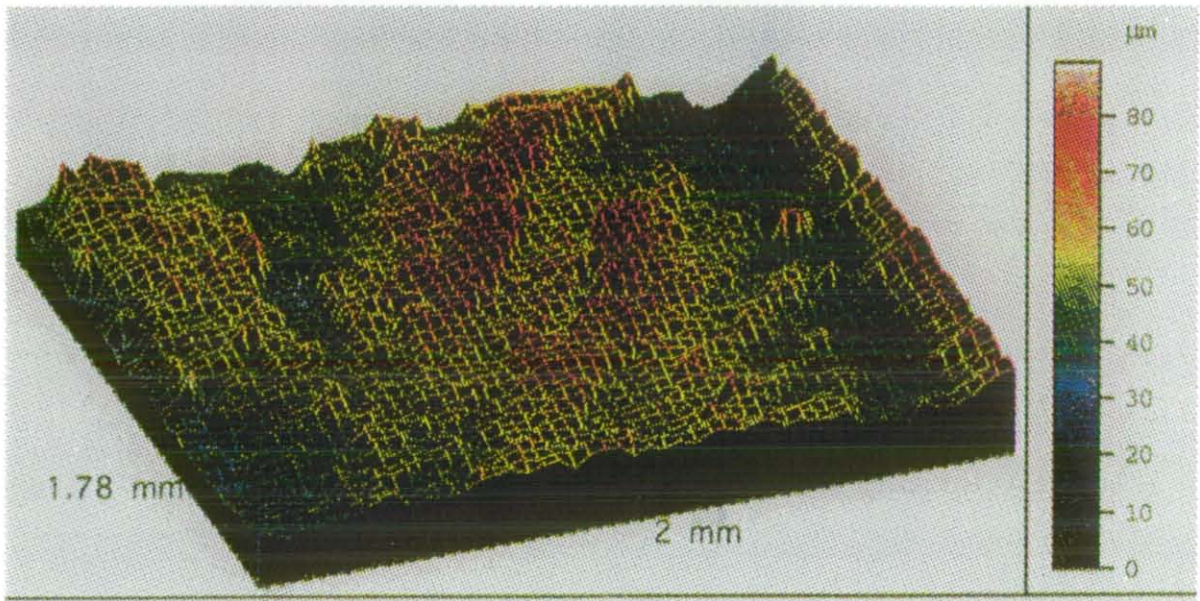


Figure 4.28 The true surface roughness after removing a least square fitting surface (a screening sample).

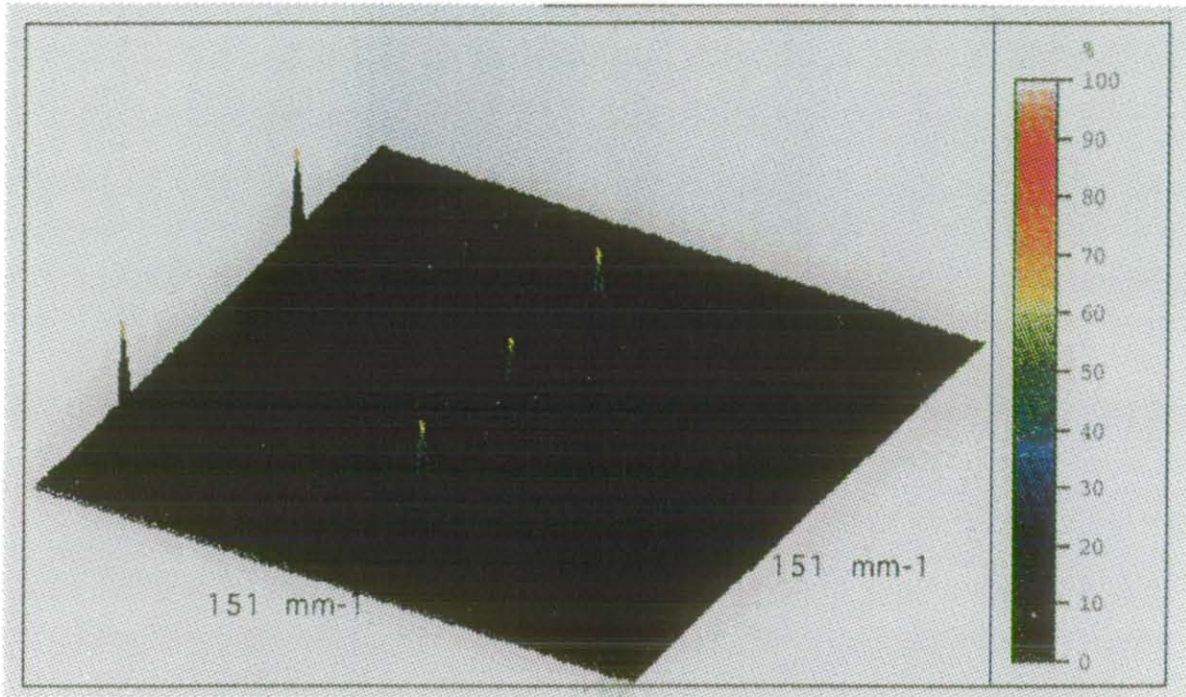


Figure 4.29 A two dimensional Power spectrum for the true roughness of fracture surface (a screening sample).

Figure 4.27 shows original data of the fracture surface of a tensile strength test sample. **Figure 4.28** shows the true roughness of **Figure 4.27** by removing the least- square fitting surface. A two dimensional Fourier transformation was applied to the surface of **Figure 4.28**. Its result is shown in **Figure 4.29**.

In **Figure 4.29**, five peaks are observed. They can be classified into two categories.

① Two peaks near the edge.

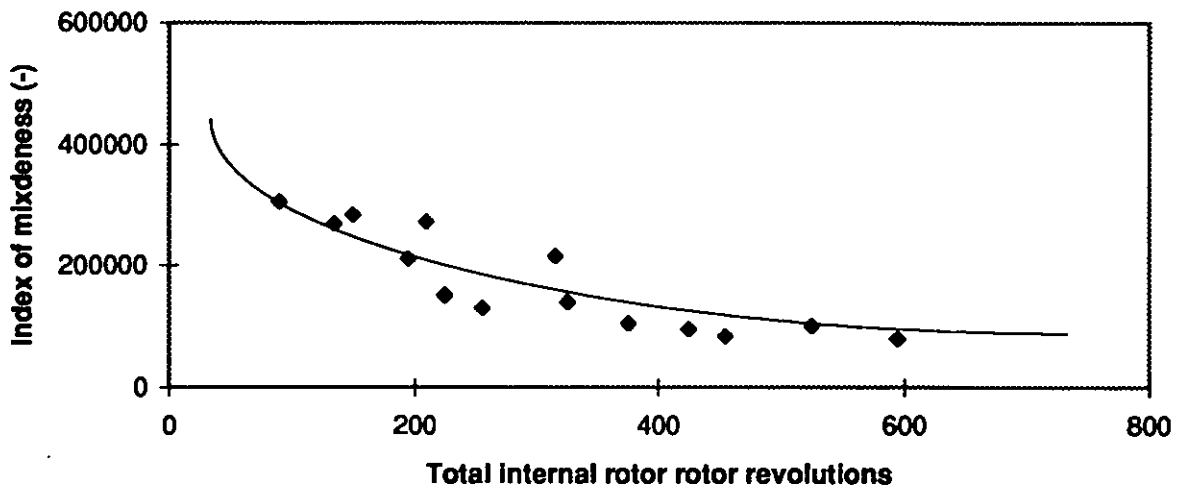
The two peaks on the edge correspond to a total slope of the fracture surface and were discussed in the light of the fractal concept in section 4.3.1.

② Three peaks in the centre of the spectrum surface.

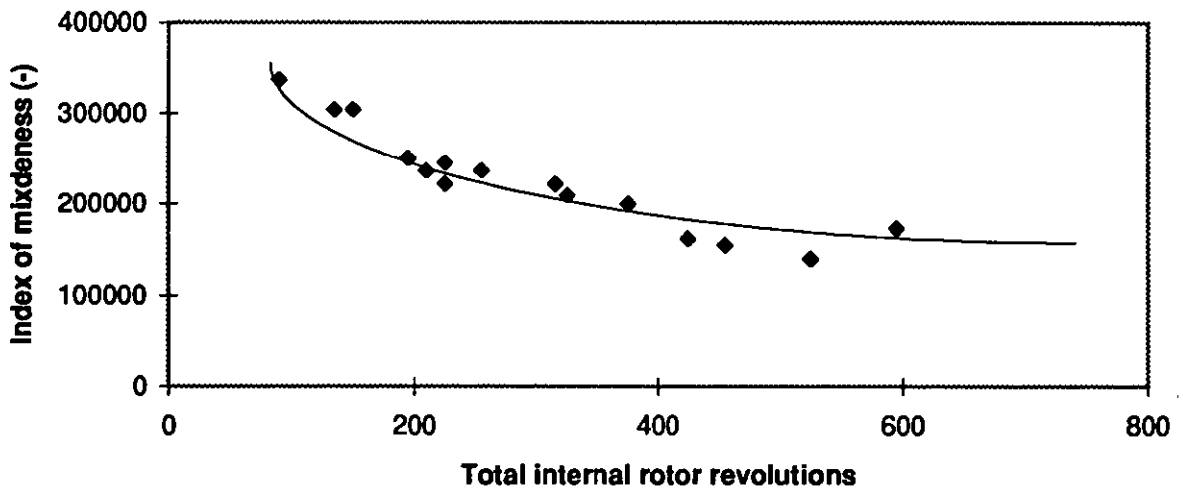
The three peaks in the centre give the quantified value of the roughness of the fracture surface.

Corresponding to ASTM D2663, two types of information were obtained for evaluating the state of mix : (1) F (Peak position in cm^{-1}) and (2) Intensity H (%). These corresponded to f (surface roughness) and h (peak height) of ASTM method, respectively, and were used to evaluate the state of mix. The procedure of ASTM D2663 uses $f^2 \times h$ as a representative value of filler agglomeration. Thus, $F^2 \times H$ was used to represent the state of mix. The data is shown in **Figure 4.30** and it demonstrates the applicability of the new method. There is some scattering in these figures. This scattering arises from the fact that only the peak position (F) was used to represent the surface roughness and the distributions of the peak are ignored.

To conclude, the fact that the proposed idea reduces experimental time and effort was interesting because such a reduction in time can be expected to play an important role in an industrial quality control procedure based on a standard method like ASTM D2663 (Method D).



(a) The representation of surface roughness as a function of the state of mix (SBR samples).



(B) The surface roughness of NR sample.

Figure 4.30 The new method to represent the state of mix by using 2D Fourier transformation. (Ref. 3.3.2)

4.4 The influence of the state of mix on rubber properties

In this section, the influence of the state of mix on thermal properties and bound rubber will be discussed. The former can be regarded as ascribed the macroscopic phenomena of the state of mix and the latter can be regarded as ascribed the microscopic characteristics of the state of mix.

4.4.1 The influence of the state of mix on thermal properties

In this subsection, two topics are discussed.

- (1) The validity of experimental work
- (2) The mechanism of thermal conduction in rubber compounds

The validity of experimental work

The importance of the state of mix for thermal properties was discussed in the literature review (section 2.2.3.3). Here the thermal diffusivity will be discussed. The experimental procedure was shown in section 3.3.5 and the analytical procedure was discussed in section 2.2.3.3. The experimental work was conducted on SBR samples (AGL). One of the results of temperature measurement is shown in Figure 4.31

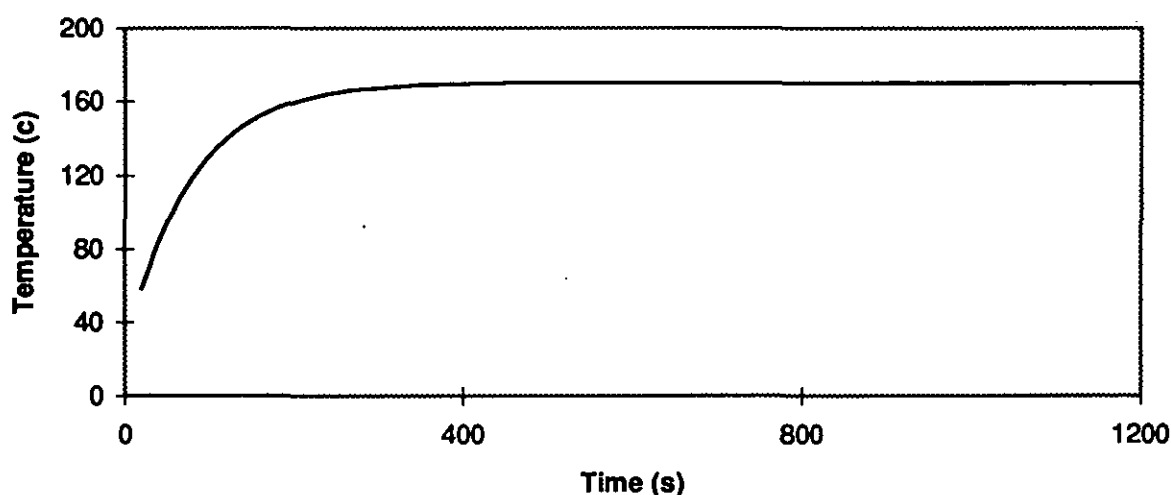


Figure 4.31 A temperature increase during vulcanisation. (Ref. 3.3.5)

Based on Equation 2.70 in section 2.2.2.3, the data was analysed to produce a thermal diffusivity. Figure 4.32 shows the results as a function of the state of mix.

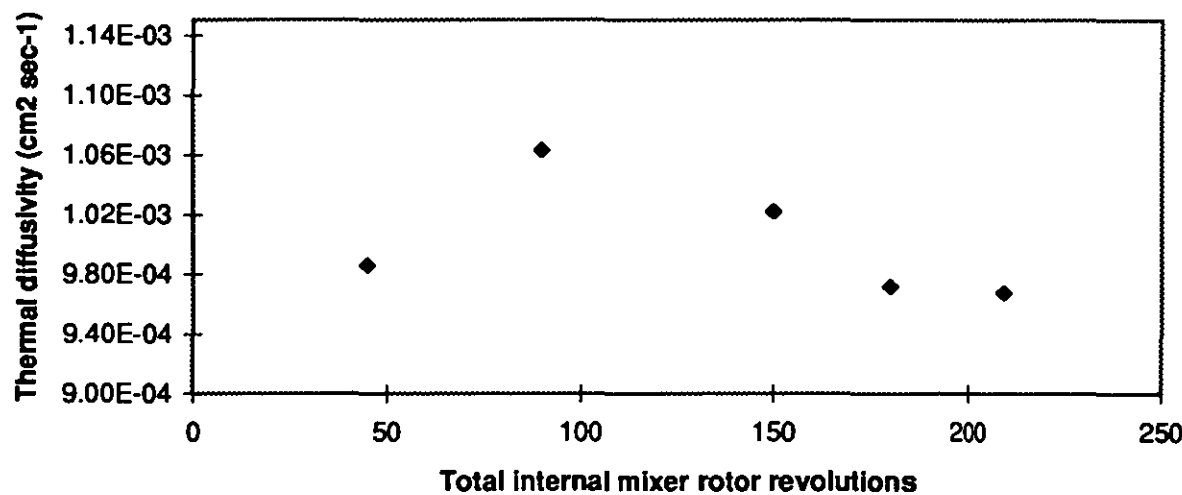


Figure 4.32 Thermal diffusivity as a function of the state of mix.

The validity of this data can be verified by referring to the reported data. Kaneko’s ¹¹⁾ data is quoted in Table 4.1 and the calculated diffusivity is listed in the same table. (There was not any data available for the specific conditions. Thus, the diffusivity is calculated here based on its definition (Equation 4.6)).

Table 4.1 Some thermal properties of polymer and carbon black (room temp).

	SBR	Carbon black
Conductivity(cal/cm ² sec ¹)	5.9×10 ⁻⁴	6.8×10 ⁻⁴
Density (g/cm ³)	0.94	1.90
Specific heat (cal/g)	0.452	0.204
Diffusivity (cm ² sec ⁻¹)	1.39×10 ⁻³	1.75×10 ⁻³

$$\alpha = \lambda / \rho C$$

α :diffusivity
 λ : conductivity

ρ : density
 C :specific heat

Equation 4.6

The measured data was found to be smaller in value compared to the calculated data. The difference arises from the fact that the reported data was based on the value at room temperature and the measured data reflected the value at the experimental temperature (180 °C). The temperature effect on thermal properties can be seen in Figure 2.33 in section 2.2.3.3. The temperature increase reduces the conductivity and results in a decrease of thermal diffusivity. Therefore, the measured data can be regarded as reasonable by considering the temperature effect on the thermal properties of rubber compounds.

The influence of carbon black dispersion on thermal property

Figure 4.32 shows the influence of carbon black dispersion on thermal diffusivity. The feature of the graph is that the thermal diffusivity is a monotonically decreasing function of the state of mix except at the short mixing time. The feature can be understood by considering the mechanism of thermal property.

The mechanism for thermal conduction is the transport phenomena and the relationship between viscosity, thermal conduction and electrical conduction is well established ^{12,13)}. For example, the relationship between viscosity and thermal conductivity follows the relationships ;

$$k = \left(C_p + \frac{5}{4} \frac{R}{M} \right) \mu \quad \text{Equation 4.7}$$

R : Gas constant, M: Molecular weight

The influence of carbon black dispersion on thermal property can be understood by referring to the model developed for electrical phenomena. Figure 4.33 is an example of electrical resistivity and shows a minimum point in Figure 4.33. This point corresponds to the maximum point of thermal diffusivity in Figure 4.32 and is explained by Cembrola. ¹⁴⁾ (The electrical resistivity is a reciprocal number of the electrical conductivity for a unit length. Therefore the graph of electrical conductivity becomes a reciprocal of Figure 4.33.)

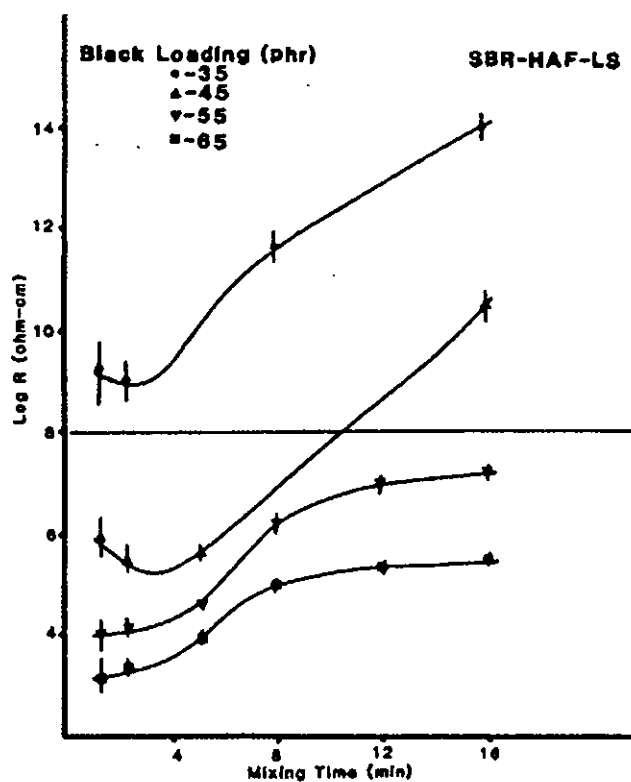


Figure 4.33 Log resistivity versus mixing time for low structure black loaded samples. ^{14, 15)}

“ In the early stages of mixing, the resistivity appears to go through a minimum. This is clearly seen for the low structure black compounds and, to a lesser extent, for the high structure black compounds. This phenomena has also been reported by Boonstra and Medalia ¹⁵⁾, although their measurements were made on vulcanised compounds. The explanation for this minimum is that, in the early stages of mixing, the black agglomerates are isolated, with few through going paths for electrical conduction. The resistivity would be governed by the gaps between agglomerates. As mixing proceeds and the agglomerates disappear, the distance of separation increases, but the resistivity of the matrix decreases owing to the increase of dispersed black. The minimum in resistivity arises as a result of these two opposing processes” ¹⁴⁾

To conclude, thermal diffusivity is a function of the state of mix. The mechanism is the one proposed by Boonstra and Medalia.

4.4.2 The relationship between bound rubber and the state of mix

In this subsection, the structure change of bound rubber will be discussed as a function of the state of mix.

The experimental procedure was explained in section 3.3.6. The NMR experimental data is shown in Table 4.2. Two types of information, (1) quality and (2) quantity of bound rubber, can be obtained from the NMR experiments. These are analysed in the following discussion.

Table 4.2 The relationship between NMR data and mixing time.

No	Mixing Time (sec)	Ratio (%)	Relaxation Time (S)
1	90	5.85×10^{-2}	1.02×10^{-2}
2	180	6.29×10^{-2}	7.66×10^{-3}
3	360	7.08×10^{-2}	9.79×10^{-3}
4	430	5.08×10^{-2}	7.94×10^{-3}
5	540	3.87×10^{-2}	7.77×10^{-3}

The quality of bound rubber (rigidity)

This quality is shown as a relaxation time in Table 4.2. (It should be noted that the more rigid the rubber around the carbon black the shorter the relaxation time.) The same data is plotted in Figure 4.34, and it indicates that the rigidity of bound rubber is a weak function of the state of mix.

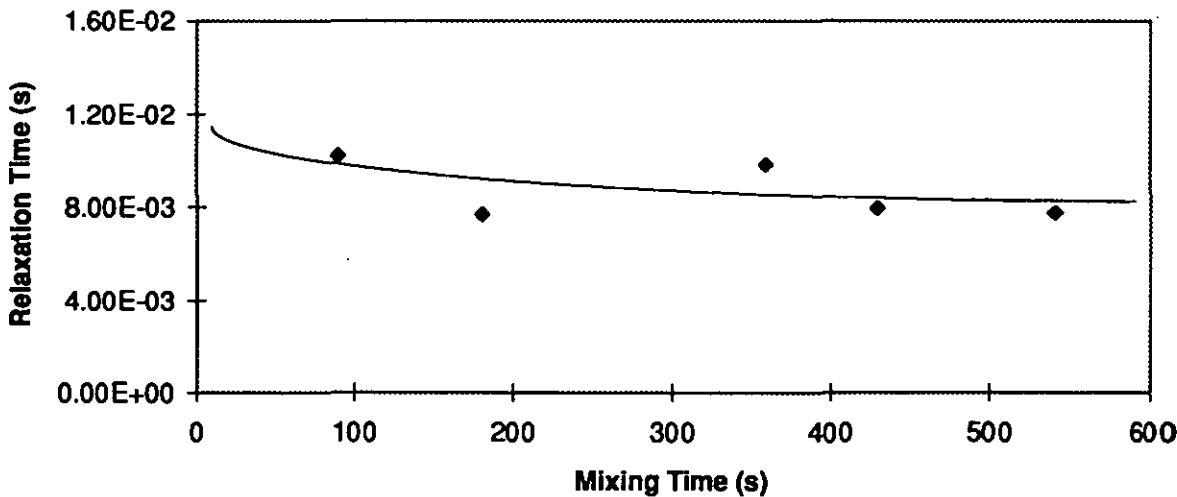


Figure 4.34 The relationship between mixing time and relaxation time of bound rubber.

The quantity of bound rubber (glassy state rubber around carbon black)

This quantity is shown as a ratio of bound rubber to the total polymer in Table 4.9, and Figure 4.35.

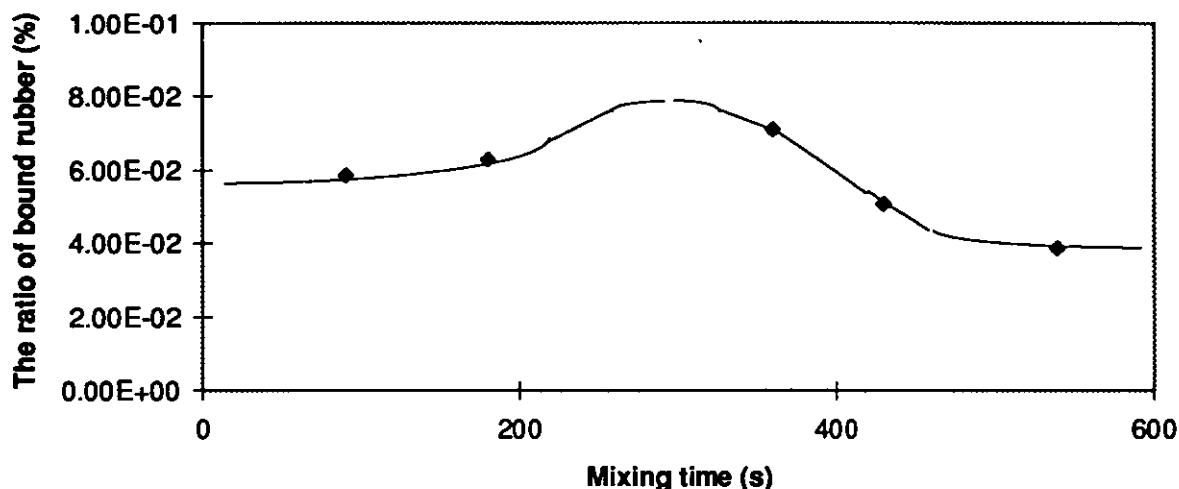


Figure 4.35 The relationship between the amount of bound rubber and mixing time. (Ref. 3.3.6)

Figure 4.35 shows a maximum point of the bound rubber as a function of mixing time. The maximum point suggests that two types of mechanism control the amount of bound rubber. These are : (a) an increase of bound rubber by the improvement of carbon black dispersion, and (b) a decrease of bound rubber by the change of segment length of bonded rubber.

(a) The amount of bound rubber is a function of the state of mix because the increase of aggregates produced by the decomposition of agglomerates results in an increase in the interaction between carbon black and the matrix polymer. This means that the amount of bound rubber is proportional to the state of mix.

(b) The mathematical model developed for proteins by de Gennes ¹⁶⁾ in Figure 4.36 can be applied to the counter effect mechanism.

At the early stage of mixing, the distribution of the bound rubber chain length is identical to the statistical random distribution because there is no preferred length for the bound

rubber. As the mixing continues, the longer chains become shorter because of scission and the adsorption of the segments in the chains on the carbon black surface. This model deduces two results :

- ① The first one is the reduction of relaxation time because a shorter chain cannot move freely like a long chain. This deduction agrees with **Figure 4.34**.
- ② The second is the reduction of the amount of bound rubber. The reduction of bound rubber will be balanced by the increase of the bound rubber arising from the increase of carbon black aggregates with the improvement of the state of mix. These phenomena balance each other and produce a maximum point as seen in **Figure 4.35**.

These agreement of the above deductions with the experimental data suggests the validity of the application of the de Gennes's model to bound rubber.

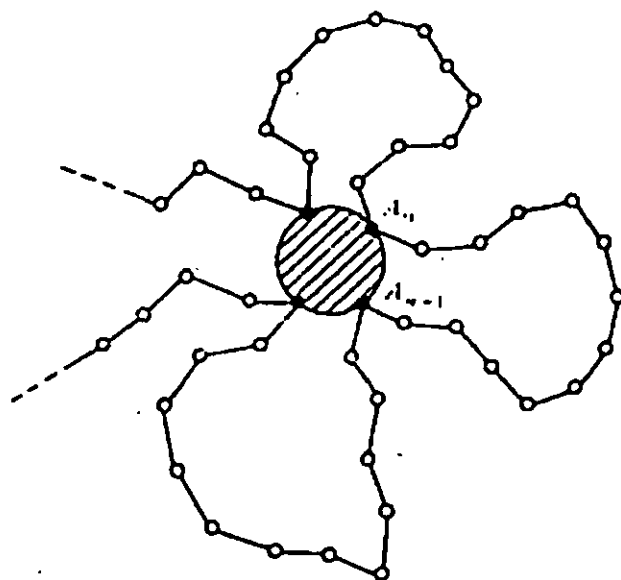


Figure 4.36 deGennes' model gives an ideal model for bound rubber. ¹⁶⁾

To conclude, it is shown that the quality and quantity of bound rubber is a function of the carbon black dispersion.

- 1) J. Clark, P. K. Freakley, *Rubb. Chem. Tech.*, 67 (4), 700 (1994)
- 2) C. M. Blow, C. Hepburn, "Rubber Technology and Manufacture", 2nd ed., Butterworth (1982)
- 3) J. D. Ferry, "Viscoelastic properties of polymers", John Wiley and Sons, (New York, 1960)
- 4) F. Bueche, "Physical Properties of Polymer", John Wiley & Sons., (1962)
- 5) A. V. Toborski, "Property and Structure of Polymer", John Wiley & Sons., (1960)
- 6) R. B. Bird, R. C. Armstrong, O. Hassager, "Dynamics of Polymer Liquid" 2nd ed., John Wiley & Sons., (1987)
- 7) L. R. G. Treloar "The physics of rubber elasticity", Oxford Univ. Press, (London, 1975)
- 8) K. Nishimoto, N. Urabe, *Nippon Gomu Kyokaishi* 65 (7), 82 (1992)
- 9) S. L. Lovejoy, *Science*, 216, 185 (1982)
- 10) H. Takayasu, "Fractal in Physical Science", Manchester Univ. Press (1990)
- 11) H. Kanako, "Ouyo Gomu Busseiron 20 kou", Taisei pub. (Tokyo 1985)
- 12) R. B. Bird, W. E. Stewart, E. N. Lightfoot, "Transport Phenomena", John Wiley and Sons (1960)
- 13) F. Reif, "Fundamentals of Statistical and Thermal Physics", McGraw Hill (1965)
- 14) R. J. Cembrola., *Polym. Eng. Sci.*, 22 (10), 601 (July, 1982)
- 15) B. B. Boonstra, A. I. Medalia, *Rub. Chem. Tech.*, 36, 115 (1963)
- 16) Y. Bayazitoglu, M. N. Ozisik, "Elements of Heat Transfer", McGrawhill (1988)
- 17) P. G. de Gennes, "Simple Views on Condensed Matter", World Science (1995)

Chapter 5

Conclusion and Recommendations

5.1 Conclusions

5.1.1 Fractal applications

1. The fractal concept has been applied successfully to characterise :

(1) The mixer power trace

MEM (Maximum entropy method) is applied to obtain a fractal dimension of mixing from a mixer power-trace. The fractal dimension decreases steadily as total rotor revolutions increase. The mechanisms which contribute to the fractal dimensions are disagglomeration of carbon black and mastication.

(2) Carbon black dispersion

The state of mix of carbon black is characterised by the fractal concept with the help of a box-counting method. The fractal dimension of the state of mix decreases steadily as mixing time evolves due to the disagglomeration of carbon black resulting in a decrease of carbon black agglomerates.

(3) Fracture surfaces

The fracture surface of the tensile sample is characterised by the MEM (Maximum entropy method). The fractal dimension of the fracture surface decreases as the state of mix is improved. Tensile strength at break of SBR and NR compounds are proportional to the fractal dimension of the fracture surface except for NR compounds with a long mixing time when mastication dominate the tensile strength. The fracture mechanism proposed by Medalia ¹⁾ gives a fundamental interpretation of the fractal dimension of fracture surfaces.

2. The relationship between mixing treatment (power trace), state of mix (carbon black dispersion) and fracture surfaces.

The relationship between the fractal dimensions of mixing, the state of mix and fracture surface are discussed and relatively straightforward linear and quadratic relationships are found. This simple relationships arise from the fact that the carbon black dispersion and its dispersion process dominate such properties in the experiments in this thesis.

3. Relationships between properties characterised by fractal analysis and characterised by conventional methods.

The results of fractal method of the carbon black dispersion are compared to two conventional methods : the measurement of electrical resistance and the Payne effect. It is shown that the fractal method is more closely related to the Payne effect than the electrical resistance. The fractal method in this thesis is a macroscopic evaluation method, and the influence of the state of mix on the Payne effect is dominated by macroscopic dispersion (volume fraction of agglomerates), whereas the electrical resistance measurement is also sensitive to micro-dispersion (aggregate breakage). The results follow the physics of the system. Therefore, the agreement of the fractal analysis and the conventional analysis gives the confidence of the validity of the fractal methods.

5.1.2 A new method to evaluate the state of mix of filler dispersion

Because of improvements in instrumentation, an up-dated method of ASTM D2663 (Method D) is proposed. The information from the new method is discussed using the procedure described in ASTM D2663 and is used to characterise the state of mix. It is shown that a new instrument (Rodestock RM600) provides a two dimensional evaluation method of carbon black dispersion, resulting in more suitable data than the conventional one dimensional method. The new two dimensional method did not require experimental repetition to obtain a statistical value. This resulted in the reductions of experimental time and effort in comparison with the conventional method.

5.1.3 The influence of the state of mix on rubber properties

The influence of the state of mix on 1) heat transfer and 2) bound rubber is discussed, based on the measured thermal diffusivity and NMR data, respectively.

1) Thermal diffusivity takes a maximum value at a certain point of carbon black dispersion and this phenomena is discussed with the relation to transport phenomena.

The mechanism is based on the disagglomeration of added carbon black, which results in the decrease of electrical path through carbon black agglomerates and the increase of electrical conductivity of the matrix during the mixing process.

2) Based on relaxation time and the amount of bound rubber, the influence of the state of mix on bound rubber is discussed. Two types of mechanisms are proposed. The first is an increase of bound rubber due to the improvement of the state of mix. The second is a change of segment length of the bound rubber (which is measured by relaxation time) resulting in a decrease in the amount of bound rubber.

These results suggest an improved understanding of the extent of the state of mix on rubber properties.

5.2 Recommendations

In this project, the fractal dimensions of mixing, carbon black dispersion and fracture surfaces are evaluated by comparing them to existing data. Some mechanisms are proposed, based on these experimental results. Further investigation is necessary for a better understanding and should include the mathematical modelling for mixing, carbon black dispersion process and fracture processes.

1. Mixing

The fractal dimensions of mixing in this thesis is evaluated based on existing data, but there is no fundamental explanation of the values. Thus, it is necessary to derive fractal dimensions from basic theories such as the Navier-Stokes' equation.

2. The state of mix of carbon black

The experimental data in this thesis reflect two dimensional evaluation of carbon black dispersion, and it is necessary to search three dimensional evaluations method for a better understanding of the influence of carbon black dispersion on rubber properties. The

starting point to obtain a theoretical model for the three dimensional carbon black dispersion and its dispersion process could be the Random Sierpinski Sponge mentioned in the literature review.

3. Fracture surface

A carbon black agglomerate is an initiating point of the fracture process and a fracture path reflects the state of mix of carbon black because the fracture path has to avoid bound rubbers, which has a higher hardness than normal bulk rubber. It could be possible to include the effect of carbon black dispersion in Takayasu's model ²⁾ by choosing a suitable parameters.

4. The other properties of rubber compounds

It is possible to search the relationship between mixing, the state of mix and the rubber properties. Some fractal application to evaluate the rubber properties, such as wear and fatigue, are already reported and it is necessary to discuss the relationship between such properties and the carbon black dispersion for the better understanding of the role of carbon black dispersion.

5. The method proposed to replace D2663 for filler dispersion measurement requires further interpretation. The peak position and its strength obtained by two dimensional Fourier transformation from Rodenstock RM 600 are used in this thesis, but it is possible to obtain more information from the instruments such as the dispersions of the peaks.

6. The microscopic model for bound rubber was discussed based on NMR data. It is necessary to discuss the validity of the proposed model by considering other properties such as the amount of bound rubber determined by solution extraction, and by calculating the amount of rigid rubber and its relaxation time based on de Gennes's model. ³⁾

References

- 1) A. I. Medalia, *Rubb. Chem. Tech.*, 60, 45 (1987)
- 2) H. Takayasu, *Phys. Rev. Lett.*, 1099, 54 (1985) ; *Prog. Theor. Phys.*, 1343, 74 (1985) ; "Fractals in Physics", ed. by L. Pietronero and E. Tosatti, (Elsevier Science Publisher B. V., 1986)
- 3) P. G. de Gennes, "Simple Views of Condensed Matter", World Science (1995)

Appendix 1 : The definition of the Peano Curve

A line on a plane can be expressed by the relationship between x and y .

$$y = f(x) \quad \text{Equation 1}$$

In some cases, it is convenient to use a parameter (t) to express the same line. So, Equation 1 is modified to

$$\begin{aligned} x &= \varphi(t) \\ y &= \phi(t) \end{aligned} \quad \text{Equation 2}$$

That the only restriction for these functions is their continuity for identifying a line without any ambiguity.

Imagine a line (T) and a triangle (Δ) (Figure 1). A correspondence will be considered between the line (one dimension) and the triangle (two dimensions).

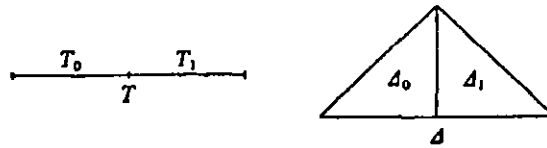


Figure 1. A correspondence between a line and a triangle by means of a parameter.¹⁾

In the first step, divide the line into two pieces. The right and left side and the centre are identified by T_0, T_1, T respectively. The triangle is divided into two pieces and a right and left side and a centre are labelled as $\Delta_0, \Delta_1, \Delta$, respectively.

As a second step, the same procedure continues again (Figure 2). The line T_0, T_1 are divided into two pieces and the resultant four lines are named $T_{00}, T_{01}, T_{10}, T_{11}$. The triangles are also divided into four pieces and they are named $\Delta_{01}, \Delta_{01}, \Delta_{10}, \Delta_{11}$. In the second step, the divided lines are in the sequence of $T_{00}, T_{01}, T_{10}, T_{11}$ from left to right.

The adjacent divided triangles share their sides. The relationship between the lines and the triangles are shown in **Figure 3**.

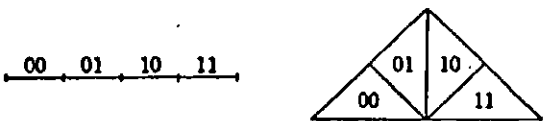


Figure 2. A second step to identify a position on a triangle. ¹⁾

By the same procedure, further divisions are carried out. The relationship are shown in **Figure 3** for a third step.

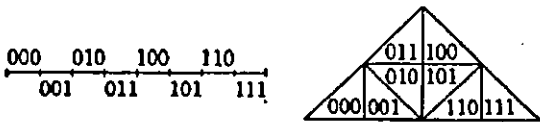


Figure 3. The third step of identify a correspondence between a line and a triangle.

It is possible to regard the identity symbol (abc.....l) as corresponding to a line T_{abc.....l}, which is mathematically unambiguous.

In addition, if parameter “t” is expressed by a binary form in the range of [0,1]

$$t = 0.C_1C_2C_3C.....C_n.....$$

Equation 3

the following topological relation is achieved.

$$\Delta_{c_1} \supset \Delta_{c_1\ c_2} \supset \Delta_{c_1\ c_2\ c_3} \supset \supset \Delta_{c_1\ c_2\ c_3\c_n} \supset$$

Equation 4

The infinite triangle sequence converges to a single point. When a co-ordinate system is used to describe the triangle plane, the co-ordinate (x, y) of the point P is identified without any ambiguity (Figure 4). The trace of the points in the above procedure defines a line by using the parameter (t).

$$\begin{aligned} x &= \varphi(t) \\ y &= \phi(t) \end{aligned}$$

Equation 5

It should be recognised that the correspondence from the line to the triangle is not a one to one relationship because the two end points on the divided line correspond to the only one point on the triangle. It is expressed as,

$$t = a/2^n$$

Equation 6

For example, a point on the line

$$t = 0.0101000..... = 0.0100111..... = 5/16$$

Equation 7

corresponds to a point

$$P = (0, 1/2)$$

Equation 8

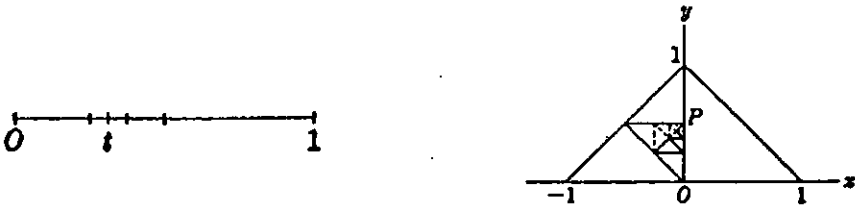


Figure 4. An example of the correspondence from the line to the triangle. ¹⁾

The above procedure gives the functions (φ(t)) a continuity. For example, if

$$|t - t'| < 1/2^{2^n}$$

Equation 9

the corresponding distance (PP') in the triangle is

$$|P - P'| < 1/2^{2-2^n}$$

Equation 10

This shows that, it is possible to approach any point by any precision.

The Koch Curve is defined by the same procedure (Figure 5).

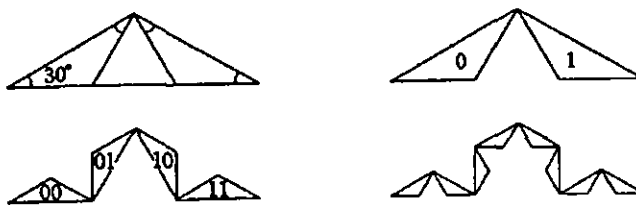


Figure 5. The Koch Curve and its mathematical definition. ¹⁾

Another example is the Jordan Curve which can be regarded as a combination of Koch Curves.(Figure 6)

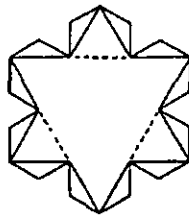


Figure 6. The Jordan Curve. ¹⁾

Appendix 2 : Fourier Transformation

The Fourier Transform ^{2,3)} is used to approximate a function by the sum of a trigonometric function series. One example is shown in Figure 7.

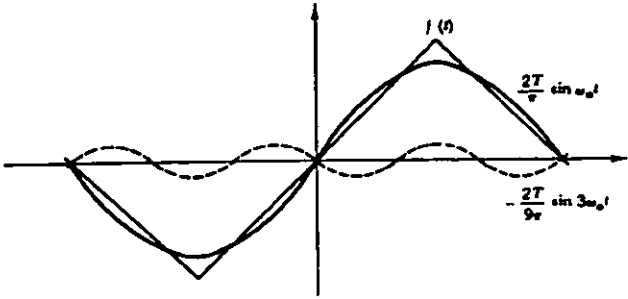


Figure 7. Fourier series approximation for a triangular wave. ²⁾

The definition of a Fourier Transform is given by

$$\begin{aligned}
 F(\omega) &= \int_{-\infty}^{\infty} f(t) \exp(-j\omega t) dt \\
 &= \int_{-\infty}^{\infty} f(t) (\cos(\omega t) - j \sin(\omega t)) dt \\
 &= S(\omega) - jC(\omega)
 \end{aligned}
 \tag{Equation 11}$$

The intensity of $S(\omega)$ and $C(\omega)$ depend on an analytical condition, but a square sum gives an intrinsic value for a system without any influence from the analytical conditions.

$$\begin{aligned}
 X(\omega) &= S(\omega)^2 + C(\omega)^2 \\
 &= |F(\omega)|^2
 \end{aligned}
 \tag{Equation 12}$$

The $X(\omega)$ is called a "Power Spectrum".

Appendix 3 : Maximum Entropy Method

To predict futures events in cosmology, earth physics or economic activities, it is very important to identify a regular pattern within irregular phenomena. Regularity can be detected by applying a Fourier Transform to observed signals. It is important to observe a signal fluctuation which is longer than the observable period. This is difficult, in the case of cosmic phenomena or geological physics because it is very difficult to collect data over long periods such as ten or more years. The maximum entropy method (MEM) ^{4,5)} is a spectrum measurement which enables us to estimate such long period phenomena with considerable accuracy by introducing the "Information Entropy" Concept ⁶⁾.

MEM A history and present situation

The maximum entropy method was introduced by Burg ⁵⁾ into mineral research and has been applied to find the relationship between solar activity and fluctuations of temperature on the earth, the wave analysis of earthquakes, and the polar rotation of the earth. The principle of MEM is that this method retains all of the estimated lags (observed intervals) without modification and uses a non-zero estimate for the lags not directly estimated. Because of this, MEM is very suitable for estimating a spectrum using only a few parts of a long - period signal. This method has attracted many researchers and it has been applied not only to time spectrum data but also to space or energy distributions. A typical example of these fields is X-ray measurement, such as computer tomography. MEM is applied to estimate unobservable data because of the restriction of observation or obstruction by human organs. A direct example is an application to Fourier Transform Spectroscopy. A resolution power is a function of maximum light path. MEM enables us to obtain the same data as that obtained by larger machines having equivalent differences of the light paths. It was once thought that MEM needed a main frame computer because of the computing time and memory capacities required. MEM is therefore not as common as Fast Fourier Transformation. Moreover recent advances of computer technology enable us to use MEM.

A problem of FFT

In this section, the problem of Discrete Fourier Transformation (DFT) and Fast Fourier Transformations (FFT) are shown. Fourier Transform is a method used to transform a signal into a spectrum. The problem of DFT or FFT arises from the difference in mathematical treatments between analogue functions and digital data. The definition of a Fourier Transformation is given by

$$X(\omega) = \int_{-\infty}^{\infty} x(t)e^{-j\omega t} dt \quad \text{Equation 13}$$

To carry out this calculation by a computer, Equation 13 has to be converted into a discrete expression.

$$\begin{aligned} X_t &= \sum_{k=0}^{N-1} x_k e^{-j\omega k \Delta t} \Delta t \\ x_k &= x(k\Delta t) \end{aligned} \quad \text{Equation 14}$$

N : The number of data

The problem of DFT and FFT arises from the difference between these two equations. The range of analytical expression is from $-\infty$ to ∞ . On the other hand, the range of the digitised equation is 0 to N-1. Because of the character of the Fourier Transformation, the latter equation assumes 'tacitly' the repetition of spectrum from 0 to N-1 at each ends of the range. It is not obvious that the signal is repeating on each side.

Another problem arises from the precision of digitised data. In the case of Equation 14, if the number of sampled data is 128, then the spectrum can be divided into the same resolution power. Originally, it was thought that these problems were not inevitable if the Fourier Transformation was calculated by using a computer. MEM is one method of overcoming these problems. The problems are explained in more detail, in order to understand them more precisely.

Figure 8 shows an example for the case of a cosine curve. The true spectrum is shown in (b) in Figure 8 and it is given as a line spectrum. It is impossible to measure a signal which continues infinitely. The (c), (e) and (f) in Figure 8 show the measured signal and (d), (f) and (h) show their spectrum, respectively, after being applied to the analogue-digital transformation and being subjected to FT. The (b) and (d) in Figure 8 give the same result but it was also found that if a sampling period became longer than (c), the spectrum developed ghost data as shown in (f).

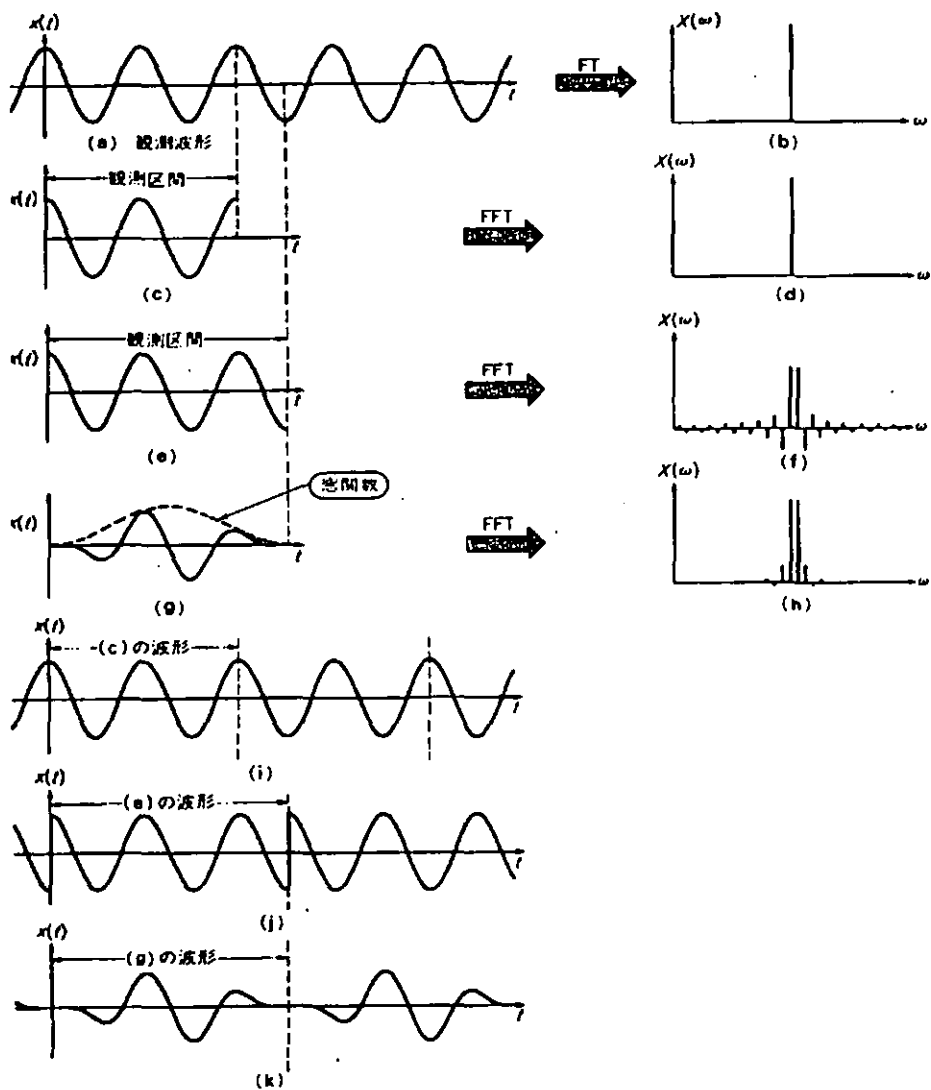


Figure 8 An explanation of Fourier Transformation. ⁴⁾

The data (e) has more information than (c) because it was collected over a longer time, thus giving more results (c). This figure illustrates that this may not be the case from the tacit repetition to change the definition of Fourier Transformation from a finite range to an infinite range. The spectra of (d), (f) was obtained from the signals in (i) and (j), respectively. In the case of (i), however, the same signal is by chance identical to the original one. But in the case of (j), the signal is deformed from the original signal by the tacit repetition. Because of the tacit repetition, it is impossible to obtain precise spectra from finite data. Sampled data must be connected smoothly at both sides of a measured range. To avoid such phenomena, it is common to apply a “window function” to the signal. The diagram (g) in Figure 8 shows an example. In this case, a cosine curve is multiplied to the measured data as a window-function. As the result of the window-unction, the error of spectra in the spectrum is reduced as can be seen (h) in Figure 8.

The principle of MEM

MEM is a method of estimating a spectrum from finite data on the basis of calculation which maximises the information entropy. This method was proposed by J.Burg in 1967. It became popular after Akaike ⁷⁾ proposed an alternative method known as the Auto Regressive Model. These two methods were proposed independently, but the latter method gives us a more comprehensive view than the former one. Although these methods give a different procedure to derive a result, the results give almost the same algorithm to carry out FT. In this research thesis, the Auto Regressive Model was used to carry out experiments.

The important point of Akaike’s model is that it assumes an auto regressive model for given data. An Auto Regressive Model is a model based on probability theory and is defined by

$$x_k = -\sum_{i=1}^m a_{mi}x_{k-i} + n_k$$

Equation 15

- x_k : data at number k
- a_m : auto regressive coefficient
- n_k : random noise
- m : the number of data points

An auto-correlation-function is assumed to take the following form.

$$Ri = R(i\Delta t) \equiv E\{x_k x_{k-i}\} \tag{Equation 16}$$

R : auto correlation function
 E : an expectation

By multiplying x_k to Equation 15,

$$\begin{aligned} R_0 = E\{x_k^2\} &= -\sum_{i=1}^m a_{mi} E\{x_k x_{k-i}\} + E\{x_k n_k\} \\ &= -\sum_{i=1}^m a_{mi} R_i + E\{n_k^2\} \end{aligned} \tag{Equation 17}$$

The independence of n from x was assumed in the derivation. Similarly, a matrix was constructed by multiplying $x_{k-1}, x_{k-2}, \dots, x_{k-m}$ to Equation 15.

$$\begin{bmatrix} R_0 & R_1 & \dots & R_m \\ R_1 & R_0 & \dots & R_{m-1} \\ \vdots & \vdots & \ddots & \vdots \\ R_m & \dots & \dots & R_0 \end{bmatrix} \begin{bmatrix} 1 \\ a_{m1} \\ \vdots \\ a_{mm} \end{bmatrix} = \begin{bmatrix} P_m \\ 0 \\ \vdots \\ 0 \end{bmatrix} \tag{Equation 18}$$

here P_m is a deviation of white noise. From the Wiener-Khinchin (Appendix 4) equation, the following relation can be obtained.

$$S(\omega) = \frac{P_m \times \Delta t}{\left| 1 + \sum_{i=1}^m a_{mi} e^{-j\omega i \Delta t} \right|^2} \tag{Equation 19}$$

$S(\omega)$: A power spectrum of datum

Using this equation, a power spectrum from the given data set can be obtained.

In the case of the Auto Regression Model, the order of regression is very important because it affects the result of the power spectrum. Akaike proposed a solution to the problem called the Final Prediction Error method (FPE). FPE is a statistical amount of Q_m and is given by

$$Q_m = E \left\{ \left(x_k - \sum_{i=1}^m \hat{a}_{mi} x_{k-i} \right)^2 \right\} \quad \text{Equation 20}$$

This value can be calculated by using the following equations.

$$Q_m = \left(1 + (m+1)/N \right) \left(1 - (m+1)/N \right)^{-1} E_m^2$$

$$E_m^2 = \sum_{k=m+1}^N \left(x_k - \sum_{i=1}^m \hat{a}_{mi} x_{k-i} \right)^2 \quad \text{Equation 21}$$

The order of regression is defined as the number which gives a minimum number of FPE.

The programme of maximum entropy method

```

1000 REM *****
1010 REM *
1020 REM * Maximum Entropy Method *
1030 REM *
1040 REM *****
1050 REM
1060 REM Main Routine
1070 REM
1071 CLS : SCREEN 12
1080 DEFINT I-N
1090 WIDTH 80, 60: CLS
1100 PRINT SPC(6); "***** MEM *****": PRINT
1110 INPUT "Number of Sample = "; nd: PRINT
1120 INPUT "delta time = "; DT: PRINT
1130 INPUT "Do you want to define the model index? (Y/N) "; AN$: PRINT
1140 IF AN$ = "Y" THEN ISW = 1: P$ = "**** Model Index =" ELSE
    IF AN$ = "N" THEN ISW = 0: P$ = "**** Max Model Index =" ELSE 1130
1150 PRINT P$; : INPUT MMAX: PRINT
1160 DIM x(1024)
1170 GOSUB 1310
1180 REM CONSOLE 1, 1, 0, 0

```

```

1190 ns = nd: wnmin = 0: wnmax = nd
1200 N$ = " Data ": GOSUB 2110
1210 GOSUB 1420
1220 INPUT " Minimum Frequency = "; wnmin
1230 INPUT " Maximum Frequency = "; wnmax
1240 INPUT " Number of Spectra "; ns
1250 WNINT = (wnmax - wnmin) / ns: GOSUB 1960
1260 ns$ = " MEM spectrum ": GOSUB 2401
1261 LOCATE 58, 1: PRINT SPC(20);
1270 INPUT " Do you want to try it again? (Y/N)"; AN$
1280 IF AN$ = "Y" THEN 1220 ELSE IF AN$ <> "N" THEN 1270
1290 REM CONSOLE 0, 20, 0, 0
1300 STOP
1310 REM
1320 REM   Data Input Routine
1330 REM
1340 INPUT " ***   Data File Name   = "; NM$
1350 OPEN "A:" + NM$ FOR INPUT AS #1
1360 FOR i = 1 TO nd: INPUT #1, x(i): NEXT
1370 CLOSE #1
      xxmax = x(1): xxmin = x(1)
      FOR i = 2 TO nd
        IF x(i) > xxmax THEN xxmax = x(i)
        IF x(i) < xxmin THEN xxmin = x(i)
      NEXT
      FOR i = 1 TO nd
        x(i) = 100 * x(i) / (xxmax - xxmin)
      NEXT

1380 RETURN
1390 REM
1400 REM   AR-Model Estimation Routine
1410 REM
1420 DIM y(nd), FPE(MMAX), R(MMAX), RR(MMAX), RFPE(MMAX)
1421 CLS : PRINT "Calculating AR-model"
1430 SUM = 0
1440 FOR i = 1 TO nd
1450   SUM = SUM + x(i)
1460 NEXT
1470 AV = SUM / nd
1480 SUM = 0
1490 FOR i = 1 TO nd
1500   Z = x(i) - AV: x(i) = Z: y(i - 1) = Z
1510   SUM = SUM + Z * Z
1520 NEXT
1530 PM = SUM / nd
1540 FPEMIN = (nd + 1) / (nd - 1) * PM: FPE(0) = FPEMIN
1550 REM
1560 FOR M = 1 TO MMAX
1570   SUMN = 0: SUMD = 0
1580   FOR i = 1 TO nd - M
1590     SUMN = SUMN + x(i) * y(i)
1600     SUMD = SUMD + x(i) * x(i) + y(i) * y(i)
1610   NEXT

```

```

1620 RM = -2 * SUMN / SUMD: R(M) = RM
1630 PM = PM * (1 - RM * RM)
1640 IF M = 1 THEN 1680
1650 FOR i = 1 TO M - 1
1660   R(i) = RR(i) + RM * RR(M - i)
1670 NEXT
1680 FOR i = 1 TO M
1690   RR(i) = R(i)
1700 NEXT
1710 FOR i = 1 TO nd - M - 1
1720   x(i) = x(i) + RM * y(i)
1730   y(i) = y(i + 1) + RM * x(i + 1)
1740 NEXT
1750 IF ISW = 0 THEN GOSUB 1800
1760 NEXT
1770 IF ISW = 1 THEN GOSUB 1880
1780 RETURN
1790 REM
1800 FPE(M) = (nd + M + 1) / (nd - M - 1) * PM
1801 PRINT M, FPE(M)
1810 IF FPE(M) > FPEMIN THEN RETURN
1820 FPEMIN = FPE(M): MINM = M: PMM = PM
1830 FOR i = 1 TO M
1840   RFPE(i) = R(i)
1850 NEXT
1860 RETURN
1870 REM
1880 MINM = MMAX: PMM = PM
1890 FOR i = 1 TO MMAX
1900   RFPE(i) = R(i)
1910 NEXT
1920 RETURN
1930 REM
1940 REM   Power Spectrum Estimation Routine
1950 REM
1960 CI = 2 * 3.14159 * DT
1970 i = 0
1980 FOR F = wnmin TO wnmax STEP WNINT
1990   SUM1 = 1: SUM2 = 0
2000   FOR j = 1 TO MINM
2010     SUM1 = SUM1 + RFPE(j) * COS(CI * F * j)
2020     SUM2 = SUM2 + RFPE(j) * SIN(CI * F * j)
2030   NEXT
2040   x(i) = PMM * DT / (SUM1 * SUM1 + SUM2 * SUM2)
2050   i = i + 1
2060 NEXT
2070 RETURN
2080 REM
2090 REM   Output Routine
2100 REM
2110 x0 = 75: y0 = 400: xl = 512: yl = 380: ms = 10
2120 xmax = x(1)
2130 FOR i = 2 TO ns
2140   IF x(i) > xmax THEN xmax = x(i)

```

```

2150 NEXT
2160 CLS : SCREEN 12
2170 LINE (x0, y0 + 3)-(x0, y0 - y1), 4: REM y-axis
2180 LINE (x0 - 3, y0)-(x0 + x1, y0), 4: REM x-axis
2190 FOR i = 1 TO ms
2200   xx = x0 + x1 / ms * i: LINE (xx, y0 + 1)-(xx, y0 + 4): REM x-axis scale
2210 NEXT
2220 A$ = STR$(wnmin): XXX = INT((x0 - 8 * LEN(A$) - 8) / 8 + 1): YYY = INT((y0 + 8) / 8 + 1)
2221 LOCATE YYY, XXX: PRINT A$
2230 A$ = STR$(wnmax)
2231 YYY = INT(((x0 + x1 - 8 * LEN(A$) - 8) / 8 + 4)): XXX = INT((y0 + 6) / 8 + 2)
2232 LOCATE XXX, YYY: PRINT A$
2240 REM LOCATE Y0 - 3, X0 - 22: PRINT "0";
2250 A$ = STR$(xmax)
2251 XXX = INT((y0 - y1 - 10) / 8): YYY = ((x0 - 8 * LEN(A$) - 8) / 8 + 4)
2252 LOCATE YYY, XXX: PRINT A$
2260 sc = x1 / ns: xmax = xmax / y1
      PSET (x0 + sc, y0 - x(i) / xmax)
2270 FOR i = 2 TO ns: REM dada plot
2280   LINE -(x0 + sc * i, y0 - x(i) / xmax)
2290 NEXT
2300 NN = 15 - INT(LEN(NS) / 2): N$ = STRING$(NN, "*") + N$ + STRING$(NN, "*")
2310 REM PRINT N$
2320 LOCATE 57, 1: PRINT SPC(20); : INPUT "Hard Copy(Y/N)"; AN$
2330 IF AN$ = "Y" THEN copy = 1 ELSE IF AN$ <> "N" THEN 2320
2340 PRINT SPC(20); : INPUT "Data Save(Y/N)"; AN$
2350 IF AN$ = "N" THEN 2400 ELSE IF AN$ <> "Y" THEN 2340
2360 INPUT "Data file name = "; NM$
2370 OPEN "A:" + NM$ FOR OUTPUT AS #2
2380 FOR i = 1 TO ns: WRITE #2, i, x(i): NEXT
2390 CLOSE #2
2400 RETURN
2401 REM log - log plot
      CLS 2
2402 x0 = 75: y0 = 400: x1 = 380: y1 = 380: ms = 10
      LINE (x0, y0)-(x0 + x1, y0 - y1), 4, B: REM OUTLINE

2403 xmax = x(1): REM RENORMALIZATION
2404 FOR i = 2 TO ns
2405   IF x(i) > xmax THEN xmax = x(i)
2406 NEXT
2408 rex = INT(.4343 * LOG(wnmax / wnmin))
2409 rey = INT(.4343 * LOG(xmax))
2410 cwx = 380 / rex: cwy = 380 / rey: REM X-AXIS AND ITS SCALE
2411 FOR j = 1 TO rex
2412   FOR i = 2 TO 10 STEP 2
2413     x = x0 + cwx * (j - 1) + (LOG(i) / LOG(10)) * cwx
2414     IF j = rex AND i = 10 THEN 2417
2415     IF i = 10 THEN LINE (x, y0)-(x, y0 - 6) ELSE LINE (x, y0)-(x, y0 - 3)
2416   NEXT i
2417 NEXT j
      REM X AXIS SCALE FIGURE
      FOR j = 1 TO rex + 1
        py = INT((cwx * (j - 1) + x0) / 8)

```



```

        LOCATE 52, py - 1
        PRINT USING "###^"; wnmin * 10 ^ (j - 1)
    NEXT j
    LOCATE 53, 25
    PRINT " Freq (Hz) "
    REM Y AXIS
2418 FOR j = 1 TO rey
2419     FOR i = 2 TO 10 STEP 2
2420         y = y0 - (cwy * (j - 1) + LOG(i) / LOG(10) * cwy)
2421         IF j = rey AND i = 10 THEN 2424
2422         IF i = 10 THEN LINE (x0, y)-(x0 + 6, y) ELSE LINE (x0, y)-(x0 + 3, y)
2423     NEXT i
2424 NEXT j
    FOR j = 1 TO rey + 1
        py = INT((y0 - cwy * (j - 1) + LOG(j * 10) / LOG(10)) / 8)
        LOCATE py + 1, 6
        PRINT USING "###"; 10 ^ (j - rey - 1)
    NEXT j

    PSET (x0, y0 - y1)
2425 FOR i = 1 TO ns - 1
2426     xx = x0 + 380 * (LOG(wnmin + i / ns * (wnmax - wnmin)) - LOG(wnmin)) / (LOG(wnmax) -
LOG(wnmin))
2427     yy = y0 - 380 * LOG(x(i)) / LOG(xmax)
2428     PSET (xx, yy)
2429 NEXT i
    FOR i = 1 TO 1000 STEP 10
        xp = wnmin + i / ns * (wnmax - wnmin)
        LPRINT USING "###.###^"; xp;
        LPRINT SPC(20);
        LPRINT USING "###.###^"; x(i)
    NEXT i
2430 RETURN
2500 REM
2510 END

```

Appendix 4 : Analysis of random data

An concept of random data is shown in Figure 9.

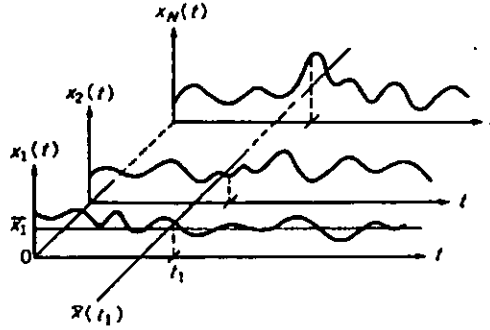


Figure 9 Random data series. ⁸⁾

Statistical quantities and its definition

(1) Mean time

Mean time is defined for each time sequence data in Figure 9. It is defined as an average value in each time sequence.

$$\overline{x_k} = \lim_{T \rightarrow \infty} \frac{1}{T} \int_0^T x_k(k) dt$$

Equation 22

(2) An ensemble mean

An ensemble mean is defined as an average value of an ensemble at one time t_1 . It is defined by ;

$$\overline{x(t_1)} = \lim_{N \rightarrow \infty} \frac{1}{N} \sum_{k=1}^N x_k(t_1)$$

Equation 23

(3) Dispersion and correlation function

A dispersion gives information about the broadness of a distribution and the definition is

$$\sigma^2 = \lim_{T \rightarrow \infty} \frac{1}{T} \int_0^T [x(t) - \bar{x}]^2 dt \quad \text{Equation 24}$$

A correlation function gives information about the relationship between two points with a time interval $\Delta\tau$, and it is defined as

$$R(\tau) = \lim_{T \rightarrow \infty} \frac{1}{T} \int x(t)x(t+\Delta\tau)dt \quad \text{Equation 25}$$

(4) Probability density function

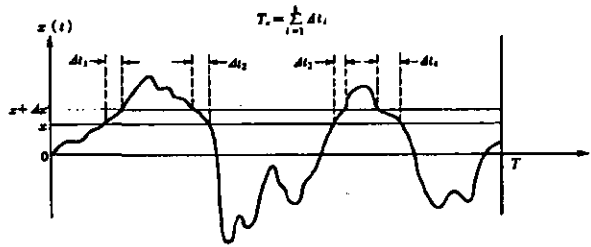


Figure 10 An explanation of a probability density function.⁸⁾

A probability density function gives us information about a frequency in standard form. Imagine that the ratio of data between $x + \Delta x$ to whole data in **Figure 10** has to be calculated. The probability is given by

$$T_x = \sum_{i=1}^k \Delta t_i$$

$$\text{Pr ob}[x < x(t) < x + \Delta x] = \lim_{T \rightarrow \infty} \frac{T_x}{T} \quad \text{Equation 26}$$

For a continuous function, it is possible to take a limit of $\Delta x \rightarrow \infty$,

$$p(x) = \lim_{T \rightarrow \infty} \frac{\text{Pr ob}[x < x(t) < x + \Delta x]}{\Delta x} = \lim_{\Delta x \rightarrow \infty} \lim_{T \rightarrow \infty} \frac{1}{\Delta x} \left(\frac{T_x}{T} \right) \quad \text{Equation 27}$$

Relationship between a power spectrum and a correlation function

The correlation function is related to a power spectrum by

$$\begin{aligned} S_x(\omega) &= \int_{-\infty}^{\infty} R_x(\tau) \exp(-j\omega\tau) d\tau \\ R_x(\tau) &= \int_{-\infty}^{\infty} S_x(\omega) \exp(j\omega\tau) d\omega \end{aligned} \quad \text{Equation 28}$$

Equation 28 is called The Wiener-Khinchin Relationship and is a starting point for random data analysis.

Appendix 5 : A random flight model as an example of a random walk

A case of arranging a chain in a line will be discussed. It is assumed that the segment length of the chain is “a”, and the chain molecule consists of “n” segments. Each segment can take a direction without any influence from adjacent segments. This assumption is called a free joint model. At first, it is necessary to determine a thermodynamical weight “W₁” under the condition of a constant end segment length “x”. Assume that the symbols of “+” and “-” stand for right or left in direction, respectively, and that the number of segments which have right and left direction are labelled as “n₊” and “n₋”. In this case, the distance between the ends is

$$x = (n_+ - n_-) \times a \quad \text{Equation 29}$$

When the segment number n₊ and n₋ are fixed, the thermodynamical weight is equal to

$$W = n! / n_+! n_-! \quad \text{Equation 30}$$

Because a molecular length is fixed, then the total segment number has to follow the following equation :

$$n_+ + n_- = n \quad \text{Equation 31}$$

From these equations,

$$n_+ = \frac{na + x}{2a} = \frac{n}{2} \times \left(1 + \frac{x}{an}\right), \quad n_- = \frac{na - x}{2a} = \frac{n}{2} \times \left(1 - \frac{x}{an}\right) \quad \text{Equation 32}$$

If “n” is big enough, it can be considered that W is a continuous function of x. In such a case, Stirling’s Formula is applicable.

$$\log n! = n \log n - n \quad \text{Equation 33}$$

By using the formula, the thermodynamical weight may be approximated ;

$$\log W = n \log n - n_+ \log n_+ - n_- \log n_- \quad \text{Equation 34}$$

Assume $(x/an) \ll 1$, then the following relation is obtained.

$$\log n_+ = \log\left(\frac{n_+}{2}\right) + \log\left(1 + \frac{x}{an_+}\right) = \log\left(\frac{n_+}{2}\right) + \frac{x}{n_+a} - \frac{1}{2}\left(\frac{x}{n_+a}\right)^2 \quad \text{Equation 35}$$

Substituting Equation 35 into Equation 33, then

$$\begin{aligned} \log W &= n \log 2 - \frac{x^2}{2na^2} \\ (\because) W &= 2^n \times \exp\left(-\frac{x^2}{2na^2}\right) \times C \end{aligned} \quad \text{Equation 6.36}$$

Here, C is a constant. Since the probability of all cases is $2n$, C has to satisfy the equation below.

$$\int_{-\infty}^{\infty} W(x) dx = 2^n \quad \text{Equation 37}$$

From this restriction, the constant C is decided and becomes

$$W = \frac{2^n}{\sqrt{2\pi na}} \times \exp\left(-\frac{x^2}{2na^2}\right) \quad \text{Equation 38}$$

To get a relationship between stress and strain, it is assumed that the chain molecule system contacts to a thermal reservoir of temperature T. From Boltzman's Principle,

$$S = k \log W(x) \quad \text{Equation 39}$$

In addition, the following thermodynamical relationship is adopted here.

$$dA = dU - TdS \quad \text{Equation 40}$$

Differentiating this equation by dx

$$F = -T \frac{\partial S}{\partial x} = -kT \frac{\partial \log W}{\partial x} = \frac{kT}{2a} \log \frac{na + x}{na - x} \quad \text{Equation 41}$$

$$(\therefore) F = \frac{kT}{2a} \log \frac{na + x}{na - x}$$

This equation is the conclusion of Guth's Theory ⁹⁾ of rubber elasticity. It is impossible to regard this conclusion as a model of rubber elasticity because there are many chain molecules in bulk rubber, and each molecule affects each other so that they produce a complicated behaviour under the specific force. Furthermore, this treatment neglects the volume of each segment. If each segment has no volume, the distance between the end segments has to be zero under no force. In addition, the intrinsic angle of chemical bonds are neglected. A chemical bond has its own specific direction. Oka ¹¹⁾ treated this problem and concluded that the stationary volume of macromolecules becomes bigger than for the free joint model because of the exclusive volume effect.

The meaning of Guth's model lies in the fact that he showed us how to treat the micro Brownian Movement of macromolecules and that the essential mechanism of rubber elasticity is an entropy effect arising from the thermal micro Brownian Movement of segments. The subsequent researches on rubber elasticity are based on Guth's Model ¹¹⁾.

Appendix 6 : Smith's failure envelope

Based on experimental results, Smith ¹²⁾ found that the relationship between a tensile strength (S_b) or an elongation (y_b) at break and the strain rate (R) at temperature (T) produces one master curve. As a strain rate increases, tensile strength increases continuously but an ultimate strain approaches a maximum point at a certain strain rate and decreases after exceeding that point. **Figure 11** and **Figure 12** show the results.

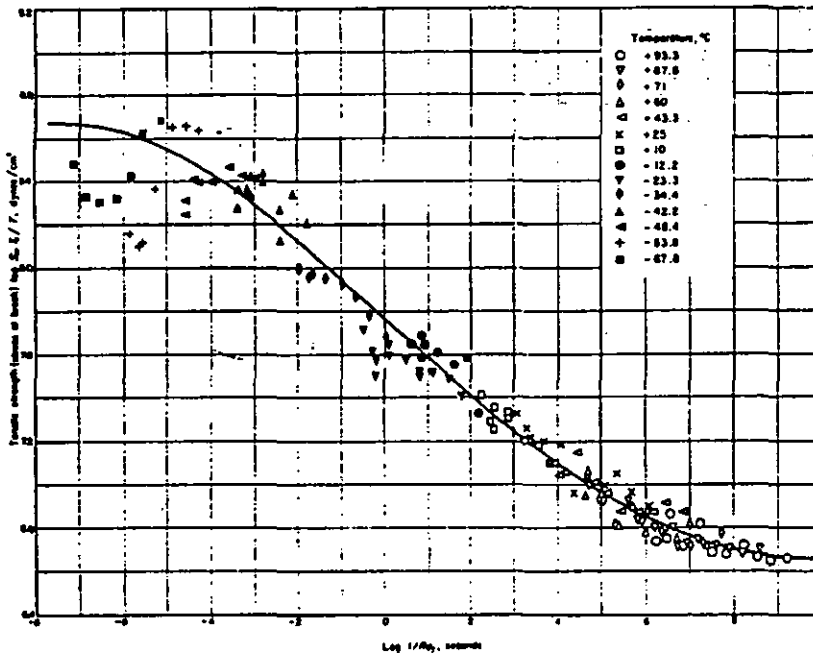


Figure 11 The variation of tensile strength with reduced strain rate. ¹²⁾

In this graph, a strain rate is expressed as reciprocal form $1/Ra$. In the case of viscoelasticity, **Figure 11** corresponds to storage modulus and **Figure 12** corresponds to the loss modulus, respectively. To evaluate the analogy between ultimate properties and viscoelasticity, Smith compared a shift factor to the theoretical value based on the Williams, Landel and Ferry (WLF) Equation.

$$\log a_i = \frac{-8.86(T - T_i)}{101.6 + (T - T_i)} \quad \text{Equation 42}$$

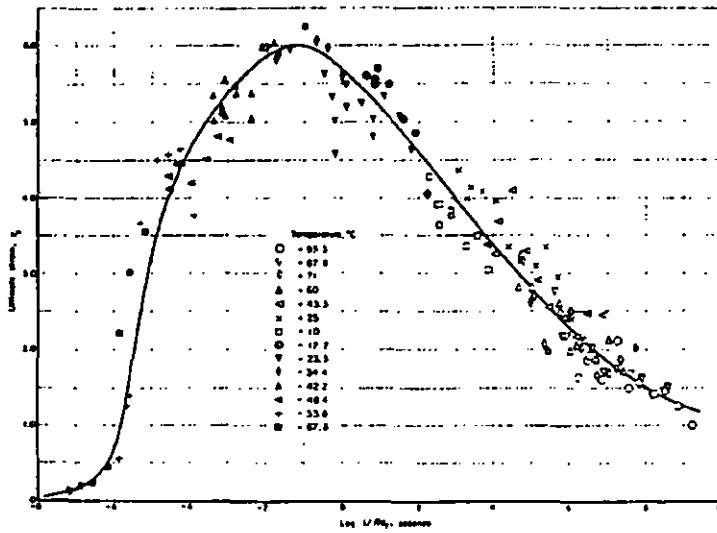


Figure 12 The variation of ultimate strain with reduced strain rate. ¹²⁾

where T_s is a standard reference temperature which has been found to be about 50 ± 5 above T_g for a wide variety of polymers, organic glass - forming liquids and inorganic glasses. The comparison is shown in Figure 13.

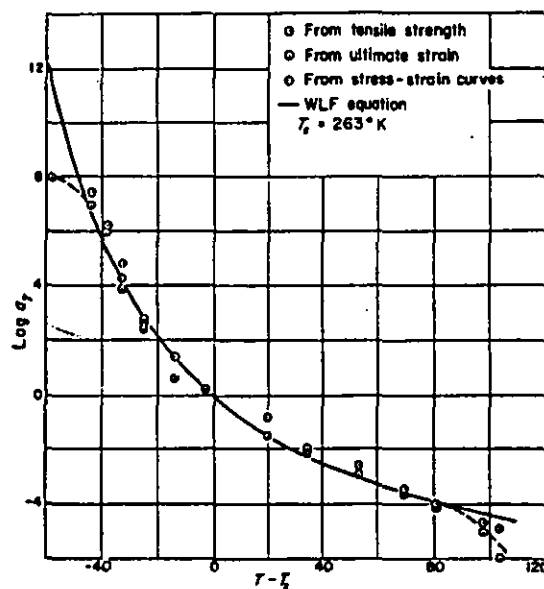


Figure 13 Experimental value of $\log(a_T)$ compared with the WLF equation. ¹²⁾

Considering that the WLF equation was derived from free volume theory and that it is usually only used for a small deformation range, it is interesting to find that the WLF equation is applicable to ultimate properties. This result may end to new theory because it gives us an essential variable which does not depend on materials. To establish such a theory which can explain Smith's Failure Envelope, it is necessary to explore researches which give a basic concept of the viscoelastic behaviour of ultimate properties.

Appendix 7 : Hashizume's model for carbon mixing

Hashizume¹³⁾ gives a basis for fractal analysis. Hashizume's analysis treated Newtonian and non - Newtonian fluids and discussed a flow property in each case.

To analyze the flow mathematically, Hashizume simplified the shape of the rotor in an internal mixer as shown in Figure 14.

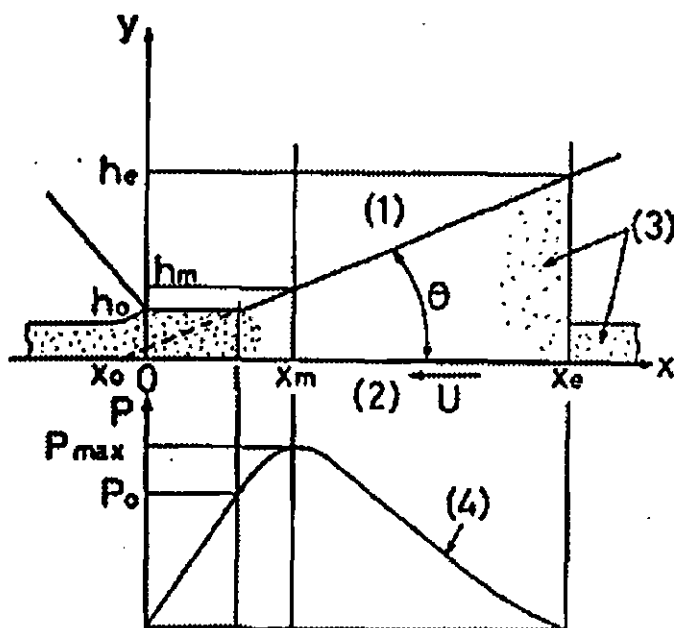


Figure 14 The magnified picture about the rotor tip. To analyse rubber flow mathematically, this simplified picture is adopted.¹¹⁾

Based on this simplification, the following equations are derived from the equations of continuity and momentum,

$$\frac{\partial}{\partial x}(\rho v_x) = 0$$

$$\rho v_x \frac{\partial v_x}{\partial x} = -\frac{\partial P}{\partial x} + \frac{\partial \tau_{xy}}{\partial y}$$

Equation 43

ρ : Density of materials

P, τ : Normal force and shear applied on sample

v : Velocity of materials

There are several types of non - Newtonian flow. Hashizume adopted the flow which follows the power law. In this case, a rheological equation can be written by

$$\frac{dP}{dx} = k \frac{d}{dy} \left\{ \left(\frac{dv_x}{dy} \right)^n \right\}$$

Equation 44

Combining these three equations, it is possible to obtain the pressure distribution for material flow. Integrating **Equation 44** by y , then,

$$\left(\frac{dv_x}{dy} \right)^n = \frac{1}{k} \left(\frac{dP}{dx} \right) y + c_1$$

Equation 45

dv_x/dy may be integers although it is not necessary for "n" to be an integer. This equation was to be solved by division into three regions. **Figure 15** shows these regions and some explanation of the nomenclature. The derivation for each case is as follows ;

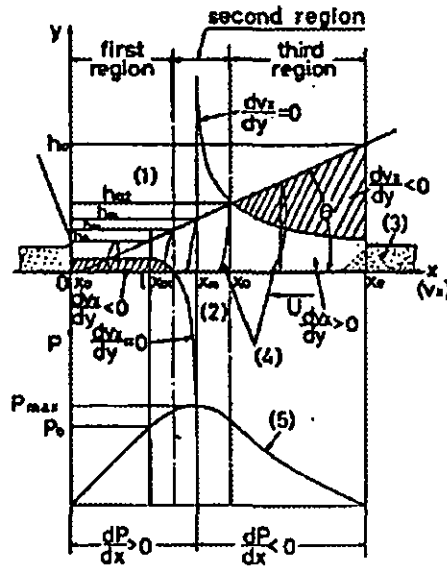


Figure 15. Three regions of rubber flow and the pressure distribution.

First region

In the first region, the condition is $dP/dx > 0$. Furthermore, $dv_x/dy < 0$ in the case of $0 < y < h_{01}$.

Then,

$$v_x = \left\{ \frac{1}{k} \left(\frac{dP}{dx} \right)^{1/n} \right\} \frac{n}{n+1} \left\{ (y_0 - y)^{1+1/n} - y_0^{1+1/n} \right\} - U \quad \text{Equation 46}$$

considering the boundary condition $v_x = -U$ when $y=0$. By expanding right term under the condition $y_0 < h$, then,

$$y_0 = \frac{n}{n+1} h + \frac{U}{\left\{ -\frac{1}{k} \left(\frac{dP}{dx} \right)^{1/n} \right\} h^{1/n}} \quad \text{Equation 47}$$

As seen in the analysis of another region, this equation governs the flow property for all regions, even those which are derived from other conditions.

Second region

The condition of this region is $dv_x/dy > 0$. Integration of Equation 47 by y , gives

$$U = \frac{n}{n+1} \left\{ \frac{1}{k} \left(\frac{dP}{dx} \right) \right\}^{1/n} h^{1+1/n} \left\{ (1+\alpha)^{n+1/n} - \alpha^{n+1/n} \right\}$$

Equation 48

$$\alpha = \frac{c_1}{\frac{1}{k} \left(\frac{dP}{dx} \right) h}$$

considering a boundary condition, $v_x = -U$ when $y=0$. By expanding $(1+\alpha)^{n+1/n}$ until the second term, an approximation equation of Equation 49 will be obtained.

$$U \equiv c_1^{1/n} \left\{ 1 + \frac{h}{2nc_1} \frac{1}{k} \left(\frac{dP}{dx} \right) \right\}$$

Equation 49

From this equation, it is possible to decide c_1 , and substituting it to Equation 49, a flow of material is expressed by,

$$Q_x = \frac{UH}{2} + \frac{h^3}{12nk} \left(\frac{U}{h} \right)^{1-n} \left(\frac{dP}{dx} \right)$$

Equation 50

At the pressure maximum point, $dP/dx=0$. So, we get

$$Q_x = \frac{Uh_m}{2}$$

Equation 51

From this equation, the final equation about pressure distribution is obtained.

$$\frac{dP}{dx} = 6nk \left(\frac{U}{h} \right)^n \frac{h_m - h}{h^2} \quad \text{Equation 52}$$

The result is shown in **Figure 15**. The important point of this equation is the location of pressure where maximum pressure occurs. This derivation tells us that the location of maximum pressure is located in front of the rotor tip.

Third region and total analysis

The condition of the third region is $dp/dx < 0$. Using the same analysis in section 6.1.7.2, the following relation is obtained.

$$y_0 = \frac{n}{n+1} h + \frac{U}{\left\{ -\frac{1}{k} \left(\frac{dP}{dx} \right) \right\}^{1/n} h^{1/n}} \quad \text{Equation 6.53}$$

Using the angle between rotor and chamber wall, θ , Equation 6.53 can be written as

$$\frac{dP}{dh} = \frac{6nk}{\tan \theta} \left(\frac{U}{h} \right)^n \frac{h_m - h}{h^2} \quad \text{Equation 6.54}$$

Integrating Equation 6.54 by h under a boundary condition $P=0$ when $h=h_0$, a general expression for P can be obtained.

$$P = \frac{6nk}{\tan \theta} U^n \left[\frac{1}{n} \left\{ \frac{1}{(x-x_0)^n \tan^n \theta} - \frac{1}{h_e^n} \right\} - \frac{h_m}{n+1} \left\{ \frac{1}{(x-x_0)^{n+1} \tan^{n+1} \theta} - \frac{1}{h_e^{n+1}} \right\} \right]$$

Equation 6.55

This equation is the conclusion of Hashizume's treatment. The results of Hashizume's treatment are ;

- 1) A maximum pressure occurs just in front of a rotor tip
- 2) This pressure distribution causes a second flow
- 3) This second flow is a recirculation

To develop Hashizume's proposal, it is necessary to refer to some research concerning turbulence as a model of a flow in an internal mixer. Procaccia ¹⁴⁾ discussed the relationship between turbulence and the fractal dimension assuming that the turbulence is the assembly of a flow tube and produced the relationship ;

$$W(|u|) = 4\pi^2 |u|^2 W(u) = \begin{cases} |u|^2 \dots |u| \rightarrow 0 \\ |u|^{-d/2-1} \dots |u| \rightarrow \infty \end{cases} \quad \text{Equation 56}$$

W : Distribution function of vortex tube
u : Velocity of vortex tube

The interesting result from his analysis is that the distribution of the flow tube is subject to the power rule which means that the distribution of the flow tube has a fractal structure through the power of the equation.

Appendix 8 : ASTM D2663 Method B (Evaluation of carbon black dispersion)

This section is a direct quotation from ASTM. For details such as sample preparation and test procedures, reference should be made to the standard.

12.1 Test Method B is a quantitative test method. Dispersion is evaluated by measuring with a light microscope, the percentage area covered by black agglomerates in microtomed (a sledge type equipped with specimen clamp and holder for glass knives) sections of the compound. Since this test method involves direct measurement, it is quantitative and more accurate than the visual test method. The test is applicable to the analysis of carbon black dispersion in compounds that contain other fillers.

13. Summary of Test Method

13.1 The compounded rubber is microtomed into sections which are sufficiently thin to permit observation of the carbon agglomerates by transmitted light with the aid of a light microscope. The total cross-sectional area of all agglomerates 5 μm or larger is counted, and from the known content of carbon black in the stock, the percentage of carbon black below the 5 μm size is calculated and expressed as "Percentage of Carbon Black Dispersed."

21. Calculation and Interpretation of Results

21.1 Percent Dispersion-Calculates the percent dispersion, representing the percentage of carbon black that has been dispersed below the 5 μm agglomerate size, as follows:

$$\text{Dispersion, \%} = 100 - \text{SU/L}$$

where:

U = total number of graticule squares that are at least half filled with carbon black. (This represents an average of the five graticule counts on the section. See Note 2.)

Most agglomerates are not composed entirely of carbon black. They may contain substantial amounts of polymer or extender oil. In extreme cases, where U is very large, negative dispersion ratings are possible. Such stocks are extremely poor and may simply be classified at a "0" or "no dispersion" rating. It must also be assumed that the absolute level of all the percent dispersion values is probably higher than reported. A satisfactory test method is not presently available for determining the precise amount of carbon black in each agglomerate.

S = Area swelling factor from the action of the solvent used to uncurl the sections (a ratio of the section area after swelling to the area before swelling), and

L = volume percentage of black in the compound.

For maximum accuracy, the black volume percentage can be calculated from the following expression:

$$L_1 = \frac{\text{density of compound} \times \text{mass of black}}{\text{density of black} \times \text{total mass of compound} \times 100}$$

However, when dealing with hydrocarbon rubbers; for practical purposes the density of the carbon black can simply be considered as being twice that of the polymer and oil, and the weight contribution of the curing agents can be disregarded. Then, the volume percentage of black can be calculated from the following simplified expression where: .

$$L_2 = \frac{\text{mass of black} \times 100}{\text{mass of black} + 2 \times (\text{total mass of polymer} + \text{oil})}$$

Appendix 9 : Experimental data
physicla properties of rubber samples

Table 1 AGL

No.	1	2	3	4	5
Power Trace β (-)	1.106	1.690	1.871	2.074	1.970
D_f (-)	1.947	1.655	1.564	1.463	1.515
State of Mix D_f (-)	0.7287	0.6318	0.6117	0.5771	---
Cure F_{max} (Nm)	4.23	4.26	4.13	3.96	3.83
F_{min} (Nm)	1.02	0.98	0.86	0.84	0.75
$T_{0.9}$ (s)	1588	1664	1692	1728	1764
Elec. Resistance(Ω cm)	4.23×10^4	8.46×10^4	2.60×10^5	7.57×10^5	2.02×10^6
Fracture Surface D_f (-)	2.797	2.512	2.488	2.476	2.453
Peak P (mm^{-1})	67	70	63	56	66
Intensity (%)	68	55	53	48	30
Payne effect (%)	55.5	52.7	46.1	43.9	42.6
Stress Strain 50 %	1.42	1.66	1.73	1.57	1.60
(MPa) 100	2.49	3.19	3.17	2.74	2.52
200	7.14	9.3	9.75	8.28	6.78
300	13.95	17.94	18.8	16.44	13.49
400	21.3	27.0	---	24.9	21.1
Tb	26.3	27.1	27.5	27.7	28.0
Eb	465	402	396	434	49.7

Table 2 AGM

No.	1	2	3	4	5
Power Trace β (-)	1.68	1.98	2.35	2.30	2.38
D_f (-)	1.66	1.51	1.32	1.35	1.31
State of Mix D_f (-)	0.6293	---	0.6140	0.5803	0.6169
Cure F_{max} (Nm)	2.11	2.21	2.15	2.1	2.1
F_{min} (Nm)	0.44	0.31	0.41	0.39	0.27
$T_{0.9}$ (s)	1608	1696	1688	1712	1712
Elec. Resistance(Ω cm)	4.24×10^4	---	4.38×10^7	9.97×10^9	2.37×10^9
Fracture Surface D_f (-)	2.687	2.482	2.389	2.475	2.384
Peak P (mm^{-1})	70	54	54	50	49
Intensity (%)	58	52	48	42	40
Payne effect (%)	40.9	34.5	30.0	26.5	28.0
Stress Strain 50 %	1.46	1.56	1.47	1.61	1.70
(MPa) 100	2.41	2.73	2.82	2.83	3.08
200	6.50	8.4	8.54	8.69	9.11
300	13.46	17.25	17.07	17.44	18.09
400	22.15	27.3	25.5	26.8	27.4
Tb	27.1	27.45	28.0	27.0	28.4
Eb	423	410	427	402	411

Table 3 AGN

No.	1	2	3	4	5
Power Trace β (-)	1.88	2.506	2.724	2.868	2.722
D_f (-)	1.56	1.247	1.138	1.066	1.139
State of Mix D_f (-)	0.7451	0.6372	0.5210	0.4530	0.4351
Cure F_{max} (Nm)	3.54	2.16	2.12	1.98	2.03
F_{min} (Nm)	0.58	0.42	0.38	0.33	0.26
$T_{0.9}$ (s)	1680	1696	1732	1668	1736
Elec. Resistance(Ω cm)	1.61×10^5	7.16×10^7	7.56×10^9	9.43×10^{10}	4.81×10^{10}
Fracture Surface D_f (-)	2.389	2.314	2.342	2.381	2.332
Peak P (mm^{-1})	68	67	42	53	50
Intensity (%)	59	48	48	36	32
Payne effect (%)	43.3	38.8	15.5	20.3	23.7
Stress Strain 50 %	1.31	1.55	1.52	1.43	1.85
(MPa) 100	2.23	2.68	2.58	2.21	3.24
200	5.90	7.84	7.54	6.36	9.46
300	12.06	16.1	15.5	13.51	18.52
400	19.27	25.1	24.2	21.8	---
Tb	27.7	28.0	27.8	27.5	26.9
Eb	514	434	442	478	390

Table 4 AGO

No.	1	2	3	4	5
Power Trace β (-)	1.28	1.49	1.84	1.67	1.70
D_f (-)	1.86	1.76	1.58	1.67	1.65
State of Mix D_f (-)	0.6474	0.4742	0.5418	0.4543	---
Cure F_{max} (Nm)	3.37	3.57	3.62	3.55	2.71
F_{min} (Nm)	1.31	1.33	1.13	1.25	0.97
$T_{0.9}$ (s)	640	948	984	1020	904
Elec. Resistance Ω cm)	1.12×10^4	2.33×10^4	7.90×10^4	8.33×10^4	1.05×10^5
Fracture Surface D_f (-)	2.560	2.409	2.381	2.370	2.343
Peak P(mm^{-1})	75	78	70	64	68
Intensity (%)	69	50	51	54	51
Payne effect (%)	71.2	61.2	56.5	58.5	---
Stress Strain 50 %	1.33	1.27	1.34	1.26	0.76
(Mpa) 100	2.38	2.20	2.47	2.33	1.23
200	5.79	5.28	6.31	6.07	2.75
300	11.00	10.07	11.94	11.64	5.76
400	17.27	15.78	18.49	18.02	10.56
Tb	28.9	229.7	30.2	29.7	29.4
Eb	448	509	485	466	540

Table 5 AGP

No.	1	2	3	4	5
Power Trace β (-)	1.72	1.88	1.78	1.79	1.80
D_f (-)	1.64	1.56	1.61	1.60	1.60
State of Mix D_f (-)	0.5179	0.5030	0.4920	0.4345	0.4799
Cure F_{max} (Nm)	1.51	1.50	1.53	1.45	1.48
F_{min} (Nm)	0.53	0.55	0.43	0.23	0.29
$T_{0.9}$ (s)	640	992	1072	972	1068
Elec. Resistance(Ω cm)	1.82×10^4	8.01×10^4	3.02×10^5	4.67×10^5	7.35×10^5
Fracture Surface D_f (-)	2.463	2.387	2.289	2.309	2.387
Peak P (mm^{-1})	70	68	60	68	62
Intensity (%)	62	53	58	43	42
Payne effect (%)	65.4	56.8	48.3	26.9	---
Stress Strain 50 %	1.21	1.31	1.34	1.08	1.35
(MPa) 100	2.15	2.36	2.55	2.03	2.71
200	5.77	5.96	7.14	6.50	7.72
300	11.54	11.66	14.03	13.61	14.49
400	19.05	18.94	18.9	21.87	22.1
Tb	29.4	30.3	29.5	26.5	28.4
Eb	515	535	510	453	482

Table 6 AGQ

No.	1	2	3	4	5
Power Trace β (-)	1.883	---	1.63	1.90	1.71
D_f (-)	1.558	---	1.68	1.55	1.65
State of Mix D_f	0.5700	0.521	0.3622	0.3454	0.3219
Cure F_{max} (Nm)	3.13	3.08	3.96	3.85	3.62
F_{min} (Nm)	1.24	0.92	1.08	1.13	0.99
$T_{0.9}$ (s)	936	872	940	1060	956
Elec. Resistance(Ω cm)	3.19×10^4	1.41×10^5	2.53×10^6	5.15×10^6	1.57×10^7
Fracture Surface D_f (-)	2.431	2.335	2.293	2.226	2.247
Peak P (mm^{-1})	68	64	58	57	60
Intensity (%)	51	54	46	43	48
Payne effect (%)	63.8	51.5	35.2	24.3	18.6
Stress Strain 50 %	1.17	0.97	1.66	1.40	1.36
(MPa) 100	2.13	1.75	3.06	2.73	2.59
200	6.04	4.94	8.84	8.00	7.28
300	12.71	10.13	16.46	15.75	14.35
400	21.15	16.69	24.4	24.1	22.2
Tb	29.9	29.6	27.7	27.2	27.1
Eb	492	557	443	440	462

Viscoelastic property Temperature dependence

SAMPLE AGO-04 DATA.
TYPE RHEOLO SOLID IR
96/11/16 NAME
XTENSION TYPE SAMPLE'

		DIMENSION(C.M)		LENGTH		WIDTH		THICKNESS	
				2.154		4.700		2.200	
		FREQUENCY		(Hz)		52.05			
		AMPLITUDE		(%)		0.10			
TEMP	E'	E"	TANDEL	STEEES	STRAIN	E'	E"		
°C	Pa	Pa	(-)	GRAM	%	dyne/cm^2	dyne/cm^2		
-69.1	3.246E+09	1.523E+08	0.0469	3.324E+03	0.10	3.246E+10	1.323E+09		
-67.5	3.208E+09	1.607E+08	0.0501	3.270E+03	0.10	3.208E+10	1.607E+09		
-66.5	3.194E+09	1.524E+08	0.0477	3.331E+03	0.10	3.194E+10	1.524E+09		
-65.5	3.146E+09	1.710E+08	0.0546	3.301E+03	0.10	3.146E+10	1.719E+09		
-64.2	3.082E+09	1.975E+08	0.0641	3.237E+03	0.10	3.082E+10	1.975E+09		
-63.6	3.053E+09	1.879E+08	0.0615	3.217E+03	0.10	3.053E+10	1.879E+09		
-62.2	2.991E+09	1.917E+08	0.0641	3.145E+03	0.10	2.991E+10	1.917E+09		
-61.2	2.886E+09	2.356E+08	0.0817	3.049E+03	0.10	2.886E+10	2.356E+09		
-60.4	2.854E+09	2.376E+08	0.0833	3.025E+03	0.10	2.854E+10	2.376E+09		
-59.4	2.737E+09	2.629E+08	0.0961	2.828E+03	0.10	2.737E+10	2.629E+09		
-58.4	2.654E+09	3.044E+08	0.1147	2.773E+03	0.10	2.654E+10	3.044E+09		
-57.3	2.478E+09	3.707E+08	0.1496	2.602E+03	0.10	2.478E+10	3.707E+09		
-56.2	2.324E+09	4.295E+08	0.1848	2.475E+03	0.10	2.324E+10	4.295E+09		
-55.5	2.174E+09	4.719E+08	0.2180	2.332E+03	0.10	2.174E+10	4.739E+09		
-54.1	1.946E+09	5.587E+08	0.2871	2.137E+03	0.10	1.946E+10	5.587E+09		
-53.6	1.799E+09	6.128E+08	0.3407	2.000E+03	0.10	1.799E+10	6.128E+09		
-52.0	1.499E+09	6.757E+08	0.4506	1.717E+03	0.10	1.499E+10	6.757E+09		
-51.6	1.314E+09	6.872E+08	0.5231	1.576E+03	0.10	1.314E+10	6.872E+09		
-50.3	1.026E+09	6.758E+08	0.6590	1.308E+03	0.10	1.026E+10	6.758E+09		
-49.5	8.497E+08	6.409E+08	0.7542	1.124E+03	0.10	8.497E+09	6.409E+09		
-48.1	6.198E+08	5.572E+08	0.8990	8.802E+02	0.10	6.198E+09	5.572E+09		
-47.6	5.514E+08	5.272E+08	0.9562	8.081E+02	0.10	5.514E+09	5.272E+09		
-46.4	3.937E+08	4.207E+08	1.0687	6.058E+02	0.10	3.037E+09	4.207E+09		
-44.9	3.015E+08	3.415E+08	1.1325	4.761E+02	0.10	3.015E+09	3.415E+09		
-44.5	2.550E+08	2.954E+08	1.1683	4.140E+02	0.10	2.550E+09	2.954E+09		
-43.1	1.866E+08	2.192E+08	1.1749	3.061E+02	0.10	1.865E+09	2.192E+09		
-42.4	1.636E+08	1.917E+08	1.1716	2.658E+02	0.10	1.636E+09	1.917E+09		
-41.3	1.375E+08	1.587E+08	1.1542	2.227E+02	0.10	1.375E+09	1.587E+09		
-40.4	1.141E+08	1.278E+08	1.1207	1.791E+02	0.10	1.141E+09	1.278E+09		
-38.8	9.321E+07	1.002E+08	1.0752	1.434E+02	0.10	9.321E+08	1.002E+09		
-38.4	8.362E+07	8.717E+07	1.0425	1.272E+02	0.10	8.362E+08	8.717E+09		
-37.0	7.082E+07	7.027E+07	0.9922	1.046E+02	0.10	7.082E+08	7.027E+08		
-36.5	6.545E+07	6.319E+07	0.9654	9.436E+02	0.10	6.545E+08	6.319E+08		
-35.2	5.571E+07	5.088E+07	0.9133	8.006E+01	0.10	5.571E+08	5.088E+08		
-33.8	5.028E+07	4.360E+07	0.8672	7.070E+01	0.10	5.028E+08	4.360E+08		
-33.5	4.641E+07	3.882E+07	0.8365	6.309E+01	0.10	4.641E+08	3.882E+08		
-31.6	4.074E+07	3.228E+07	0.7923	5.438E+01	0.10	4.074E+08	3.228E+08		
-31.8	3.997E+07	3.132E+07	0.7834	5.262E+01	0.10	3.997E+08	3.132E+08		
-30.8	3.519E+07	2.601E+07	0.7391	4.557E+01	0.10	3.519E+08	2.601E+08		
-29.2	3.085E+07	2.152E+07	0.6976	3.938E+01	0.10	3.085E+08	2.152E+08		
-27.1	2.875E+07	1.935E+07	0.6731	3.585E+01	0.10	2.875E+08	1.935E+08		

-27.6	2.799E+07	1.842E+07	0.6582	3.494E+01	0.10	2.799E+08	1.842E+08
-26.4	2.458E+07	1.524E+07	0.6200	3.003E+01	0.10	2.458E+08	1.524E+08
-23.8	2.323E+07	1.365E+07	0.5877	2.813E+01	0.10	2.323E+08	1.365E+08
-24.6	2.252E+07	1.266E+07	0.5623	2.700E+01	0.10	2.252E+08	1.266E+08
-22.8	2.018E+07	1.065E+07	0.5278	2.380E+01	0.10	2.018E+08	1.065E+08
-22.7	2.022E+07	1.077E+07	0.5328	2.396E+01	0.10	2.022E+08	1.077E+08
-21.7	1.818E+07	8.841E+06	0.4863	2.116E+01	0.10	1.818E+08	8.841E+07
-18.9	1.702E+07	8.065E+06	0.4738	1.973E+01	0.10	1.702E+08	8.065E+07
-19.3	1.659E+07	7.305E+06	0.4403	1.884E+01	0.10	1.659E+08	7.304E+07
-16.7	1.555E+07	6.422E+06	0.4131	1.751E+01	0.10	1.555E+08	6.422E+07
-18.1	1.545E+07	6.514E+06	0.4216	1.744E+01	0.10	1.545E+08	6.514E+07
-15.4	1.435E+07	5.524E+06	0.3875	1.602E+01	0.10	1.435E+08	5.524E+07
-15.7	1.438E+07	5.408E+06	0.3760	1.603E+01	0.10	1.438E+08	5.408E+07
-13.5	1.342E+07	4.473E+06	0.3333	1.472E+01	0.10	1.342E+08	4.473E+07
-14.3	1.353E+07	4.603E+06	0.3402	1.488E+01	0.10	1.353E+08	4.603E+07
-11.1	1.261E+07	3.733E+06	0.2957	1.371E+01	0.10	1.263E+08	3.733E+07
-11.1	1.231E+07	3.831E+06	0.3112	1.343E+01	0.10	1.231E+08	3.831E+07
-8.3	1.209E+07	3.378E+06	0.2794	1.314E+01	0.10	1.209E+08	3.378E+07
-9.2	1.155E+07	3.000E+06	0.2598	1.254E+01	0.10	1.155E+08	3.000E+07
-7.1	1.142E+07	2.844E+06	0.2491	1.228E+01	0.10	1.142E+08	2.844E+07
-7.3	1.119E+07	2.624E+05	0.2345	1.217E+01	0.10	1.119E+08	2.624E+07
-4.8	1.092E+07	2.393E+06	0.2192	1.173E+01	0.10	1.092E+08	2.393E+07
-5.1	1.087E+07	2.339E+06	0.2152	1.162E+01	0.10	1.087E+08	2.339E+07
-3.6	1.052E+07	2.048E+06	0.1947	1.130E+01	0.10	1.052E+08	2.048E+07
-3.7	1.056E+07	1.980E+06	0.1875	1.119E+01	0.10	1.056E+08	1.980E+07
-2.7	1.038E+07	1.953E+06	0.1881	1.105E+01	0.10	1.038E+08	1.953E+07
-1.4	1.025E+07	1.812E+06	0.1769	1.091E+01	0.10	1.025E+08	1.812E+07
0.0	8.036E+06	1.909E+06	0.2376	8.881E+01	1.02	8.036E+07	1.909E+07
0.6	7.939E+06	1.861E+06	0.2344	8.783E+01	1.02	7.939E+07	1.861E+07
1.6	7.848E+06	1.764E+06	0.2248	8.643E+01	1.02	7.848E+07	1.764E+07
2.7	7.741E+06	1.683E+06	0.2175	8.539E+01	1.02	7.741E+07	1.683E+07
3.6	7.669E+06	1.626E+06	0.2120	8.436E+01	1.02	7.669E+07	1.626E+07
4.8	7.572E+06	1.552E+06	0.2050	8.308E+01	1.02	7.572E+07	1.552E+07
5.6	7.458E+06	1.485E+06	0.1991	8.307E+01	1.04	7.580E+07	1.485E+07
6.7	7.557E+06	1.463E+06	0.1936	8.280E+01	1.02	7.557E+07	1.463E+07
7.6	7.487E+06	1.413E+06	0.1887	8.267E+01	1.03	7.487E+07	1.413E+07
8.6	7.415E+06	1.361E+06	0.1835	8.150E+01	1.02	7.415E+07	1.361E+07
9.7	7.358E+05	1.329E+06	0.1806	8.027E+01	1.02	7.358E+07	1.329E+07
10.5	7.290E+06	1.282E+06	0.1758	8.008E+01	1.03	7.290E+07	1.282E+07
11.8	7.238E+05	1.251E+06	0.1729	7.942E+01	1.02	7.238E+07	1.251E+07
12.9	7.140E+05	1.202E+06	0.1684	7.954E+01	1.04	7.140E+07	1.202E+07
13.8	7.097E+06	1.180E+06	0.1662	7.741E+01	1.02	7.097E+07	1.180E+07
14.8	7.047E+06	1.150E+06	0.1632	7.727E+01	1.03	7.047E+07	1.150E+07
15.6	6.996E+06	1.122E+06	0.1604	7.643E+01	1.02	6.996E+07	1.122E+07
16.6	6.935E+06	1.098E+06	0.1584	7.613E+01	1.03	6.936E+07	1.098E+07
17.7	6.864E+06	1.058E+06	0.1542	7.624E+01	1.04	6.864E+07	1.058E+07
18.7	6.833E+06	1.048E+06	0.1534	7.476E+01	1.02	6.833E+07	1.048E+07
19.8	6.783E+06	1.017E+06	0.1499	7.374E+01	1.02	6.783E+07	1.017E+07
20.7	6.748E+06	1.003E+06	0.1486	7.377E+01	1.02	6.748E+07	1.003E+07
21.7	6.705E+06	9.790E+05	0.1460	7.342E+01	1.03	6.705E+07	9.790E+07
22.7	6.658E+06	9.821E+05	0.1445	7.280E+01	1.03	6.658E+07	9.621E+06
23.6	6.597E+06	9.353E+05	0.1418	7.294E+01	1.04	6.597E+07	9.353E+06
24.7	6.568E+06	9.356E+05	0.1424	7.217E+01	1.03	6.568E+07	9.356E+06
25.7	6.539E+06	9.354E+05	0.1430	7.227E+01	1.04	6.539E+07	9.354E+06

26.7	6.528E+06	9.051E+05	0.1386	7.134E+01	1.03	6.528E+07	9.051E+06
27.7	6.481E+06	8.980E+05	0.1386	7.088E+01	1.03	6.481E+07	8.980E+06
28.7	6.464E+06	8.799E+05	0.1361	7.018E+01	1.02	6.464E+07	8.799E+06
29.8	6.403E+06	8.682E+05	0.1356	6.962E+01	1.02	6.403E+07	8.682E+06
30.7	6.373E+06	8.530E+05	0.1338	6.976E+01	1.03	6.373E+07	8.530E+06
31.7	6.337E+06	8.297E+05	0.1309	6.925E+01	1.03	6.337E+07	8.297E+06
32.7	6.300E+06	8.200E+05	0.1301	6.866E+01	1.02	6.300E+07	8.200E+06
33.7	6.257E+06	8.248E+05	0.1318	8.894E+01	1.04	6.257E+07	8.248E+06
34.7	6.251E+06	8.062E+05	0.1288	6.815E+01	1.02	6.251E+07	8.052E+06
35.7	6.219E+06	8.058E+05	0.1296	6.898E+01	1.04	6.219E+07	8.058E+06
36.6	6.173E+06	7.862E+05	0.1274	6.932E+01	1.06	6.173E+07	7.862E+06
37.7	6.156E+06	7.755E+05	0.1260	6.840E+01	1.04	6.156E+07	7.755E+06
38.7	6.130E+06	7.782E+05	0.1269	6.798E+01	1.04	6.130E+07	7.782E+06
39.7	6.097E+06	7.641E+05	0.1253	6.739E+01	1.04	6.097E+07	7.641E+06
40.7	6.066E+06	7.663E+05	0.1263	6.731E+01	1.04	6.066E+07	7.663E+06
41.7	6.045E+06	7.448E+05	0.1232	6.689E+01	1.04	6.045E+07	7.448E+06
42.6	6.012E+06	7.282E+05	0.1211	6.687E+01	1.05	6.012E+07	7.282E+06
43.7	5.990E+06	7.211E+05	0.1204	6.644E+01	1.04	5.990E+07	7.211E+06
44.7	5.989E+06	7.283E+05	0.1216	6.630E+01	1.04	5.989E+07	7.283E+06
45.7	5.979E+06	7.142E+05	0.1194	6.508E+01	1.02	5.979E+07	7.142E+06
46.7	5.932E+06	7.039E+05	0.1187	6.476E+01	1.03	5.932E+07	7.039E+06
47.7	5.923E+06	7.055E+05	0.1191	6.475E+01	1.03	5.923E+07	7.055E+06
48.6	5.905E+06	6.961E+05	0.1179	6.458E+01	1.03	5.905E+07	5.951E+06
49.7	5.865E+06	6.898E+05	0.1176	6.617E+01	1.06	5.865E+07	5.898E+06
50.7	5.867E+06	6.986E+05	0.1191	6.496E+01	1.04	5.867E+07	6.986E+06
51.7	5.846E+06	6.708E+05	0.1148	6.432E+01	1.04	5.846E+07	6.708E+06
52.7	5.830E+06	6.817E+05	0.1169	6.367E+01	1.03	5.830E+07	6.817E+06
53.7	5.809E+06	6.710E+05	0.1155	6.388E+01	1.04	5.809E+07	6.710E+06
54.6	5.794E+06	6.704E+05	0.1157	6.395E+01	1.04	5.794E+07	6.704E+06
55.7	5.796E+06	6.637E+05	0.1145	6.317E+01	1.03	5.796E+07	6.637E+06
56.7	5.757E+06	6.549E+05	0.1138	6.349E+01	1.04	5.757E+07	6.549E+06
57.7	5.737E+06	6.611E+05	0.1135	6.245E+01	1.03	5.737E+07	6.511E+06
58.8	5.709E+06	6.372E+05	0.1116	6.246E+01	1.03	5.709E+07	6.372E+06
59.7	5.682E+06	6.346E+05	0.1117	6.220E+01	1.03	5.682E+07	6.346E+06
60.8	5.664E+06	6.336E+05	0.1119	6.235E+01	1.04	5.664E+07	6.336E+06
61.7	5.659E+06	6.349E+05	0.1122	6.198E+01	1.03	5.689E+07	6.349E+06
62.7	5.631E+06	6.306E+05	0.1120	6.221E+01	1.04	5.631E+07	6.306E+06
63.7	5.620E+06	6.359E+05	0.1132	6.092E+01	1.02	5.620E+07	6.359E+06
64.7	5.585E+06	6.122E+05	0.1096	6.109E+01	1.03	5.585E+07	6.122E+06
65.7	5.560E+06	6.144E+05	0.1105	6.106E+01	1.03	5.560E+07	6.144E+06
66.7	5.532E+06	6.994E+05	0.1083	6.075E+01	1.03	5.532E+07	5.994E+06
67.7	5.511E+06	5.957E+05	0.1081	6.050E+01	1.04	5.511E+07	5.957E+06
68.8	5.482E+06	5.962E+05	0.1088	6.009E+01	1.03	5.482E+07	5.962E+06
69.8	5.448E+06	5.911E+05	0.1085	6.063E+01	1.05	5.448E+07	5.911E+06

SAMPLE AGL- 05 DATA
 TYPE RHEOLO SOLID IR
 96/11/16 NAME
 XTENSION TYPE

SAMPLE' DIMENSION(C.M) LENGTH WIDTH THICKNESS							
			2.105		4.700	2.290	
			FREQUENCY (Hz)		52.05		
			AMPLITUDE (%)		0 10		
TEMP	E'	E''	TANDEL	STRESS	STRAIN	E'	E''
	Pa	Pa		GRAM	%	dyn /cm^2	dyn/cm
-69.1	2.343E+09	3.940E+07	0.0168	2.447E+03	0.10	3. 940E+08	3.940E+08
-67.3	2.337E+09	3.805E+07	0.0163	2.444E+03	0.10	2.337E+10	3.805E+08
-66.6	2.330E+09	3.833E+07	0.0155	2.465E+03	0.10	2.330E+10	2.833E+08
-65.4	2.321E+09	3.785E+07	0.0163	2.442E+03	0.10	2.321E+10	3.785E+08
-64.3	2.314E+09	3.796E+07	0.0161	2.458E+03	0.10	2.314E+10	3.796E+08
-63.4	2.304E+09	3.805E+07	0.0165	2.438E+03	0 10	2.304E+10	3.803E+08
-62.4	2.306E+09	3.652E+07	0.0158	2.399E+03	0.09	2.306E+10	3.652E+08
-61.4	2.297E+09	3.683E+07	0.0160	2.427E+03	0.10	2.297E+10	3.683E+08
-60.3	2.285E+09	3.755E+07	0.0164	2.411E+03	0.10	2.285E+10	3.755E+08
-59.3	2.272E+09	3.779E+07	0.0166	2.395E+03	0.10	2.272E+10	3.779E+08
-58.3	2.260E+09	3.866E+07	0.0173	2.404E+03	0.10	2.260E+10	3.866E+08
-57.5	2.245E+09	4.106E+07	0.0183	2.377E+03	0.10	2.245E+10	4.106E+08
-56.4	2.227E+09	4.346E+07	0.0195	2.352E+03	0.10	2.227E+10	4.346E+08
-55.3	2.205E+09	4.624E+07	0.0210	2.343E+03	0.10	2.205E+10	4.624E+08
-54.4	2.188E+09	5.004E+07	0.0229	2.333E+03	0.10	2.188E+10	5.004E+08
-53.3	2.167E+09	5.620E+07	0.0259	2.303E+03	0.10	2.167E+10	5.620E+08
-52.4	2.134E+09	6.258E+07	0.0293	2.268E+03	0.10	2.134E+10	6.258E+08
-51.5	2.105E+09	7.107E+07	0.0338	2.240E+03	0.10	2.105E+10	7.1076E+08
-50.5	2.058E+09	8.240E+07	0.0400	2.189E+03	0.10	2.058E+10	8.240E+08
-49.5	1.999E+09	9.673E+07	0.0484	2.103E+03	0.10	1.999E+10	9.673E+08
-48.3	1.921E+09	1.213E+08	0.0631	2.055E+03	0.10	1.921E+10	1.213E+09
-46.9	1.819E+09	1.544E+08	0.0849	1.930E+03	0.10	1.819E+10	1.544E+09
-46.6	1.739E+09	1.795E+08	0.1032	1.864E+03	0.10	1.739E+10	1.795E+09
-44.8	1.597E+09	2.290E+08	0.1434	1.707E+03	0.10	1.597E+10	2.290E+09
-44.7	1.519E+09	2.541E+08	0.1673	1.636E+03	0.10	1.519E+10	2.541E+09
-43.2	1.355E+09	3.045E+08	0.2246	1.470E+03	0.10	1.355E+10	3.045E+09
-42.0	1.213E+09	3.404E+08	0.2805	1.342E+03	0.10	1.213E+10	3.404E+09
-41.2	1.063E+09	3.687E+08	0.3468	1.189E+03	0.10	1.063E+10	3.687E+09
-39.8	8.876E+08	3.857E+08	0.4346	1.038E+03	0.10	8.876E+09	3.857E+09
-39.5	7.863E+08	3.865E+08	0.4915	9.317E+02	0.10	7.863E+09	3.865E+09
-37.9	6.123E+08	3.749E+08	0.6124	7.609E+02	0.10	6.123E+09	3.749E+09
-37.6	5.501E+08	3.618E+08	0.6576	6.998E+02	0.10	5.501E+09	3.618E+09
-36.1	3.945E+08	3.105E+08	0.7871	5.309E+02	0.10	3.945E+09	3.105E+09
-35.2	3.405E+08	2.855E+08	0.8386	4.719E+02	0.10	3.405E+09	2.855E+09
-34.3	2.574E+08	2.380E+08	0.9243	3.726E+02	0.10	2.574E+09	2.380E+09
-32.4	1.728E+08	1.736E+08	1.0047	2.591E+02	0.10	1.728E+09	1.736E+09
-32.4	1.615E+08	1.637E+08	1.0138	2.433E+02	0.10	1.615E+09	1.637E+09
-30.9	1.208E+08	1.243E+08	1.0284	1.839E+02	0.10	1.208E+09	1.243E+09
-30.7	1.160E+08	1.192E+08	1.0277	1.763E+02	0.10	1.160E+09	1.192E+09
-29.2	8.946E+07	8.961E+07	1.0000	1.343E+02	0.10	8.946E+08	8.951E+08
-27.6	7.194E+07	6.871E+07	0.9552	1.028E+02	0.09	7.194E+08	6.871E+08
-27.6	7.015E+07	6.652E+07	0.9482	1.010E+02	0.10	7.015E+08	6.652E+08
-26.4	5.722E+07	5.048E+07	0.8822	8.037E+01	0.10	5.722E+08	5.048E+08
-24.8	5.007E+07	4.098E+07	0.8185	6.769E+01	0.10	5.007E+08	4.098E+08

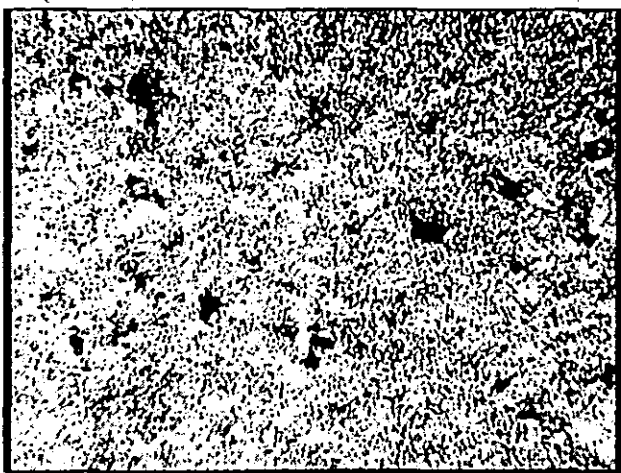
-24.1	4.948E+07	4.004E+07	0.9101	6.595E+01	0.09	4.949E+08	4.004E+08
-23.4	4.311E+07	3.249E+07	0.7537	5.738E+01	0.10	4.311E+08	3.249E+08
-21.5	3.867E+07	2.718E+07	0.7028	5.007E+01	0.10	3.867E+08	2.718E+08
-21.4	3.631E+07	2.468E+07	0.6796	4.601E+01	0.10	3.631E+08	2.468E+08
-19.5	3.286E+07	2.076E+07	0.6317	4.097E+01	0.10	3.286E+08	2.076E+08
-19.7	3.160E+07	1.937E+07	0.6131	3.892E+01	0.13	3.160E+08	1.937E+08
-18.0	2.829E+07	1.582E+07	0.5591	3.363E+01	0.09	2.829E+08	1.582E+08
-16.1	2.653E+07	1.384E+07	0.5215	3.148E+01	0.10	2.653E+08	1.384E+08
-16.5	2.598E+07	1.334E+07	0.5135	3.076E+01	0.10	2.598E+08	1.337E+08
-14.7	2.357E+07	1.099E+07	0.4663	2.724E+01	0.10	2.357E+08	1.099E+08
-14.6	2.369E+07	1.111E+07	0.4688	2.729E+01	0.09	2.369E+08	1.111E+08
-13.4	2.135E+07	9.082E+06	0.4532	2.466E+01	0.10	2.135E+08	9.082E+07
-10.8	2.031E+07	8.036E+06	0.3957	2.299E+01	0.10	2.031E+08	8.036E+07
-12.1	2.023E+07	7.803E+06	0.3857	2.295E+01	0.10	2.023E+08	7.803E+07
-9.2	1.871E+07	6.378E+06	0.3408	2.081E+01	0.10	1.871E+08	6.378E+07
-9.6	1.852E+07	6.451E+06	0.3483	2.063E+01	0.10	1.852E+08	6.451E+07
-7.1	1.760E+07	5.529E+06	0.3142	1.953E+01	0.10	1.760E+08	5.529E+07
-7.7	1.762E+07	5.533E+06	0.3141	1.947E+01	0.10	1.762E+08	5.533E+07
-5.6	1.668E+07	4.548E+06	0.2726	1.803E+01	0.09	1.668E+08	4.548E+07
-6.1	1.682E+07	4.751E+06	0.2825	1.836E+01	0.10	1.682E+08	4.751E+07
-4.4	1.589E+07	3.996E+06	0.2515	1.726E+01	0.10	1.589E+08	3.996E+07
-2.1	1.555E+07	3.771E+06	0.2426	1.704E+01	0.10	1.555E+08	3.771E+07
-2.0	1.527E+07	3.434E+06	0.2248	1.651E+01	0.10	1.527E+08	3.434E+07
-0.6	1.507E+07	3.217E+06	0.2136	1.616E+01	0.10	1.507E+08	3.217E+07
-0.8	1.231E+07	3.327E+06	0.2702	1.420E+02	1.01	1.231E+08	3.327E+07
1.5	1.214E+07	3.207E+06	0.2642	1.419E+02	1.03	1.214E+08	3.207E+07
2.5	1.171E+07	2.854E+06	0.2437	1.346E+02	1.01	1.171E+08	2.854E+07
1.9	1.183E+07	2.958E+06	0.2499	1.356E+02	1.01	1.183E+08	2.958E+07
5.8	1.140E+07	2.631E+06	0.2307	1.309E+02	1.02	1.140E+08	2.631E+07
4.0	1.143E+07	2.658E+06	0.2326	1.291E+02	1.00	1.143E+08	2.658E+07
6.3	1.127E+07	2.523E+06	0.2239	1.284E+02	1.01	1.127E+08	2.523E+07
10.0	1.098E+07	2.368E+06	0.2157	1.263E+02	1.02	1.098E+08	2.368E+07
10.2	1.063E+07	2.179E+06	0.2049	1.213E+02	1.02	1.063E+08	2.179E+07
11.0	1.057E+07	2.145E+06	0.2029	1.199E+02	1.03	1.057E+08	2.146E+07
11.5	1.050E+07	2.106E+06	0.2007	1.192E+02	1.01	1.050E+08	2.106E+07
12.1	1.042E+07	2.073E+06	0.1990	1.180E+02	1.01	1.042E+08	2.073E+07
12.8	1.034E+07	2.036E+06	0.1960	1.176E+02	1.02	1.034E+08	2.036E+07
13.6	1.026E+07	1.994E+06	0.1946	1.165E+02	1.01	1.026E+08	1.994E+07
14.0	1.020E+07	1.976E+06	0.1937	1.154E+02	1.01	1.020E+08	1.976E+07
14.7	1.015E+07	1.995E+06	0.1906	1.136E+02	1.00	1.015E+08	1.935E+07
15.5	1.005E+07	1.904E+06	0.1895	1.141E+02	1.02	1.005E+08	1.904E+07
16.6	9.955E+06	1.864E+06	0.1872	1.125E+02	1.01	9.955E+07	1.864E+07
17.6	9.849E+06	1.814E+06	0.1841	1.124E+02	1.02	9.849E+07	1.814E+07
18.6	9.746E+06	1.777E+06	0.1823	1.109E+02	1.02	9.745E+07	1.777E+07
19.7	9.674E+06	1.746E+06	0.1806	1.098E+02	1.02	9.674E+07	1.746E+07
20.7	9.589E+06	1.715E+06	0.1789	1.085E+02	1.01	9.589E+07	1.715E+07
21.7	9.486E+06	1.695E+06	0.1787	1.075E+02	1.02	9.485E+07	1.695E+07
22.8	9.394E+06	1.674E+06	0.1782	1.064E+02	1.02	9.394E+07	1.674E+07
23.6	9.320E+06	1.639E+06	0.1758	1.047E+02	1.01	9.320E+07	1.639E+07
24.7	9.235E+06	1.599E+06	0.1732	1.054E+02	1.02	9.235E+07	1.599E+07
25.7	9.172E+06	1.597E+06	0.1741	1.049E+02	1.03	9.172E+07	1.597E+07
26.7	9.074E+06	1.562E+06	0.1721	1.034E+02	1.02	9.074E+07	1.562E+07
27.7	9.010E+06	1.555E+06	0.1726	1.015E+02	1.01	9.021E+07	1.555E+07
28.5	8.927E+06	1.535E+06	0.1720	1.011E+02	1.02	8.927E+07	1.535E+07

29.7	8.859E+06	1.514E+06	0.1709	1.003E+02	1.02	8.859E+07	1.514E+07
30.1	8.791E+06	1.492E+06	0.1697	9.934E+01	1.01	8.791E+07	1.492E+07
31.6	8.701E+06	1.458E+06	0.1675	9.789E+01	1.01	8.701E+07	2.458E+07
32.7	8.641E+06	1.444E+06	0.1671	9.723E+01	1.01	8.641E+07	1.444E+07
33.7	8.564E+06	1.440E+06	0.1682	9.734E+01	1.02	8.564E+07	1.440E+07
34.6	8.494E+06	1.420E+06	0.1672	9.687E+01	1.02	8.494E+07	1.420E+07
35.8	8.443E+06	1.392E+06	0.1649	9.647E+01	1.03	8.443E+07	1.392E+07
36.7	8.391E+06	1.389E+06	0.1655	9.433E+01	1.01	8.391E+07	1.389E+07
37.7	8.331E+06	1.369E+06	0.1643	9.362E+01	1.01	8.331E+07	1.369E+07
38.7	8.272E+06	1.356E+06	0.1539	9.257E+01	1.01	8.272E+07	1.356E+07
39.7	8.214E+06	1.332E+06	0.1622	9.171E+01	1.00	8.214E+07	1.332E+07
40.7	8.144E+06	1.325E+06	0.1627	9.138E+01	1.01	8.144E+07	1.325E+07
41.7	8.077E+06	1.311E+06	0.1623	9.190E+01	1.02	8.077E+07	1.311E+07
42.7	8.010E+06	1.297E+06	0.1619	9.102E+01	1.02	8.010E+07	1.297E+07
43.7	7.966E+06	1.272E+06	0.1596	8.965E+01	1.01	7.965E+07	1.272E+07
44.7	7.898E+06	1.266E+06	0.1603	8.997E+01	1.02	7.898E+07	1.266E+07
45.7	7.858E+06	1.261E+06	0.1605	8.876E+01	1.02	7.858E+07	1.261E+07
46.6	7.805E+06	1.256E+06	0.1610	8.918E+01	1.03	7.805E+07	1.256E+07
47.7	7.775E+06	1.237E+06	0.1591	8.682E+01	1.00	7.775E+07	1.237E+07
48.8	7.682E+06	1.192E+06	0.1551	8.548E+01	1.00	7.682E+07	1.192E+07
49.7	7.642E+06	1.193E+06	0.1561	8.638E+01	1.02	7.642E+07	1.193E+07
50.7	7.566E+06	1.184E+06	0.1564	8.585E+01	1.02	7.566E+07	1.184E+07
51.6	7.547E+06	1.173E+06	0.1555	8.440E+01	1.01	7.547E+07	1.173E+07
52.7	7.481E+06	1.146E+06	0.1532	8.462E+01	1.02	7.481E+07	1.146E+07
53.7	7.434E+06	1.141E+06	0.1535	8.271E+01	1.00	7.434E+07	1.141E+07
54.8	7.366E+06	1.132E+06	0.1537	8.200E+01	1.00	7.366E+07	1.132E+07
55.8	7.306E+06	1.118E+06	0.1531	8.285E+01	1.02	7.306E+07	1.118E+07
56.7	7.273E+06	1.108E+06	0.1524	8.088E+01	1.00	7.273E+07	1.108E+07
57.8	7.373E+06	1.109E+06	0.1504	8.218E+01	1.00	7.373E+07	1.109E+07
58.8	7.320E+06	1.087E+06	0.1485	8.175E+01	1.01	7.320E+07	1.087E+07
59.0	7.263E+06	1.086E+06	0.1496	8.192E+01	1.02	7.263E+07	1.086E+07
60.7	7.229E+06	1.065E+06	0.1474	8.084E+01	1.01	7.229E+07	1.065E+07
61.7	7.153E+06	1.048E+06	0.1466	8.070E+01	1.02	7.153E+07	1.048E+07
62.8	7.096E+06	1.051E+06	0.1481	7.915E+01	1.00	7.096E+07	1.051E+07
63.7	7.042E+06	1.014E+06	0.1440	7.886E+01	1.01	7.042E+07	1.014E+07
64.6	6.983E+06	1.019E+06	0.1459	7.797E+01	1.01	6.983E+07	1.019E+07
65.7	6.907E+06	9.956E+05	0.1441	7.801E+01	1.02	6.907E+07	9.956E+06
66.8	6.876E+06	9.843E+05	0.1432	7.580E+01	0.99	6.876E+07	9.843E+06
67.8	6.790E+06	9.685E+05	0.1426	7.682E+01	1.02	6.790E+07	9.685E+06
68.7	6.759E+06	9.696E+05	0.1435	7.645E+01	1.01	6.759E+07	9.696E+06
69.7	6.704E+06	9.588E+05	0.1430	7.463E+01	1.00	6.704E+07	9.588E+06

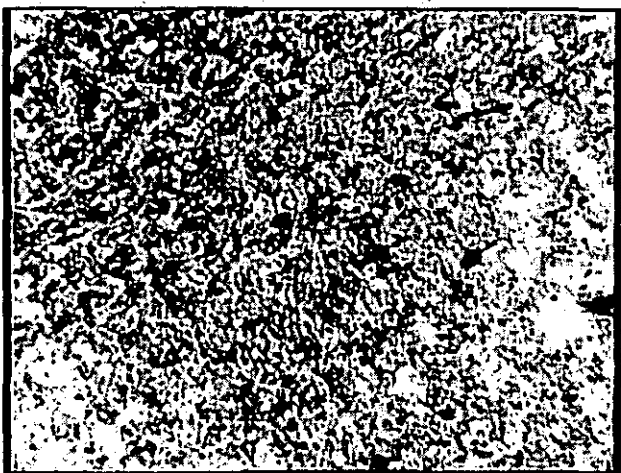
Appendix

The photograph of the state of mix

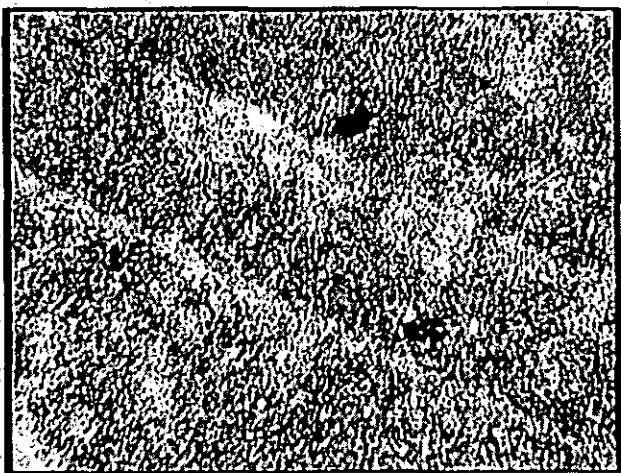
AGL1



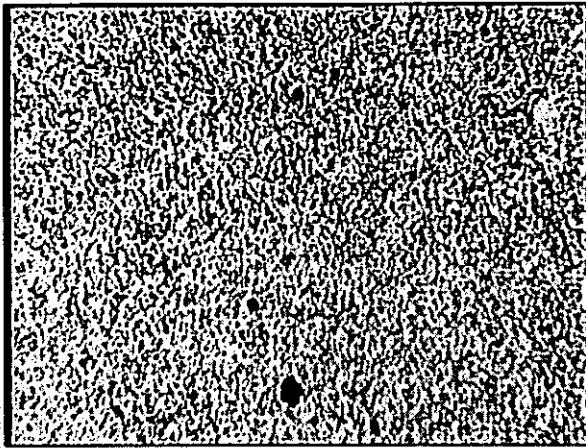
AGL2



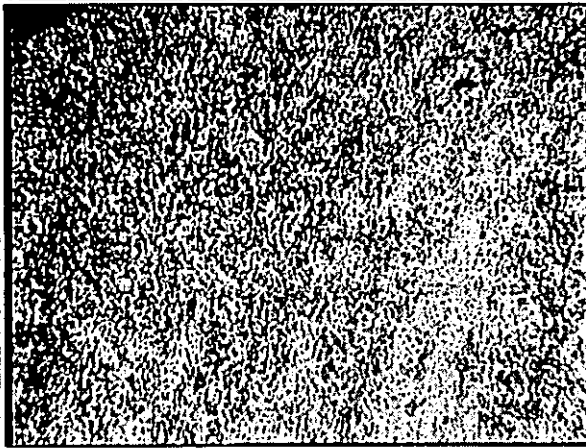
AGL3



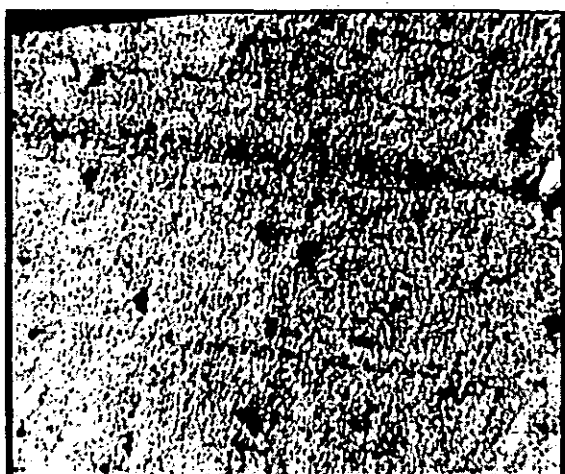
AGL4



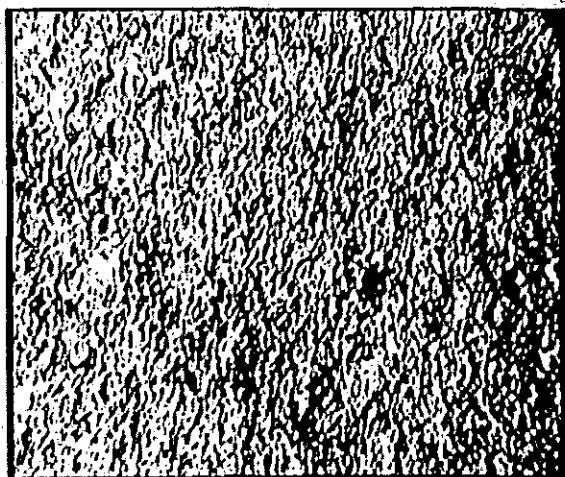
AGL5



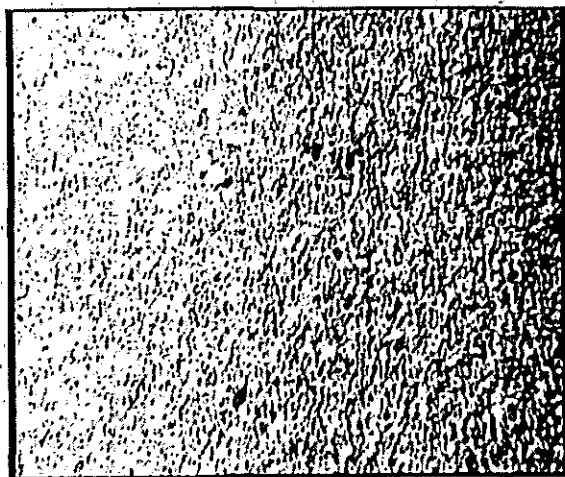
AGM1



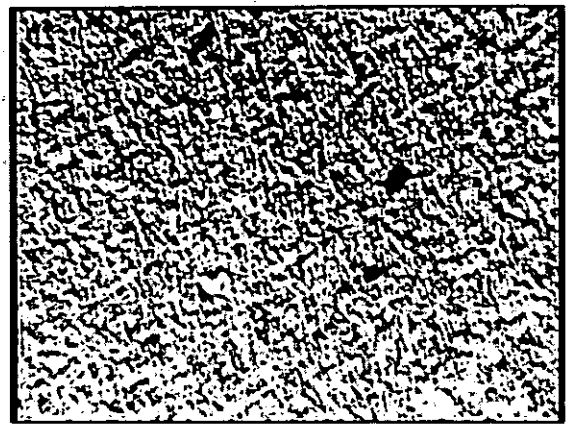
AGM2



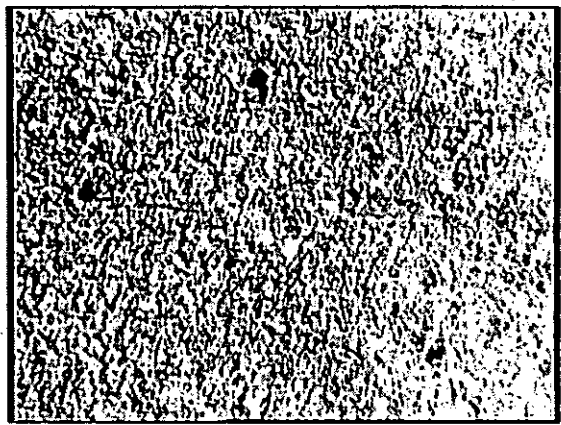
AGM3



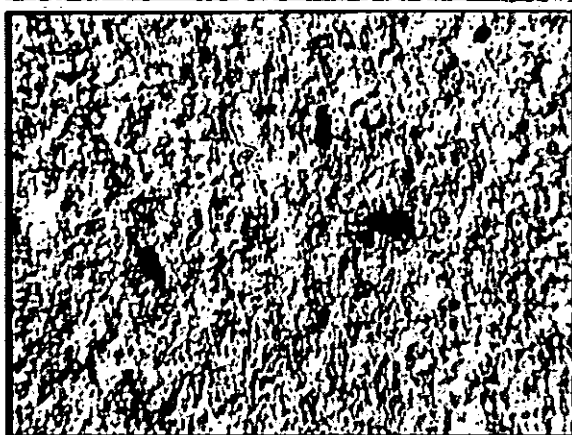
AGM4



AGM5



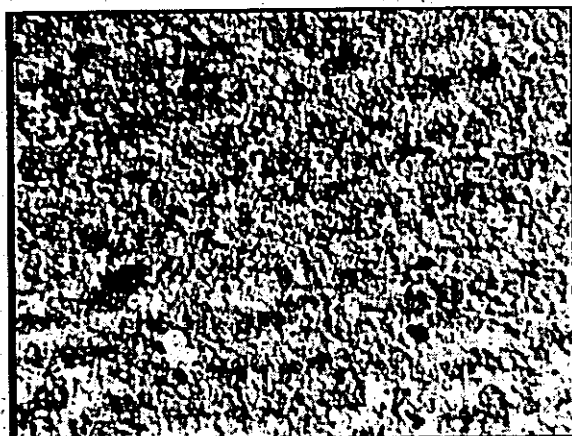
AGN1



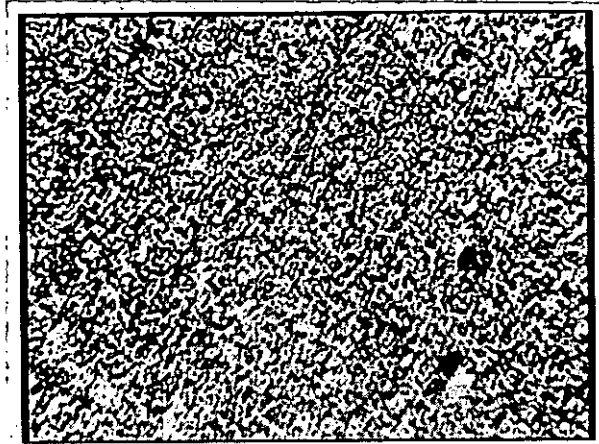
AGN2



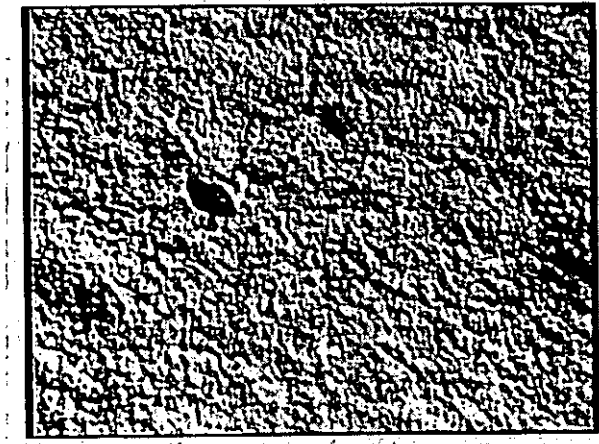
AGN3



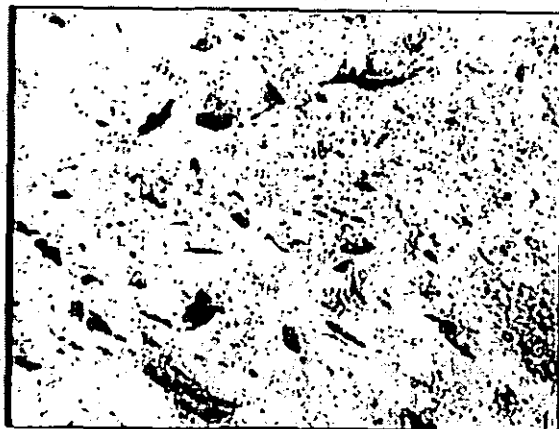
AGN4



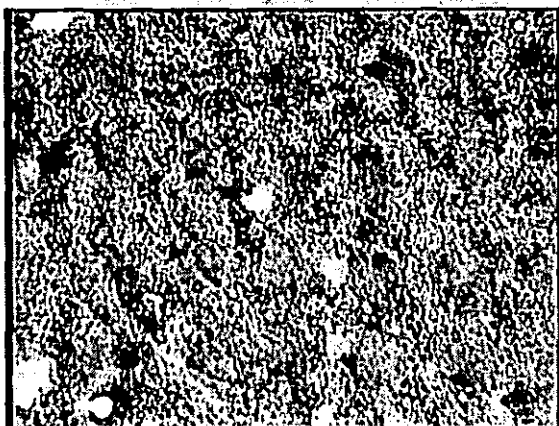
AGN5



AGO 1



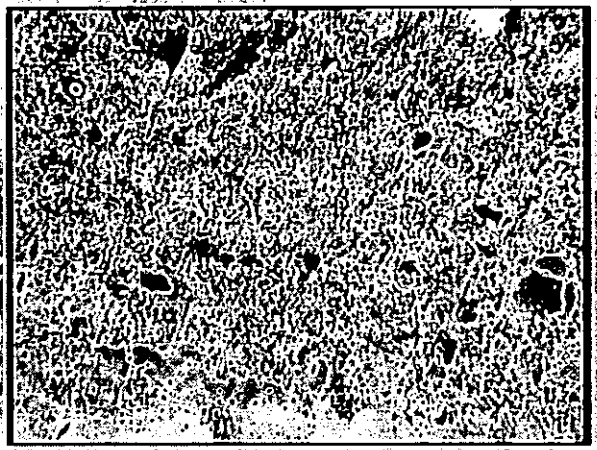
AGO2



AGO3



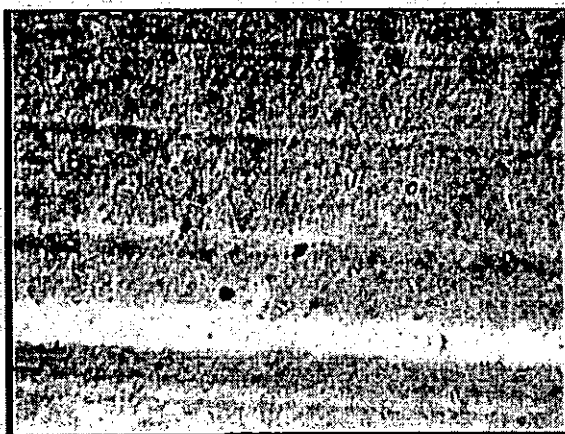
AG04



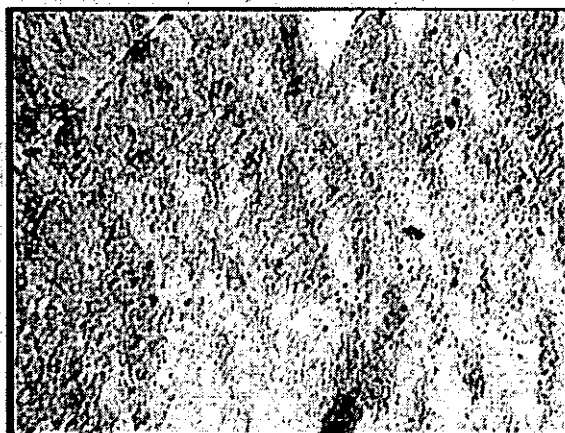
AGP1



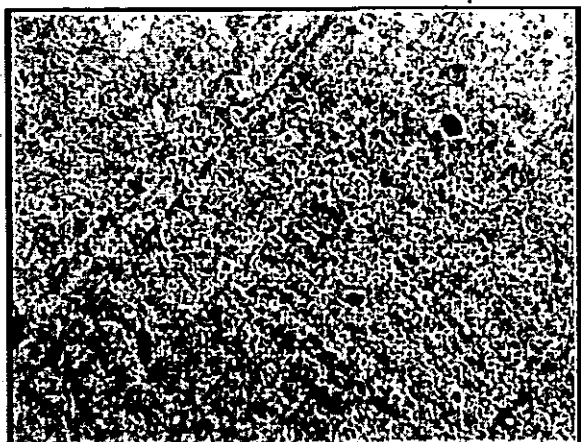
AGP3



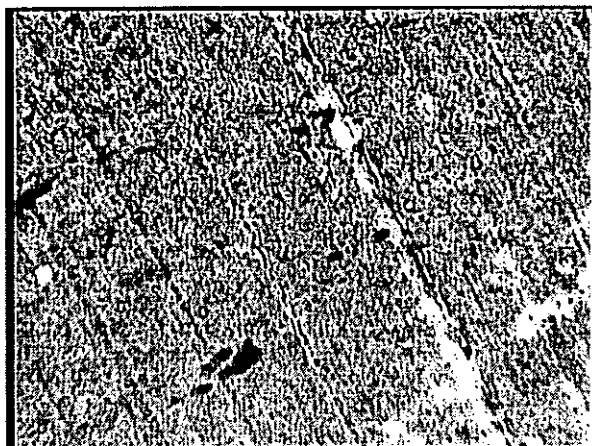
AGP4



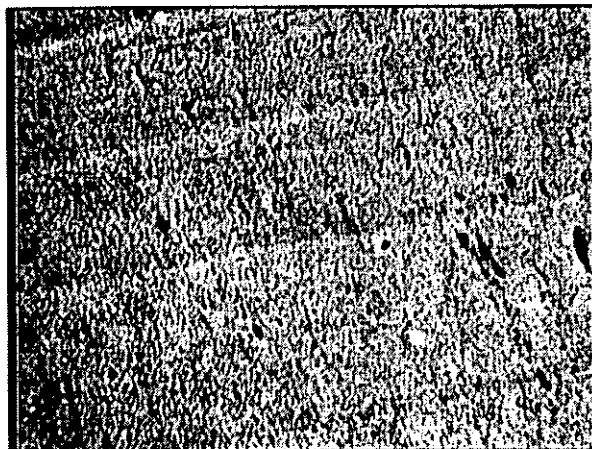
AGP5



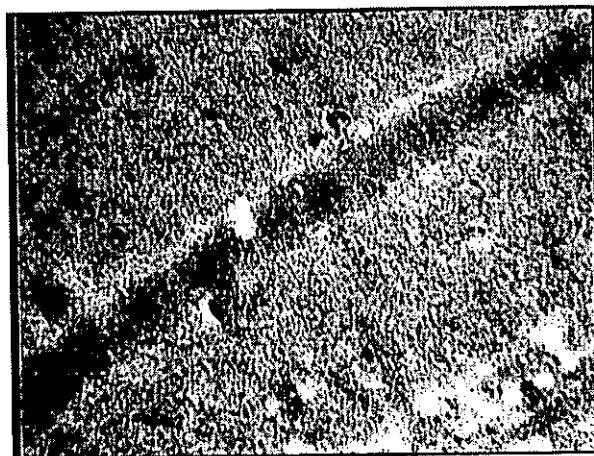
AGQ1



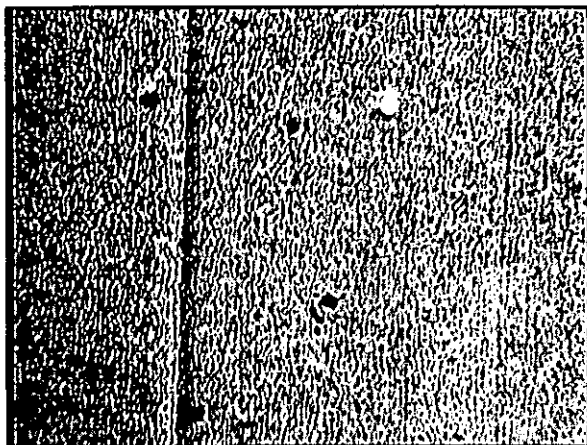
AGQ2



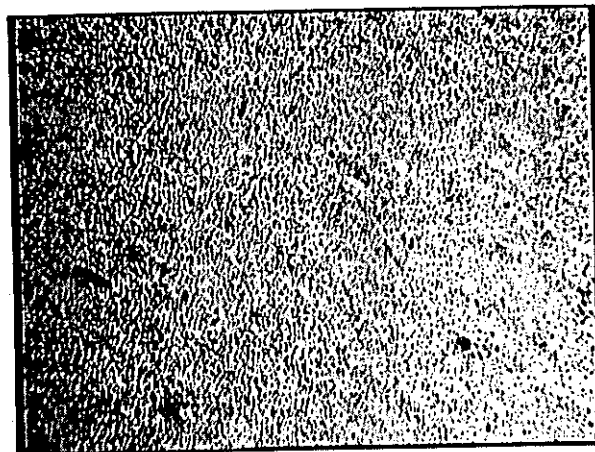
AGQ3

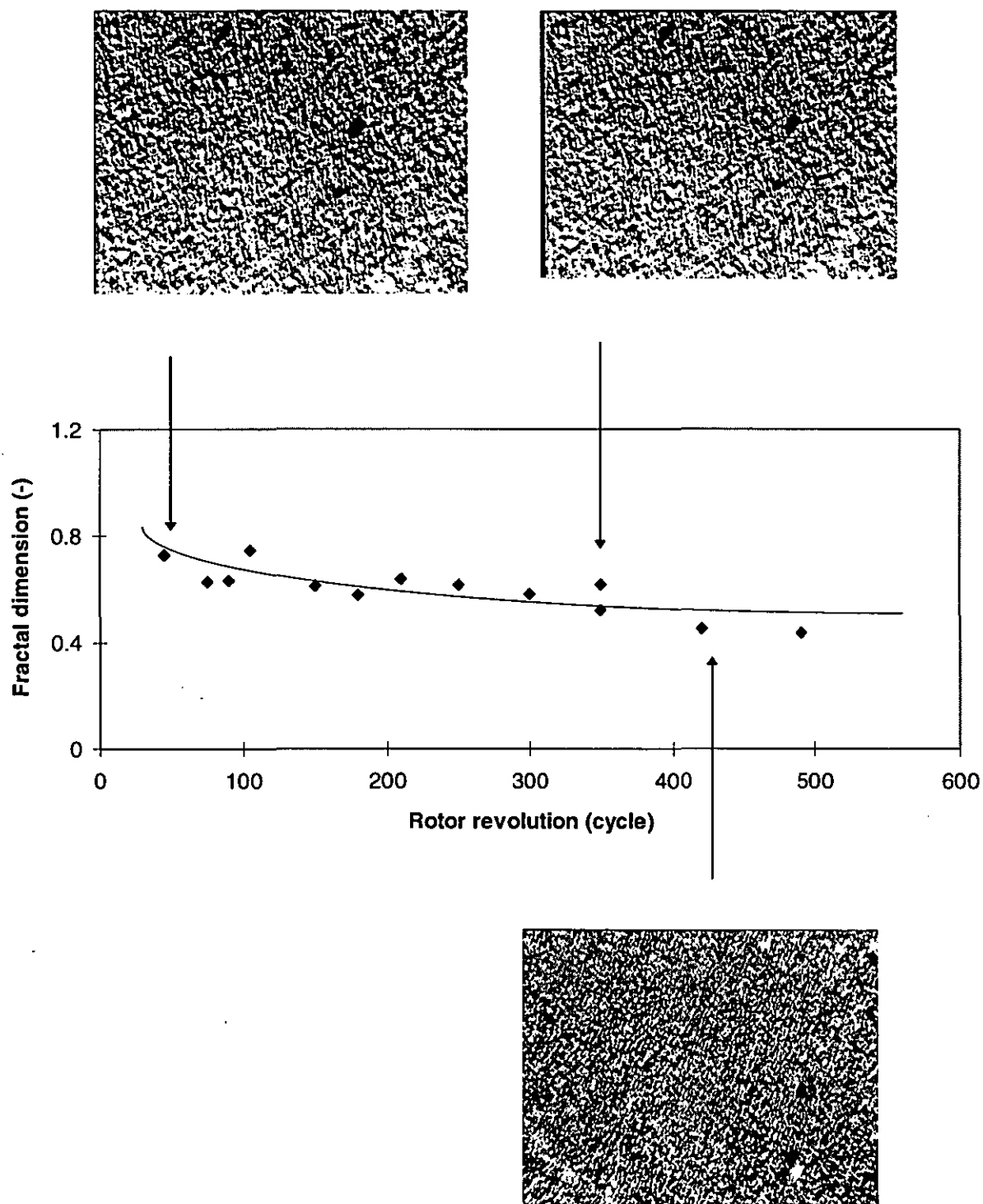


AGQ4



AGQ5





The relationship between the fractal dimension and the state of mix. (SBR sample)

Reference

- 1) T. Takagi, "Kaiseki gaku", Iwanami Pub. (1918)
- 2) A. Paulis, "The Fourier Integral and its application", McGraw Hill (1962)
- 3) R. N. Bracewell, "The Fourier Integral and its application", McGraw Hill (1965)
- 4) S. Minami, "Hakei Deta Syori", CQ Pub. (1986)
- 5) J. P. Burg, "Advanced Study institute on Signal Processing", NATO, Enschede, Netherlands (1968)
- 6) C. E. Shannon, "The Mathematical Theory of Communication", The university of Illinois press (1949)
- 7) H. Akaike "Statistical Predictor Identification", Ann. Inst. Stat. Math., vol(2), 203(1969)
- 8) J. S. Bendat, A. G. Piersol, "Measurement and Analysis of Random Data", John Wiley & Sons., (New York 1958)
- 9) E. Guth, H. Mark, Mh. Chem., 65, 93 (1934)
- 10) S. Oka, J. Phy. Soc. Jap., 3, 119 (1948)
- 11) W. Kuhn, Kolloid-Z., 2, 68 (1934)
- 12) T. L. Smith, J. Poly. Sci., 32, 99 (1958)
- 13) S. Hashizume, Nihon Rheorogi Gakaishi, 15, 19 (1987)
- 14) I. Procaccia, J. Stat. Phys., 36, 655 (1984)

